CHALMERS
UNIVERSITY OF TECHNOLOGY

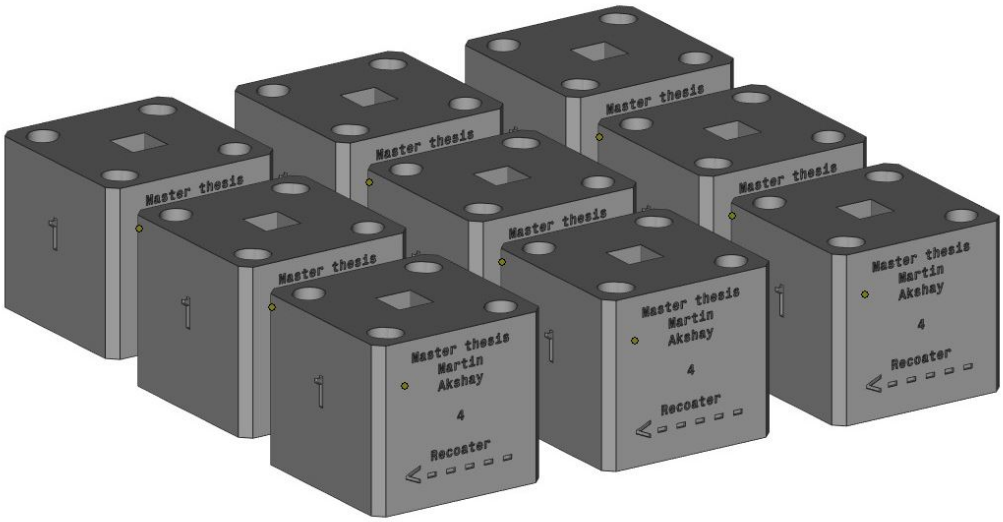

PRECISION MANUFACTURING USING ADDITIVE MANUFACTURING

A Study Focused on Geometrical Deviation in Laser Based Powder Bed Fusion

Master's thesis in Product Development

Akshaykumar Pasupulate Suresh

Martin Ohlsson

DEPARTMENT OF INDUSTRIAL AND MATERIAL SCIENCE (IMS)

CHALMERS UNIVERSITY OF TECHNOLOGY
Gothenburg, Sweden 2021
www.chalmers.se

Master's thesis 2021

Precison Manufacturing using Additive Manufacturing

A Study Focused on Geometrical Deviation in Laser Based Powder Bed Fusion



CHALMERS
UNIVERSITY OF TECHNOLOGY

Department of Industrial and Material Science
Division of Materials and Manufacturing
Chalmers University of Technology
Gothenburg, Sweden 2021

Precision Manufacturing using Additive Manufacturing
A Study Focused on Geometrical Deviation in Laser Based Powder Bed Fusion
Akshaykumar Pasupulate Suresh
Martin Ohlsson

© AKSHAYKUMAR PASUPULATE SURESH, 2021.
© MARTIN OHLSSON, 2021.

Supervisor Company: Sepehr Hatami, Research Institute of Sweden
Supervisor: Eric Bojestig, Chalmers University of Technology
Examiner: Lars Nyborg, Chalmers University of Technology

Master's Thesis 2021
Department of Industrial and Material Science
Division of Materials and Manufacturing
Chalmers University of Technology
SE-412 96 Gothenburg
Telephone +46 31 772 1000

Typeset in LaTeX
Printed by Chalmers Reproservice
Gothenburg, Sweden 2021

Precision Manufacturing using Additive Manufacturing
A Study Focused on Geometrical Deviation in Laser Based Powder Bed Fusion
Akshaykumar Pasupulate Suresh
Martin Ohlsson
Department of Industrial and Material Science
Chalmers University of Technology

Abstract

Additive Manufacturing can be used for additive manufacturing complex parts with limitations to size of the feature and capability of the machine. There exist several technologies for metal additive manufacturing but this project focuses its case study on the laser based powder bed fusion process. In order to find the geometrical deviation and variation for the small features, artifact models were designed, printed and analyzed. Ten different prints were done in order to analyse the geometrical deviation of the features different process parameters. A measurement strategy is introduced in the thesis to standardize measurement procedure to reduce the errors. A comparison between the different measuring techniques with their advantages and disadvantages are mentioned for the case study. Finally, a comparison between the parts printed using LB-PBF and Binder Jetting was done. All the results provided are subject to the scope of the project and provides a learning outcome to carry out the future research. The results indicate that the orientation of the features with respect to the recoater and the setting of amount of gas flow and its direction has an effect on the accuracy of the parts. From the analysis, the least deviation is achieved using 65% gas flow in relation to standard settings for most of the features. These results can be verified and concluded only with the further investigations. There is a high possibility for the bending of arrows of the waveguide in the first and the last positions when additive manufactured. The selection of measurement technique and strategies based on the feature size and shape is important and the human error during measurements is dependent on the magnification of the measuring instrument and has to be selected wisely. A human error of 3 to 5 μm during measurements was seen in this thesis project. From the electrical evaluation of waveguide, it was seen that there is a repeatability and geometrical accuracy for the prints 3, 4 and 5.

Cover: 3D printing of gap waveguides.

Keywords: *Accuracy, Additive Manufacturing, Artifact, Binder Jetting, Deviation, Dimensions, Geometrical Accuracy, Measurements, Strategy, Variation, LB-PBF*

Acknowledgements

Firstly, we would like to thank Chalmers University of Technology, Research Institutes of Sweden, Ericsson, Digital Metal and EOS for giving us the opportunity to be part of a master thesis project and providing their valuable suggestions and feedback throughout the thesis. I would like to thank my examiner Lars Nyborg, Professor and my supervisor Eric Bojestig, PhD Student, at the Division of Material and Manufacture, Department of Industrial and Materials Science for their constant support, feedback and guidance throughout this journey. Moreover, I would like to express my sincere gratitude to my company supervisor, Sepehr Hatami from Metal Additive Manufacturing Department, Research Institutes of Sweden.

At last, we would like to thank my family and friends for their constant support and care throughout this journey.

Akshaykumar Pasupulate Suresh, Gothenburg, June 2021
Martin Ohlsson, Gothenburg, June 2021

Nomenclature

5G: Fifth Generation of cellular network

AM: Additive manufacturing

BJ: Binder jetting

Catia: A CAD software

DFAM: Design for additive manufacturing

ESEM: Environmental Scanning Electron Microscope

ImageJ: A image analysis software well suited for taking measurements and calculating area from ESEM images.

IoT: Internet of Things

LB-PBF: Laser based powder bed fusion

Materialise Magics: A printing preparation software for additive manufacturing

MATLAB: A computational software used for plotting the results

PBF: Powder bed fusion

SD: Standard deviation

SOM: Stereo optical microscopy

Tracker: A image and physics analysis software allowing taking measurements from a calibratable image

Contents

List of Figures **xv**

List of Tables **xxi**

1 Introduction **1**
1.1 Background . . . 1
1.2 Objectives and research questions . . . 1
1.3 Scope . . . 2
1.4 Problem definition . . . 2

2 Theoretical framework **3**
2.1 Waveguide for Telecom . . . 3
2.2 Additive Manufacturing . . . 3
2.2.1 Laser based powder bed fusion . . . 3
2.3 Design for additive manufacturing . . . 5
2.3.1 Precision manufacturing . . . 5
2.3.2 Orientation . . . 5
2.3.3 Residual stresses . . . 6
2.3.4 Gas flow and build position . . . 6
2.3.5 Scan speed . . . 7
2.3.6 Machine capabilities . . . 7
2.4 Test artefact for geometric features . . . 7

3 Methodology **9**
3.1 Product description and modelling . . . 10
3.2 Test artefact model . . . 12
3.2.1 Print preparation . . . 13
3.2.1.1 EOS M290 . . . 13
3.2.1.2 EOS M100 . . . 14
3.2.1.3 Selection of process parameters . . . 15
3.2.2 Measurement using environmental scanning electron microscopy (ESEM) . . . 16
3.2.3 Measurement using stereo optical microscopy (SOM) . . . 21
3.2.4 Deviation analysis . . . 23
3.3 Gap waveguide model . . . 23
3.3.1 Print preparation . . . 23
3.3.2 Electrical evaluation . . . 24

4 Results **27**
4.1 Comparison between ESEM and SOM measurements 27
4.2 Deviation analysis of test artefact features 28
4.2.1 Deviation analysis of pins 28
4.2.2 Deviation analysis of ribs 32
4.2.3 Deviation analysis of arrowhead base 35
4.2.4 Deviation analysis of grooves 39
4.2.5 Deviation analysis of gaps 42
4.2.6 Deviation analysis of angles 45
4.2.7 Deviation analysis of arrowfoot angles and arrowhead height . 48
4.2.8 Deviation analysis of arrowfoot 51
4.3 Process variation 54
4.4 Defects in test artefact prints 58
4.4.1 Bending in geometrical features 58
4.4.2 Cracks 59
4.4.3 Pores 59
4.4.4 Attachment of half molten particles 60
4.4.5 Discontinuous print 61
4.5 Comparison between LB-PBF and Binder Jetted Parts 61
4.6 Electrical evaluation 62

5 Discussion **65**
5.1 Work progression 65
5.2 Accuracy in the results 65
5.3 Feature control 66
5.4 Ethics 67

6 Conclusions **69**

7 Recommendations for Future Work **71**

A Appendix A - Prints **I**
A.1 First print EOS M290 40μm I
A.2 Second print EOS M100 40μm III
A.3 Third print EOS M100 20μm VI
A.4 Fourth print EOS M100 65% gas-flow VIII
A.5 Fifth print EOS M100 58% gas-flow X
A.6 Sixth print EOS M100 15% scan-speed XII
A.7 Seventh print EOS M100 30% scan-speed XIV
A.8 Eight print EOS M100 50% scan-speed XVI
A.9 Ninth print repeatability of fourth print XVIII
A.10 Tenth print binder jetting XX

B Appendix B - ESEM measurements & deviation tables **XXI**
B.1 Pins XXI
B.2 Ribs XXXI
B.3 Arrowhead base XLI

B.4 Grooves LI
B.5 Arrowfoot LXII
B.6 Arrow shape area LXXII

C Appendix C - SOM measurements & deviation tables LXXIII
C.1 Print 1 comparison between ESEM & SOM measurements LXXIII
C.1.1 Pins LXXIII
C.1.2 Arrowhead base LXXIV
C.1.3 Grooves LXXV
C.2 Gaps LXXVI
C.3 Angles LXXXIV
C.4 Arrow angle & height XCI

List of Figures

2.1 Laser powder bed fusion process *[9]*. 4

3.1 Cross sectional view of the gap waveguide. 10
3.2 Critical dimensions represented in the arrow model. 11
3.3 Reverse engineered arrow model. 12
3.4 Final artefact model. 13
3.5 Orientation of the artefacts on the build plate for the EOS M290 printer in *Materialize Magics*. 14
3.6 Orientation of the artefacts on the build plate for the EOS M100 printer in *Materialize Magics*. 15
3.7 Setup of the artefact inside of the ESEM. 17
3.8 Measurement strategy for the pins. 18
3.9 Measurement strategy for the ribs. 18
3.10 Measurement strategy for arrowhead base. 19
3.11 Measurement strategy for the grooves. 19
3.12 Measurement strategy for arrowfoot. 20
3.13 Measurement strategy for arrow shape deviation. 21
3.14 Measurement strategy for the gaps. 22
3.15 Measurement strategy for the angle. 22
3.16 Measurement strategy for arrowhead height. 22
3.17 3D model of gap waveguide 23
3.18 Build orientation showcasing the configurations, recoating direction and gas-flow direction for the gap waveguides for 50%, 58% and 65% gas-flow. 24
3.19 Measuring equipment and waveguide setup for the electrical evaluation. 25

4.1 Comparison between ESEM and SOM measurements. 28
4.2 Deviation plot for pins with 0.10 mm radius in different orientations. 29
4.3 Deviation plot for pins with 0.15 mm radius in different orientations. 29
4.4 Deviation plot for pins with 0.20 mm radius in different orientations. 30
4.5 Deviation plot for pins with 0.25 mm radius in different orientations. 31
4.6 Deviation plot for pins with 0.30 mm radius in different orientations. 31
4.7 Deviation plots for ribs with 0.20 mm diameter in different orientations. 32
4.8 Deviation plots for ribs with 0.30 mm diameter in different orientations. 33
4.9 Deviation plots for ribs with 0.40 mm diameter in different orientations. 33
4.10 Deviation plots for ribs with 0.50 mm diameter in different orientations. 34

4.11 Deviation plots for ribs with 0.60 mm diameter in different orientations. 35
4.12 Deviation plots for arrowhead with 0.849 mm base in different orientations. 36
4.13 Deviation plots for arrowhead with 1.131 mm base in different orientations. 36
4.14 Deviation plots for arrowhead with 1.414 mm base in different orientations. 37
4.15 Deviation plots for arrowhead with 1.697 mm base in different orientations. 38
4.16 Deviation plots for arrowhead with 1.980 mm base in different orientations. 38
4.17 Deviation plots for grooves with 0.30 mm diameter in different orientations. 39
4.18 Deviation plots for grooves with 0.40 mm diameter in different orientations. 40
4.19 Deviation plots for grooves with 0.50 mm diameter in different orientations. 40
4.20 Deviation plots for grooves with 0.60 mm diameter in different orientations. 41
4.21 Deviation plots for grooves with 0.70 mm diameter in different orientations. 42
4.22 Deviation plots for 0.1 mm gaps in different orientations. 43
4.23 Deviation plots for 0.2 mm gaps in different orientations. 43
4.24 Deviation plots for 0.3 mm gaps in different orientations. 44
4.25 Deviation plots for 0.4 mm gaps in different orientations. 45
4.26 Deviation plots for angles in orientation 1. 46
4.27 Deviation plots for angles in orientation 2. 46
4.28 Deviation plots for angles in orientation 3. 47
4.29 Deviation plots for angles in orientation 4. 47
4.30 Deviation plots for arrowfoot angle and arrowhead height for orientation 1. 48
4.31 Deviation plots for arrowfoot angle and arrowhead height for orientation 2. 49
4.32 Deviation plots for arrowfoot angle and arrowhead height for orientation 3. 50
4.33 Deviation plots for arrowfoot angle and arrowhead height in orientation 4. 50
4.34 Deviation plots for arrowfoot in orientation 1. 51
4.35 Deviation plots for arrowfoot in orientation 2. 52
4.36 Deviation plots for arrowfoot in orientation 3. 53
4.37 Deviation plots for arrowfoot in orientation 4. 54
4.38 Process variation for pins. 55
4.39 Process variation for ribs. 55
4.40 Process variation for grooves. 56
4.41 Process variation for arrowhead base. 57
4.42 Process variation for the arrowfoot 58

4.43 Examples of bending in the prints. 59
4.44 Cracks in print 7. 59
4.45 Example of pore formation seen in arrowfoot. 60
4.46 Example of half molten particles attached to the surface. 60
4.47 Example of half molten particles attached to the surface. 61
4.48 Comparison between deviation in binder jetted and sintered as well as LB-PBF features of the fabricated test artefact samples. 62
4.49 Electrical measurements for the gap waveguide transitions. 62
4.50 Q-values and resonance frequencies histograms for gap waveguide samples. 63

A.1 First print of the artefact model where the recoating direction is shown and the orientation number from bottom left is 1, 2, 3 and 4 for each artefact. I
A.2 Front- and back -view of the artefact printed in orientation 1. II
A.3 Front- and back -view of the artefact printed in orientation 2. II
A.4 Front- and back -view of the artefact printed in orientation 3. II
A.5 Front- and back -view of the artefact printed in orientation 4. III
A.6 Second print of the artefact model where the recoating direction is shown and the orientation number from bottom left is 1, 2, 3 and 4 for each artefact. III
A.7 Front- and back -view of the artefact printed in orientation 1. IV
A.8 Front- and back -view of the artefact printed in orientation 2. IV
A.9 Front- and back -view of the artefact printed in orientation 3. IV
A.10 Front- and back -view of the artefact printed in orientation 4. V
A.11 Third print of the artefact model where the recoating direction is shown and the orientation number from bottom left is 1, 2, 3 and 4 for each artefact. VI
A.12 Front- and back -view of the artefact printed in orientation 1. VI
A.13 Front- and back -view of the artefact printed in orientation 2. VII
A.14 Front- and back -view of the artefact printed in orientation 3. VII
A.15 Front- and back -view of the artefact printed in orientation 4. VII
A.16 Fourth print of the artefact model where the recoating direction is shown and the orientation number from bottom left is 1, 2, 3 and 4 for each artefact. VIII
A.17 Front- and back -view of the artefact printed in orientation 1. VIII
A.18 Front- and back -view of the artefact printed in orientation 2. IX
A.19 Front- and back -view of the artefact printed in orientation 3. IX
A.20 Front- and back -view of the artefact printed in orientation 4. IX
A.21 Fifth print of the artefact model where the recoating direction is shown and the orientation number from bottom left is 1, 2, 3 and 4 for each artefact. X
A.22 Front- and back -view of the artefact printed in orientation 1. X
A.23 Front- and back -view of the artefact printed in orientation 2. XI
A.24 Front- and back -view of the artefact printed in orientation 3. XI
A.25 Front- and back -view of the artefact printed in orientation 4. XI

A.26 Sixth print of the artefact model where the recoating direction is shown and the orientation number from bottom left is 1, 2, 3 and 4 for each artefact. XII
A.27 Front- and back -view of the artefact printed in orientation 1. XII
A.28 Front- and back -view of the artefact printed in orientation 2. XIII
A.29 Front- and back -view of the artefact printed in orientation 3. XIII
A.30 Front- and back -view of the artefact printed in orientation 4. XIII
A.31 Seventh print of the artefact model where the recoating direction is shown and the orientation number from bottom left is 1, 2, 3 and 4 for each artefact. XIV
A.32 Front- and back -view of the artefact printed in orientation 1. XIV
A.33 Front- and back -view of the artefact printed in orientation 2. XV
A.34 Front- and back -view of the artefact printed in orientation 3. XV
A.35 Front- and back -view of the artefact printed in orientation 4. XV
A.36 Eight print of the artefact model where the recoating direction is shown and the orientation number from bottom left is 1, 2, 3 and 4 for each artefact. XVI
A.37 Front- and back -view of the artefact printed in orientation 1. XVI
A.38 Front- and back -view of the artefact printed in orientation 2. XVII
A.39 Front- and back -view of the artefact printed in orientation 3. XVII
A.40 Front- and back -view of the artefact printed in orientation 4. XVII
A.41 Ninth print of the artefact model where the recoating direction is shown and the orientation number from bottom left is 1, 2, 3 and 4 for each artefact. XVIII
A.42 Front- and back -view of the artefact printed in orientation 1. XVIII
A.43 Front- and back -view of the artefact printed in orientation 2. XIX
A.44 Front- and back -view of the artefact printed in orientation 3. XIX
A.45 Front- and back -view of the artefact printed in orientation 4. XIX
A.46 Tenth print of the artefact where two artefacts were binder jetted. . XX
A.47 Recoatin direction of the binder jetted artefacts. XX

B.1 ESEM images of pins of print 1. XXII
B.2 ESEM images of pins of print 2. XXIII
B.3 ESEM images of pins of print 3. XXIV
B.4 ESEM images of pins of print 4. XXV
B.5 ESEM images of pins of print 5. XXVI
B.6 ESEM images of pins of print 6. XXVII
B.7 ESEM images of pins of print 7. XXVIII
B.8 ESEM images of pins of print 8. XXIX
B.9 ESEM images of the pins for print 9. XXX
B.10 ESEM images of the binder jetted pins of print 10. XXXI
B.11 ESEM images of ribs of print 1. XXXII
B.12 ESEM images of ribs of print 2. XXXIII
B.13 ESEM images of ribs of print 3. XXXIV
B.14 ESEM images of ribs of print 4. XXXV
B.15 ESEM images of ribs of print 5. XXXVI

B.16 ESEM images of ribs of print 6. XXXVII
B.17 ESEM images of ribs of print 7. XXXVIII
B.18 ESEM images of ribs of print 8. XXXIX
B.19 ESEM images of the ribs for print 9. XL
B.20 ESEM images of the binder jetted ribs of print 10. XLI
B.21 ESEM images of arrowhead base of print 1. XLII
B.22 ESEM images of arrowhead base of print 2. XLIII
B.23 ESEM images of arrowhead base of print 3. XLIV
B.24 ESEM images of arrowhead base of print 4. XLV
B.25 ESEM images of arrowhead base of print 5. XLVI
B.26 ESEM images of arrowhead base of print 6. XLVII
B.27 ESEM images of arrowhead base of print 7. XLVIII
B.28 ESEM images of arrowhead base of print 8. XLIX
B.29 ESEM images of the arrowhead base for print 9. L
B.30 ESEM images of the binder jetted arrowhead of print 10. LI
B.31 ESEM images of the grooves for print 1. LII
B.32 ESEM images of the grooves for print 2. LIII
B.33 ESEM images of the grooves for print 3. LIV
B.34 ESEM images of the grooves for print 4. LV
B.35 ESEM images of the grooves for print 5. LVI
B.36 ESEM images of the grooves for print 6. LVII
B.37 ESEM images of the grooves for print 7. LVIII
B.38 ESEM images of the grooves for print 8. LIX
B.39 ESEM images of the grooves for print 9. LX
B.40 ESEM images of the binder jetted grooves of print 10. LXI
B.41 ESEM images of arrowfoot of print 1. LXII
B.42 ESEM images of arrowfoot of print 2. LXIII
B.43 ESEM images of arrowfoot of print 3. LXIV
B.44 ESEM images of arrowfoot of print 4. LXV
B.45 ESEM images of arrowfoot of print 5. LXVI
B.46 ESEM images of arrowfoot of print 6. LXVII
B.47 ESEM images of arrowfoot of print 7. LXVIII
B.48 ESEM images of arrowfoot of print 8. LXIX
B.49 ESEM images of the arrowfoot of print 9. LXX
B.50 ESEM images of the binder jetted arrowfoot of print 10. LXXI
B.51 Images of arrow shape area of print 1. LXXII

C.1 SOM images of pins for print 1. LXXIII
C.2 SOM images of arrowhead base for print 1. LXXIV
C.3 SOM images of grooves for print 1. LXXV
C.4 SOM images of the gaps for print 1. LXXVI
C.5 SOM images of the gaps for print 2. LXXVII
C.6 SOM images of the gaps for print 3. LXXVIII
C.7 SOM images of the gaps for print 4. LXXIX
C.8 SOM images of the gaps for print 5. LXXX
C.9 SOM images of the gaps for print 6. LXXXI

C.10 SOM images of the gaps for print 7. LXXXII
C.11 SOM images of the gaps for print 8. LXXXIII
C.12 SOM images of angle 1 and 5 for print 2. LXXXIV
C.13 SOM images of angle 1 and 5 for print 3. LXXXV
C.14 SOM images of angle 1 and 5 for print 4. LXXXVI
C.15 SOM images of angle 1 and 5 for print 5. LXXXVII
C.16 SOM images of angle 1 and 5 for print 6. LXXXVIII
C.17 SOM images of angle 1 and 5 for print 7. LXXXIX
C.18 SOM images of angle 1 and 5 for print 8. XC
C.19 SOM images of arrow 1 and 5 for print 2. XCI
C.20 SOM images of arrow 1 and 5 for print 3. XCII
C.21 SOM images of arrow 1 and 5 for print 4. XCIII
C.22 SOM images of arrow 1 and 5 for print 5. XCIV
C.23 SOM images of arrow 1 and 5 for print 6. XCV
C.24 SOM images of arrow 1 and 5 for print 7. XCVI
C.25 SOM images of arrow 1 and 5 for print 8. XCVII

List of Tables

3.1 Critical dimensions in the arrow model. 11
3.2 Dimensions of features in the test artefact model. 13
3.3 Processing variants included in the test plan. 16
3.4 Process parameter settings used for the gap waveguide prints. 24

5.1 Deviation for the features, repeatability and human error expressed as min, max, mean and standard deviation. 67

A.1 Dimensions and weight of the binder jetted artefacts. XX

B.1 Deviation of the pins for print 1. XXII
B.2 Deviation of the pins for print 2. XXIII
B.3 Deviation of the pins for print 3. XXIV
B.4 Deviation of the pins for print 4. XXV
B.5 Deviation of the pins for print 5. XXVI
B.6 Deviation of the pins for print 6. XXVII
B.7 Deviation of the pins for print 7. XXVIII
B.8 Deviation of the pins for print 8. XXIX
B.9 Deviation of the pins for print 9. XXX
B.10 Deviation of the pins for print 10. XXXI
B.11 Deviation of the ribs for print 1. XXXII
B.12 Deviation of the ribs for print 2. XXXIII
B.13 Deviation of the ribs for print 3. XXXIV
B.14 Deviation of the ribs for print 4. XXXV
B.15 Deviation of the ribs for print 5. XXXVI
B.16 Deviation of the ribs for print 6. XXXVII
B.17 Deviation of the ribs for print 7. XXXVIII
B.18 Deviation of the ribs for print 8. XXXIX
B.19 Deviation of the ribs for print 9. XL
B.20 Deviation of the ribs for print 10. XLI
B.21 Deviation of the arrowhead base for print 1. XLII
B.22 Deviation of the arrowhead base for print 2. XLIII
B.23 Deviation of the arrowhead base for print 3. XLIV
B.24 Deviation of the arrowhead base for print 4. XLV
B.25 Deviation of the arrowhead base for print 5. XLVI
B.26 Deviation of the arrowhead base for print 6. XLVII
B.27 Deviation of the arrowhead base for print 7. XLVIII

B.28 Deviation of the arrowhead base for print 8. XLIX
B.29 Deviation of the arrowhead base for print 9. L
B.30 Deviation of the binder jetted arrowhead base for print 10. LI
B.31 Deviation of the grooves for print 1. LII
B.32 Deviation of the grooves for print 2. LIII
B.33 Deviation of the grooves for print 3. LIV
B.34 Deviation of the grooves for print 4. LV
B.35 Deviation of the grooves for print 5. LVI
B.36 Deviation of the grooves for print 6. LVII
B.37 Deviation of the grooves for print 7. LVIII
B.38 Deviation of the grooves for print 8. LIX
B.39 Deviation of the grooves for print 9. LX
B.40 Deviation of the grooves for print 10. LXI
B.41 Deviation of arrowfoot of print 1. LXII
B.42 Deviation of arrowfoot of print 2. LXIII
B.43 Deviation of arrowfoot of print 3. LXIV
B.44 Deviation of arrowfoot of print 4. LXV
B.45 Deviation of arrowfoot of print 5. LXVI
B.46 Deviation of arrowfoot of print 6. LXVII
B.47 Deviation of arrowfoot of print 7. LXVIII
B.48 Deviation of arrowfoot of print 8. LXIX
B.49 Deviation of arrowfoot of print 9. LXX
B.50 Deviation of the arrowfoot for print 10. LXXI
B.51 Deviation for the arrow area expressed in distance and percentage. . . LXXII

C.1 Deviation of the gaps for print 1. LXXVI
C.2 Deviation of the gaps for print 2. LXXVII
C.3 Deviation of the gaps for print 3. LXXVIII
C.4 Deviation of the gaps for print 4. LXXIX
C.5 Deviation of the gaps for print 5. LXXX
C.6 Deviation of the gaps for print 6. LXXXI
C.7 Deviation of the gaps for print 7. LXXXII
C.8 Deviation of the gaps for print 8. LXXXIII
C.9 Deviation of angles for print 2 LXXXIV
C.10 Deviation of angles for print 3 LXXXV
C.11 Deviation of angles for print 4 LXXXVI
C.12 Deviation of angles for print 5 LXXXVII
C.13 Deviation of angles for print 6 LXXXVIII
C.14 Deviation of angles for print 7 LXXXIX
C.15 Deviation of angles for print 8 XC
C.16 Deviation of arrowfoot angle for print 2. XCI
C.17 Deviation of arrowhead height for print 2. XCI
C.18 Deviation of arrowfoot angle for print 3. XCII
C.19 Deviation of arrowhead height for print 3. XCII
C.20 Deviation of arrowfoot angle for print 4. XCIII
C.21 Deviation of arrowhead height for print 4. XCIII

C.22 Deviation of arrowfoot angle for print 5. XCIV
C.23 Deviation of arrowhead height for print 5. XCIV
C.24 Deviation of arrowfoot angle for print 6. XCV
C.25 Deviation of arrowhead height for print 6. XCV
C.26 Deviation of arrowfoot angle for print 7. XCVI
C.27 Deviation of arrowhead height for print 7. XCVI
C.28 Deviation of arrowfoot angle for print 8. XCVII
C.29 Deviation of arrowhead height for print 8. XCVII

1
Introduction

When a part is manufactured using additive manufacturing, the dimensions of the features of the part and their build orientation are standardized for larger parts but when the features are very small in size of μm, it's hard to manufacture them with precision. The project's main focus is on manufacturing the small arrow features in a gap waveguide which play a major role in high-frequency transmission in 5G antennas. This project aims to develop and evaluate the repeatability and precision of the small arrow features of a gap waveguide using laser based powder bed fusion. The knowledge gained from this project will be useful to Ericsson for their antenna production.

1.1 Background

Precision is very important when it comes to manufacturing thousands of parts. In many industries, parts are manufactured using traditional manufacturing processes, and the variation that occurs in the process is already known. The purpose of this thesis is to get knowledge about the possibilities of precision manufacturing using metal additive manufacturing for small parts which are suitable for AM. Furthermore, it is of interest to see how additive manufacturing can be implemented on the application "gap waveguide".

1.2 Objectives and research questions

The objectives of the project are to find solutions on how to produce tiny features with high precision using AM, get to know where the limits are and what type of critical dimensions exist. Furthermore, one more goal is to learn more about AM and design for AM in general for small features. The main challenge of the project is that the precision of the features not only depends on the design and build orientation but also on other parameters such as the type of machine used, size, and quality of the material used. Another challenge is that there are very few materials available regarding precision manufacturing using AM for small features.
From the objectives of the project, the following research questions are defined:

- How to print small features with high precision using LB-PBF?
- Does the orientation from the recoater and the gas flow affect the accuracy of the parts?
- Where is the limit of the technology?

- What kind of measurement strategy needs to be used for fine features to get high accuracy in measurements?
- What are the advantages and disadvantages of different measurement systems?
- How should one act to reduce the human error during measurement?
- What are the capabilities for high precision in LB-PBF?
- What kind of defects can be expected when printing small features using LB-PBF and what could be the cause for it?
- How precise can the variation be controlled?

1.3 Scope

The thesis is performed at Chalmers in co-operation with RISE, and Ericsson. The scope of the thesis is limited to laser based powder bed fusion (LB-PBF), and only 316L stainless steel is used. Furthermore, the thesis focuses only on design for AM and certain process parameters for the EOS M290 and M100 LB-PBF machines.

1.4 Problem definition

The problem that the project aims to solve is to find the machine and process parameters suitable for printing the arrow features with high precision so that they are able to transmit high-frequency waves. This relates to reducing geometrical deviations of the part when printing. The project aims to design a test artefact for the arrow model in a demonstrator gap waveguide, find a relevant measurement strategy and do a relevant deviation analysis strategy.

2
Theoretical framework

This chapter provides necessary theoretical knowledge about the product, AM method used in the project, definitions, process parameters, and test artefacts for geometrical features.

2.1 Waveguide for Telecom

In telecom industries, waveguides are used to transfer energy over a physical medium with low loss when a frequency greater than 30 GHz is used. Rectangular waveguides are used normally for radio frequencies in many applications. These waveguides play an important role in millimeter wavelengths and act as a transmission line feeding the antenna elements [10].

2.2 Additive Manufacturing

Additive Manufacturing (AM) is a technology where the part is built layer by layer. AM technology can be used to print plastics, metals, and ceramics. According to the American Society for Testing and Materials (ASTM F2792-12a) there are over 50 different AM technologies, which are classified into seven different processing categories: binder jetting, material jetting, material extrusion, vat photopolymerization, powder bed fusion, energy deposition, and sheet lamination [18]. Additive manufacturing or also called 3D-printing has undergone three phases of evolution. In the first phase, architects, artists, and product designers used 3D-printing technology to make prototypes or mockups of new designs. In the second phase, they were used in creating finished goods. This has also been referred to as "direct digital manufacturing" or "rapid tooling". In the third evolution phase, the technology will be owned and used by end consumers. It is said that in the future, people will be having their own factories in their home for manufacturing for their personal needs [4]. In this thesis, laser based powder bed fusion technique is used.

2.2.1 Laser based powder bed fusion

Laser based powder bed fusion or in short LB-PBF is most common technique used for printing metal parts [17]. In this section, the technology of the process and process parameters are explained. The process starts with the dispenser dispensing powder and the powder is then applied to the building platform with the recoater where the excrescent powder is stored in the collector for later use. The powder is

then fused with a laser beam that selectively melts the powder locally with the help of mirrors to provide for the scanning of the beam. This is all done under protective gas, normally argon. Each layer undergoes a cycle of selective local melting according to the pattern laid out in the layer followed by cooling and solidification. The building platform is then lowered and the process starts over again [3]. A visualization of the LB-PBF process can be seen in Figure 2.1.

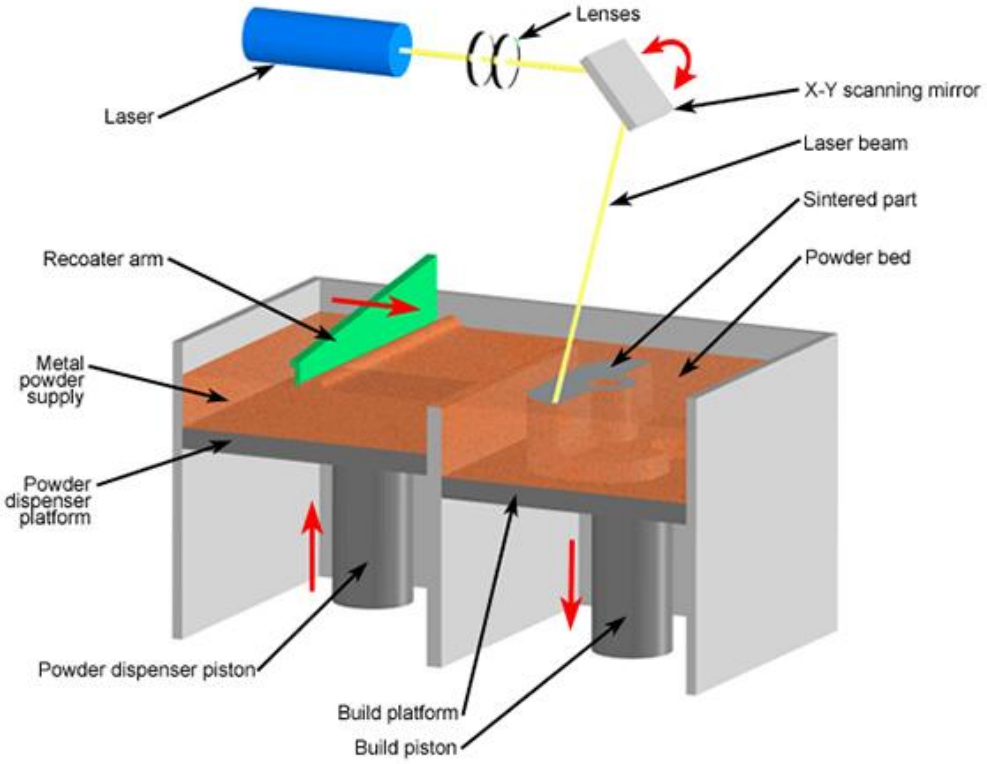

Figure 2.1: Laser powder bed fusion process *[9]*.

There are four main categories of process parameters for laser based powder bed fusion where the parameter categories are firmly independent and mutually interacting with each other. Each category of parameters has to be balanced with one another in order to provide the best possible trade-off between the parameters [5]. The four process parameter categories are as follows.

1. Laser-related parameters that include laser power, spot size, pulse duration, and pulse frequency.
2. Scan-related parameters including scan speed, scan spacing and scan pattern.
3. Powder-related parameters including powder bed density, layer thickness, material properties and the powder characteristics particle shape, size, and its distribution.
4. Temperature-related parameters which include the powder bed temperature and temperature distribution.
   In this project different scan speeds, different layer thickness, and different gas flow settings are used.

2.3 Design for additive manufacturing

Design for additive manufacturing (DFAM) is a design for manufacturability strategy that is applied to additive manufacturing. It is a general type of design method or tool where functional performance and other key product life-cycle considerations such as manufacturability, reliability, and cost can be optimized subject to the capabilities of additive manufacturing technologies. Parts that have not been designed for AM might require a lot of supports, and would require post-processing for their removal. Hence the parts have to be designed for AM. Some of the critical key factors that drive the success rate and productivity of the AM builds are discussed below.

2.3.1 Precision manufacturing

The demand for increasing precision has evolved in all industry sectors from automobile and aerospace to 3D printers. These evolving technologies enable us to achieve precision in the prints. One possible way of defining precision is by determining accuracy, repeatability, resolution, uncertainty, and deviation. It is considered precision if these attain 1 defect in 10^6 parts [7]. It is always that the lack of precision comes with a lack of repeatability that leads the process. In this project since LB-PBF is used some of the factors like porosity, warpage, residual stress, and cracking could affect the precision. These factors directly or indirectly contribute to the dimensional deviation of the finished parts during printing of metal AM parts [17]. The precision of the parts is also affected by the process parameter settings of the machine [6].

2.3.2 Orientation

In LB-PBF, the parts are produced layer by layer in a powder bed. When a layer is melted it relies on the previous layer in order to provide support and remove excess heat, which makes the correlation of the layers important [14]. When the laser beam is melting an area where the layer below consists out of solid metal and not powder, the heat can flow through the metal, and therefore be cooled rapidly, and create a stronger bonding. If the layer below consists of powder the bound will consist out of solid metal, and partially melted powder due to insulating properties of the powder heat will be reattained longer, and give additional sintering of surrounding powder. This behavior can result in additional material being connected to the overhanging regions of the part, which in turn can result in distortions such as misshapen surfaces, and rough finishes.

As stated before, down-skins have an increased risk to have bad surface finishes, which is important to take into account when orienting a part. In order to be able to produce finer features can the down-skins be moved to the top surface of the part. Another important thing to consider is the recoater direction. When a new layer of powder is applied, the recoater pushes it across the bed and it gets sequentially squeezed in order to produce a densely packed layer. This results in that the recoater

can interact with feature surfaces that are inclined towards the recoater which can cause the recoater to come into contact with the feature leading to distortions, and even build failure [14]. Orienting inclined features away from the recoater results in that the recoater hits the feature with an oblique angle which reduces the probability of distortions.

2.3.3 Residual stresses

Residual stresses are the result of fast heating followed by cooling in the manufacturing process under geometrical constraint which is inevitable for LB-PBF. In LB-PBF, the most common types of distortion are caused by shrinkage, and deformations created by residual stresses during the manufacturing process [2]. When a new hot layer is created by the process it is created on top of a cold layer, the new layer then cools on top of the cold layer which results in contraction and shear forces emerge between the two layers. This results in stresses adding up together with each layer being added, which can create distortions of the part and even in some cases cracking of the part. Furthermore, can heat caused by swelling create local deformation.

A way to minimize residual stresses is by changing the scanning pattern that has a shorter scan vector, and hence mitigate the residual stresses that are likely to be built into the part [14]. Furthermore, the orientation of the scan vectors can be rotated for each layer so that residual stresses do not build up in the same plane.
There are 3 types of common scanning patterns: Meander Hatching Pattern, Stripe Hatching Pattern, Chessboard Hatching Pattern. Each has its own advantage.

1. Meander Hatching Pattern
   The pattern uses 67-degree rotation after each layer and is suitable for higher build rate and small as well as thin features. The drawback is that it increases the residual stresses.
2. Stripe Hatching Pattern
   This type of pattern is suitable for larger parts and has higher build rate than the chessboard hatching patterns. It also has a homogeneous distribution of residual stresses.
3. Chessboard Hatching Pattern
   This type of pattern divides each layer into 5 mm by 5 mm islands. This Pattern is rotated 67 degrees after each layer. It has a homogeneous distribution of residual stresses and is suitable for large parts.
   In this project, the Meander hatching pattern is used since it is more suitable for the size of part that is being printed.

2.3.4 Gas flow and build position

Gas flow and build position play an important role in the geometrical variation of the parts. In recent studies, it is seen that the gas flow direction and the amount of gas flow has a secondary effect on geometry deviation [17]. The gas flow direction differs from machine to machine. Moreover, it is seen that the parts that are built near

the chamber door and away from the gas inlet have the higher accuracy and less geometrical deviation. The geometrical deviation increases towards the gas inlet and increases away from the chamber door. The parts have to be manufactured with all these aspects in mind. In order to have the highest dimensional accuracy, it is suggested to have a uniform gas flow rate, and pressure along with the build chamber.

2.3.5 Scan speed

The scan speed impacts the level of details when the scanning direction changes. Several studies show that the effects of balling, and wetting can be controlled by changing the scan speed [8]. Changing the scan speed affects the laser line energy density, which makes it hard to predict the impact on a certain feature. A common strategy is to maintain the same energy density by adapting the laser power to the scan speed, thus changing only one process parameter at the time which makes it easier to analyze the impacts on the feature.

2.3.6 Machine capabilities

Apart from the process parameters, the machine capabilities contribute to the variation in the process. Different machines use different position systems to direct the laser beam which affects the achievable accuracy [11]. Furthermore, the hardware affecting process parameters are gas flow and powder distribution which makes the selection of process parameters different for different machines.

2.4 Test artefact for geometric features

Different types of test artefacts can be used in order to test the printer's geometrical accuracy and performance [16]. The artefacts enable us to have a common reference to be able to compare additive manufacturing machine limitations [13]. It is important to have a good understanding of how variations in the process may affect the particular part, machine and material in order to be able to predict the effect of the variation on the features of the part. This makes test artefacts easy and straightforward to inspect for specific features relevant to the manufacturing process. Furthermore, test artefacts can be divided into three different categories depending on what they are testing, which can be testing geometric, mechanical, and process features.

The type of artefact that is of particular interest for the current thesis project is the artefact that tests geometric features. There exist a lot of recommendations when designing an artefact for testing geometric features as stated in [13], more precisely it is of significant importance that the artefact is large enough to be able to test the performance of borders, while the main body of the manufactured part should not be too big as this will increase time to build, material use and manufacturing cost. Furthermore, the artefact should carry the real features of parts that the AM system will manufacture as different holes, bosses, thin walls and surfaces. The features of

the artefact should be of different sizes, i.e. large, medium, and small in order for it to be easy to identify the limits of the system and the features need to be easy to measure.

The Swedish Standard Institute (ISO) claims that there exist mainly three different types of measures related to features that can test the capability of the AM system when it comes to evaluating the geometry of an artefact; these are the accuracy, the resolution, and the surface texture of a feature [15].

artefacts that test the accuracy of a feature can either depict the linear positioning or dynamic accuracy of the machine in order to be able to compensate for the positioning or to be intended to evaluate the activation energy of projection of the machine. The artefacts can either be shaped like rectangles on a solid base where the spacing between the rectangles increases between each rectangle or like thin circular rings placed inside one another on a solid base where the radius decreases for each ring.

Resolution artefacts aim to access the ability to manufacture fine features which are represented from a real part with high accuracy from the machine or material. The artefacts consist out of multiple copies of the feature that are going to be tested, which are linearly spaced, and decreased in size. Common features that are used in order to evaluate the resolution are pins, holes, ribs, and slots.

There are artefacts that can evaluate the surface texture of features produced by the AM system. Such artefacts make it possible to evaluate the surface texture by taking profile and areal measurements. The layer-by-layer process of applying the material in additive manufacturing leaves often a rough surface caused by several factors such as powder size, gravity, heat dissipation, build direction and the setup of the machine. The artefacts typically consist of flat taps joined together with struts at different angles.

3
Methodology

In order to get the needed knowledge to be able to perform each step in the thesis study, a literature study was performed. At the beginning of the thesis work, the main purpose is to get a basic understanding of the subjects, basic approaches, and methods. Once the basics were covered, the purpose of the literature study was shifted to get a more depth and detailed understanding of findings that were important to the project.

The literature study was performed by reviewing articles, books, and relevant information from passed courses. The reading material were mostly provided through *Google Scholar*, *Chalmers Library* and the course *MTT120 - Additive manufacturing*. The result of the literature study can be seen in *Chapter 2 - Theoretical framework* in the report.

Keywords used for the Literature study: *AM standards, Accuracy, Additive Manufacturing, Benchmark, Dimensional Deviations, Material Science, Environmental Scanning Electron Microscope, Gas Flow, Laser Based Powder Bed Fusion, Precision, Process Qualification, Scan Speed, Test artefact, artefact Design Guidelines, Measurement Strategies*

3.1 Product description and modelling

Precision manufacturing is used for Ericsson's test part "gap waveguide" where the arrows are the main focus. The gap waveguide consists of 4 arrows that are shown in Figure 3.1. The test part is supposed to transmit 100 GHz of frequency signals. Any deviation in the geometry or the critical dimensions means that the performance will be affected. Deviation of 1 μm will result in 10 MHz frequency deviation from the desired frequency.

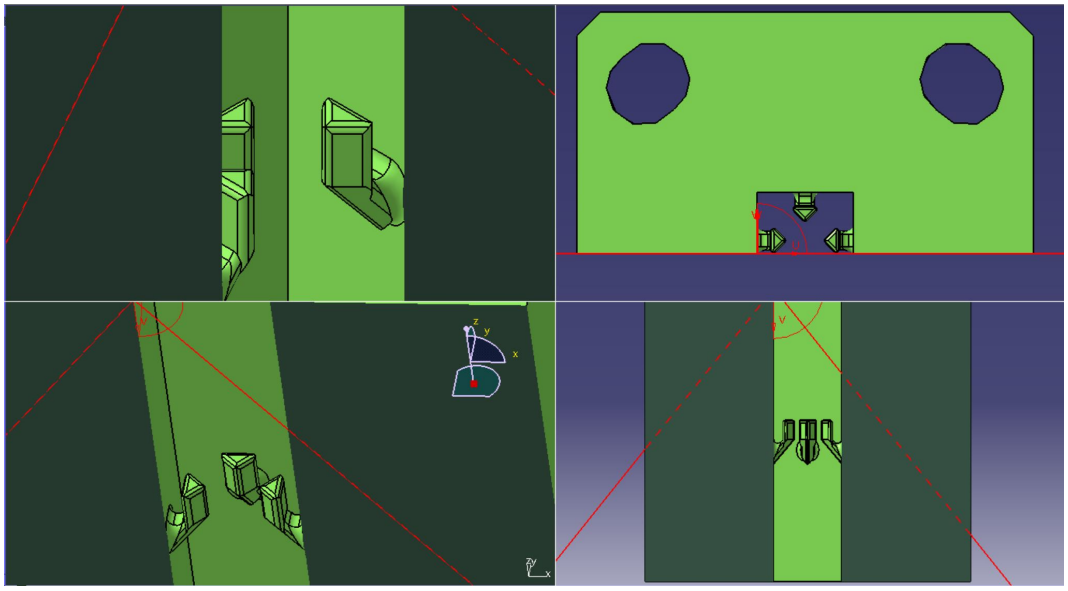

Figure 3.1: Cross sectional view of the gap waveguide.

Some of the critical dimensions of the arrows are shown in the table 3.1 below. Corresponding dimensions are represented in the arrows as shown in the figure 3.2. Here the "arrow gap" is just the distance between the two opposite arrows. "Arrowfoot angle" is the angle between the bottom surface of the arrow and the wall. "Arrow fillet" is the fillet given to the arrow both vertically and horizontally. "Arrow foot" is the distance between the wall and the surface of the arrow. "Arrowhead height" is the height of the arrow from the top of the arrow till the arrow makes a bend.

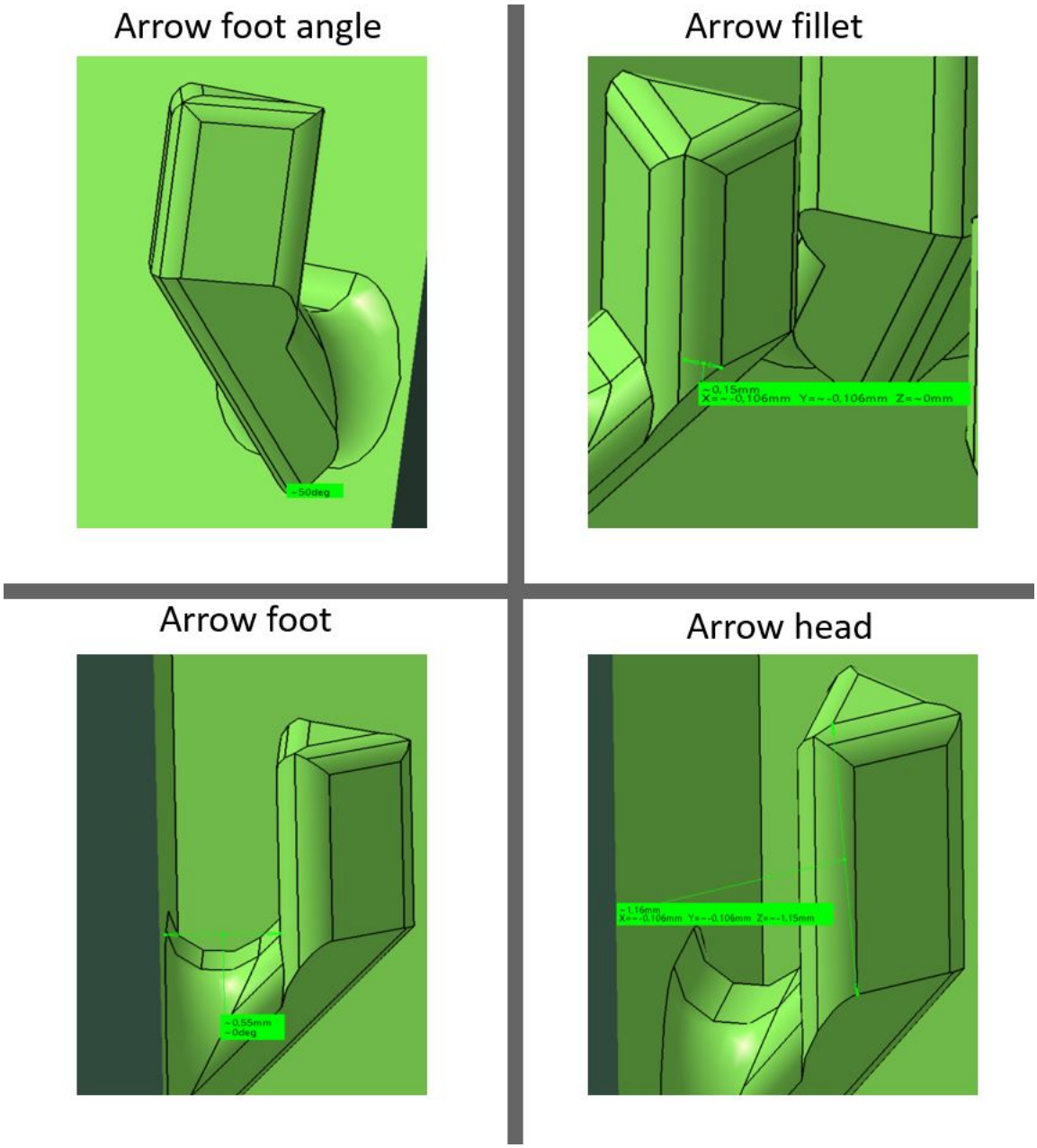

Figure 3.2: Critical dimensions represented in the arrow model.

Table 3.1: Critical dimensions in the arrow model.

Dimensions	Value
Arrow gap	1.5 mm
Arrowhead height	1.15 mm
Arrowfoot	0.5 mm
Arrow fillet	0.15 mm
Arrowfoot angle	40 degrees

A reverse engineering approach was used to extract the exact dimensions and surfaces from the arrow in the original model to create a new 3D model of the arrow that can be modified at any time of the project. CATIA V5 software was used to design the arrow model that is shown below in Figure 3.3.

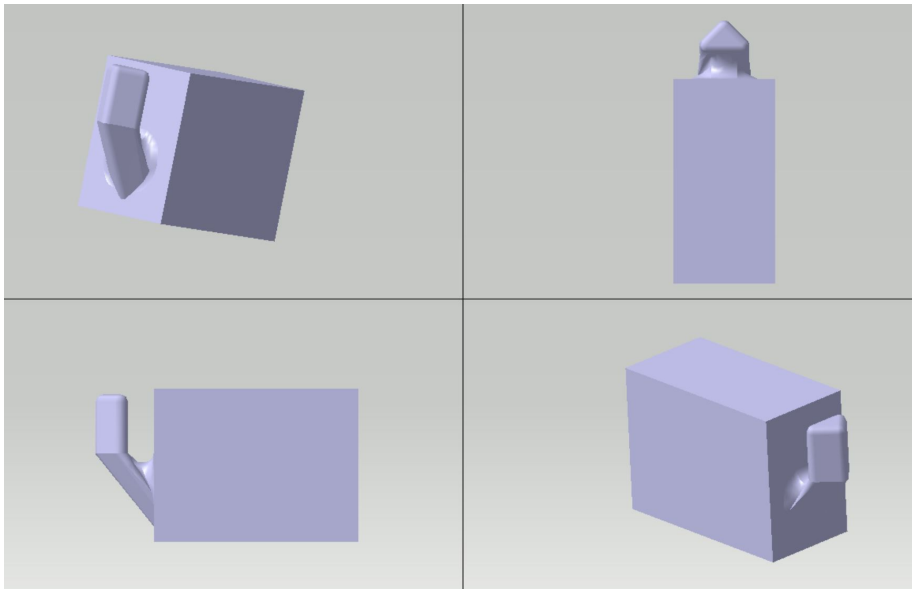

Figure 3.3: Reverse engineered arrow model.

3.2 Test artefact model

A test artefact was developed in order to evaluate the different features of the arrow model. Each feature of the arrow was designed with varying dimensions. The features were then created as a row with each feature increasing in the size of 0.05 mm and 5 degrees for the angles with equal spacing in between the features. The artefact model can be seen in Figure 3.4. The arrow model consisted of vertical and horizontal fillets which were represented as cylindrical pins standing up in the first row from the top, pins laying down horizontally in the second row. The arrowhead represented with a triangle which could be interpreted from the ISO standard as testing accuracy in the third row, cylindrical grooves in the fourth row which represented the up skin in the arrow model, down skins were represented by designing different down skin angles for the arrow model.

Furthermore, the thickness of the bottom plate is increased to be able to cut the artefacts from the build-plate to reduce the risk of damaging the artefacts and the space between the features decreased after considering the capabilities of the printer and powder usage for the print. Lastly, the five identical models of the arrow were added to the artefact. This was done to be able to study how well the printer would perform on the repeatability of the arrows with respect to the same process parameter and to be able to compare them with the other features on the artefact.

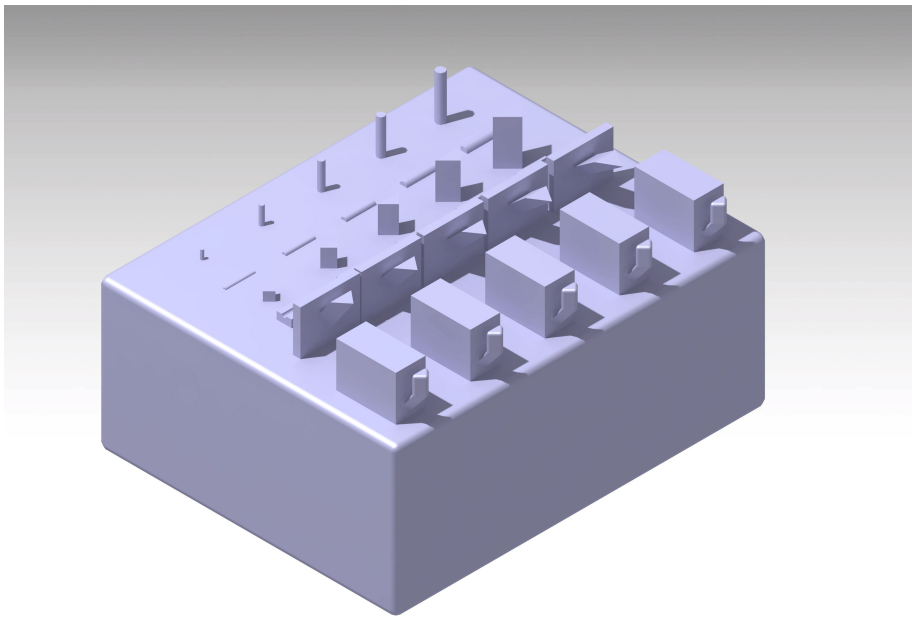

Figure 3.4: Final artefact model.

Table 3.2 below shows the dimensions of each feature in the test artefact model from left to right.

Table 3.2: Dimensions of features in the test artefact model.

Dimension [mm]					
Pin [ϕ]	0.2	0.3	0.4	0.5	0.6
Rib [ϕ]	0.2	0.3	0.4	0.5	0.6
Arrowhead base	0.849	1.131	1.414	1.697	1.98
Groove [ϕ]	0.3	0.4	0.5	0.6	0.7
Angle [°]	35	40	45	50	55
Gap	0.1	0.2	0.3	0.4	
Arrow foot	0.5	0.5	0.5	0.5	0.5

3.2.1 Print preparation

artefacts were printed with EOS M290 and EOS M100 printer with different placement, orientations, and process parameter settings as described below.
The prints were prepared in the *Materialize Magics* for the EOS M290 and EOS 100 printer using 316L stainless steel powder as the source material.

3.2.1.1 EOS M290

The first print was prepared in *Materialize Magics* for the EOS M290 printer using 316L stainless steel as the material. Four identical artefacts were placed close to one another with a rotation of 90 degrees at the upper-center of the build plate to

investigate the impact of the re-coating direction on the arrows. The placement of the artefacts can be seen in Figure 3.5 below.

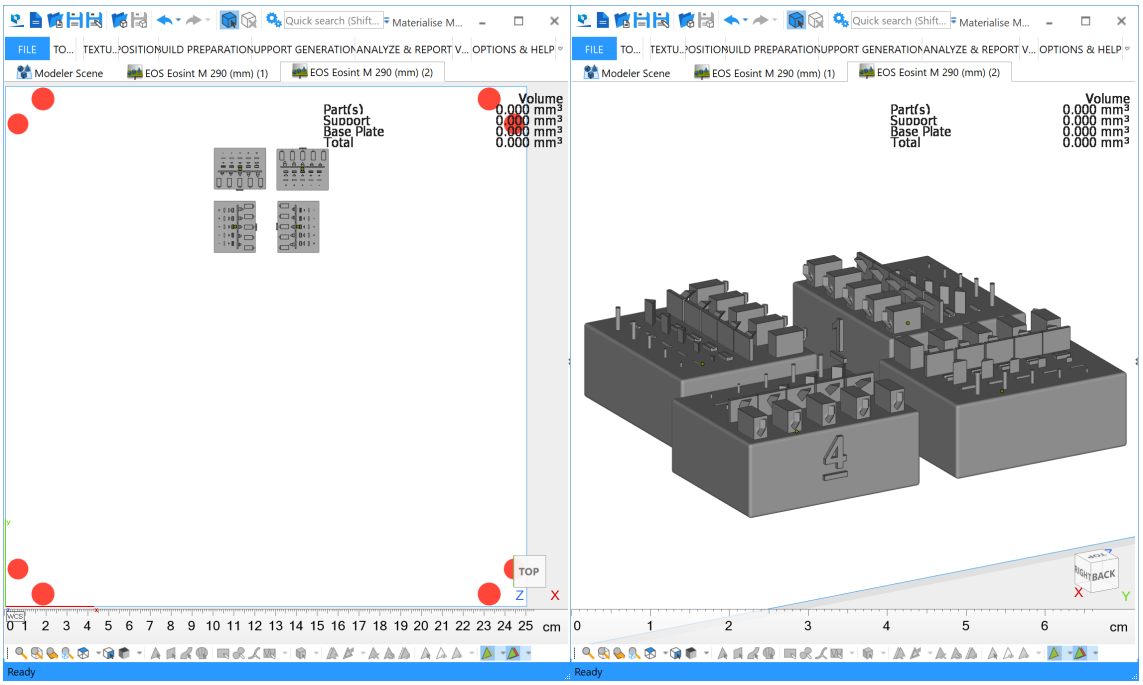

(a) Top-view showcasing the build plate. **(b)** Zoomed in side-view.

Figure 3.5: Orientation of the artefacts on the build plate for the EOS M290 printer in *Materialize Magics*.

3.2.1.2 EOS M100

The rest of the prints were done in an EOS M100 printer using 316L stainless steel as build material. The prints were prepared in *Materialize Magics* by rotating the EOS 290 preparation 180 degrees and centered in the middle of the build plate in order to match the new recoating direction. The placement of the artefacts is seen in Figure 3.6 below.

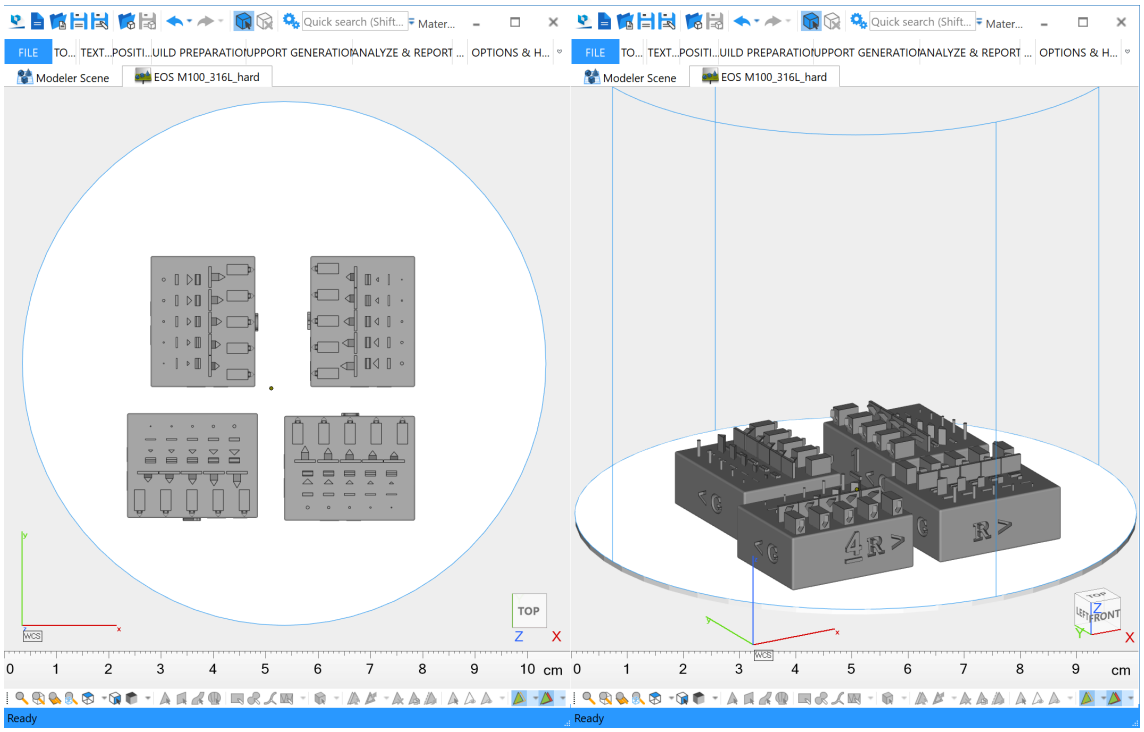

(a) Top-view showcasing the build plate. **(b)** Zoomed in side-view.

Figure 3.6: Orientation of the artefacts on the build plate for the EOS M100 printer in *Materialize Magics*.

3.2.1.3 Selection of process parameters

Each job was printed with different process parameter settings in order to find the capability of each type of setting. Layer thickness was changed from $40\mu m$ to $20\mu m$ to study the impact of the powder size on the features. Amount of gas flow was changed to 65% and 58% of the standard gas flow with standard process parameters for $20\mu m$ layer thickness to evaluate the ability to produce better shapes. Furthermore the scan-speed was varied to 15%, 30% and 50% of standard setting by changing the laser power while thus maintaining the same energy density in order to investigate the capabilities to produce smooth surfaces of the features without any balling effect. Lastly, the repeatability of print 4 was tested and a comparison print with binder jetting (BJ) was done provided by Digital Metal using 316L stainless steel powder as well. The binder jetting constitute a two-stage processing route with final sintering stage after the printing. The different processing variants are shown in Table 3.3.

Table 3.3: Processing variants included in the test plan.

Print	Machine	Parameters
1	EOS M290	Standard with layer thickness 40μm
2	EOS M100	Standard with layer thickness 40μm
3	EOS M100	Standard with layer thickness 20μm
4	EOS M100	Standard with 65% gas flow
5	EOS M100	Standard with 58% gas flow
6	EOS M100	Standard with scan speed 15%
7	EOS M100	Standard with scan speed 30%
8	EOS M100	Standard with scan speed 50%
9	EOS M100	Standard with 65% gas flow
10	Digital Metal	BJ: Standard with layer thickness 20μm

3.2.2 Measurement using environmental scanning electron microscopy (ESEM)

The ESEM instrument used for measurements is Philips ESEM XL 30. The measurements done using ESEM were pin diameter, rib diameter, groove diameter, gap distance, arrowhead base, and arrowfoot. The purpose of the analysis is to find some of the measurements of the features and to analyze the impact of process parameter settings like defects on the prints. This will help in identifying the correct process parameters for the next print. The samples were analyzed starting from the smallest dimension in each row to the largest dimension in each row. Each row of the feature was analyzed and visualized in the same way. The features with different heights were measured with different magnifications which could have an impact on the accuracy of measurements within the same feature. For pins, the magnification used was around 250x. For the arrowhead base, the magnification used was around 130x. For ribs, grooves, gaps and arrowfoot the magnification used was 130x. The setup of the test artefact in the ESEM can be seen in Figure 3.7.

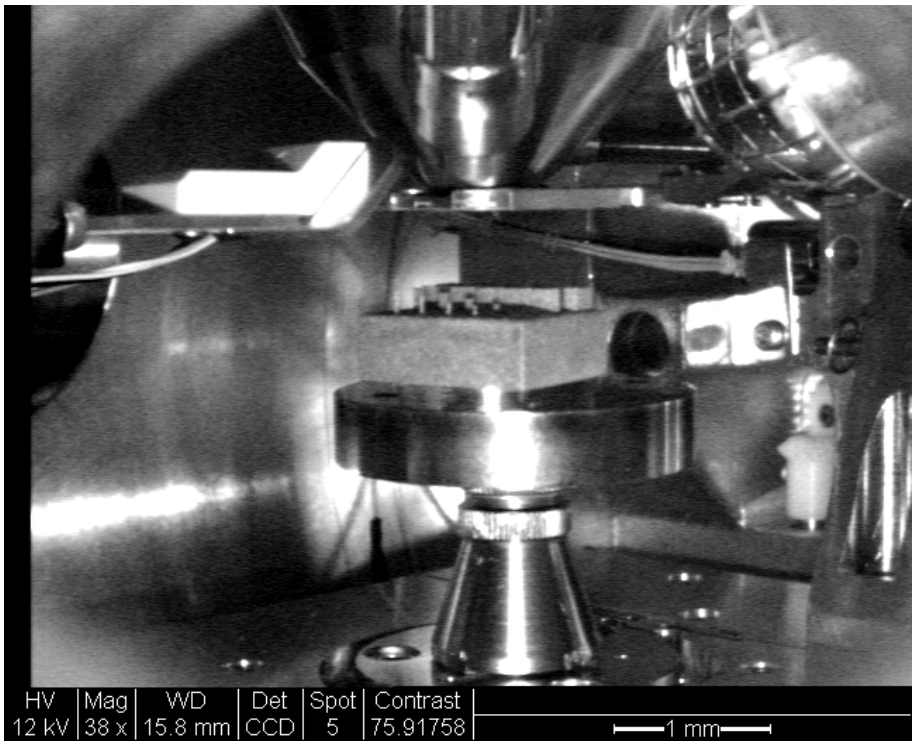

Figure 3.7: Setup of the artefact inside of the ESEM.

For measurements, Tracker software was used and all the images were calibrated to the ESEM scale. In all the feature measurements half molten particles are not included. Since the printed parts are expected to deviate from the CAD model, a measurement strategy had to be standardized for all the features so that inaccuracy is mitigated. The measurement strategy for each feature is different. They are formulated in the best way to get the best possible measurements for the features. The strategies to measure these features are summarized below.

- **Pins**
  The measurement starts by placing four points in a cross-like shape on the edges of the pin. The software will then approximate the best fitting circle based on the points. If the pin has large distortions, more points need to be placed in order to create more accurate result. The radius of the circle is then calculated. The procedure for measurement can be seen in Figure 3.8.

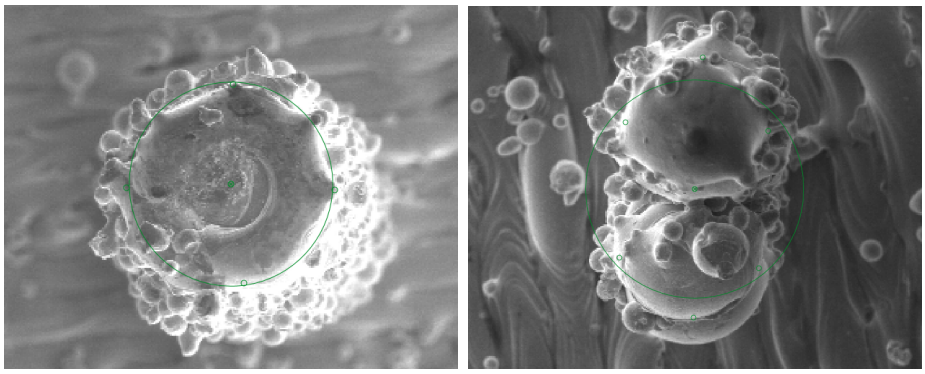

(a) Point placement for low-distortions.

(b) Point placement for high-distortions.

Figure 3.8: Measurement strategy for the pins.

- **Ribs**
  The ribs were measured by doing the measurement closer to the center of the rib where the print is continuous. The measurement is defined by two endpoints where each point should be approximately placed at each edge line at which the ribs start. The procedure for measurement can be seen in Figure 3.9.

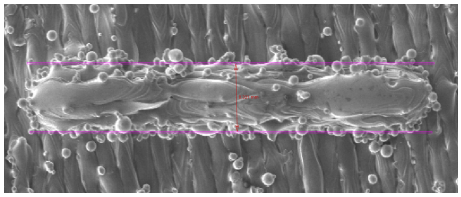

Figure 3.9: Measurement strategy for the ribs.

- **Arrowhead base**

  The arrowhead base was measured by taking the points on the baseline of the arrowhead where the curved edges end as shown in Figure 3.10.

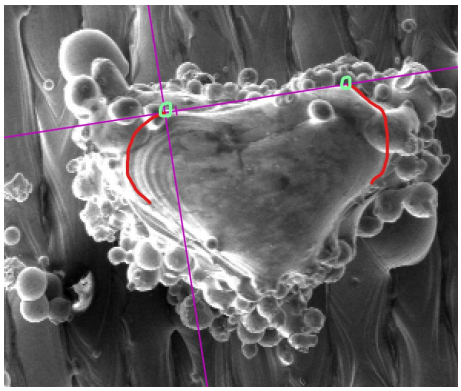

Figure 3.10: Measurement strategy for arrowhead base.

- **Grooves**
  The grooves were measured by taking a measurement at the center of the groove. The measurement is defined by two endpoints where each point should be approximately placed at each edge line at which the groove starts. The procedure for measurement can be seen in Figure 3.11.

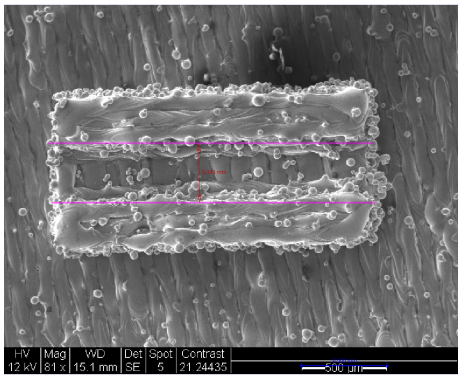

Figure 3.11: Measurement strategy for the grooves.

- **Arrowfoot**
  The arrowfoot was measured by taking the points as shown in Figure 3.12 below. The blue circles represent the edges of the fillets where the line joins these from which the distance is measured to the wall.

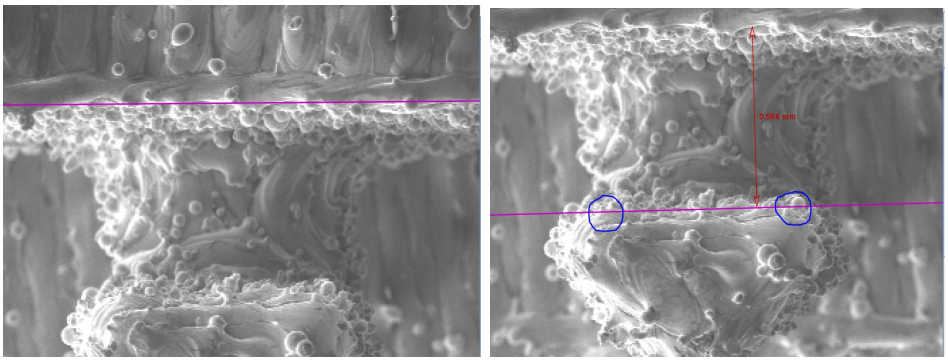

(a) First point. **(b)** Second point.

Figure 3.12: Measurement strategy for arrowfoot.

- **Area shape analysis**

  ImageJ software is used to get the shape of the arrow, which will give an approximate understanding of the shape deviation with respect to different recoater directions. In order to do so, first, the image is calibrated and then only the arrow shape is selected. The next step "Find Edges" option is used to get edges focused and sharpened. If the edges are still not clearly visible, then the "sharpen" option is used. In the next step, only the arrow shape is selected using the "Clear outside" option. Then Auto threshold is then used to get the approximate shape. Since the shape is not perfect, the binary option "fill hole" is applied to fill the gaps. If the shape is yet not completed, the binary option "dilate" is used to expand the pixel which closes the outer boundary of the shape. Now the "fill hole" option is applied again to fill the gaps. These steps are repeated until the shape is filled entirely. Now binary option "erode" is used to bring back the shape to its original size at the end. Erode option is hence used the same number of times as dilate, i.e. using erode two times in the end when applying dilate two times. Since there are many contribution to noises in the shape like the particles attached to the arrow, such noise is reduced by using the "remove outliers" option with a 20-25%. The remaining noise is mostly removed by using the "subtract" option. Finally, the shape is selected and then measured for the area. This is then compared with the original CAD model area to find the deviation using Excel.

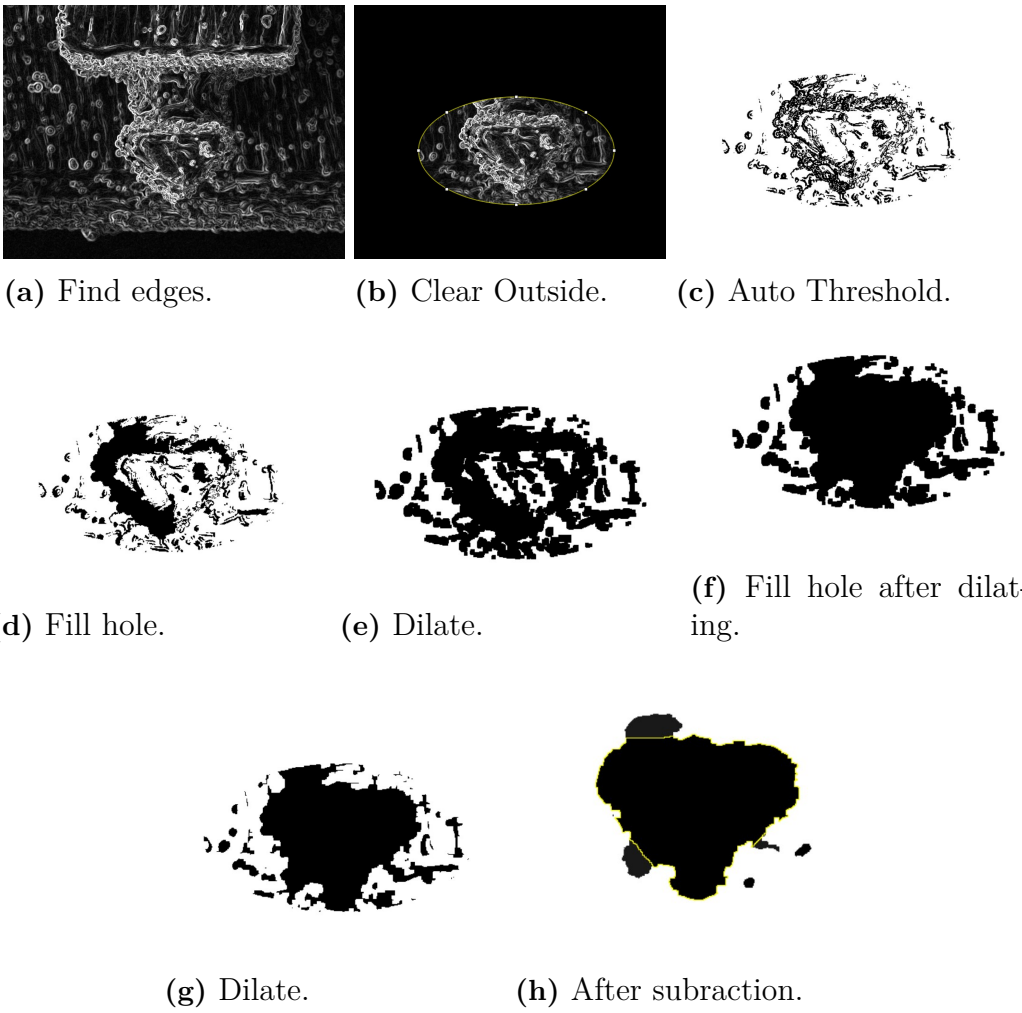

(a) Find edges. **(b)** Clear Outside. **(c)** Auto Threshold.

(d) Fill hole. **(e)** Dilate. **(f)** Fill hole after dilating.

(g) Dilate. **(h)** After subraction.

Figure 3.13: Measurement strategy for arrow shape deviation.

3.2.3 Measurement using stereo optical microscopy (SOM)

The stereo optical microscopy (SOM) used for geometrical analysis was ZEISS Discovery V20. This was done to measure gaps, angles and arrowhead heights. In order to measure using SOM, the Axio Vision software was applied. The area that needs to be measured was focused and magnified to get better accuracy. For most of the measurements, the partially attached metal particles were include in the measurements because of the lower magnification of SOM. Moreover, the angles of the arrowroot and arrowhead height in the artefact are easier to measure using SOM with the ESEM even though the measurement accuracy is higher in the latter case ESEM.

- **Gaps**
  The gaps were measured by taking the measurement between the two walls created by the gap. The procedure for measurement can be seen in Figure 3.14.

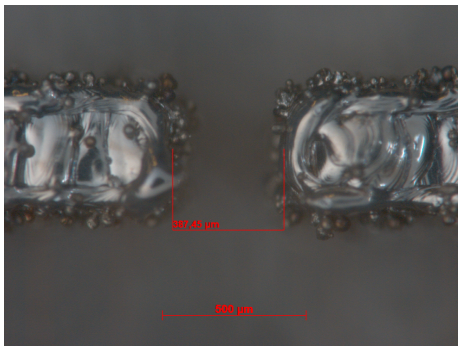

Figure 3.14: Measurement strategy for the gaps.

- **Angles**
  In order to measure the angles in the artefact and the arrowfoot angles, the points were taken at the joint between arrowfoot and the wall, at the endpoint of the arrowfoot, and at the endpoint of the wall. The procedure for measurement can be seen in Figure 3.15.

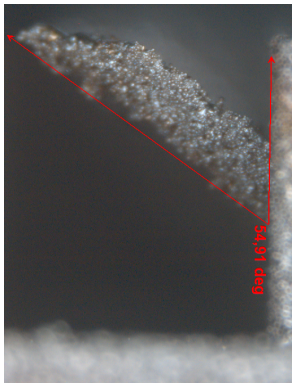

Figure 3.15: Measurement strategy for the angle.

- **Arrowhead height**
  In order to measure the arrowhead height, the measurement was done from endpoint of the arrowhead top to the line where the half molten particles are becoming straight from an angled manner.

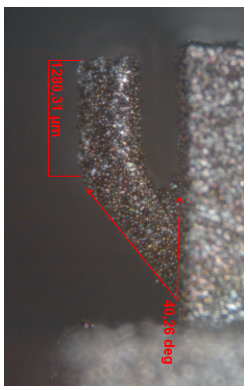

Figure 3.16: Measurement strategy for arrowhead height.

3.2.4 Deviation analysis

Once all the measurements are done for all the test artefacts of different prints, deviation from the nominal CAD model dimensions are calculated. The measurements calculated are subtracted from the nominal CAD dimensions. These deviations are plotted versus print identification using MATLAB software through which interpretations are done.

3.3 Gap waveguide model

A model of the gap waveguide was created with the reverse engineered arrow and the critical dimensions provided by Ericsson to check for repeatability in frequency for the prints printed with gas flow settings. The model was created in CATIA V5 and can be seen in Figure 3.17 below.

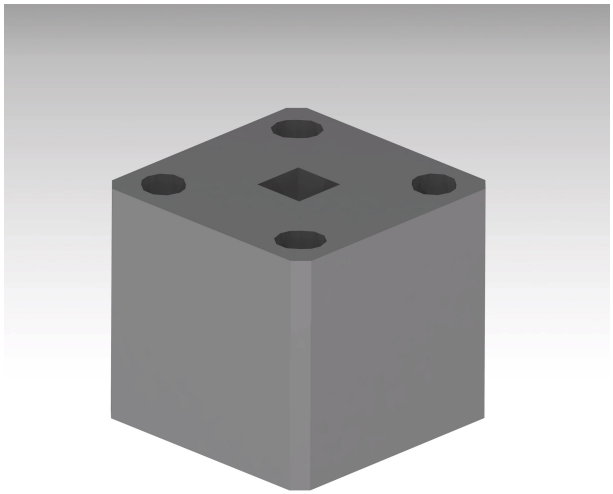

Figure 3.17: 3D model of gap waveguide

3.3.1 Print preparation

The waveguide parts were prepared in the EOS M100 printer to provide test samples for studying the potential correlation between electrical properties and gas flow. The waveguides were printed in the configurations on the build plate as seen in Figure 3.18 with 50%, 58% and 65% gas flow and standard process parameter settings for 20 μm layer thickness. A waveguide cut across the diagonal was added to the prints to enable microscope measurements or 3D-scanning. In total five prints were done, where the process parameters used can be seen in Table 3.4.

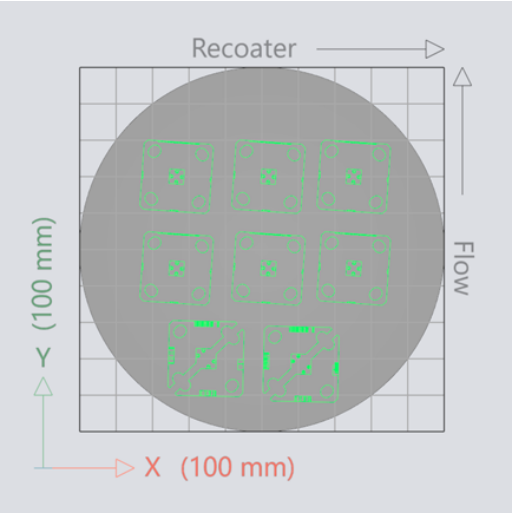

(a) 50% GF configuration.

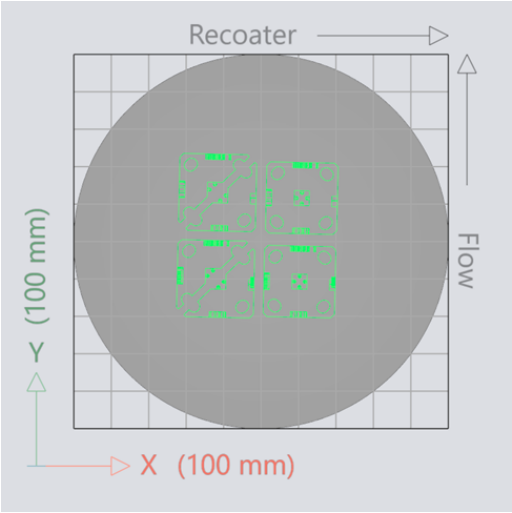

(b) 58% and 65% GF configuration.

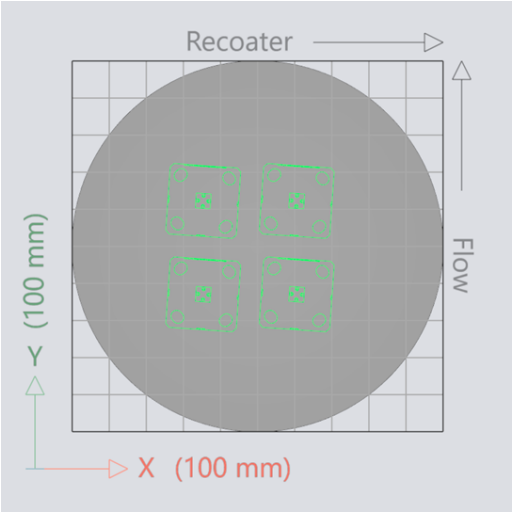

(c) 58% and 65% GF configuration.

Figure 3.18: Build orientation showcasing the configurations, recoating direction and gas-flow direction for the gap waveguides for 50%, 58% and 65% gas-flow.

Table 3.4: Process parameter settings used for the gap waveguide prints.

Print	Machine	Parameters
1	EOS M100	Standard with 50% gas flow
2	EOS M100	Standard with 58% gas flow
3	EOS M100	Standard with 65% gas flow
4	EOS M100	Standard with 58% gas flow
5	EOS M100	Standard with 65% gas flow

3.3.2 Electrical evaluation

The electrical evaluation was done by Lars Manholm and Oscar Talcoth at Ericsson. The measurement equipment used was a VNA R&S ZVA67 vector network analyser

with 1.85mm coax connectors, where the coax cables were attached to the waveguide transitions. The equipment and waveguide setup can be seen in Figure 3.19.

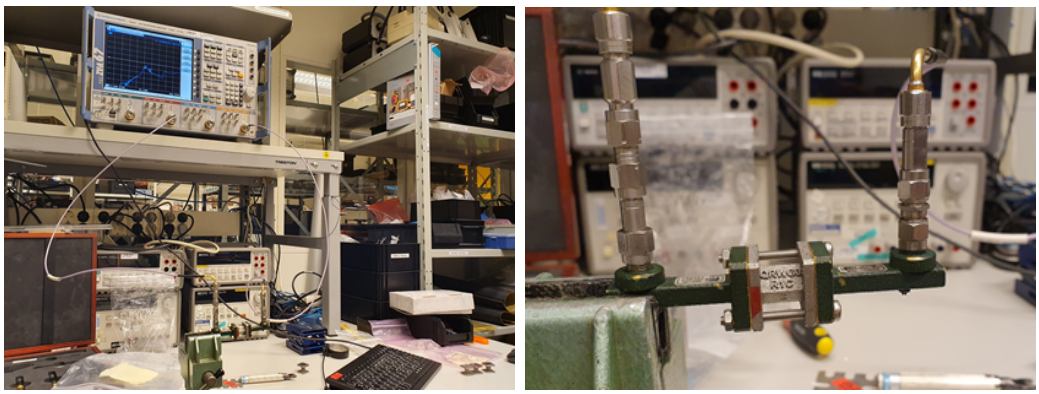

(a) Equipment setup. **(b)** Waveguide setup.

Figure 3.19: Measuring equipment and waveguide setup for the electrical evaluation.

4

Results

First, a comparison between the ESEM and the SOM measurements is done by evaluating their accuracy in measurements for the features. After this comparison, an analysis based on measurements for identifying the deviation and accuracy of the features is done for the respective process settings, followed by explaining the defects found during the analysis in each print. Finally, the analysis of repeatability is performed to evaluate the accuracy of the results. A closer view of each orientations and artefacts for the prints can be seen in Appendix A.

4.1 Comparison between ESEM and SOM measurements

In order to evaluate which measurement method is best for micron-level accuracy and precision a comparison between the ESEM and the SOM measurements was done for print 1 as seen in C.1. Printing was then done in the EOS M290 printer with standard process parameters for 40 μm layer thickness. Both measurement methods had advantages and disadvantages with respect to some feature measurements. The ESEM measurements were good and precise when compared to SOM measurements for top views for all the features but they had the disadvantage of depicting the vertical measures for all the features. On the other hand, SOM is user friendly and can provide measurements for both top view and side view, but has lower magnification than the ESEM, which reduces the precision level of the measurements. The angles and the arrowhead measurements were not easy to record in ESEM, hence SOM was used for measuring these features by compromising on the accuracy and precision of the results. Figure 4.1 below shows the measurements taken with ESEM and measurements are taken in SOM for print 1. The analysis shows that the ESEM measurements are more accurate than the SOM measurements. Therefore, the further analysis and measurements for all the features except the angles, arrowfoot angles, and arrowhead heights were taken in ESEM.

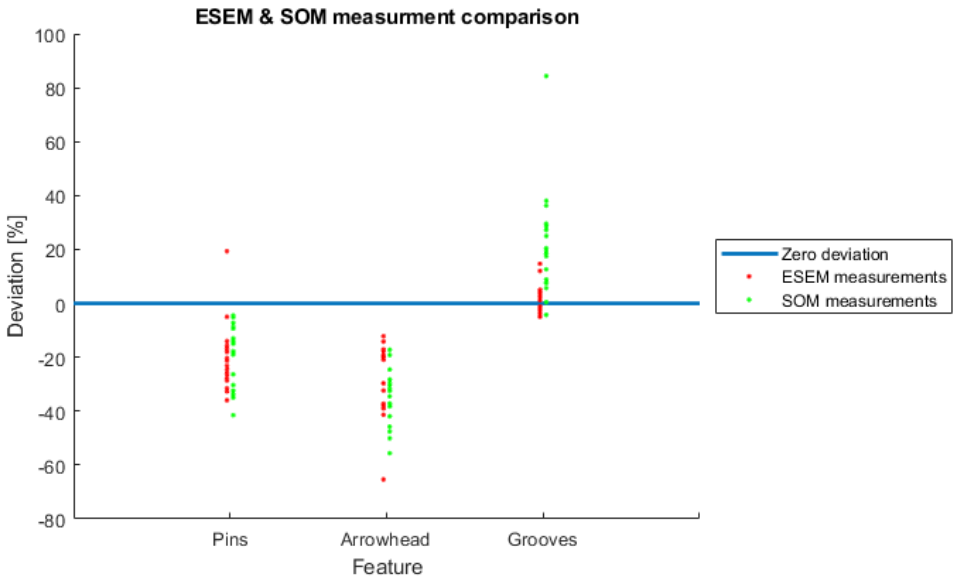

Figure 4.1: Comparison between ESEM and SOM measurements.

4.2 Deviation analysis of test artefact features

In order to analyze each feature, each feature size is measured and analyzed for deviation, accuracy in the prints, repeatability, analyzed for defect and shape of the feature. The analysis was carried out using ESEM and SOM. Finally electrical evaluation for the gap waveguide using the print 4 and print 5 settings is analyzed.

4.2.1 Deviation analysis of pins

Based on the measurements done on the pins using ESEM, the deviation measures are calculated. A negative deviation and a positive deviation indicate the oval shape in the pins. A detailed analysis using ESEM for the pins printed in different settings, its measurements, and deviation values can be seen in B.1.

Based on the deviation table from different prints, each pin size is analyzed individually below for getting detailed results on the variation in process parameters.

- **Deviation of pins with 0.10 mm radius**

  The deviation measure for all pins with a radius of 0.10 mm was plotted in MATLAB over each orientation, which can be seen in Figure 4.2 below. From the figure, it can be concluded that that the lowest deviation is observed for orientation 2 in print 4 whereas the highest deviation is observed for orientation 3 in print 6. In most of the prints there exists a pattern where orientation 3 has the highest deviation.

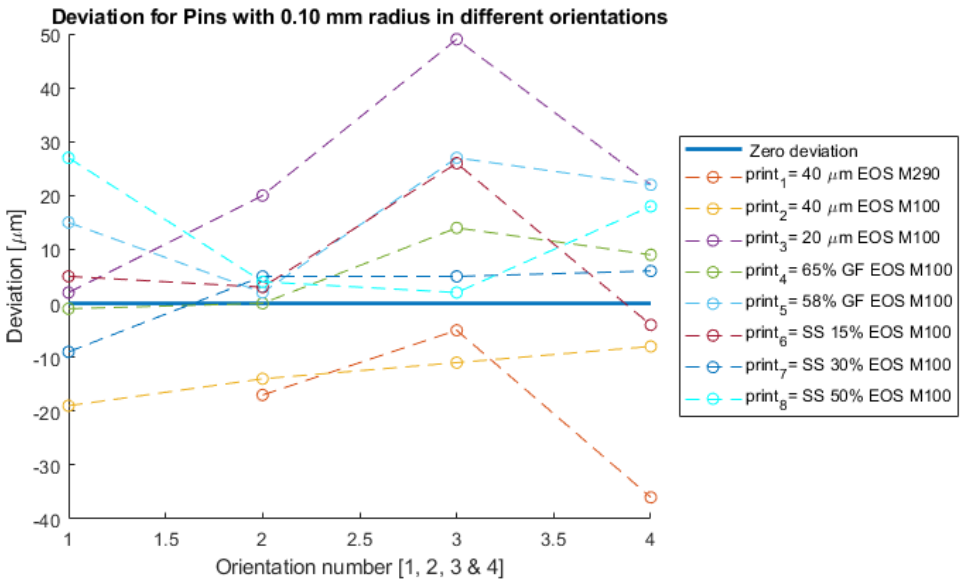

Figure 4.2: Deviation plot for pins with 0.10 mm radius in different orientations.

- **Deviation of pins with 0.15 mm radius**

  The deviation measure for all pins with a radius of 0.15 mm was plotted in MATLAB over each orientation, which can be seen in Figure 4.3 below. From the figure, it can be concluded that that the lowest deviation is observed for orientation 1 in print 4 whereas the highest is observed for orientation 2 and 3 in print 1. The deviation for all the orientations is consistent and lowest in print 6. There exists a pattern here where the deviation in all the orientations is similar.

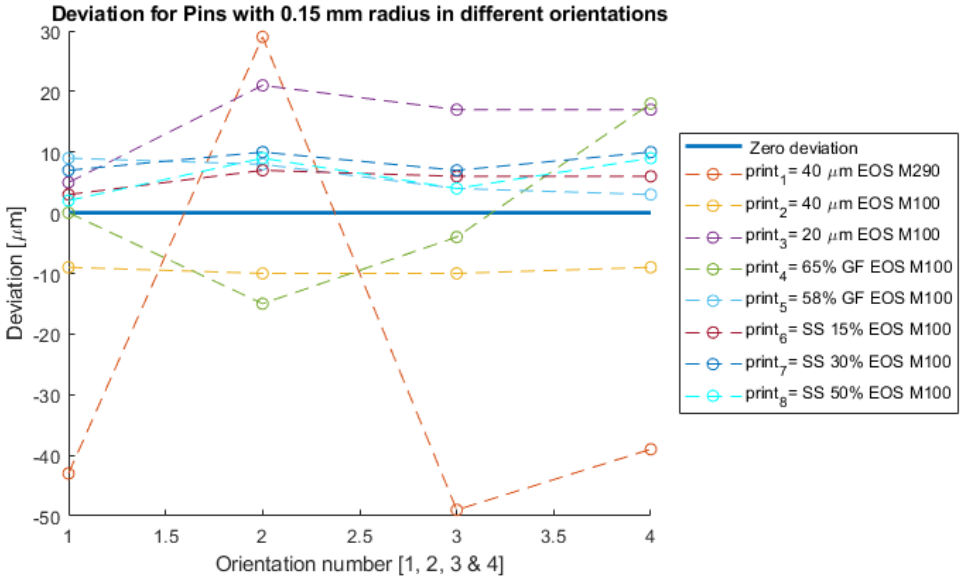

Figure 4.3: Deviation plot for pins with 0.15 mm radius in different orientations.

- **Deviation of pins with 0.20 mm radius**

  The deviation measure for all pins with a radius of 0.20 mm was plotted in MATLAB over each orientation, which can be seen in Figure 4.4 below. It can be seen that the lowest deviation is for orientation 3 in print 4 whereas the highest is for orientation 1 in print 1. The deviation for all the orientations is consistent and lowest in print 6. The highest deviation is in print 1. There exists a pattern here where the deviation in all the orientations is similar.

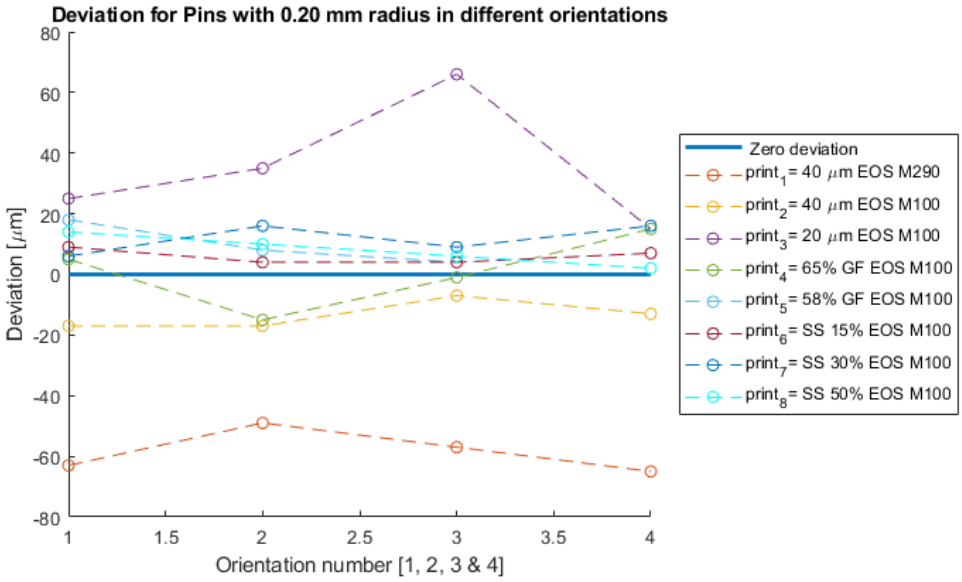

Figure 4.4: Deviation plot for pins with 0.20 mm radius in different orientations.

- **Deviation of pins with 0.25 mm radius**

  The deviation measure for all pins with a radius of 0.25 mm was plotted in MATLAB over each orientation, which can be seen in Figure 4.5 below. It can be seen that the lowest deviation is for orientation 1 in print 4 whereas the highest is for orientation 2 in print 1. The deviation for all the orientations is consistent and lowest in print 6. The highest deviation is in print 1. There exists a pattern here where the deviation in all the orientations is similar.

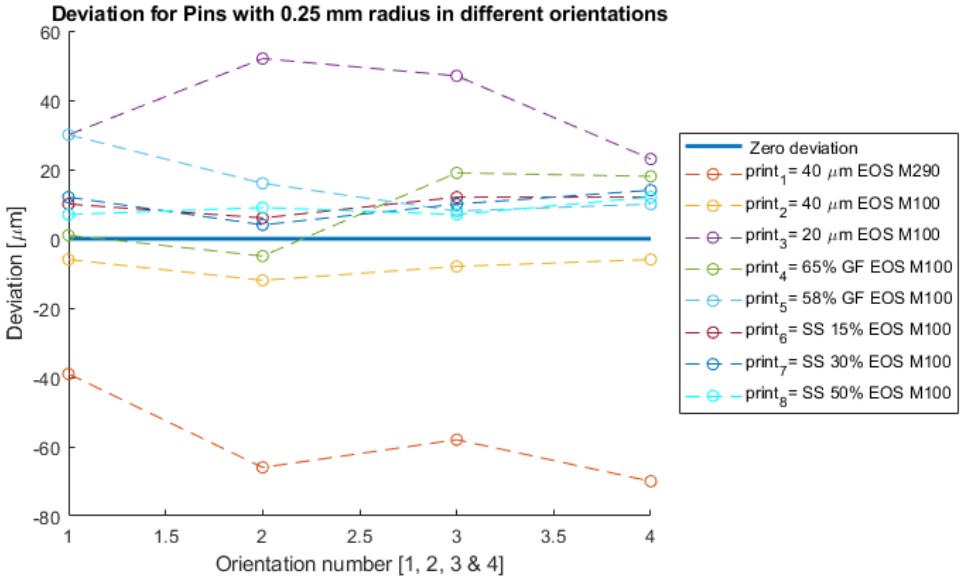

Figure 4.5: Deviation plot for pins with 0.25 mm radius in different orientations.

- **Deviation of pins with 0.30 mm radius**

  The deviation measure for all pins with a radius of 0.30 mm was plotted in MATLAB over each orientation, which can be seen in Figure 4.6 below. From the figure, it can be concluded that that the lowest deviation is observed for orientation 2 in print 4 whereas the highest is observed for orientation 2 in print 1. The deviation for all the orientations is consistent and lowest in print 4. The highest deviation is in print 1. There exists a pattern here where the deviation in all the orientations is similar in all the prints.

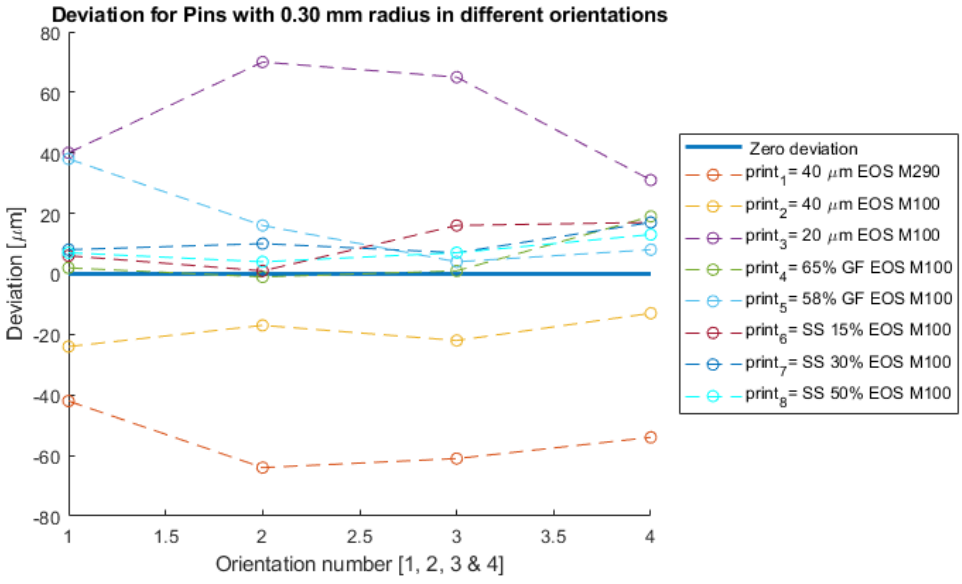

Figure 4.6: Deviation plot for pins with 0.30 mm radius in different orientations.

4.2.2 Deviation analysis of ribs

Based on the measurements done on the ribs using ESEM, the deviation measures are calculated. A negative deviation and a positive deviation indicate the oval shape in the ribs. A detailed analysis using ESEM for the ribs printed in different settings, its measurements, and deviation values can be seen in B.2.

Based on the deviation table from different prints, each rib size is analyzed individually below for getting detailed results on the variation in process parameters.

- **Deviation of ribs with 0.20 mm diameter**

  The deviation measures for all ribs with a diameter of 0.20 mm were plotted in MATLAB over each orientation, which can be seen in Figure 4.7. The lowest deviation value is found for orientations 2 and 4 and the highest is for orientations 1 and 3 in all the prints. The lowest deviation is in print 4.

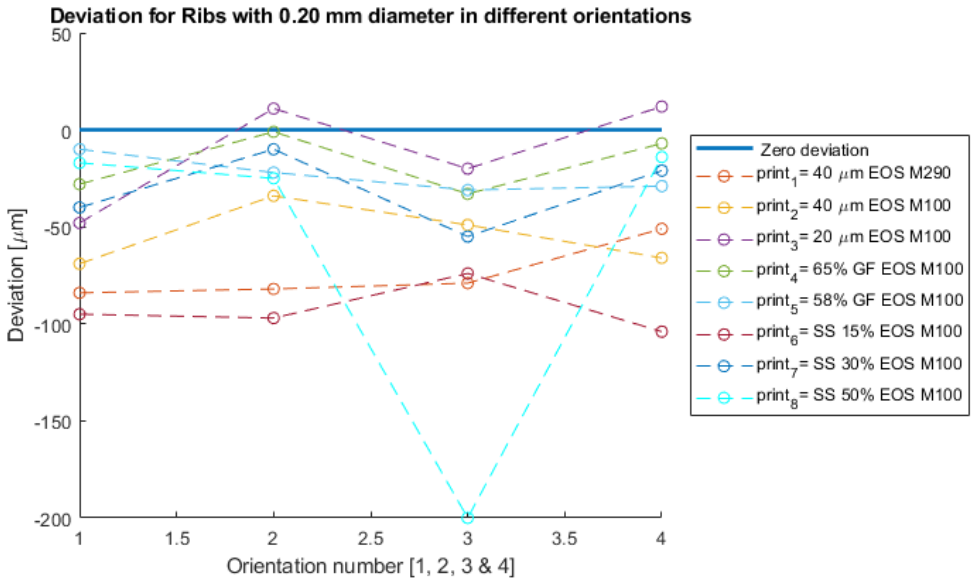

Figure 4.7: Deviation plots for ribs with 0.20 mm diameter in different orientations.

- **Deviation of ribs with 0.30 mm diameter**

  The deviation values for all the ribs with a diameter of 0.30 mm were plotted in MATLAB over each orientation, which can be seen in Figure 4.8. The lowest deviation value is found in orientations 2 and 4 and the highest is found for orientations 1 and 3 in all the prints. The lowest deviation is in print 4.

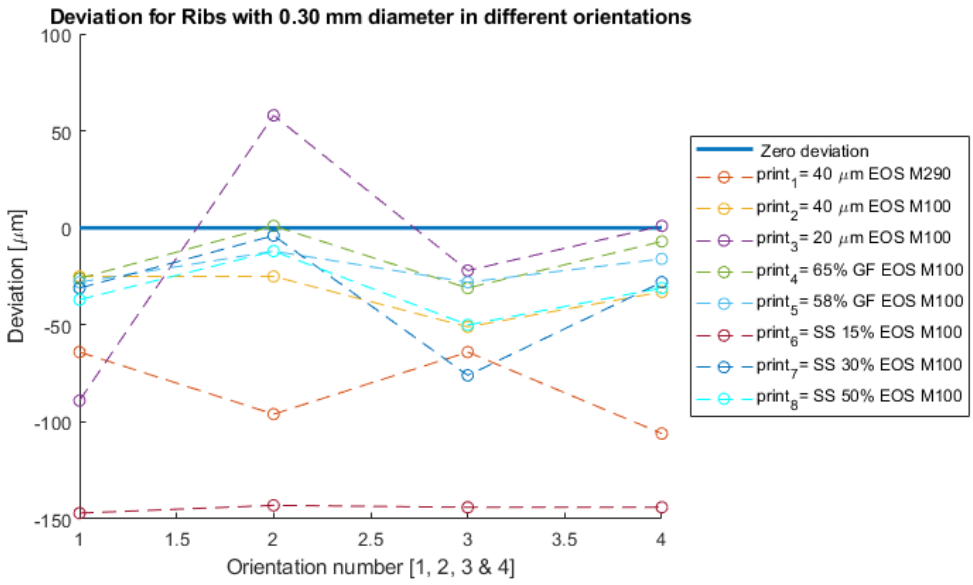

Figure 4.8: Deviation plots for ribs with 0.30 mm diameter in different orientations.

- **Deviation of ribs with 0.40 mm diameter**

  The deviation measure for all ribs with a diameter of 0.40 mm was plotted in MATLAB over each orientation, which can be seen in Figure 4.9. It can be seen that as amount of gas flow has decreased the effect of recoater direction is less and the deviation is the same for all the orientations. The lowest deviation is observed for orientation 2 of print 4

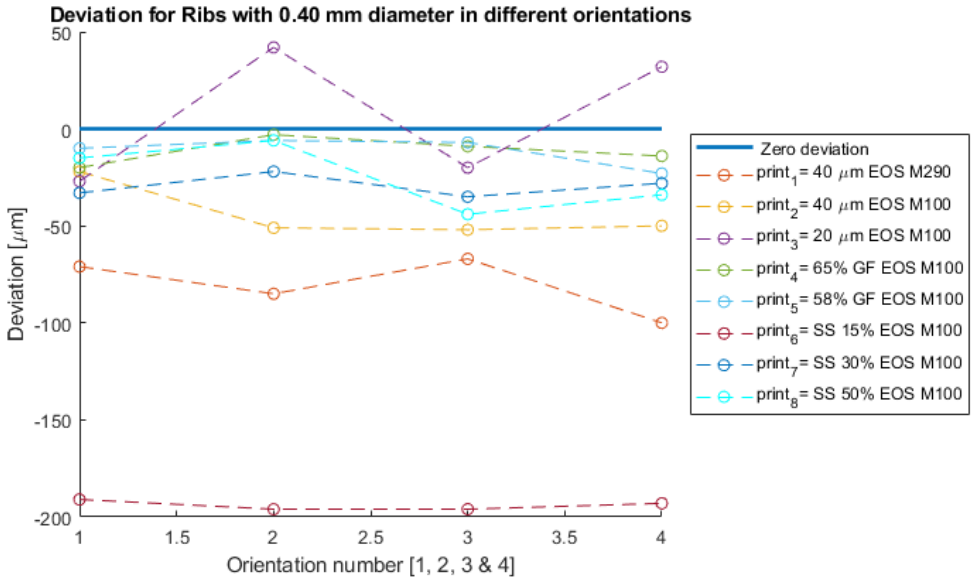

Figure 4.9: Deviation plots for ribs with 0.40 mm diameter in different orientations.

- **Deviation of ribs with 0.50 mm diameter**

  The deviation measure for all ribs with a diameter of 0.50 mm was plotted in MATLAB over each orientation, which can be seen in Figure 4.10. It can be seen that as the amount of gas flow has decreased the effect of recoater direction is less and the deviation is the same for all the orientations. The lowest deviation is observed for orientation 2 of print 4.

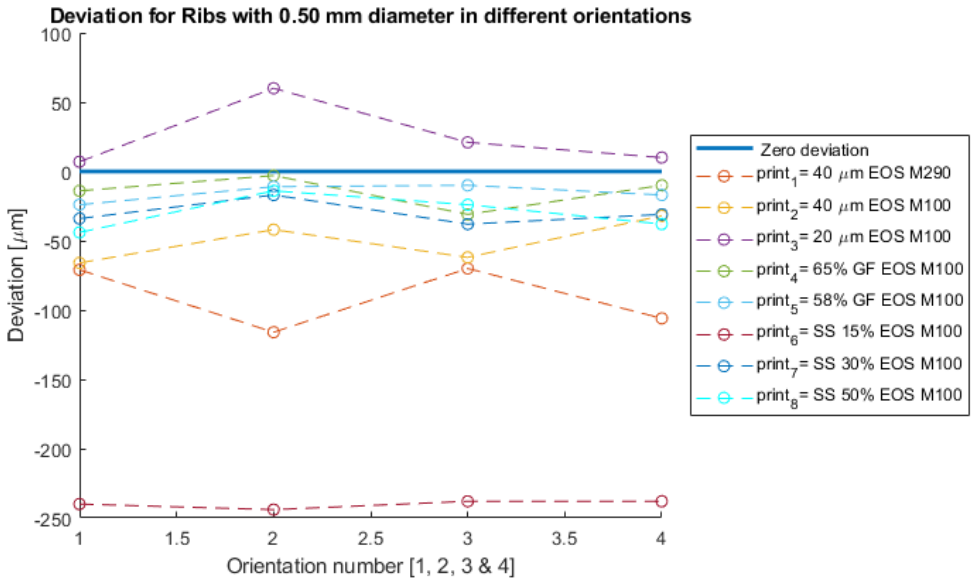

Figure 4.10: Deviation plots for ribs with 0.50 mm diameter in different orientations.

- **Deviation of ribs with 0.60 mm diameter**

  The deviation value for all ribs with a diameter of 0.60 mm was plotted in MATLAB over each orientation, which can be seen in Figure 4.11. It can be seen that as the amount of gas flow has decreased the effect of recoater direction is less and the deviation is the same in all orientations. The lowest deviation is observed for orientation 2 of print 4.

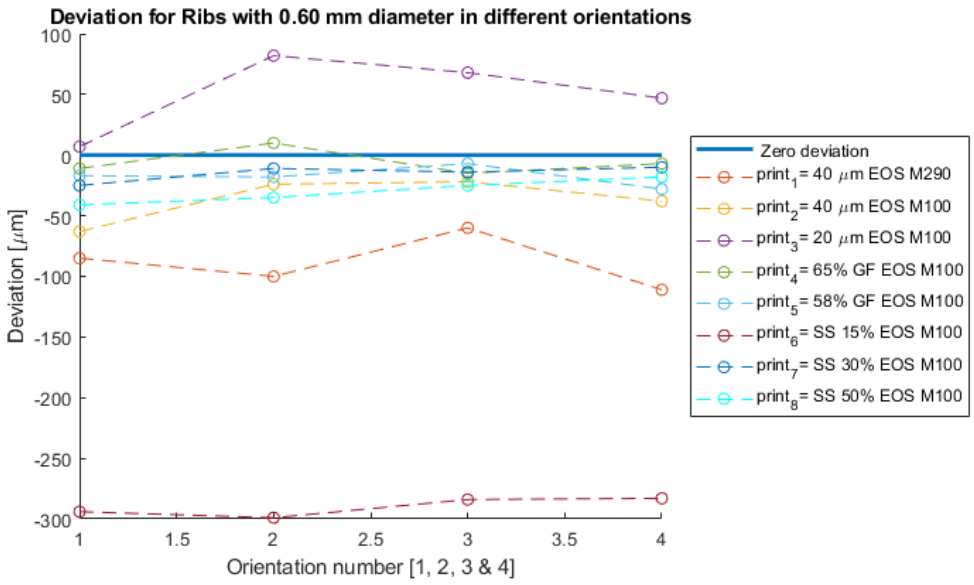

Figure 4.11: Deviation plots for ribs with 0.60 mm diameter in different orientations.

4.2.3 Deviation analysis of arrowhead base

Based on the measurements done on the arrowhead base using ESEM, the deviation values are determined. The negative deviation indicates that the base has curved edges in the corner and the positive deviation indicates that the base has half molten particles attached. A detailed analysis using ESEM for the arrowhead base printed in different settings, its measurements and deviation values can be seen in B.3.

Based on the deviation table from different prints, each arrowhead base size is analyzed individually below for getting detailed results on the variation in process parameters.

- **Deviation of arrowhead with 0.849 mm base**

  The deviation values for all the arrowheads with a base of 0.849 mm were plotted in MATLAB over each orientation, which can be seen in Figure 4.12. The deviation among the different orientations is the same. The lowest deviation can be found for all the orientations in print 5.

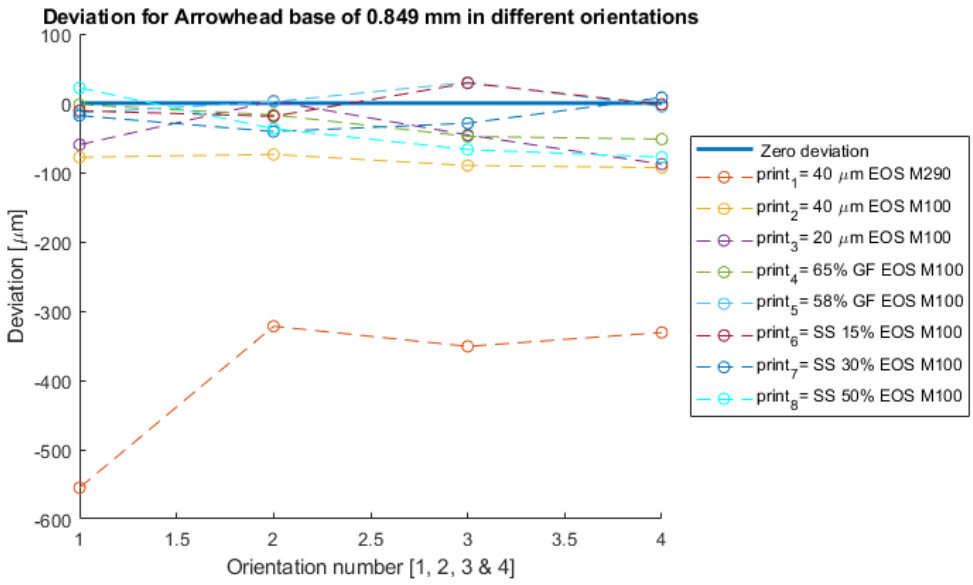

Figure 4.12: Deviation plots for arrowhead with 0.849 mm base in different orientations.

- **Deviation of arrowhead with 1.131 mm base**

  The deviation measure for all arrowheads with a base of 1.131 mm was plotted in MATLAB over each orientation, which can be seen in Figure 4.13. The deviation among the different orientations is the same. The lowest deviation can be found for all the orientations in print 5.

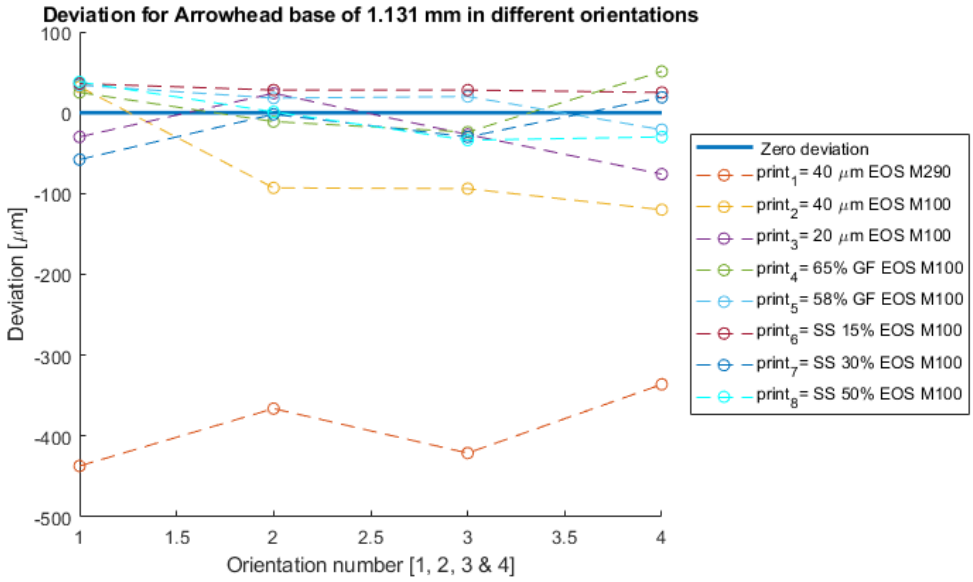

Figure 4.13: Deviation plots for arrowhead with 1.131 mm base in different orientations.

- **Deviation of arrowhead with 1.414 mm base**

  The deviation value for all arrowheads with a base of 1.414 mm was plotted in MATLAB over each orientation, which can be seen in Figure 4.14. The lowest deviation can be found in different orientations in different prints. Therefore the lowest deviation among the different orientations is considered the best outcome. Here the print 5, shows most consistent deviation among the orientations.

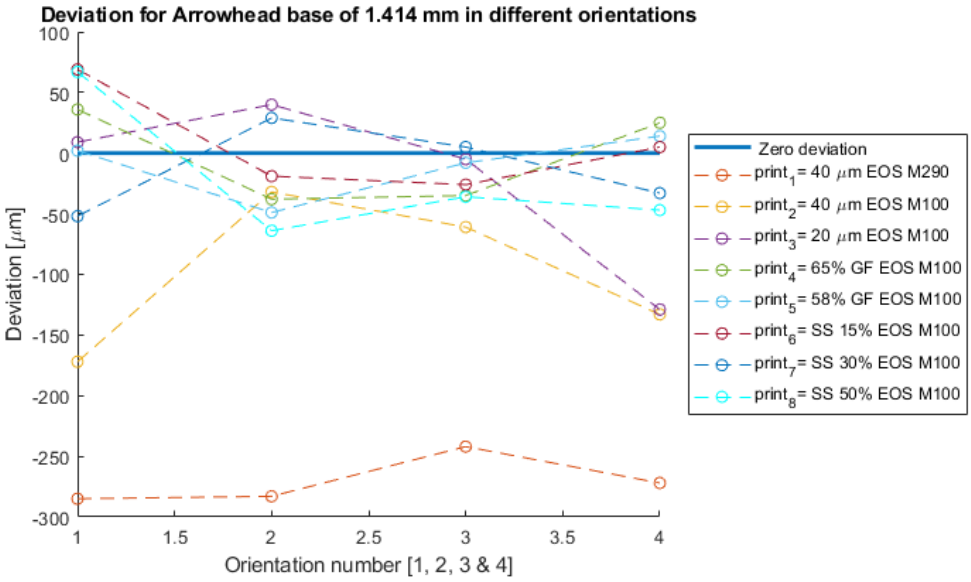

Figure 4.14: Deviation plots for arrowhead with 1.414 mm base in different orientations.

- **Deviation of arrowhead with 1.697 mm base**

  The deviation data for all arrowheads with a base of 1.697 mm was plotted in MATLAB over each orientation, which can be seen in Figure 4.15. The deviation among the different orientations is almost the same in all the prints. The lowest deviation can be seen in print 5.

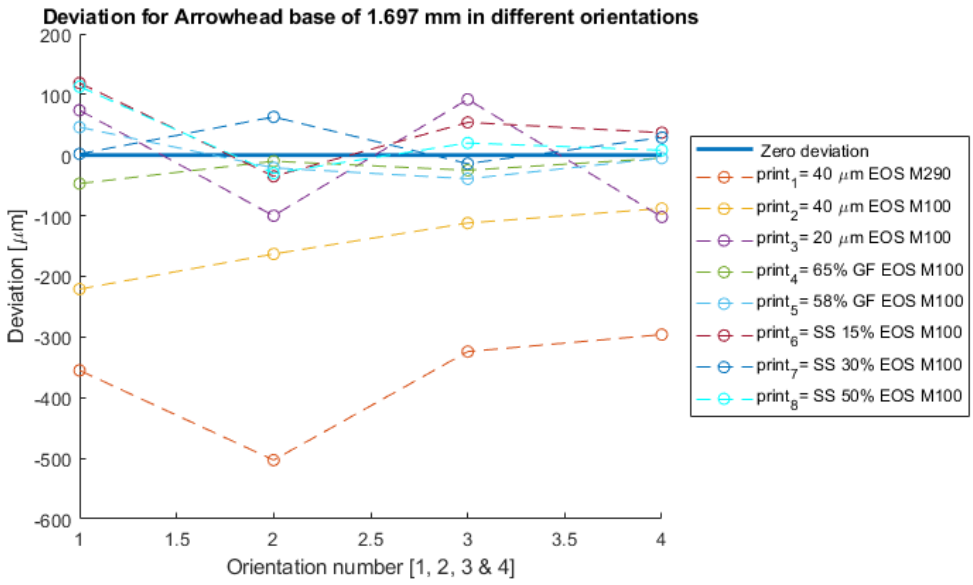

Figure 4.15: Deviation plots for arrowhead with 1.697 mm base in different orientations.

- **Deviation of arrowhead with 1.980 mm base**

  The deviation values for all arrowheads with a base of 1.980 mm were plotted in MATLAB over each orientation, which can be seen in Figure 4.16. The deviation among the different orientations are almost same for the 20μm layer thickness prints and the lowest deviation be seen in print 5.

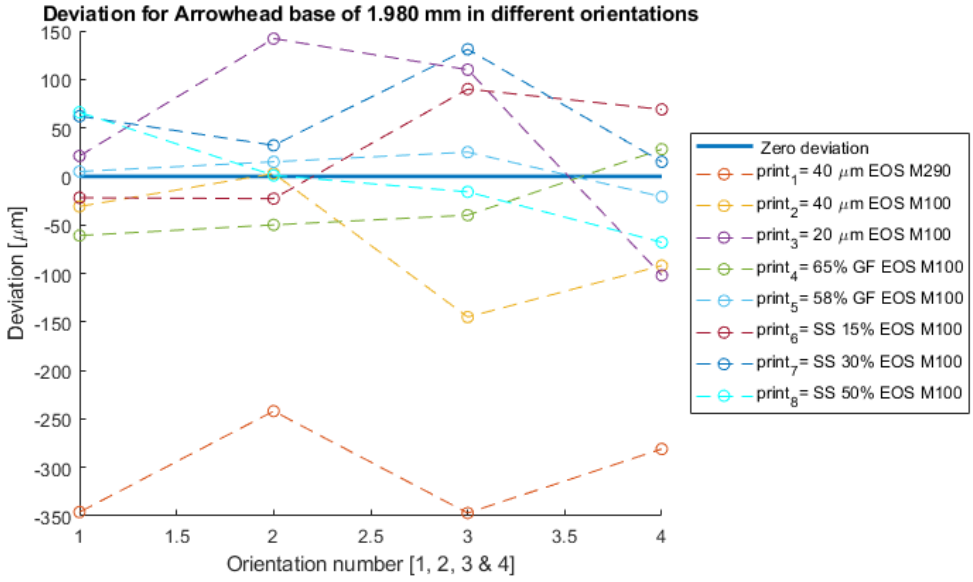

Figure 4.16: Deviation plots for arrowhead with 1.980 mm base in different orientations.

4.2.4 Deviation analysis of grooves

Based on the measurements done on the grooves using ESEM, the deviation values are determined. The negative deviation indicates that the base has curved edges in the corner and the positive deviation indicates that the base has half molten particles attached. A detailed analysis using ESEM for the arrowhead base printed in different settings, its measurements, and deviation values can be found in B.4.

Based on the deviation table from different prints, each groove size is analyzed individually below for getting detailed results on the variation in process parameters.

- **Deviation of grooves with 0.30 mm diameter**

  The deviation value for all grooves with a diameter of 0.30 mm was plotted in MATLAB over each orientation, which can be seen in Figure 4.17. The deviation in orientation 1 and orientation 3 and the deviation in orientation 2 and orientation 4 are the same in print 4 and print 3. In the print 5, print 6, print 7, and print 8 the deviation among the orientations are almost the same. The lowest deviation is for orientation 2 in print 3.

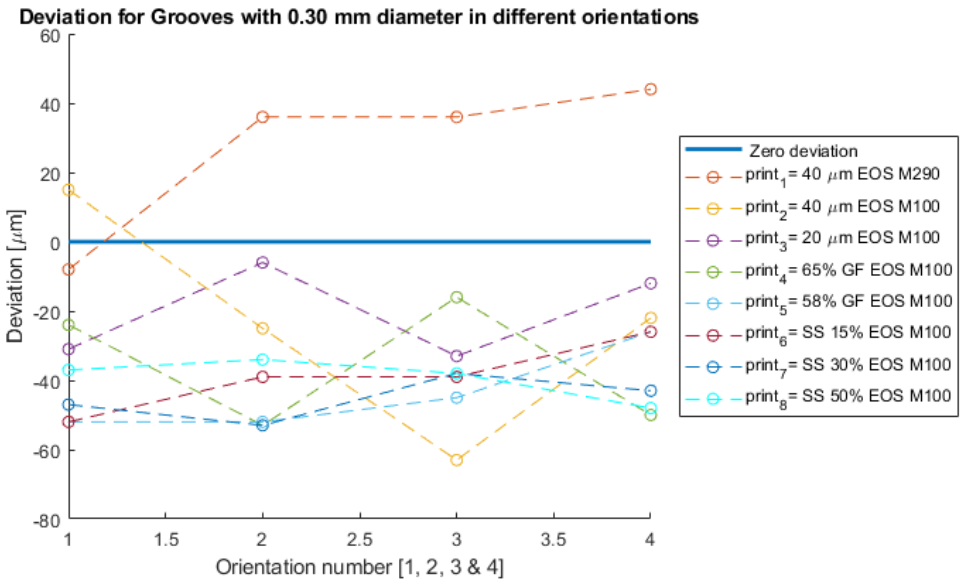

Figure 4.17: Deviation plots for grooves with 0.30 mm diameter in different orientations.

- **Deviation of grooves with 0.40 mm diameter**

  The deviation value for all grooves with a diameter of 0.40 mm was plotted in MATLAB over each orientation, which can be seen in Figure 4.18. The deviation varies a lot for each orientation in each print. However, the lowest deviation is found for orientation 4 in print 3.

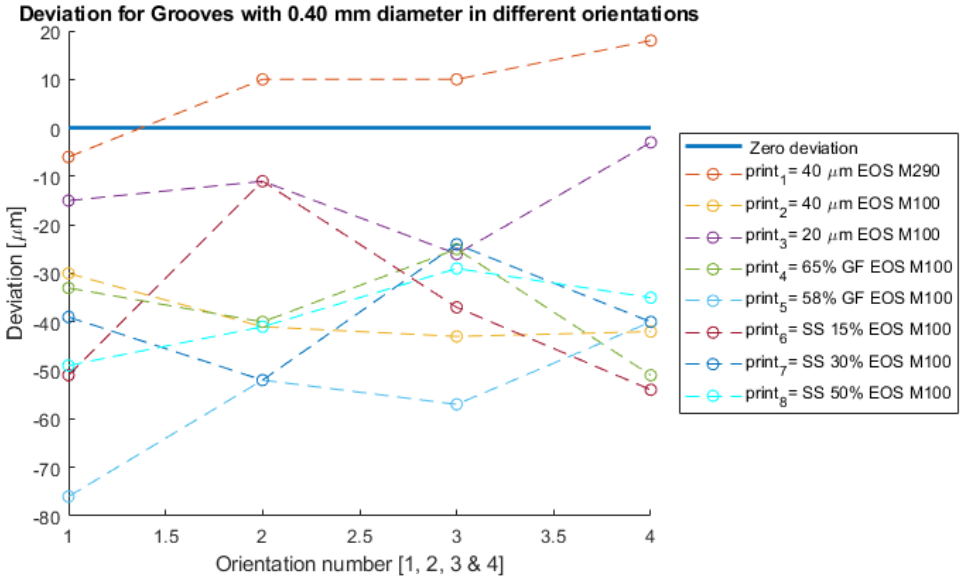

Figure 4.18: Deviation plots for grooves with 0.40 mm diameter in different orientations.

- **Deviation of grooves with 0.50 mm diameter**

  The deviation measure for all grooves with a diameter of 0.50 mm was plotted in MATLAB over each orientation, which can be seen in Figure 4.19. The patterns of orientations 1 and 3 having the same deviation and orientations 2 and 4 having the same deviation are found in some prints. The deviation varies a lot for each orientation. However, the lowest deviation is found for orientation 1 in print 3.

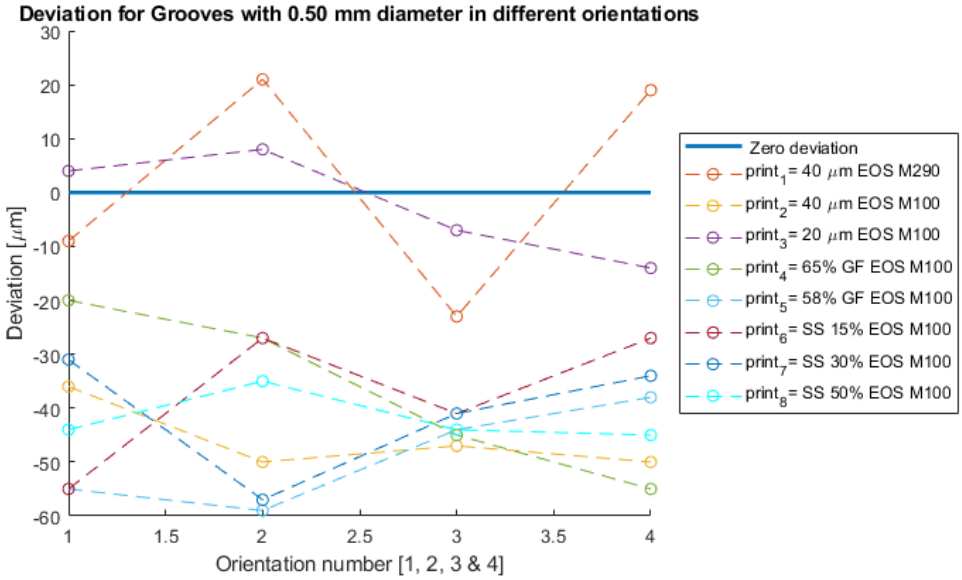

Figure 4.19: Deviation plots for grooves with 0.50 mm diameter in different orientations.

- **Deviation of grooves with 0.60 mm diameter**

  The deviation value for all grooves with a diameter of 0.60 mm was plotted in MATLAB over each orientation, which can be seen in Figure 4.20. The pattern of orientation 1 and orientation 3 having the same deviation and orientation 2 and orientation 4 having the same deviation is found in $40\mu m$ layer thickness prints. For $20\mu m$ layer thickness prints, the effect of orientation is reduced. The deviation varies a lot for each orientation. However, the lowest deviation is found for orientation 4 in print 3. The deviation among the different orientations is similar in print 3.

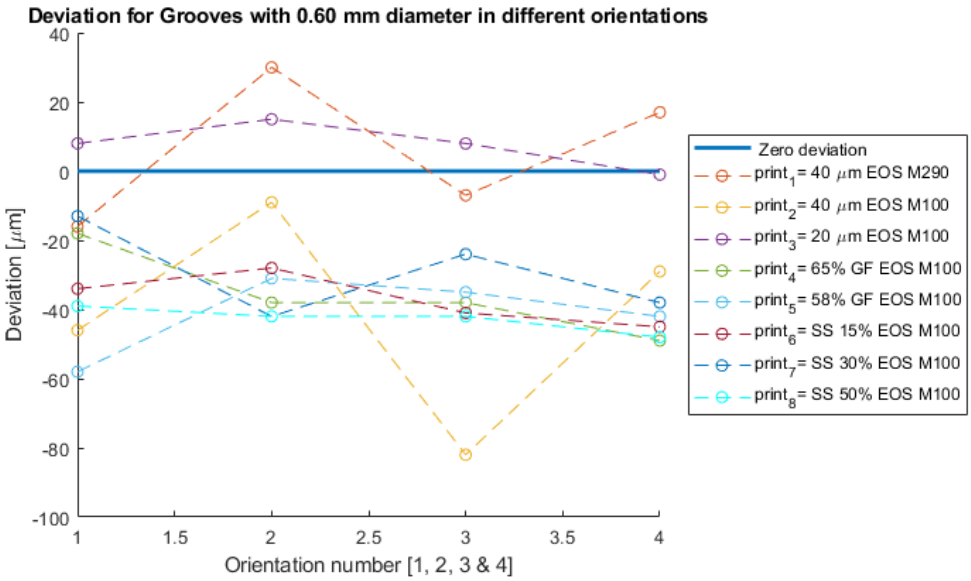

Figure 4.20: Deviation plots for grooves with 0.60 mm diameter in different orientations.

- **Deviation of grooves with 0.70 mm diameter**

  The deviation value for all grooves with a diameter of 0.70 mm was plotted in MATLAB over each orientation, which can be seen in Figure 4.21. The pattern of orientation 1 and orientation 3 having the same deviation and orientation 2 and orientation 4 having the same deviation is found for $40\mu m$ layer thickness prints. For $20\mu m$ layer thickness prints, the effect of orientation is reduced. The deviation varies a lot for each orientation. However the lowest deviation is found for orientation 4 in print 3. The deviation among the different orientations is similar in print 3.

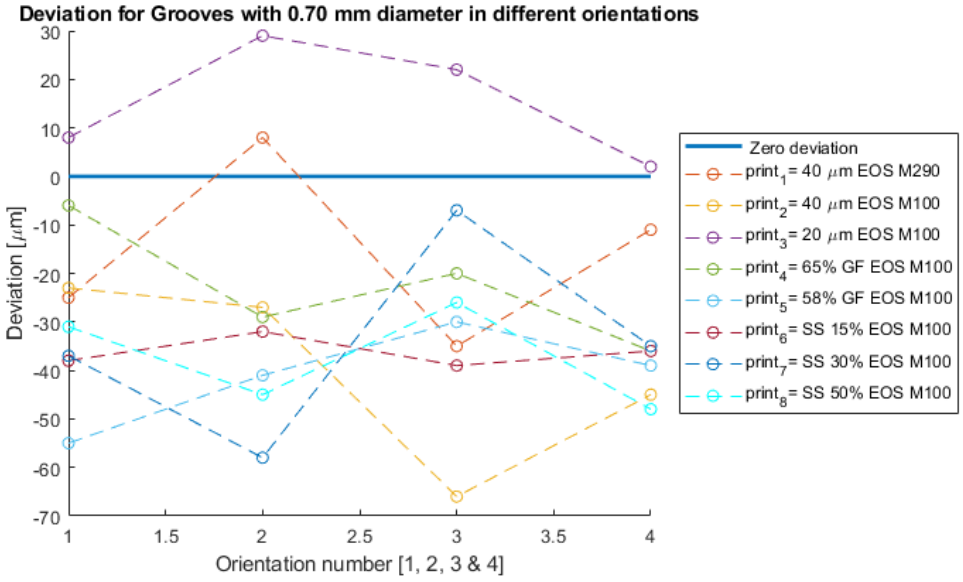

Figure 4.21: Deviation plots for grooves with 0.70 mm diameter in different orientations.

4.2.5 Deviation analysis of gaps

Based on the measurements done on the gaps using ESEM, the deviation values are determined. A negative deviation indicates that the gap distance is reduced because of too many half molten particles at the walls where the gaps are measured. The positive deviation indicates that the gap distance is increased because of the shrinkage or defects in the parts between which the gap is measured. A detailed analysis using ESEM for the gap in different settings, its measurements, and deviation values can be seen in C.2.

Based on the deviation table from different prints, each gap is analyzed individually below for getting detailed results on the variation in process parameters.

- **Deviation of 0.1 mm gap**

  The deviation for all 0.1 mm gaps was plotted in MATLAB over each orientation, which can be seen in Figure 4.22. From the figure can the lowest deviation be found in orientation 3 and the highest in orientation 4. The lowest deviation is observed in print 8 with 50% scan-speed and the highest is observed in print 1 with $40\mu m$ layer thickness.

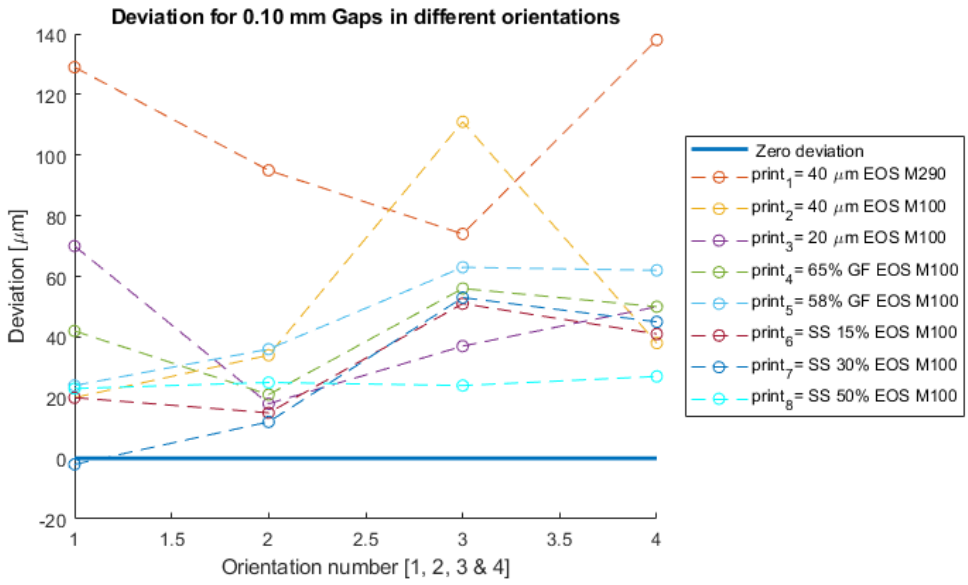

Figure 4.22: Deviation plots for 0.1 mm gaps in different orientations.

- **Deviation of 0.2 mm gap**

  The deviation value for all 0.2 mm gaps was plotted in MATLAB over each orientation, which can be seen in Figure 4.23. From the figure the lowest deviation can be found for orientation 2 and the highest for orientation 4. The lowest deviation is observed in print 3 with $20\mu m$ layer thickness and the highest is observed in print 1 with $40\mu m$ layer thickness.

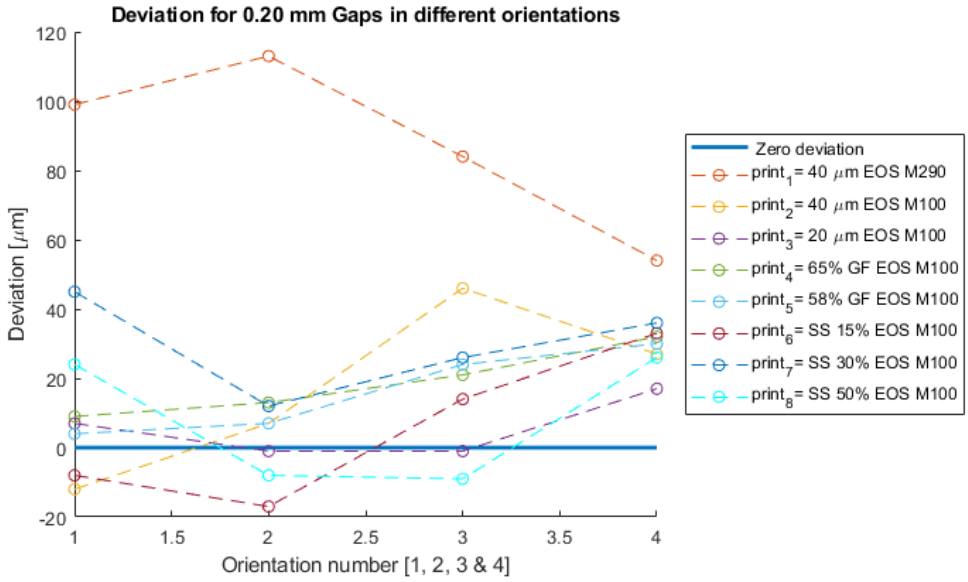

Figure 4.23: Deviation plots for 0.2 mm gaps in different orientations.

- **Deviation of 0.3 mm gap**

  The deviation data for all 0.3 mm gaps was plotted in MATLAB over each orientation, which can be seen in Figure 4.24. From the figure it can be concluded that that the lowest deviation is in orientation 2 whereas the highest is in orientation 4. The lowest deviation is in print 2 with $40\mu m$ layer thickness with the EOS M100 printer and the highest is in print 1 with $40\mu m$ layer thickness with the EOS M290 printer.

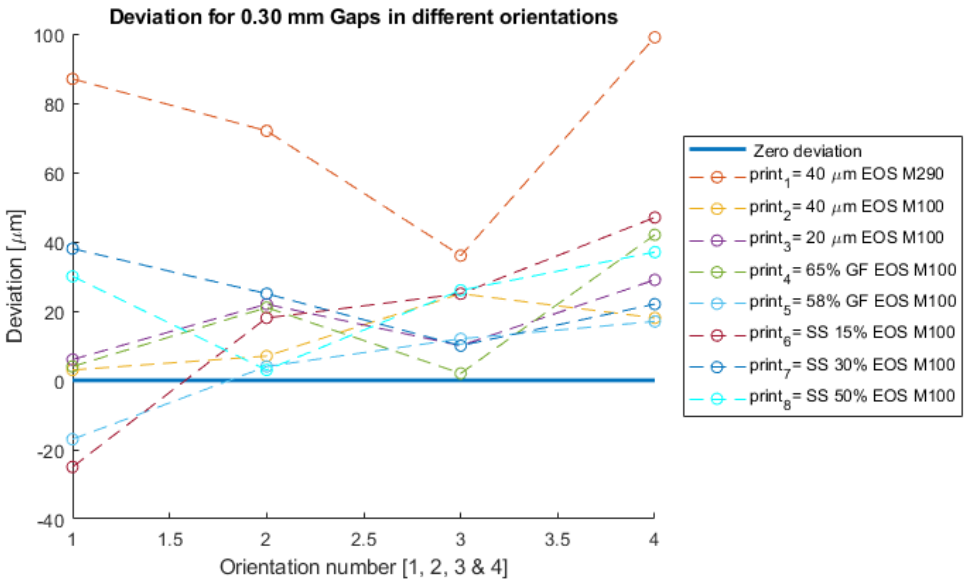

Figure 4.24: Deviation plots for 0.3 mm gaps in different orientations.

- **Deviation of 0.4 mm gap**

  The deviation measure for all 0.4 mm gaps was plotted in MATLAB over each orientation, which can be seen in Figure 4.25. From the figure can it be concluded that that the lowest deviation is for orientation 2 whereas the highest is for orientation 4. The lowest deviation is observed in print 3 with $20\mu m$ layer thickness and the highest is observed in print 1 with $40\mu m$ layer thickness.

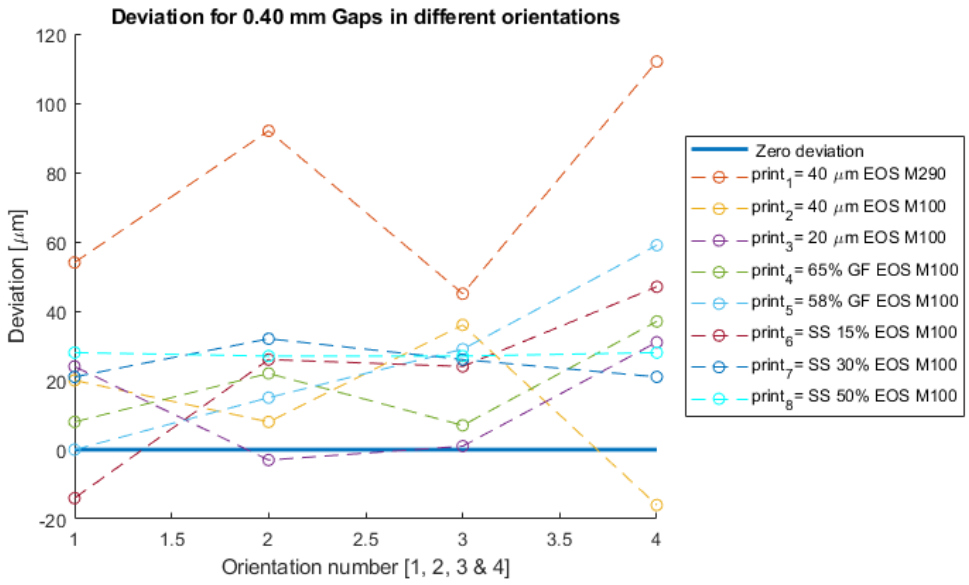

Figure 4.25: Deviation plots for 0.4 mm gaps in different orientations.

4.2.6 Deviation analysis of angles

Based on the measurements done on the angles for the positions 1 and 5 using ESEM, the deviation values are determined. Position 1 is the angle of 35° and position 5 is the angle of 55°. A detailed analysis using ESEM for the angles in different settings, their measurements, and deviation values can be seen in C.3.

Based on the deviation table from different prints, the angle for positions 1 and 5 is analyzed individually below for getting detailed results on the variation in process parameters.

- **Deviation of angles for orientation 1 build**

  The deviation for the angles of 35° and 55° were plotted in MATLAB for orientation 1, which can be seen in Figure 4.26. From the figure can it be concluded that the lowest deviation is for 35°. The lowest deviation is observed within print 2 for $40\mu m$ layer thickness with standard process parameters.

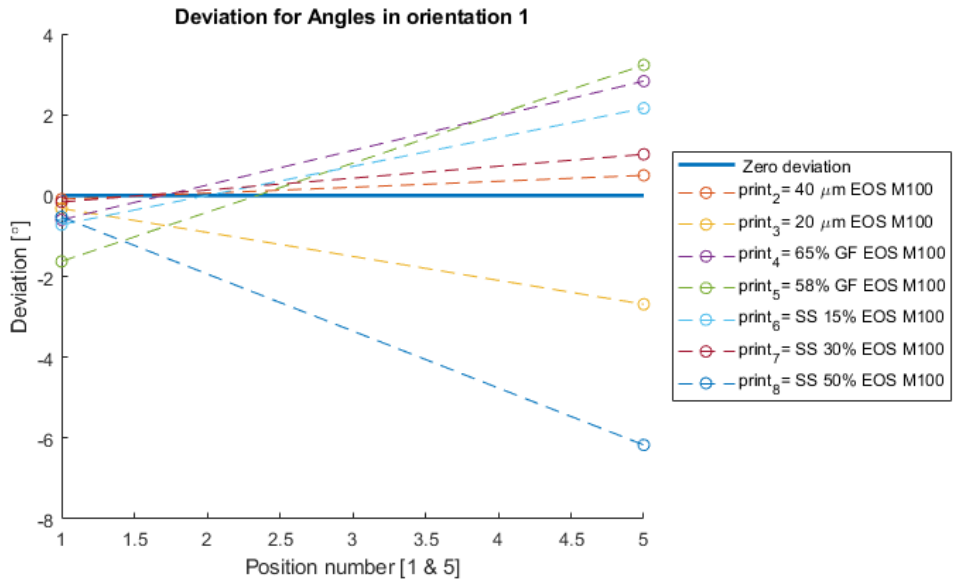

Figure 4.26: Deviation plots for angles in orientation 1.

- **Deviation of angles for orientation 2 build**

  The deviation values for the angles of 35° and 55° were plotted in MATLAB for orientation 2, which can be seen in Figure 4.27. From the figure it can be concluded that the lowest deviation is for 35°. The lowest deviation is observed for print 5 with 58% gas flow.

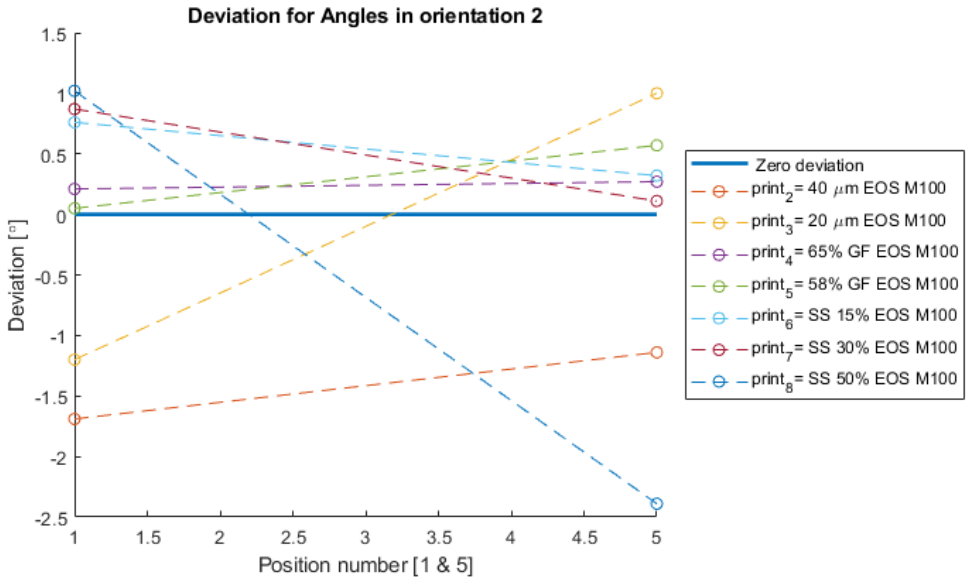

Figure 4.27: Deviation plots for angles in orientation 2.

- **Deviation of angles for orientation 3 build**

  The deviation values for the angles of 35° and 55° were plotted in MATLAB

for orientation 3, which can be seen in Figure 4.28. From the figure it can be concluded that the lowest deviation is found for 35°. The lowest deviation is observed for print 7 with 30% scan-speed.

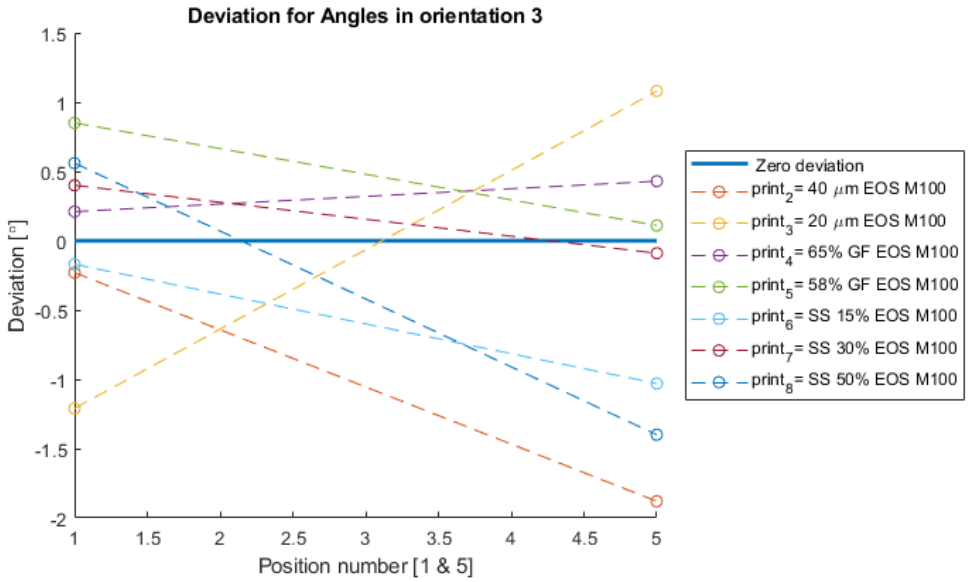

Figure 4.28: Deviation plots for angles in orientation 3.

- **Deviation of angles for orientation 4 build**

  The deviation values for the angles of 35° and 55° were plotted in MATLAB for orientation 4, which can be seen in Figure 4.29. From the figure it can be concluded that the lowest deviation is found for 35°. The lowest deviation is observed for print 4 with 65% gas flow.

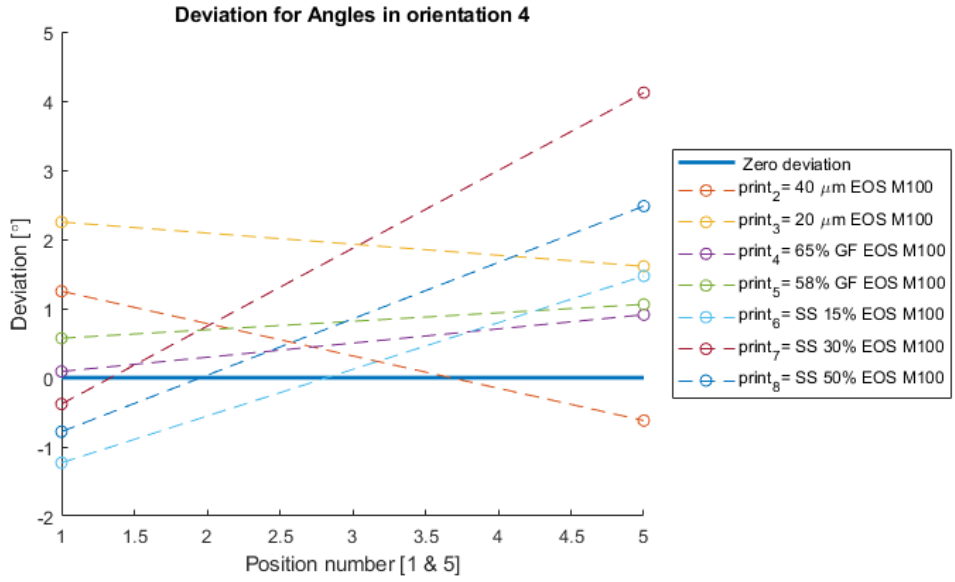

Figure 4.29: Deviation plots for angles in orientation 4.

4.2.7 Deviation analysis of arrowfoot angles and arrowhead height

Based on the measurements done on the arrowfoot angles and arrowhead height for the positions 1 and 5 using ESEM, the deviation values are determined. Position 1 represents the angle of 35° and position 5 represents the angle of 55°. Since only two angles and two arrowhead height's were measured, only linear graph is extracted, which is not accurate, but can be used to understand how the trends are for these features. The detailed analysis using ESEM for the arrowfoot angles and arrowhead heights for different processing settings, their measurements and deviation values can be seen in C.4.

Based on the deviation data from different prints, the arrowfoot angles and arrowhead height for positions 1 and 5 are analyzed individually below for getting detailed results on the variation in process parameters.

- **Deviation of arrowfoot angle and arrowhead height for orientation 1**

  For orientation 1, the deviation for the angles of 35° and 55° were plotted in MATLAB, which can be seen in Figure 4.30. From the figure it can be seen that the lowest deviation for angles of 35° and 55° is in print 7. For arrowhead height, the lowest deviation and variation is observed in print 7.

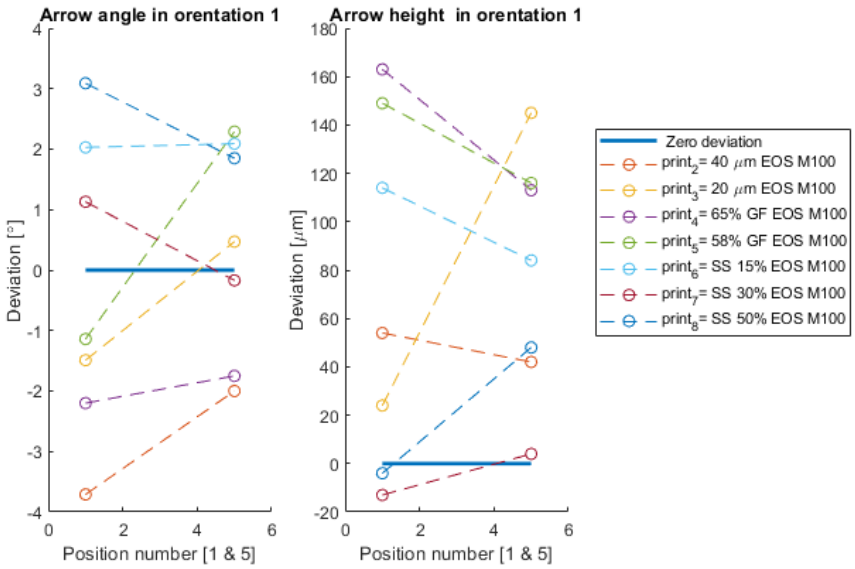

Figure 4.30: Deviation plots for arrowfoot angle and arrowhead height for orientation 1.

- **Deviation of arrowfoot angle and arrowhead height for orientation 2**

For orientation 2, the deviation for the angles of 35° and 55° were plotted in MATLAB, which can be seen in Figure 4.31. From the figure it can be seen that the lowest deviation for angles of 35° and 55° is in print 4. For arrowhead height, the lowest deviation is observed in print 2 and the lowest variation is observed in print 5.

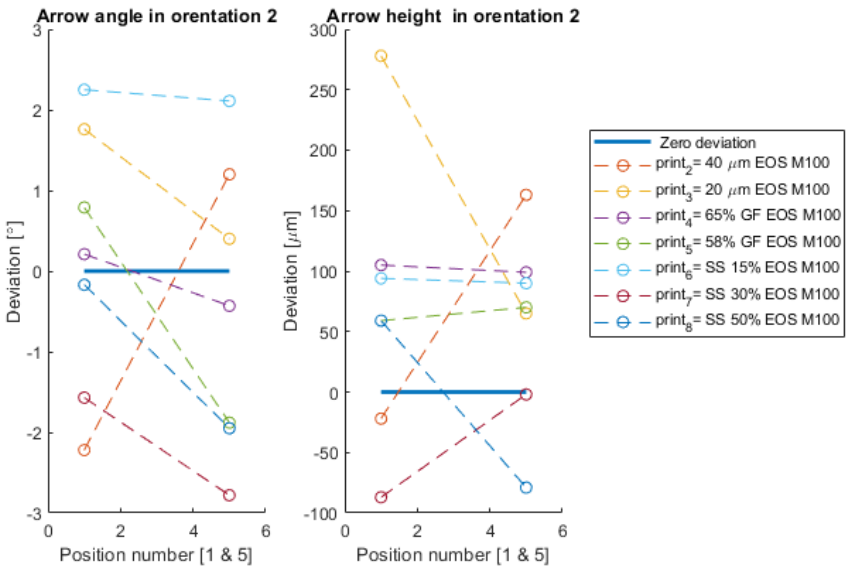

Figure 4.31: Deviation plots for arrowfoot angle and arrowhead height for orientation 2.

- **Deviation of arrowfoot angle and arrowhead height for orientation 3**

For orientation 3, the deviation for the angles of 35° and 55° were plotted in MATLAB, which can be seen in Figure 4.32. From the figure it can be seen that the lowest deviation for angles of 35° angle and 55° is in print 7. For arrowhead height, the lowest deviation and variation are observed in print 8.

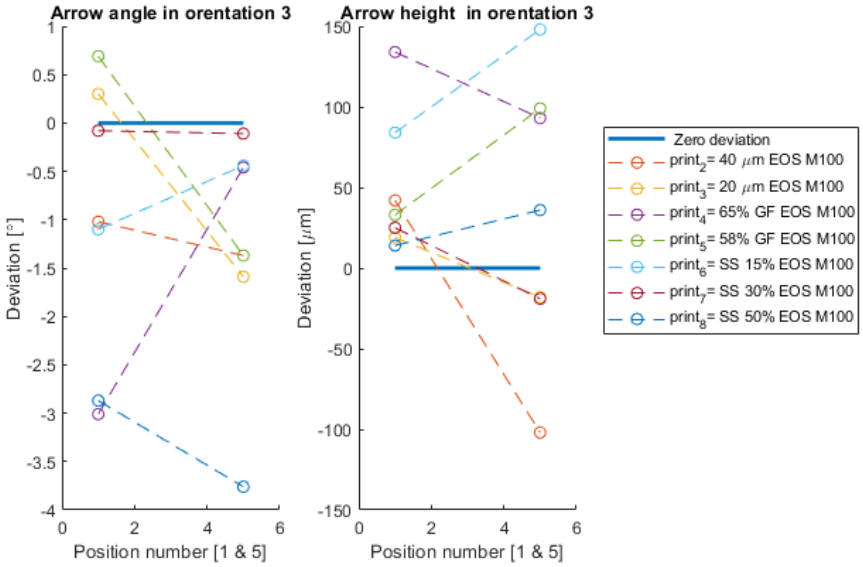

Figure 4.32: Deviation plots for arrowfoot angle and arrowhead height for orientation 3.

- **Deviation of arrowfoot angle and arrowhead height for orientation 4**

  For orientation 4, the deviation for the angles of 35° and 55° were plotted in MATLAB, which can be seen in Figure 4.33. From the figure it can be seen that the lowest deviation for 35° is observed in print 4 and for 55°, it is in print 3. For arrowhead height, the lowest deviation is observed in print 6 and the lowest variation is observed in print 8.

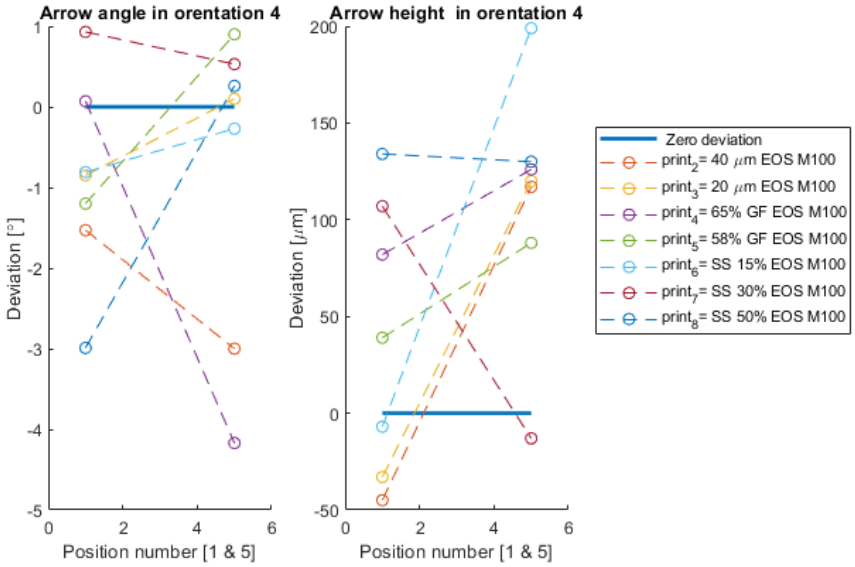

Figure 4.33: Deviation plots for arrowfoot angle and arrowhead height in orientation 4.

4.2.8 Deviation analysis of arrowfoot

Based on the measurements done on the arrowfoot using ESEM, the deviation values are calculated. A detailed analysis using ESEM for the arrowfoot angles and arrowhead height for different processing settings, their measurements, and deviation values can be seen in B.5.

Based on the deviation data from different prints, the arrowfoot is analyzed individually below for obtaining detailed results on the variation in deviation data with respect to process parameters.

- **Deviation of arrowfoot in orientation 1**

  The deviation data for the arrowfoot were plotted in MATLAB for orientation 1 in order to investigate the repeat-ability, which can be seen in Figure 4.34. From the figure, the lowest deviation can be found for print 3 with $20\mu m$ layer thickness with standard process parameters and the highest for print 1 with $40\mu m$ layer thickness.

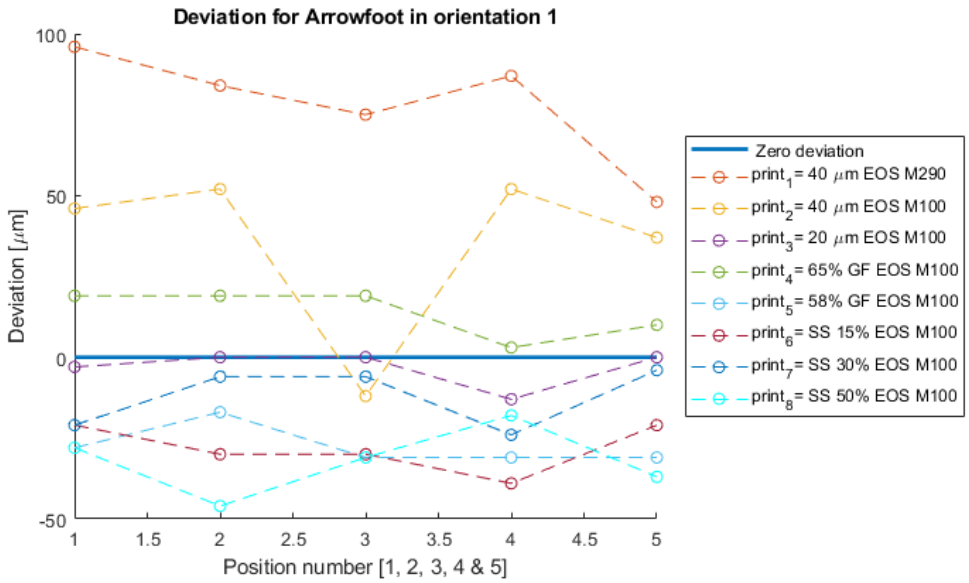

Figure 4.34: Deviation plots for arrowfoot in orientation 1.

- **Deviation of arrowfoot in orientation 2**

  The deviation data for the arrowfoot was plotted in MATLAB for orientation 2 to investigate the repeatability, which can be seen in Figure 4.35. From the figure, the lowest deviation can be found for print 3 with $20\mu m$ layer thickness with standard process parameters and the highest for print 2 with $40\mu m$ layer thickness.

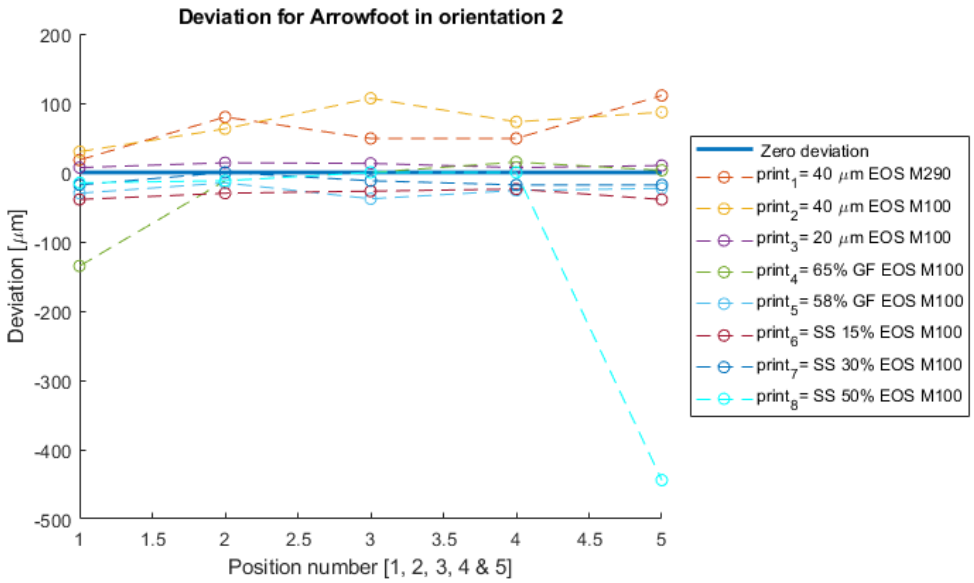

Figure 4.35: Deviation plots for arrowfoot in orientation 2.

- **Deviation of arrowfoot in orientation 3**

  The deviation data for the arrowfoot was plotted in MATLAB for orientation 3 to investigate the repeatability, which can be seen in Figure 4.36. It can be seen that the lowest deviation is for print 8 with 50% scan speed and the highest for print 1 with $40\mu m$ layer thickness.

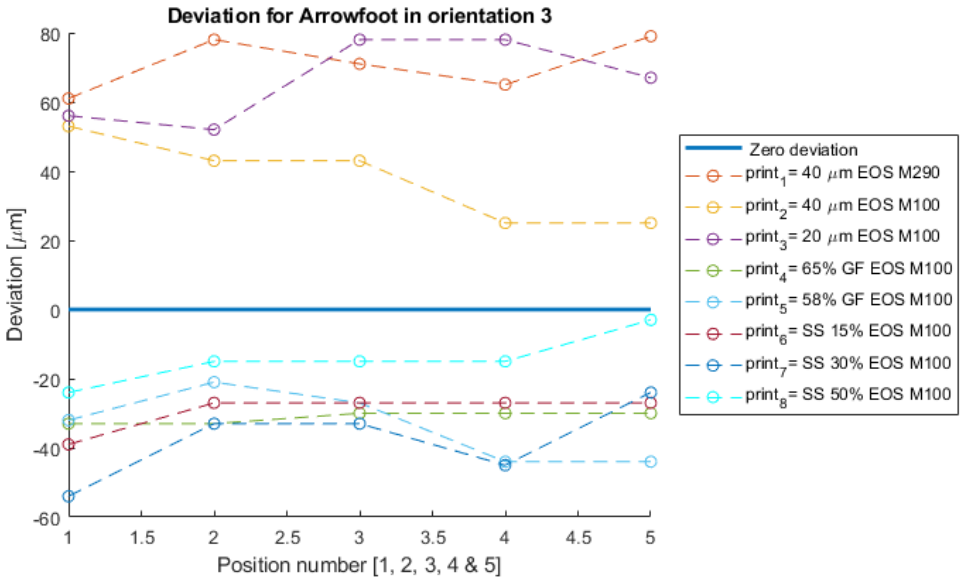

Figure 4.36: Deviation plots for arrowfoot in orientation 3.

- **Deviation of arrowfoot in orientation 4**

  The deviation measure for the arrowfoot was plotted in MATLAB for orientation 4 to investigate the repeatability, which can be seen in Figure 4.37. It can be seen that the lowest deviation is in print 8 with 50% scan speed and the highest in print 1 with $40\mu m$ layer thickness.

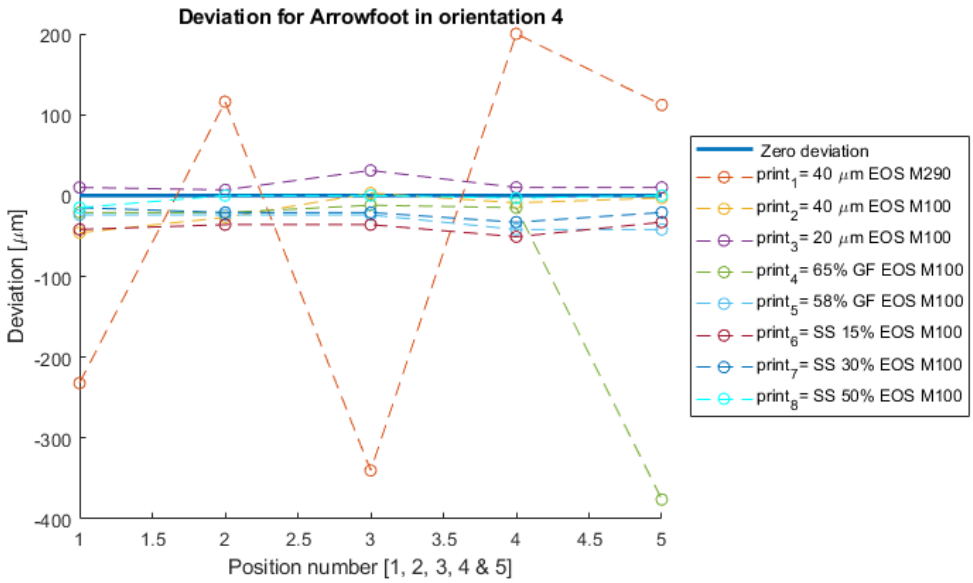

Figure 4.37: Deviation plots for arrowfoot in orientation 4.

4.3 Process variation

In order to check for repeatability, print 4 was printed again in the same manner and position. The new print is named "print 9". The variations in each feature characteristic for the respective for "print 4" and "print 9" are summarized in the Figures 4.38 to 4.42. The red solid lines in the graphs represent print 9 and the green dotted lines represent print 4. Each nominal feature size can be seen from the label for each graph. During measurements, the human errors contributed to 5 μm. This error was not taken into account while plotting the graphs but could be used to examine the range of deviation for each measurement value. In order to have the exact deviation for all the feature sizes in all the orientations refer to print 9 in appendix B.

- **Process variation for pins**

  For 0.1 mm radius pin, 10 μm to 33 μm variations are observed for all the orientations. For 0.15 mm radius pins, 10 μm to 20 μm variations are observed for all the orientations. For 0.20 mm radius pins, 5 μm to 30 μm variations are observed for all the orientations. For 0.25 mm radius pins, 2 μm to 28 μm variations are observed for all the orientations. For 0.30 mm radius pins, 5 μm to 35 μm variations are observed for all the orientations.

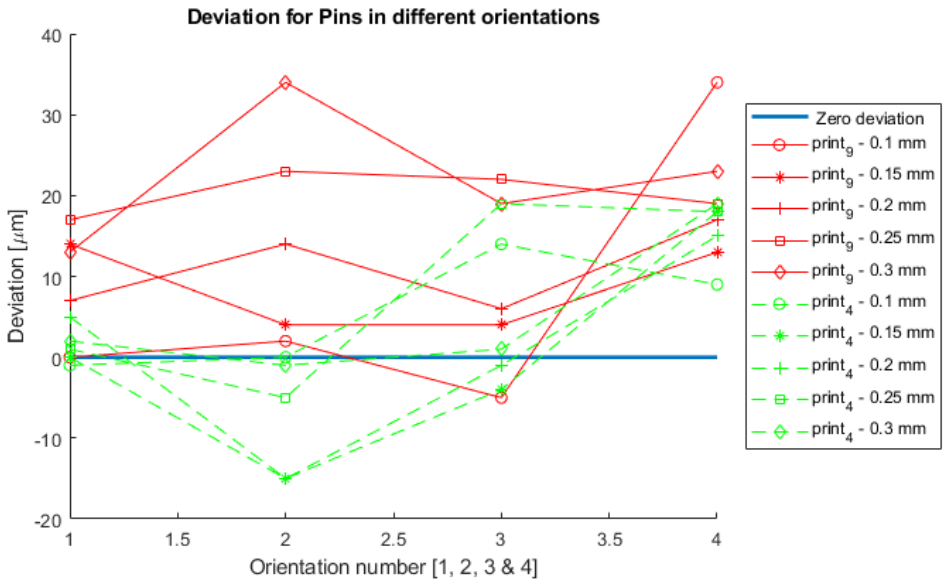

Figure 4.38: Process variation for pins.

- **Process variation for ribs**

  For 0.2 mm diameter rib, 2 μm to 15 μm variations are observed for all the orientations. For 0.3 mm diameter rib, 1 μm to 15 μm variations are observed for all the orientations. For 0.4 mm diameter rib, 1 μm to 28 μm variations are observed for all the orientations. For 0.5 mm diameter rib, 5 μm to 40 μm variations are observed for all the orientations. For 0.6 mm diameter rib, 2 μm to 30 μm variations are observed for all the orientations.

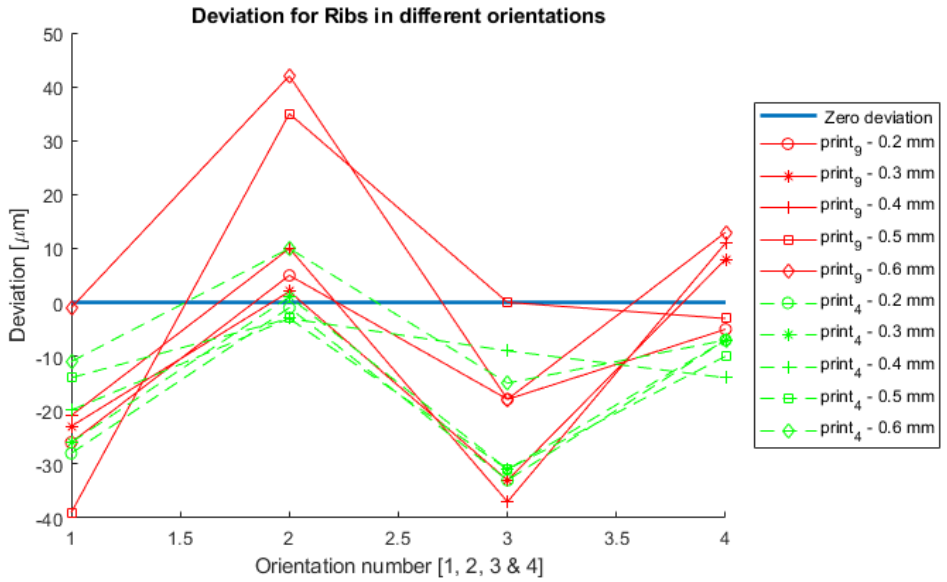

Figure 4.39: Process variation for ribs.

- **Process variation for grooves**

For 0.3 mm diameter groove, 18 μm to 30 μm variations are observed for all the orientations. For 0.4 mm diameter groove, 5 μm to 55 μm variations are observed for all the orientations. For 0.5 mm diameter groove, 8 μm to 50 μm variations are observed for all the orientations. For 0.6 mm diameter groove, 3 μm to 60 μm variations are observed for all the orientations. For 0.7 mm diameter groove, 14 μm to 60 μm variations are observed for all the orientations.

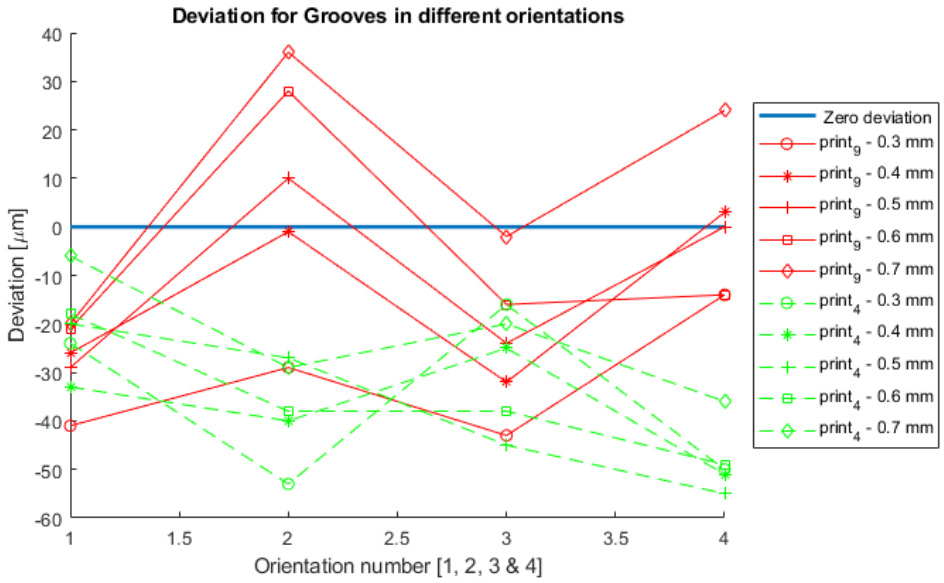

Figure 4.40: Process variation for grooves.

- **Process variation for arrowhead base**

  For 0.849 mm arrowhead base, 5 μm to 25 μm variations are observed for all the orientations. For 1.131 mm arrowhead base, 5 μm to 50 μm variations are observed for all the orientations. For 1.414 mm arrowhead base, 20 μm to 110 μm variations are observed for all the orientations. For 1.697 mm arrowhead base, 30 μm to 125 μm variations are observed for all the orientations. For 1.98 mm arrowhead base, 25 μm to 350 μm variations are observed for all the orientations.

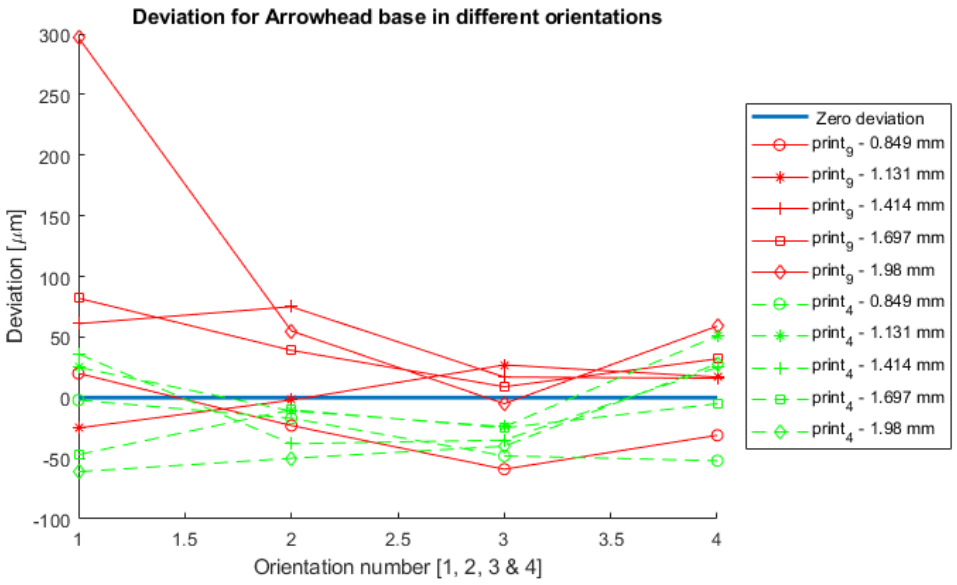

Figure 4.41: Process variation for arrowhead base.

- **Process variation for Arrowfoot**

It can be seen from the graphs that for orientations 1 and 4, the deviation in the first arrow and the fifth arrow are high. This is because of the bending in the arrows. Moreover, for orientation 2, the fifth position arrow is bent in both print 4 and print 9 which indicates that the defect is repeatable. The overall variations is expected to be between 10 μm to 60 μm. This process variations result contradicts the previous results which help us understand that the results cannot be concluded on a single run for given process settings. Hence, rather multiple runs need to be done as the variations in the process is expected to yield deviations of between 10 μm to 60 μm.

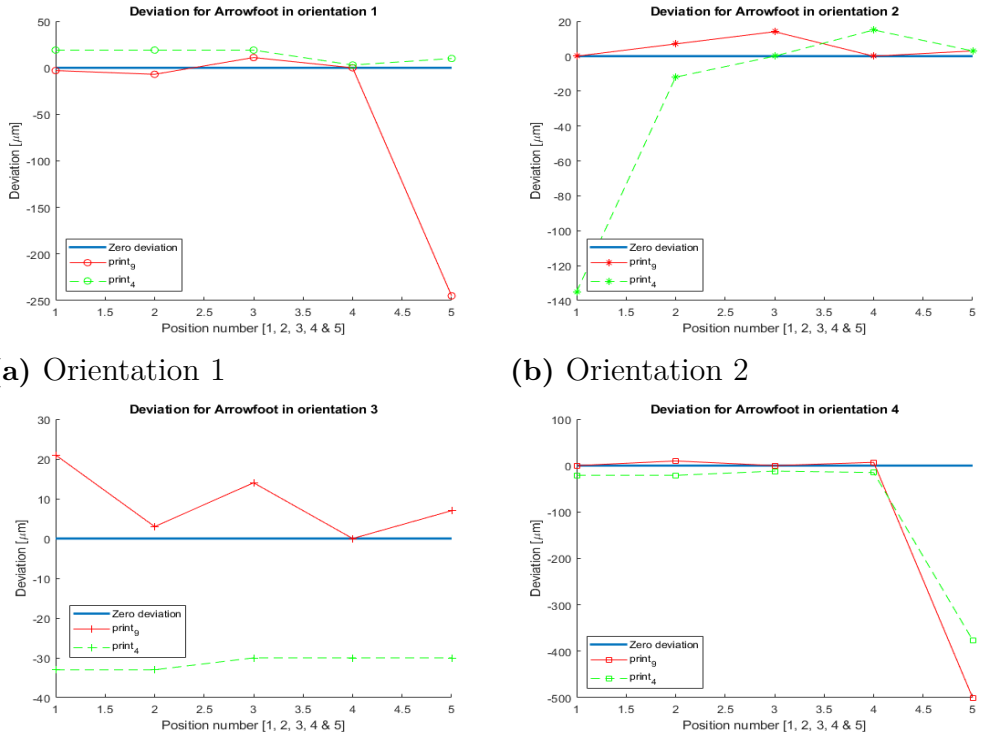

(a) Orientation 1 **(b)** Orientation 2

(c) Orientation 3 **(d)** Orientation 4

Figure 4.42: Process variation for the arrowfoot

4.4 Defects in test artefact prints

During the analysis and measurements some defects were found in the prints. Some defects are visible to the eye without any special use of characterization instruments. Some of them are not visible and can be seen only in high magnification. The defects that are found are:
i) bending in geometrical features, ii) cracks, iii) pores and iv) half molten particles. Below each defect is illustrated with an typical example. Detailed defects in each print can be found in Appendices A and B.

4.4.1 Bending in geometrical features

This defect was found in pins and arrowfoot. The bending in the pins and arrowfoot is caused by the recoater blade. The bending can be seen below in the Figure 4.43. In order to see the bending in all the prints, see the ESEM images for pins and arrowfoot that can be found in Appendix B.

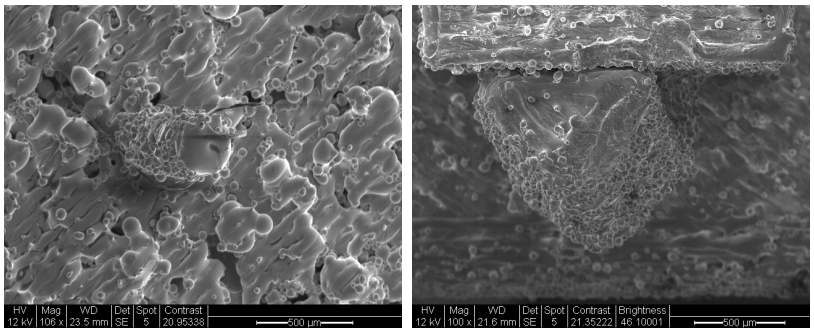

(a) Bending in pin. **(b)** Bending in arrowfoot.

Figure 4.43: Examples of bending in the prints.

4.4.2 Cracks

This defect was found in print 7. This could be due to the residual stresses. Even some part of the surface of the features looks damaged and coloured. The cracks can be seen below in Figure 4.44. The cracks are not seen in any geometrical feature, but only found in the base of the test artefact and hence not related to the fabrication of the actual features.

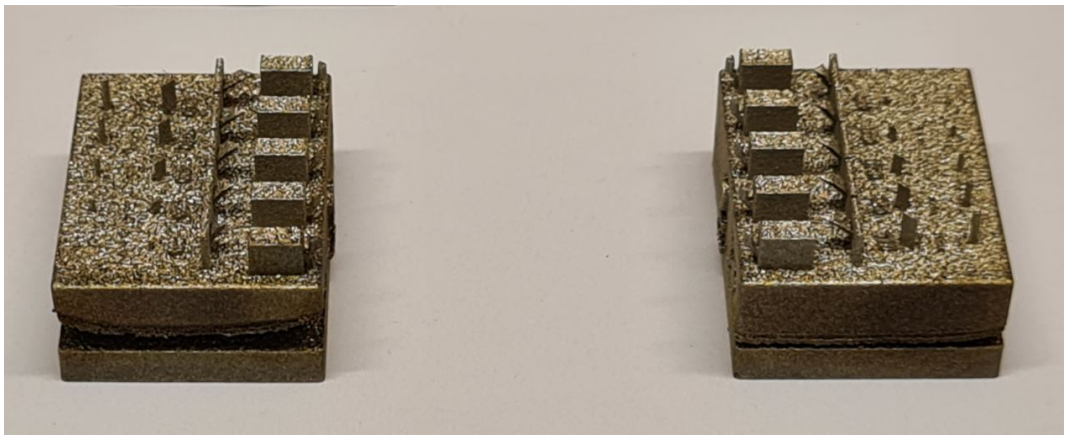

Figure 4.44: Cracks in print 7.

4.4.3 Pores

This kind of defect was found in print 2, print 6, print 7 and print 8. These prints are printed with changed scan speed and the appearance of pores could be related to this fact. The higher the scan speed and the higher the laser power is applied to keep energy density, the bigger is the size of the pores. The pores can be seen below in Figure 4.45. In order to see all the pores in print 2, print 6, print 7 and print 8 see ESEM images for geometrical features with respect to the prints discussed above in Appendices B and C.

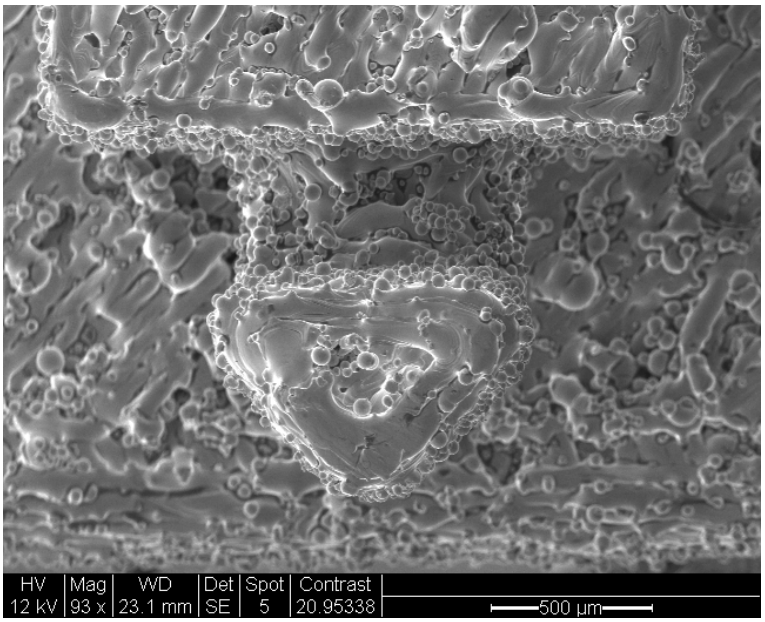

Figure 4.45: Example of pore formation seen in arrowfoot.

4.4.4 Attachment of half molten particles

This defect was found in all the features for all the prints and is basically unavoidable. This defect can be seen below in Figure 4.46 where the particles are attached to the sides of the pin. The overall documentation of the presence of half molten particles in all the prints can be found from the ESEM images of all the geometrical features in all the prints in Appendices B and C.



Figure 4.46: Example of half molten particles attached to the surface.

4.4.5 Discontinuous print

This type of defect is seen when printing ribs with 0.1 mm radius. The print was not continuous and had a discontinuity. This defect is found in prints 1 and 2.

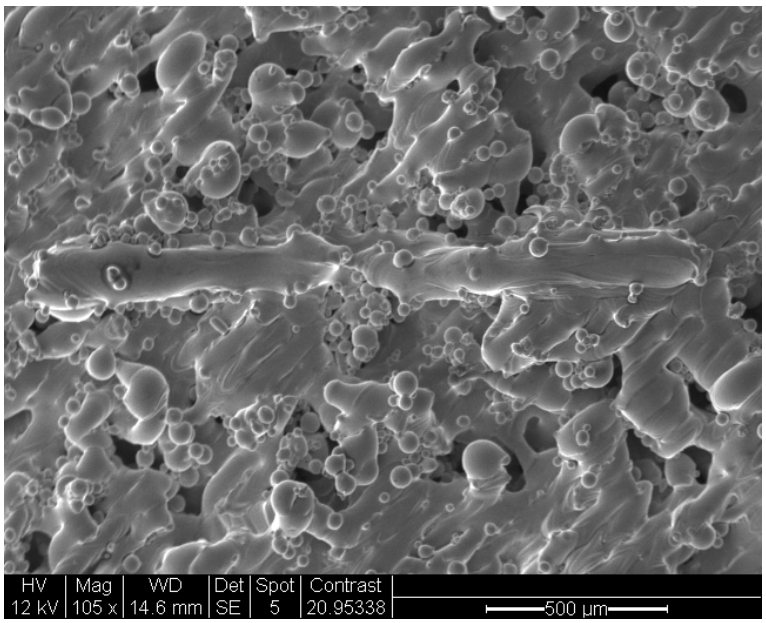

Figure 4.47: Example of half molten particles attached to the surface.

4.5 Comparison between LB-PBF and Binder Jetted Parts

In order to check for deviation, defects, repeatability, and comparison between the LB-PBF part and the binder jetted parts, two test artefacts were printed with orientation 1. They are named 'print 10'. Both the binder jetted parts were sintered at Digital Metal after printing and have weight of 38.464 grams and 38.692 grams. The measurements are done on these parts and the comparison in a deviation between the binder jetted part and the LB-PBF part is shown below in the Figure 4.48. The printed parts are shown in Figure A.46 in the Appendix.

The deviation from CAD measures is quite less for pins and ribs in the binder jetted part since the shapes of the features were good. However, arrowhead, grooves and arrowfoot were found to have less deviation in the LB-PBF print. Moreover, the defect in the Arrowfoot in position 5 for binder jetting is similar to the Arrowfoot in position 5 for LB-PBF. The surface of the features was smooth and has good quality but lower resolution for the binder-jetted part compared to the LB-PBF part. Although the parts were sintered to high relative density, there is presence of very small pores in them and which could affect the frequency transmission. Preliminary, based on the analysis and prints done, LB-PBF parts tends to show less deviation. Still, to get clear and more detailed results, further research has to be conducted for the respective technology regarding precision manufacturing of fine

features.

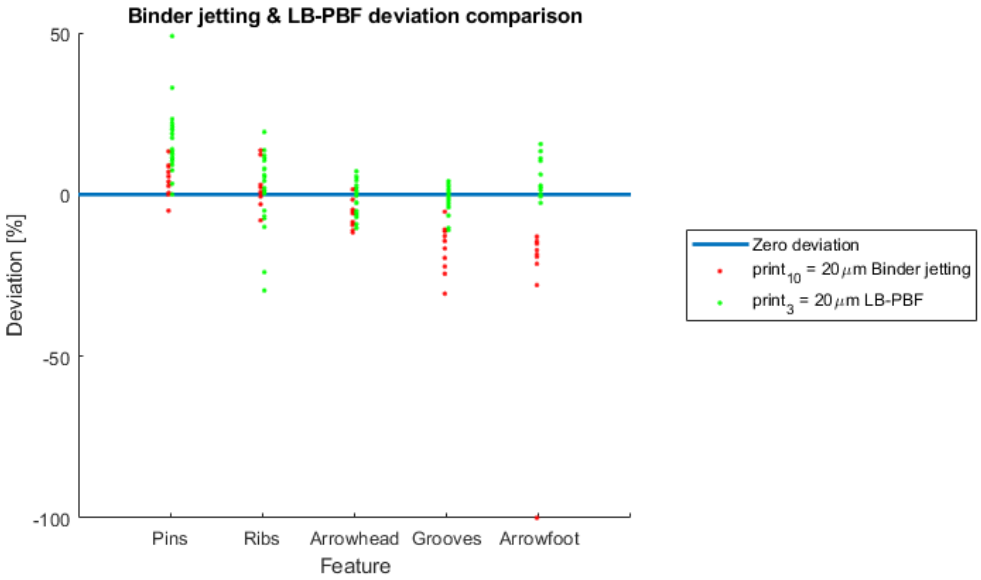

Figure 4.48: Comparison between deviation in binder jetted and sintered as well as LB-PBF features of the fabricated test artefact samples.

4.6 Electrical evaluation

The electrical evaluation was done by Lars Manholm and Oscar Talcoth at Ericsson. In order to filter away fast ripple measurements for all gap waveguides were smoothed with a 0.22 GHz hamming window, which can be seen in Figure 4.49. Furthermore, a single resonance peak can be observed which indicates good geometrical accuracy and very good consistency and repeatability for the samples.

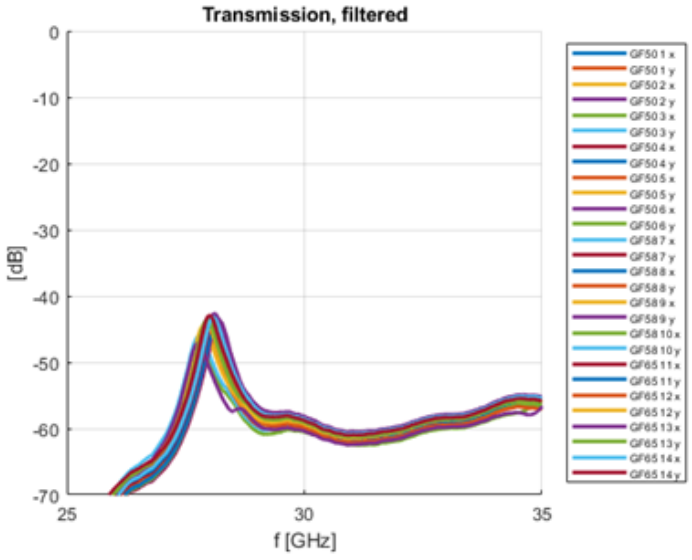

Figure 4.49: Electrical measurements for the gap waveguide transitions.

The Q-values and the resonance frequencies $f0$ were plotted in a histogram for each sample as seen in Figure 4.50. For the Q-values, there is a mean of 81 with a standard deviation of 4.35. Furthermore, possibly there could be a trend that higher gas flow when printing using LB-PBF would give slightly higher Q-value. Still, this observation is not conclusive and would need further investigation. The mean $f0$ is 28.02 GHz with a standard deviation of 112 MHz which indicates good accuracy as the mean is close to the nominal resonance frequency of 27.9 GHz.

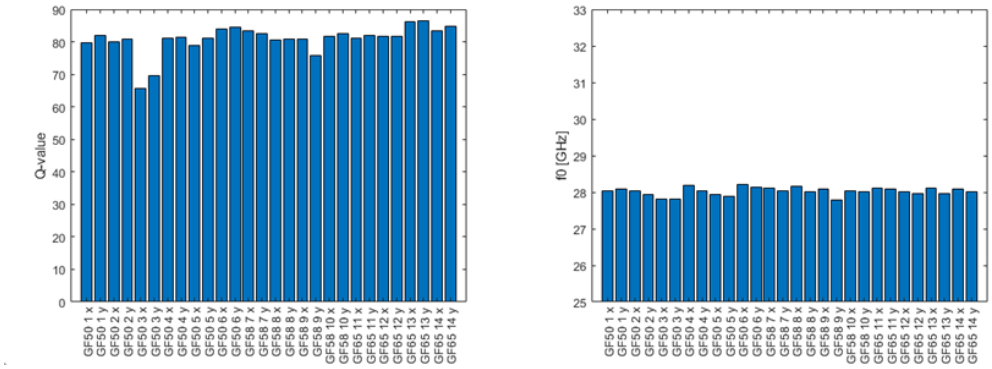

(a) Q-values. **(b)** Resonance frequencies.

Figure 4.50: Q-values and resonance frequencies histograms for gap waveguide samples.

From the conducted electrical evaluation, it is suggested that the corresponding accuracy and high repeatability be achieved for prints 3, 4 and 5, which indicates that the geometrical deviations in critical dimensions is within controllable limits.

5
Discussion

In this chapter, a discussion about the thesis work progression, accuracy in the results, feature control, and ethics are provided. The discussion is related to different challenges both from the project and additive manufacturing from technology point of view.

5.1 Work progression

The progress of this thesis was characterized by working in an agile manner, which in this context means that relevant literature findings were applied in practice in a repeating fashion. This was proven to be an efficient way to find new results and testing them. However, in the middle of the project started a measuring phase where measurements needed to be taken on the prints. Due to limited equipment availability, the measurements were taken with an ESEM and SOM microscope which were shown to be a way of taking accurate measurements as such. However, the time required for achieving proper measurements using these techniques is significant. If another method like 3D-scanning, potentially providing shorter measurements, would have been used, this may have enabled further study of process parameters of interest.

5.2 Accuracy in the results

The deviation values are measured and derived for each feature for each set of processing parameter settings and the data reported do not account for any human errors for the measurements. When measuring using ESEM and SOM, the measurements can vary from person to person for the same feature measurement and this could affect the results. Even though this error was found to be $\pm 5\ \mu m$ which is very small, the study focuses on assessing measures with a μm level precision. Hence, even $\pm 1\ \mu m$ uncertainty is important. Moreover, the repeatability is carried out for only one print and the variation was found to be between 5 μm and 60 μm. Hence the measures obtained might vary if more repeatability tests are conducted for all the process parameters. Since the scope of the project is limited to only certain parameters, the analysis was carried out only for these, and results are provided for them only.

In this thesis project, the measurements were done before surface treatment hence there were half molten particles attached to the printed features. If the parts would

have been surface treated, measurements could have been taken easily with small errors. This would have added further understanding of deviation before the surface treatment and after the surface treatment could have been added. Based on such comparison of variation in measures, the design parameters can be modified to meet the nominal CAD dimension after printing.

The accuracy of certain features like arrowhead height and arrowfoot angle have been decreased in μm scale level when using the SOM instrument since the edges were not visible clearly and had too many half molten particles attached. However, with the ESEM it was not possible to measure these features as the instrument has some limitation with respect to the size of the part to be kept inside the chamber for analysis. This disadvantage in the use of SOM and ESEM can potentially be overruled by using 3D scanning. However, the accuracy of the measurement using the 3D scanner is tentatively at best in the submillimetre range and the applicability of this technique for small feature analysis would need to be depicted. The 3D scanner would still be beneficial in order to understand the overall deviation more as it gives a direct 3-dimensional view of the part, whereas in SOM and ESEM are limited to 2D-analysis, where 3D reconstruction is to be gained for stacked and multiple orientation imaging.

In the comparison between the LB-PBF parts and the binder jetted and sintered parts, it was seen that the latter although being near fully had some very small pores. Since the final stage is the sintering this sets the final geometrical accuracy and to what extent the remaining pores has an impact here including as well the functional behaviour of the part remains to be verified. Furthermore, would applying hot isostatic pressing to eliminate any residual porosity would be of interest to depict.

5.3 Feature control

In the thesis project the deviation of features with respect to waveguide was studied. To summarize the results, the minimum, maximum, mean and standard deviation deviation of each feature for the prints 1 to 8 are calculated, contribution of repeatability from the processes and human error expressed as min, max, mean, and standard deviation for prints 4 and 9 are shown in Table 5.1 below. It could be seen that the easiest features to control were pins followed by grooves, angles, and gaps. This is connected to those features having well defined corners, thus making measurements to be placed accurately. The hardest features to control were arrowhead base, ribs, and arrowfoot. This is mainly caused by the half molten particles and the natural filleted corners for these features, thus contributing to the deviation and making it hard to take accurate measurements. Since the arrow in the waveguide consists of multiple features, the deviation increases when the deviations from all the features are combined. Lastly, the repeatability and human error results indicates that the deviation contributed from the process is greater than the deviation contributed from human error when taking measurements. From this project, it is also seen that the arrowhead height and the arrowfoot angle has higher human error

than the other features during measurement. Hence, importance should be given on standardizing the measurement strategy for these features.

Table 5.1: Deviation for the features, repeatability and human error expressed as min, max, mean and standard deviation.

	Min [μm]	**Max** [μm]	**Mean** [μm]	**SD** [μm]
Pins	-70.0	70.0	2.43	24.4
Ribs	-299	82.0	-50.4	68.6
Arrowhead base	-555	142	-55.6	126
Grooves	-82	44.0	-28.8	23.4
Gaps	-25	138	30.35	30.3
Angles	-6.17°	4.12°	0.108°	1.59°
Arrowfoot	-444	200	-6.65	71.3
Repeatability	0.00	358	32.3	48.4
Human error	-5.2	5.1	1.4	3.3

5.4 Ethics

Ethics is of high importance when developing a new product as the product may affect society. Understanding the ethical consequences is critical in order to be able to predict what impact the technology may have on society as for the individual. The ethical dilemmas created by writing this thesis were found to be a contribution to the further development of AM and 5G technologies.

Further development of LB-PBF may give rise to dilemmas of reusing metal powder in order to still get accurate results to minimize environmental waste and potential health issues. AM makes it possible to manufacture complex components easy which may cause problems regarding intellectual property and business ethics as anyone with the right 3D printer could produce copies of the components [12]. One may conclude that further development of AM is needed to process and answer these ethical issues.

The development of this product may encourage further development of 5G technologies. The potential of 5G is tremendous, however, there are also many ethical dilemmas to consider in conjunction with the rise of this new technology. 5G gives the possibility of massive data collection which in many cases is beneficial, however, this may affect the privacy of many people. Furthermore, with the rise of robots using artificial intelligence, robots could become more like people which may give rise to even more ethical issues to how people should interact with robots [1].

6
Conclusions

The conclusions aims to answer the research questions stated at the beginning of the project. These research questions are answered below.

- **How to print small features with high precision using LB-PBF?**

Small features with high procession can be produced by analyzing the impact of the process parameters on the given feature testing the capability of the machine. In this thesis the best precision results are obtained with the $20\mu m$ layer thickness together with a 65% gas flow in relation to the standard process settings. A more elaborate conclusion on the best results can be achieved by investigating more on all process parameters options since the scope in this thesis is precision manufacture of fine features rather than the normal manufacture of normal complex structural parts.

- **Does the orientation from the recoater and the gas flow affect the accuracy of the parts?**

Yes, the orientation of the part with respect to the recoater and the setting of amount of gas flow and its direction has an effect on the accuracy of the parts. Here, each feature has a different pattern with respect to the deviation and the gas flow has an high effect on the final shape of the feature and the deviation of measures compared to CAD design.

- **Where is the limit of the technology?**

When printing a component using additive manufacturing there will always be a trade-off between different targeted geometrical characteristics. During the analysis, it was seen that some of the features control contradict one another and needed different process parameters to produce good results with respect to best tolerance control(least deviations). Since all the process parameters contribute to the overall accuracy in geometrical control, trade-offs that are viable and acceptable haves to be researched and multiple process parameter optimization can be used in order to establish the best possible trade-off.

- **What kind of measurement strategy needs to be used for fine features to get high accuracy in measurements?**

In order to ascertain high accuracy in the measurements, the right measurement techniques and measurement strategies need to be used depending on the particular feature and the feature size of concern. The geometry of the feature or the part should be taken into account when deciding the instrument for measurement. A measurement strategy makes the measurements be taken systematical in a prede-

fined manner reducing the variation in the measurements.

- **What are the advantages and disadvantages of different measurement systems?**

During the analysis, the measurements were taken with ESEM, SOM, and 3D scanning. ESEM gives a good overall image of the top surfaces with high accuracy and high magnification, however, due to the high magnification, the half molten particles in the down skins and skins make it hard to distinguish the sharp edges and the changes in the geometry. Furthermore, it takes a long time to examine the samples in the ESEM. Measurements using SOM are simple and the time to examine the samples is very much less, but some trade-off has to be considered between the accuracy, importance of the measurement, and the time to measure. In SOM, as the magnification is low it is easy to follow the outer shapes of the part. Measurements using 3D scanning are fast and make it easy to determine the deviation, however, it is hard to find the right equipment which is able to determine the deviation accurately for small features. Eventhough the 3D scanning builds the approximate geometry edges, there is a possibility that it considers half molten particles which might reduce the accuracy.

- **How to reduce the human error during measurement?**

Outcome of measurements can vary from person to person. The human error can be reduced by establishing a measurement strategy making the measurements to be taken in a systematical fashion that can be understood by everyone.

- **What are the capabilities for high precision in LB-PBF?**

Due to the fine metal powder and high precision lasers, it is possible to produce the small features using LB-PBF. However, the capabilities are limited for the technology meaning that the highest possible resolution for the features is determined by the powder size and how well the process is controlled. The trade-off between accuracy and resolution must be taken into account further when manufacturing small features. Through this project, it was found that there will always be partially fused powder particles on the surfaces making the surface rough.

- **What kind of defects can be expected when printing small features using LB-PBF and what could be the cause for it?**

During the analysis, some of the defects that are found were bending, porosity, partially fused and unfused powder seen in the LB-PBF prints. These are caused by the aspect-ratio issues, damage owing to recoater, non-optimised processing involving for example too high scan speed, and to low laser power.

- **How precise can the variation be controlled?**

Variation can be controlled by selecting the process parameter that has an impact on the accuracy of the part and then varying it to the correct setting. In this project, the variation depended on the feature, size and the orientation of print. The variation might differ for each process and therefore the prints must be done multiple times to get accurate statistical data for variation analysis.

7

Recommendations for Future Work

This chapter consists of ideas on developing the project topic further. These recommendations are given based on the results. The recommendations are given below.

- Conduct more analysis with surface treated parts by analyzing the deviation of each dimension after surface treatment.
- Conduct more analysis by printing the test artefacts with different process parameters to get more knowledge on deviation and variation between them.
- Conduct research finding an optimal setting by integrating the best setting of each parameter by using Multi Objective Optimization.
- Conduct research on different machines using LB-PBF technology for precision manufacturing.
- Conduct research on build position along with the different process parameters for the test artefacts and the gap waveguide.
- Conduct research for finding the precision limits for the gap waveguide to achieve the desired frequency by doing electrical evaluation.
- Conduct research to reduce number of defects in prints.
- Conduct research about the deviation connected to different measurement instruments used for characterization.
- Conduct research by printing the test artefacts and gap waveguide using different metal AM technologies to observe the geometrical deviations.

References

[1] 5G?IoT. *WHAT ARE 5G AND THE INTERNET OF THINGS?* 2019. URL: https://whatis5g.info/?fbclid=IwAR1PGCnRGQ9n_IxfZ8AsKt7t1P13FFiehC25t_mRDxijPR_FaQ_yHDUBDbM (visited on 02/09/2021).

[2] Shukri Afazov et al. "A methodology for precision additive manufacturing through compensation". In: *Precision Engineering* 50 (2017).

[3] Claus Aumund-Kopp and Adeline Riou. *INTRODUCTION TO ADDITIVE MANUFACTURING TECHNOLOGY - A guide for Designers and Engineersm.* 3rd Edition. European Powder Metallurgy Association, 2019.

[4] Barry Berman. "3-D printing: The new industrial revolution". In: *ScienceDirect* (2012). DOI: https://doi.org/10.1016/j.bushor.2011.11.003. URL: https://www.sciencedirect.com/science/article/pii/S0007681311001790.

[5] Eduard Hryha. *Overvew of AM technologies and materials.* 2019. URL: PowerPoint (visited on 02/17/2021).

[6] T. Ingrassia et al. "Process parameters influence in additive manufacturing". In: *Springer Link* (2017).

[7] Richard Leach and eds Simone Carmignato. *Precision Metal Additive Manufacturing.* CRC Press, 2020.

[8] Ruidi Li et al. "Balling behavior of stainless steel and nickel powder during selective laser melting process". In: *The International Journal of Advanced Manufacturing Technology* 59 (2011), pp. 1025–1035.

[9] A3DM ADDITIVE MANUFACTURING. "The additive DMLS manufacturing process (direct metal laser sintering)". In: (2015). URL: https://www.a3dm-magazine.fr/news/fabrication-additive-metallique/procede-de-fabrication-additive-dmls.

[10] Mark Miller. *Waveguide Makes a Comeback in 5G—for Antennas.* 2020. URL: https://www.mwrf.com/technologies/components/article/21121323/pasternack-enterprises-waveguide-makes-a-comeback-in-5gfor-antennas.

[11] Shawn Moylan, Joseph Drescher, and M. Alkan Donmez. "Powder Bed Fusion Machine Performance Testing". In: *National Institute of Standards and Technology* AMERICAN SOCIETY FOR PRECISION ENGINEERING (2014).

[12] George Inyila Ogoh. “THE ETHICAL ISSUES OF ADDITIVE MANUFACTURING”. In: *De Montfort University* PhD thesis (2020).

[13] Marc-Antoine de Pastre, Saint-Clair Toguem Tagne, and Nabil Anwer. “Test artefacts for additive manufacturing: A design methodology review”. In: *CIRP Journal of Manufacturing Science and Technology* (2020).

[14] RENISHAW. “Design for metal AM - a beginner’s guide”. In: (2017).

[15] SIS. “Additive manufacturing – Test artifacts – Geometric capability assessment of additive manufacturing systems”. In: *ISO/ASTM 52902:2019* (2019).

[16] H.C. Taylor, E.A. Garibay, and R.B. Wicker. “Toward a common laser powder bed fusion qualification test artifact”. In: *Additive Manufacturing* 39 (2020).

[17] Jithin Kozhuthala Veetila et al. “Build position-based dimensional deviations of laser powder-bed fusion of stainless steel 316L”. In: *ScienceDirect* (2021). DOI: 10.1016/j.precisioneng.2020.09.024.

[18] Adilet Zhakeyev et al. “Additive Manufacturing: Unlocking the Evolution of Energy Materials”. In: *Wiley Online Library* (2017). DOI: https://doi.org/10.1002/advs.201700187. URL: https://onlinelibrary.wiley.com/doi/full/10.1002/advs.201700187.

A

Appendix A - Prints

A.1 First print EOS M290 40μm

From a rough inspection with the eye it can be seen that some of the resolution pins are bent in the part 1 and one of the resolution pins are missing, which can be seen in Figure A.1 below. A closer view of each printed orientation of the artefact can be found in Figure A.2, A.3, A.4 and A.5.

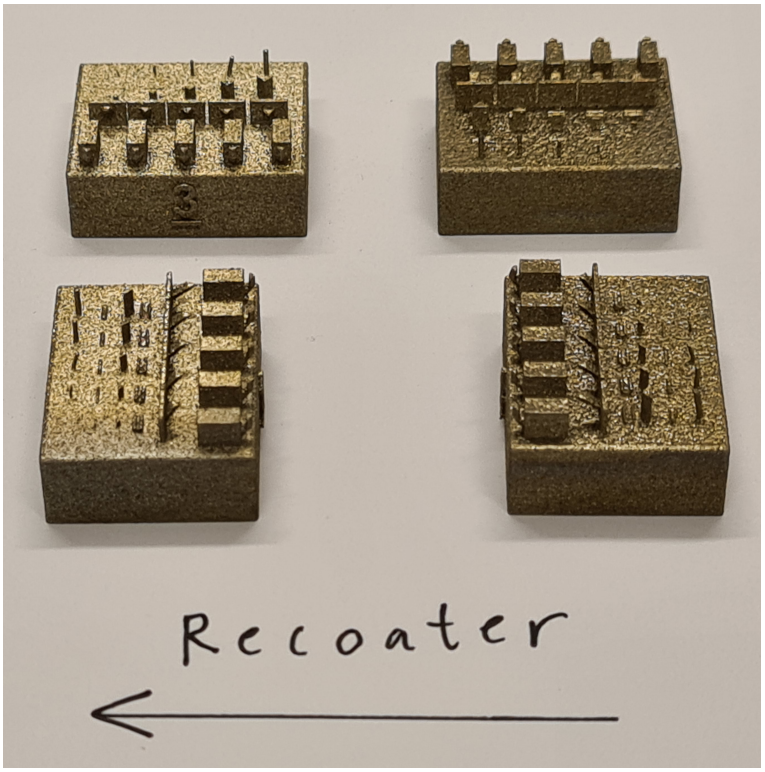

Figure A.1: First print of the artefact model where the recoating direction is shown and the orientation number from bottom left is 1, 2, 3 and 4 for each artefact.

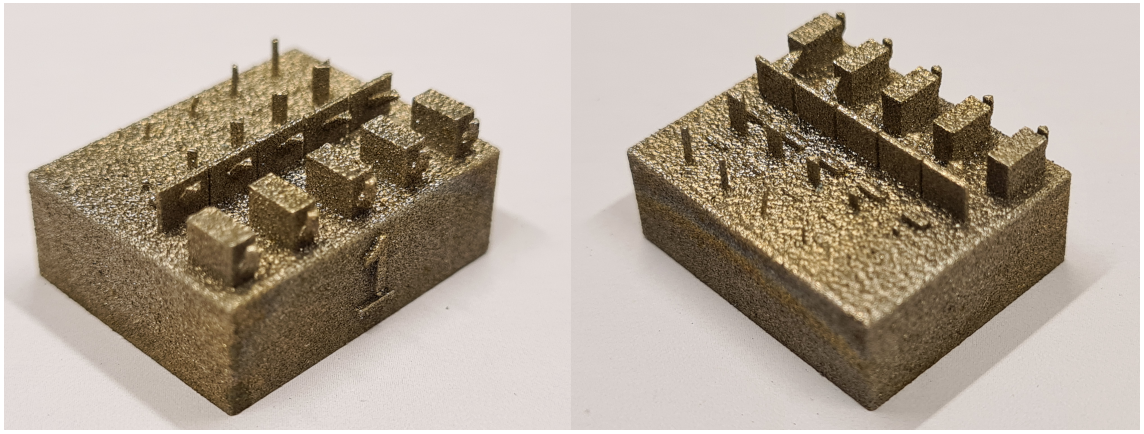

(a) Front-view of the artefact. **(b)** Back-view of the artefact.

Figure A.2: Front- and back -view of the artefact printed in orientation 1.

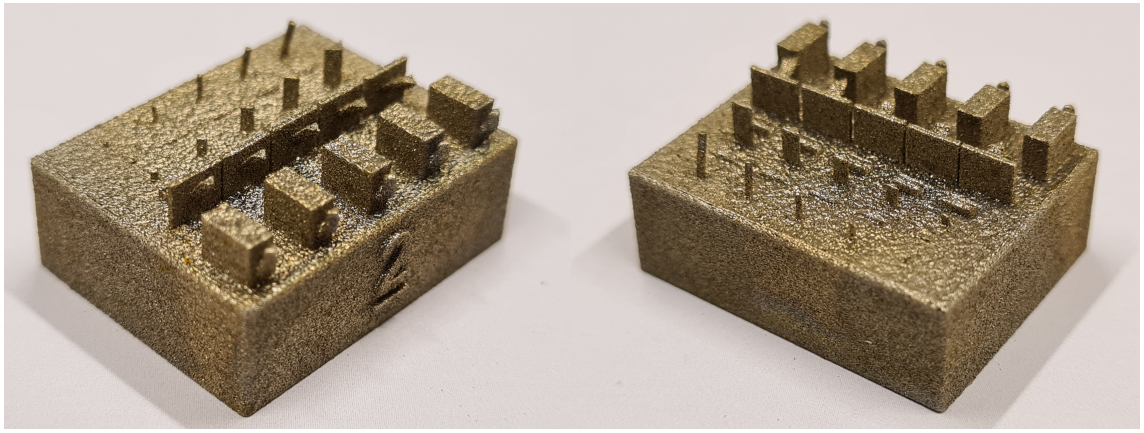

(a) Front-view of the artefact. **(b)** Back-view of the artefact.

Figure A.3: Front- and back -view of the artefact printed in orientation 2.

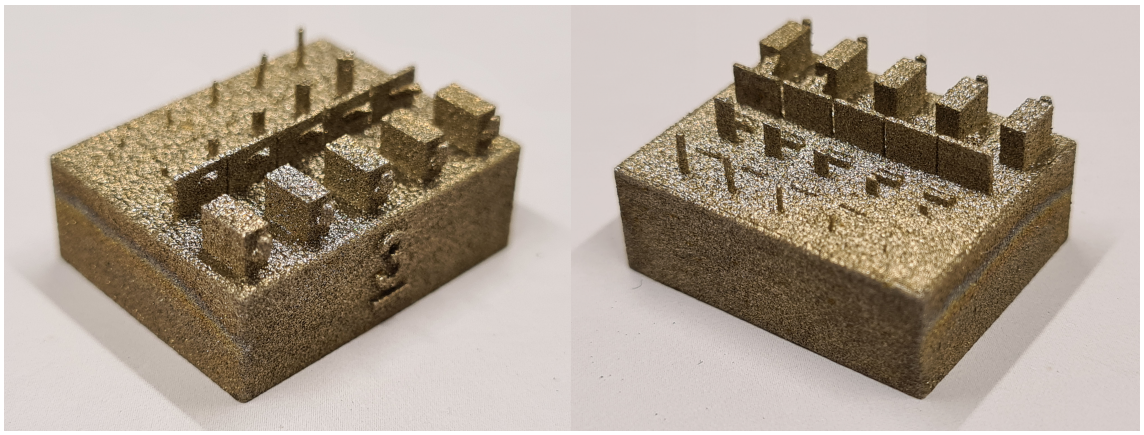

(a) Front-view of the artefact. **(b)** Back-view of the artefact.

Figure A.4: Front- and back -view of the artefact printed in orientation 3.

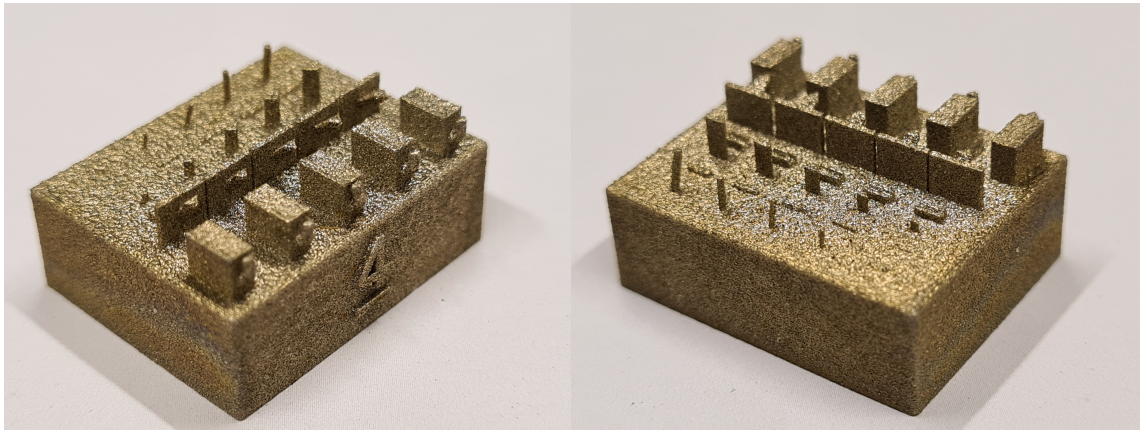

(a) Front-view of the artefact. **(b)** Back-view of the artefact.

Figure A.5: Front- and back -view of the artefact printed in orientation 4.

A.2 Second print EOS M100 40μm

It can be seen that this print is quite coarse, having a higher surface roughness than the EOS M290 print. The print can be seen in Figure A.6 where a closer view of each artefact can be found in Figure A.7, A.8, A.9 and A.10.

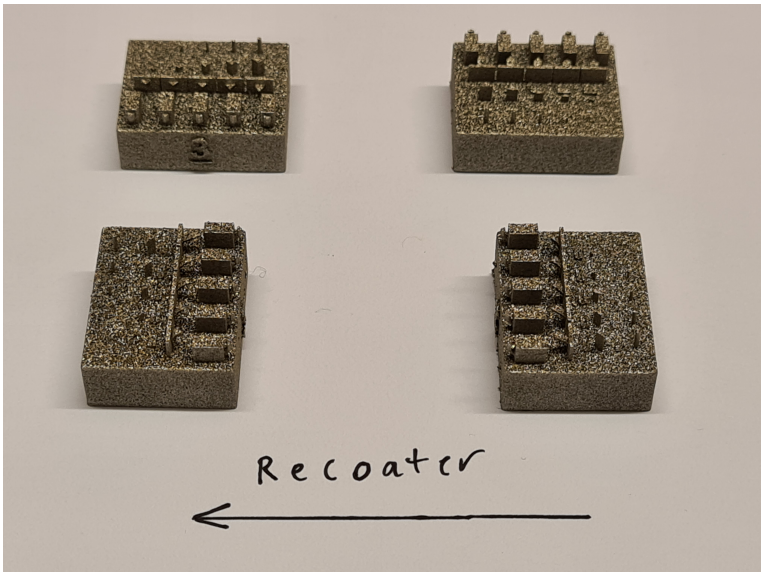

Figure A.6: Second print of the artefact model where the recoating direction is shown and the orientation number from bottom left is 1, 2, 3 and 4 for each artefact.

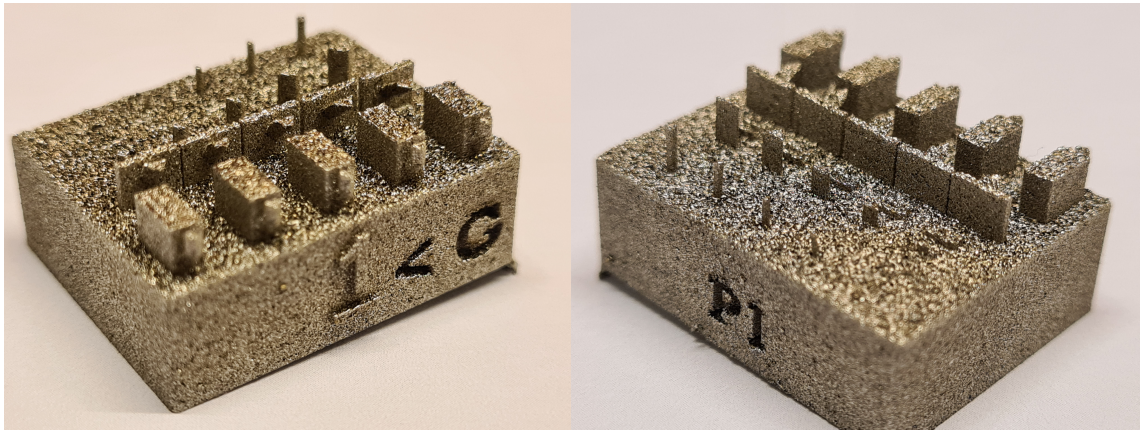

(a) Front-view of the artefact. **(b)** Back-view of the artefact.

Figure A.7: Front- and back -view of the artefact printed in orientation 1.

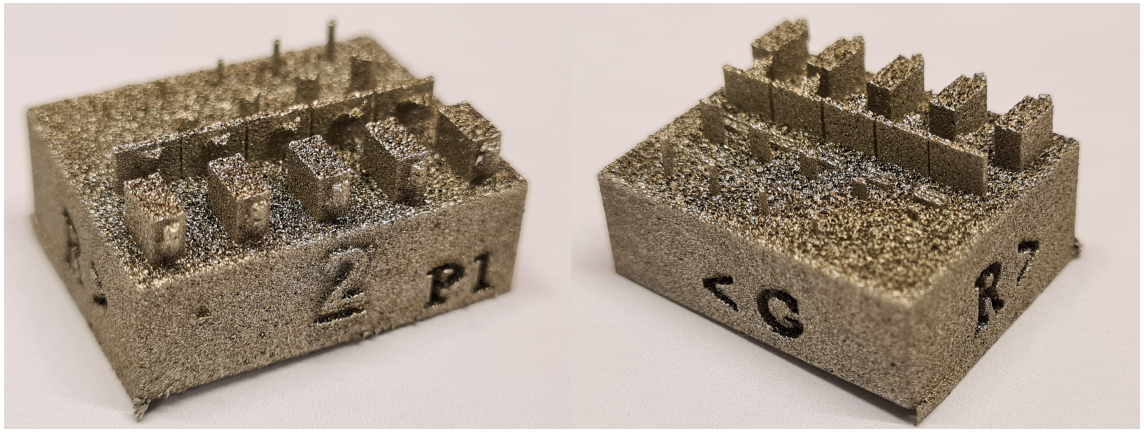

(a) Front-view of the artefact. **(b)** Back-view of the artefact.

Figure A.8: Front- and back -view of the artefact printed in orientation 2.

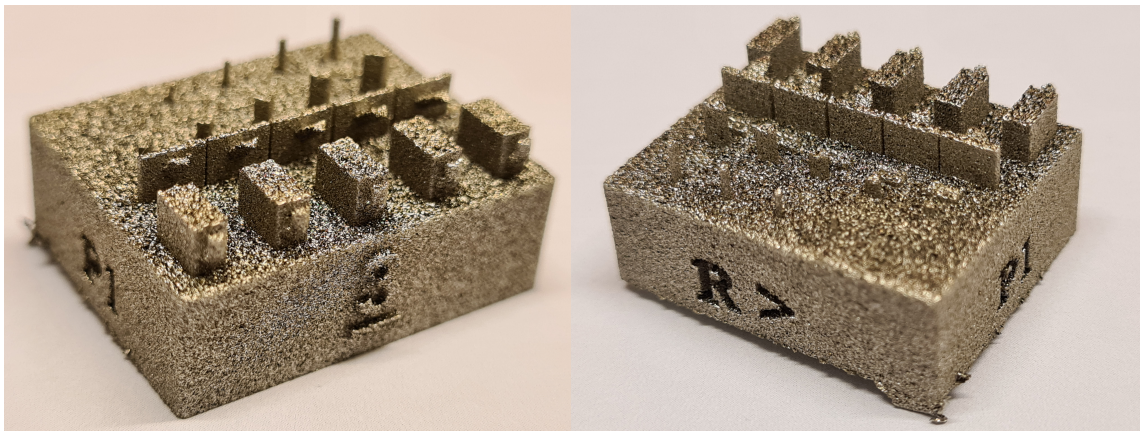

(a) Front-view of the artefact. **(b)** Back-view of the artefact.

Figure A.9: Front- and back -view of the artefact printed in orientation 3.

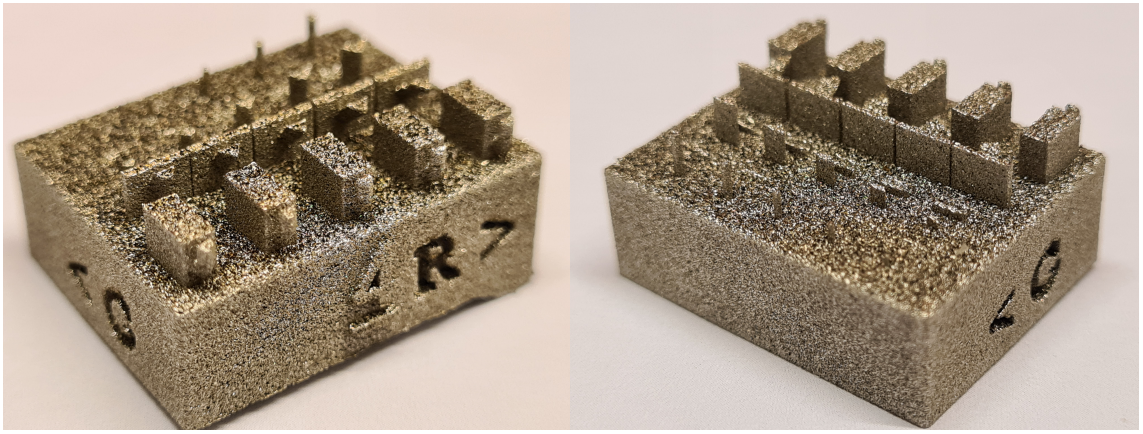

(a) Front-view of the artefact. **(b)** Back-view of the artefact.

Figure A.10: Front- and back -view of the artefact printed in orientation 4.

A.3 Third print EOS M100 20μm

From Figure A.11 below can it be seen that the surface roughness is much lower than for the previous prints due to the lower layer thickness. A closer view of each artefact can be found in Figure A.12, A.13, A.14 and A.15.

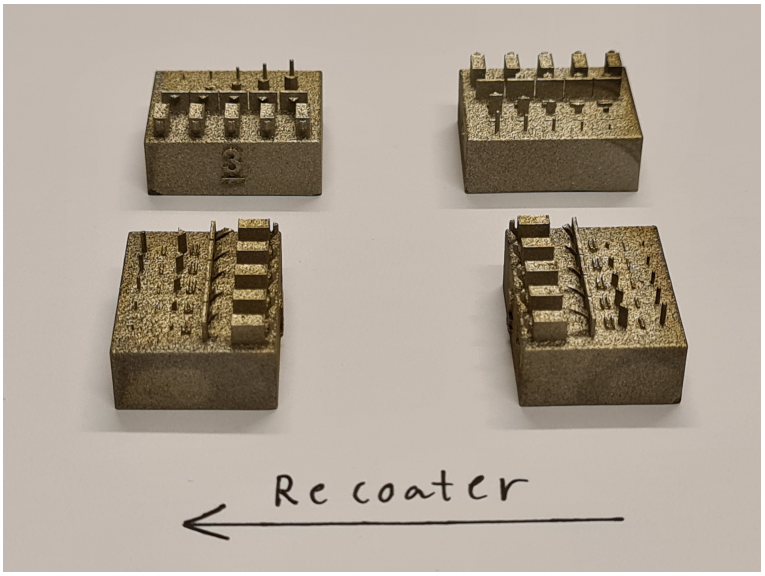

Figure A.11: Third print of the artefact model where the recoating direction is shown and the orientation number from bottom left is 1, 2, 3 and 4 for each artefact.

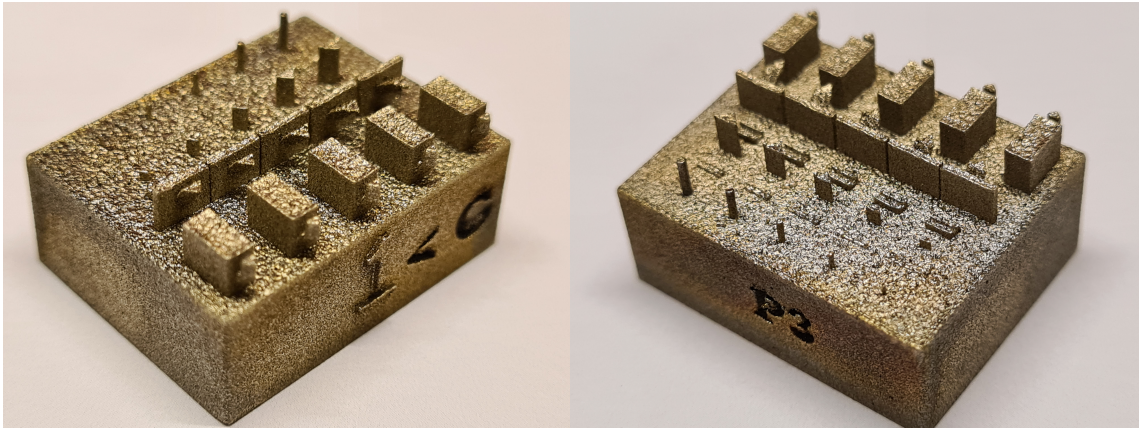

(a) Front-view of the artefact. **(b)** Back-view of the artefact.

Figure A.12: Front- and back -view of the artefact printed in orientation 1.

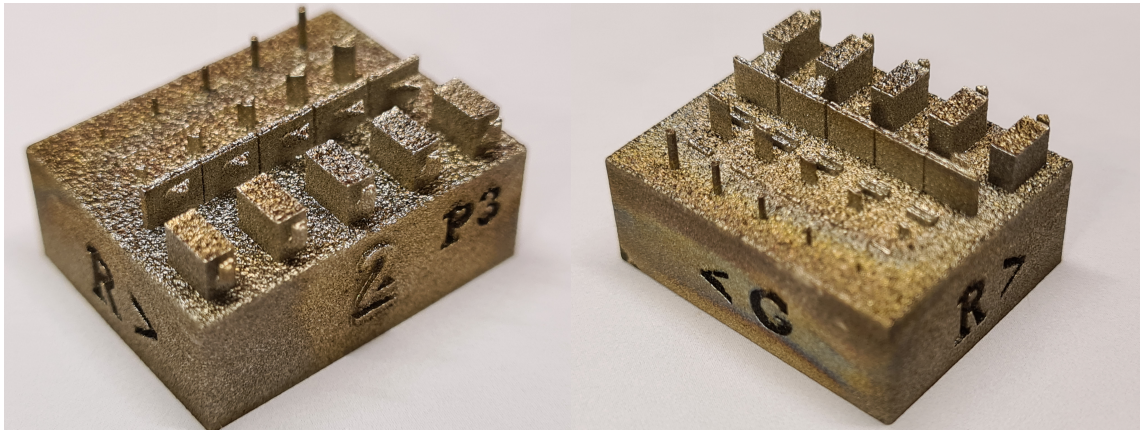

(a) Front-view of the artefact. **(b)** Back-view of the artefact.

Figure A.13: Front- and back -view of the artefact printed in orientation 2.

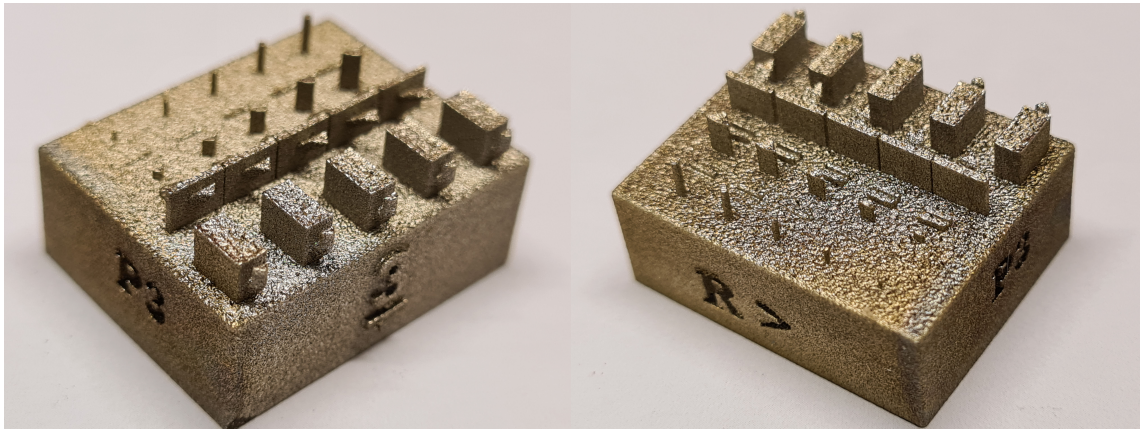

(a) Front-view of the artefact. **(b)** Back-view of the artefact.

Figure A.14: Front- and back -view of the artefact printed in orientation 3.

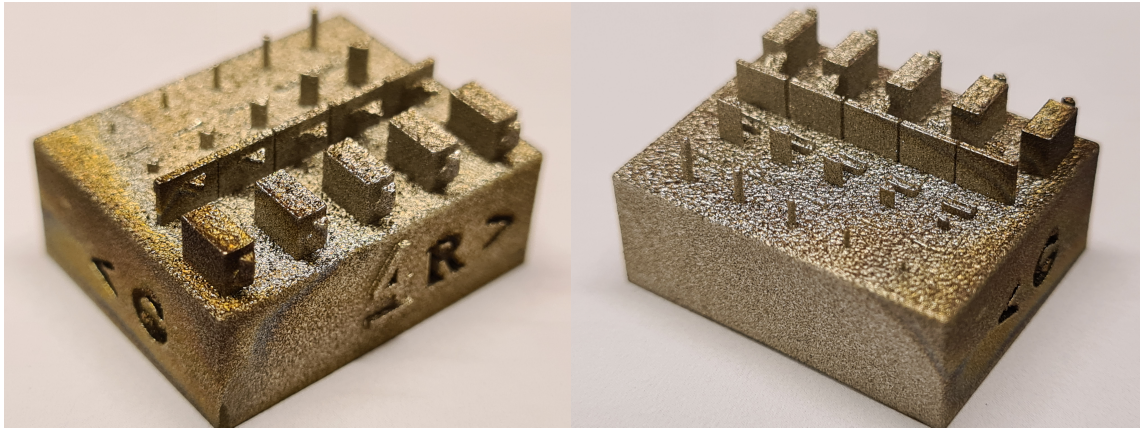

(a) Front-view of the artefact. **(b)** Back-view of the artefact.

Figure A.15: Front- and back -view of the artefact printed in orientation 4.

A.4 Fourth print EOS M100 65% gas-flow

From the figures below can it be seen that the artefacts have similar surface properties as the third print. A closer view of each artefact can be found in Figure A.17, A.18, A.19 and A.20.

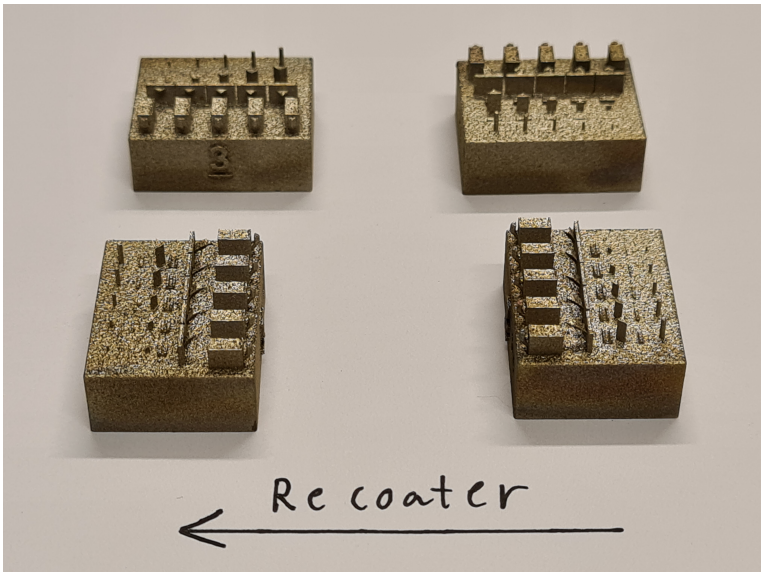

Figure A.16: Fourth print of the artefact model where the recoating direction is shown and the orientation number from bottom left is 1, 2, 3 and 4 for each artefact.

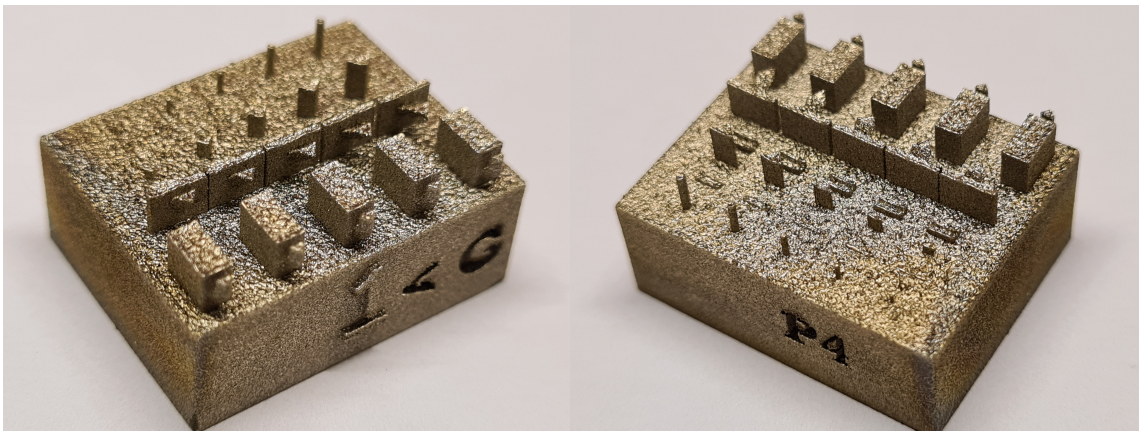

(a) Front-view of the artefact. **(b)** Back-view of the artefact.

Figure A.17: Front- and back -view of the artefact printed in orientation 1.

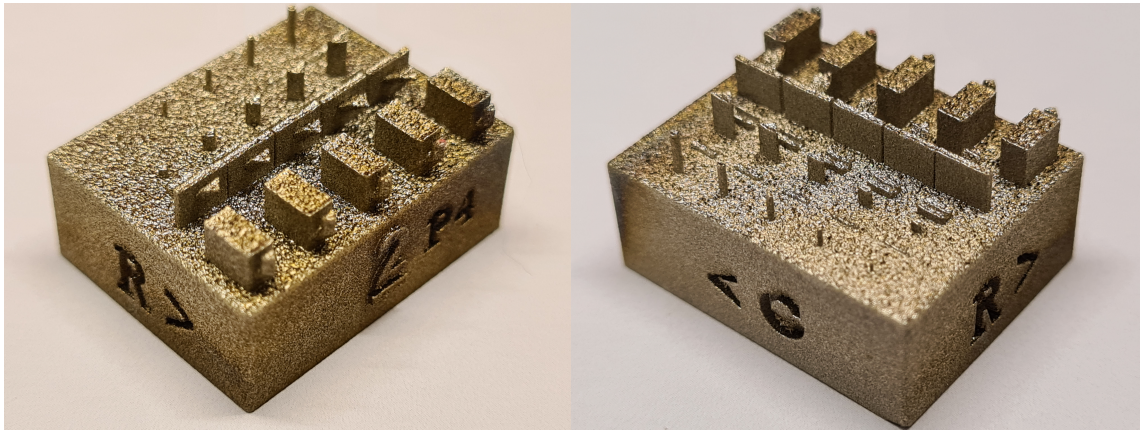

(a) Front-view of the artefact. **(b)** Back-view of the artefact.

Figure A.18: Front- and back -view of the artefact printed in orientation 2.

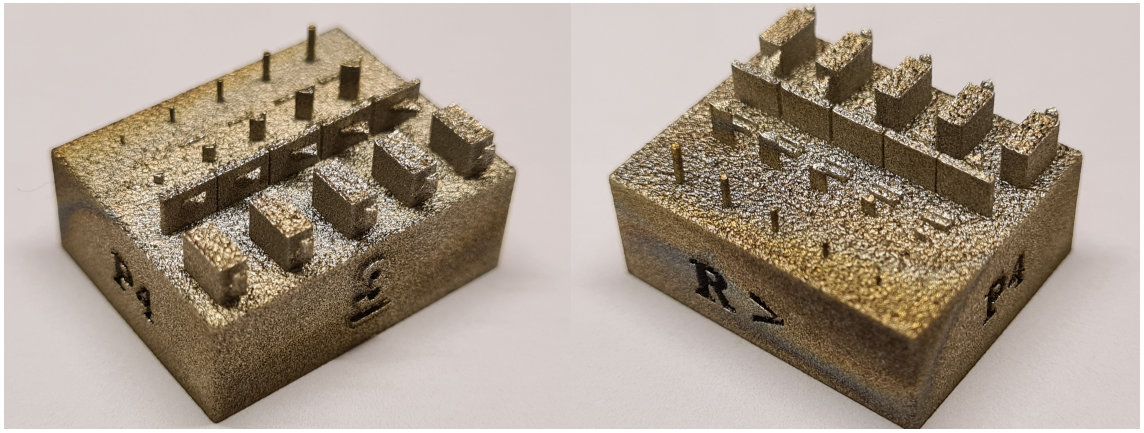

(a) Front-view of the artefact. **(b)** Back-view of the artefact.

Figure A.19: Front- and back -view of the artefact printed in orientation 3.

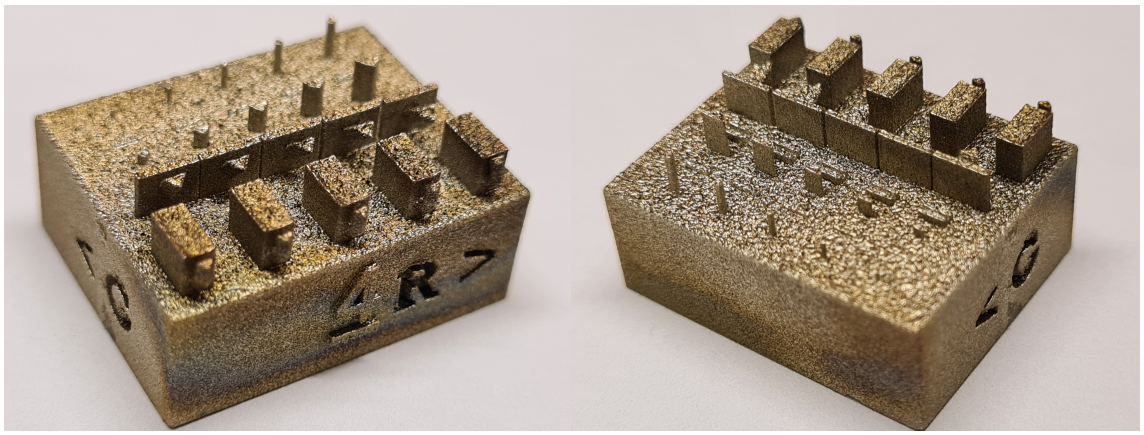

(a) Front-view of the artefact. **(b)** Back-view of the artefact.

Figure A.20: Front- and back -view of the artefact printed in orientation 4.

A.5 Fifth print EOS M100 58% gas-flow

From the figures below can it be seen that the artefacts have higher surface roughness than previous $20\mu m$ prints. A closer view of each artefact can be found in Figure A.22, A.23, A.24 and A.25.

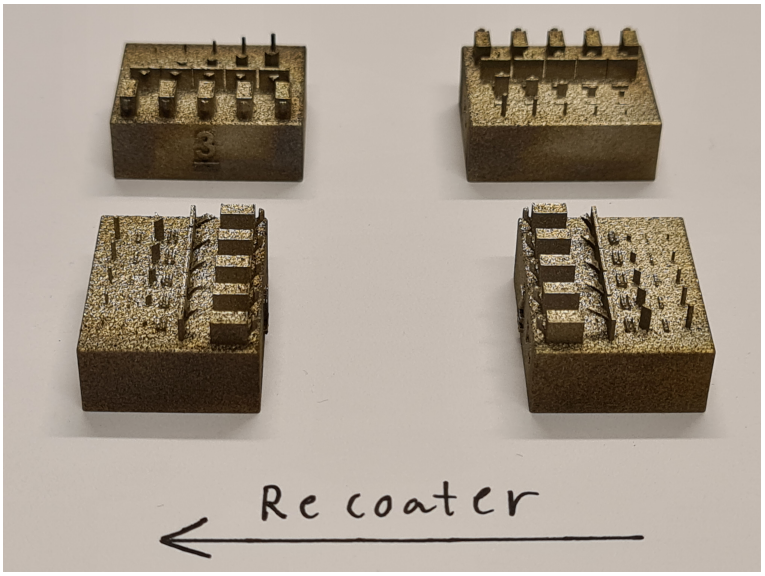

Figure A.21: Fifth print of the artefact model where the recoating direction is shown and the orientation number from bottom left is 1, 2, 3 and 4 for each artefact.

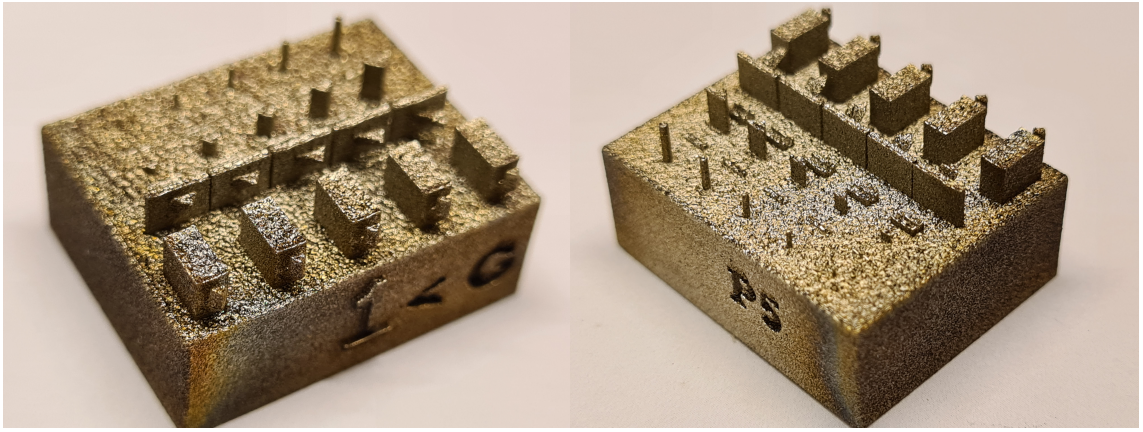

(a) Front-view of the artefact. **(b)** Back-view of the artefact.

Figure A.22: Front- and back -view of the artefact printed in orientation 1.

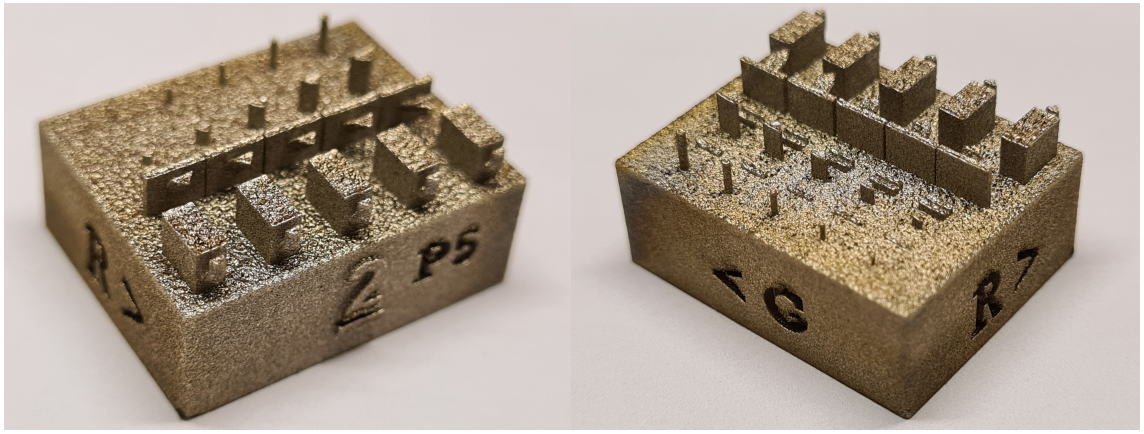

(a) Front-view of the artefact. **(b)** Back-view of the artefact.

Figure A.23: Front- and back -view of the artefact printed in orientation 2.

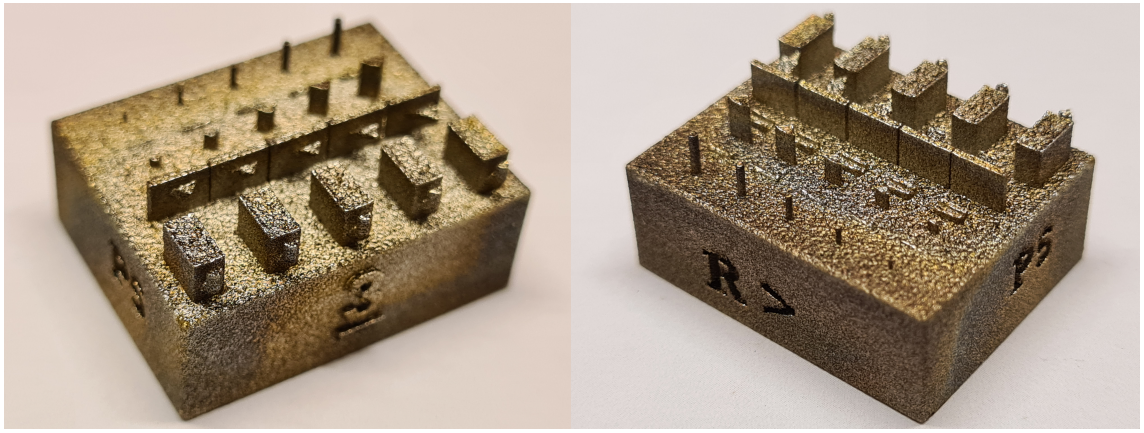

(a) Front-view of the artefact. **(b)** Back-view of the artefact.

Figure A.24: Front- and back -view of the artefact printed in orientation 3.

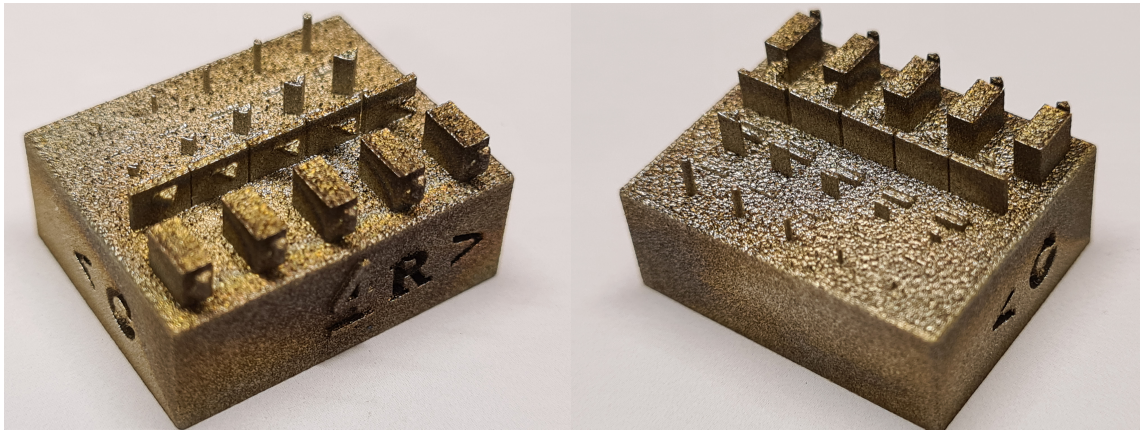

(a) Front-view of the artefact. **(b)** Back-view of the artefact.

Figure A.25: Front- and back -view of the artefact printed in orientation 4.

A.6 Sixth print EOS M100 15% scan-speed

In the figures below can it be seen that the artefacts have a high surface roughness compared to other 20μm prints. Furthermore it can be seen that the artefact in the orientation 1 and 2 have a much higher surface roughness than artefact in orientation 3 and 4. A closer view of each artefact can be found in Figure A.27, A.28, A.29 and A.30.

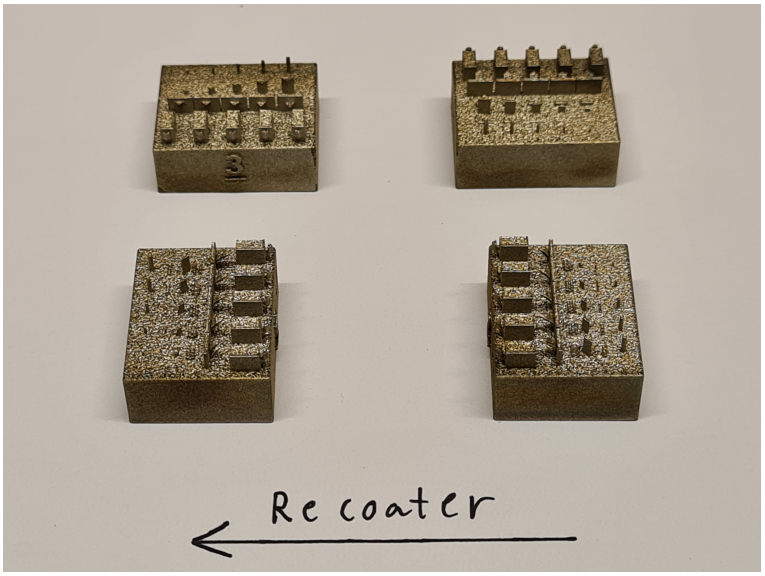

Figure A.26: Sixth print of the artefact model where the recoating direction is shown and the orientation number from bottom left is 1, 2, 3 and 4 for each artefact.

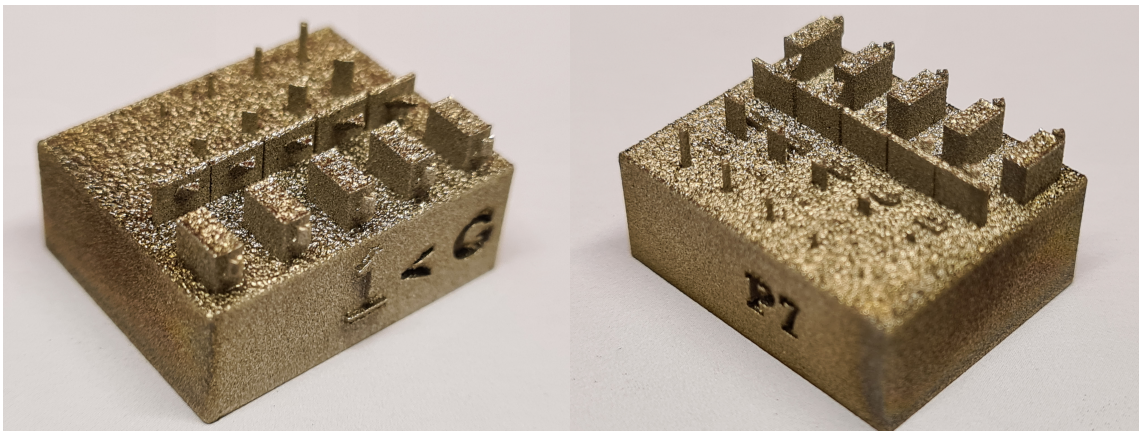

(a) Front-view of the artefact. **(b)** Back-view of the artefact.

Figure A.27: Front- and back -view of the artefact printed in orientation 1.

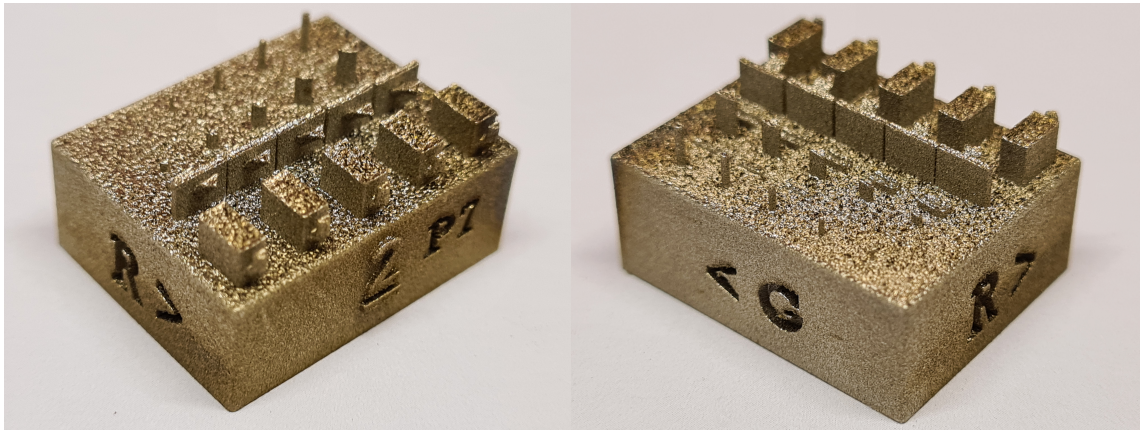

(a) Front-view of the artefact. **(b)** Back-view of the artefact.

Figure A.28: Front- and back -view of the artefact printed in orientation 2.

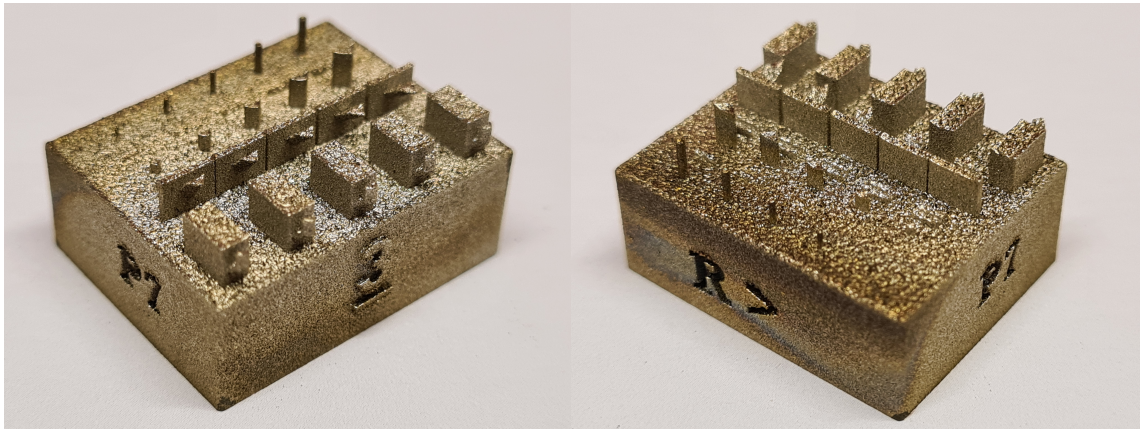

(a) Front-view of the artefact. **(b)** Back-view of the artefact.

Figure A.29: Front- and back -view of the artefact printed in orientation 3.

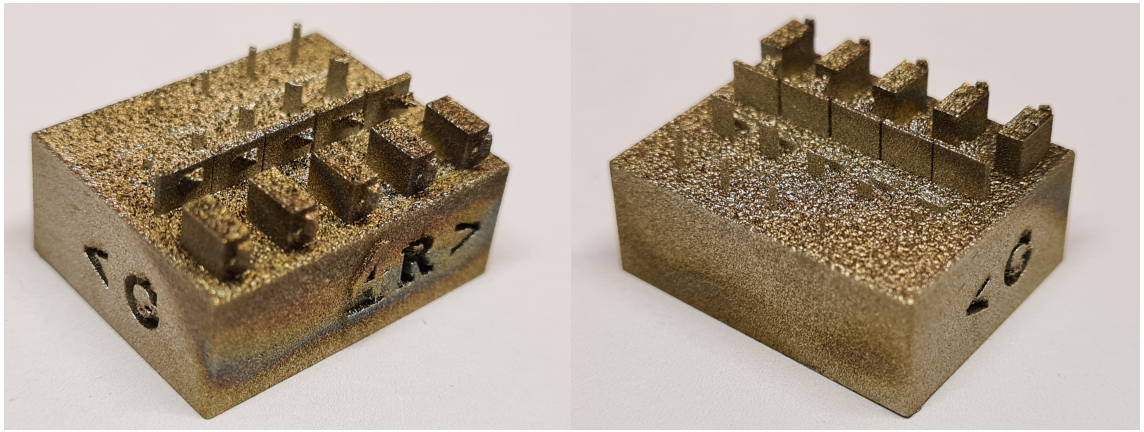

(a) Front-view of the artefact. **(b)** Back-view of the artefact.

Figure A.30: Front- and back -view of the artefact printed in orientation 4.

A.7 Seventh print EOS M100 30% scan-speed

It can be seen in the figures that the surface of the artefacts are rough. Furthermore can it be sen that powder is un-fused causing the artefacts to crack, however were the features on top of the artefacts intact. A closer view of each artefact can be found in Figure A.32, A.33, A.34 and A.35.

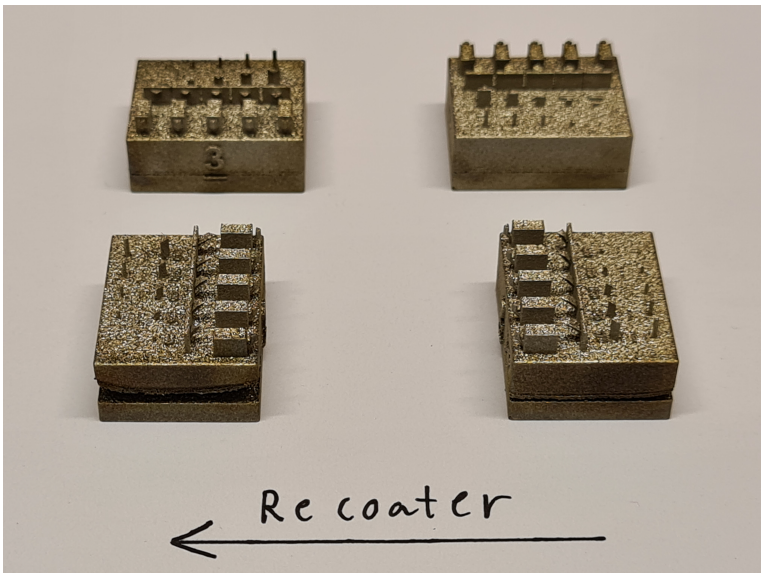

Figure A.31: Seventh print of the artefact model where the recoating direction is shown and the orientation number from bottom left is 1, 2, 3 and 4 for each artefact.

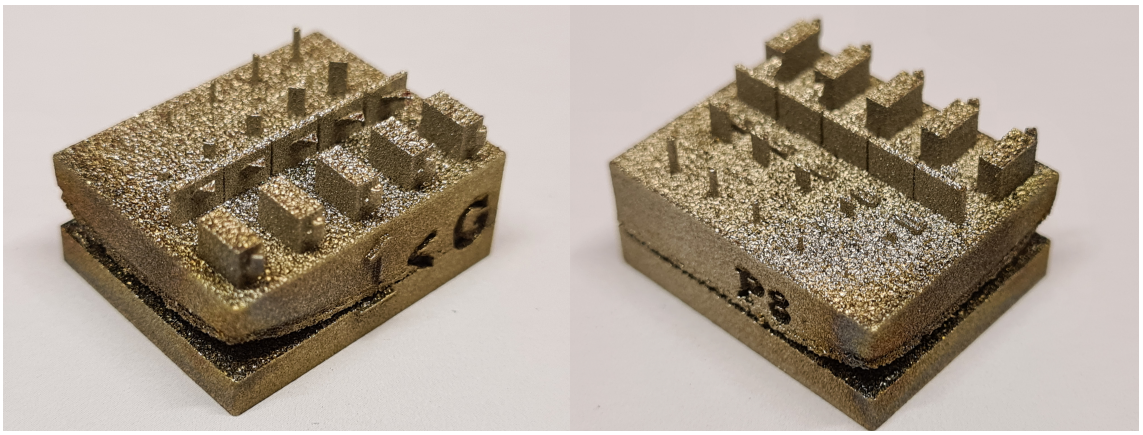

(a) Front-view of the artefact. **(b)** Back-view of the artefact.

Figure A.32: Front- and back -view of the artefact printed in orientation 1.

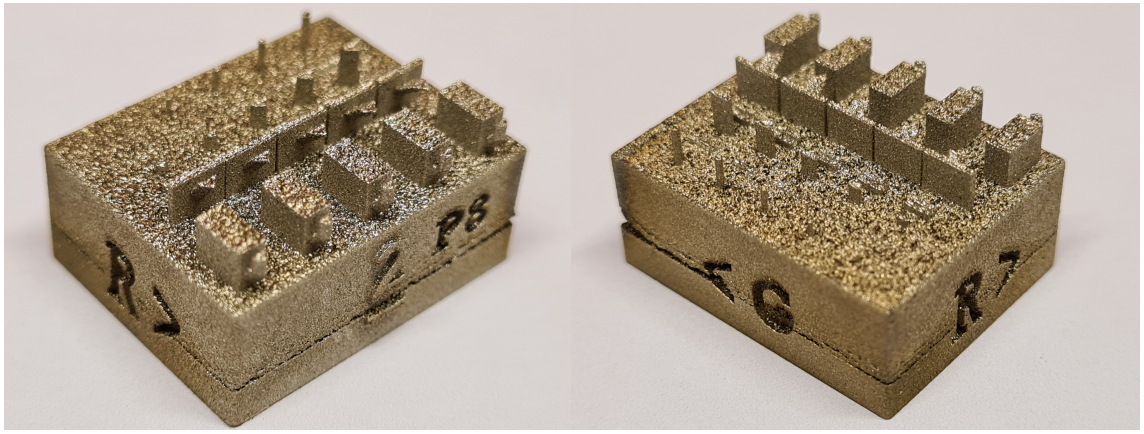

(a) Front-view of the artefact. **(b)** Back-view of the artefact.

Figure A.33: Front- and back -view of the artefact printed in orientation 2.

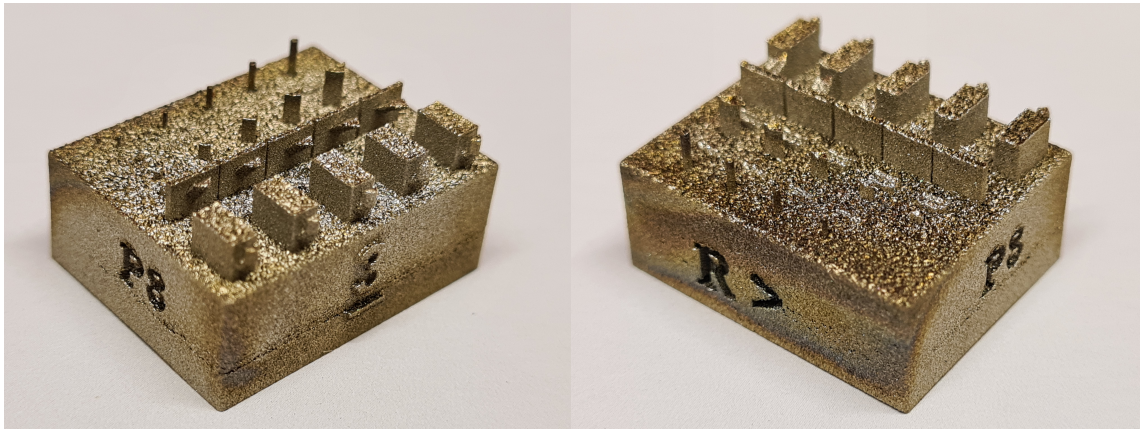

(a) Front-view of the artefact. **(b)** Back-view of the artefact.

Figure A.34: Front- and back -view of the artefact printed in orientation 3.

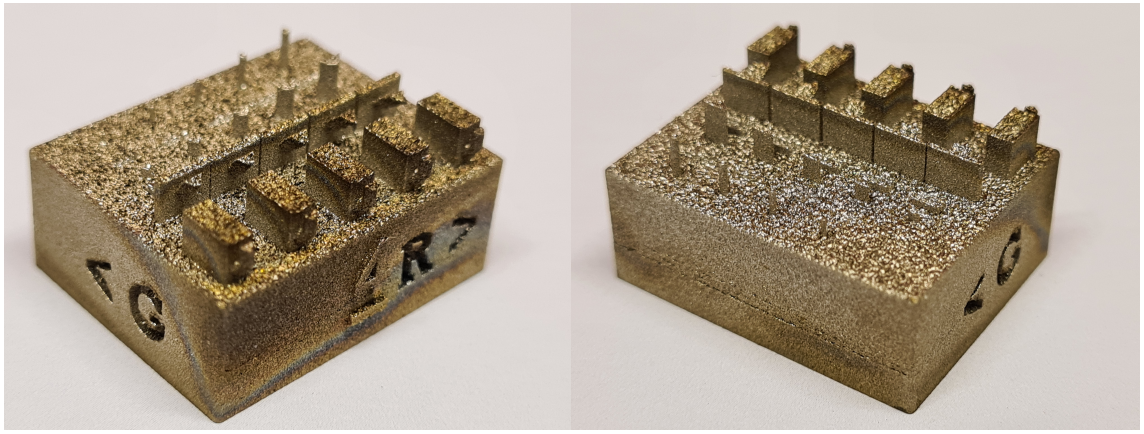

(a) Front-view of the artefact. **(b)** Back-view of the artefact.

Figure A.35: Front- and back -view of the artefact printed in orientation 4.

A.8 Eight print EOS M100 50% scan-speed

It can be seen that the artefacts in this print has the lowest surface roughness among the scan speed prints. From the figure can it be seen that the artefacts have higher surface roughness than previous 20μm prints. A closer view of each artefact can be found in Figure A.37, A.38, A.39 and A.40.

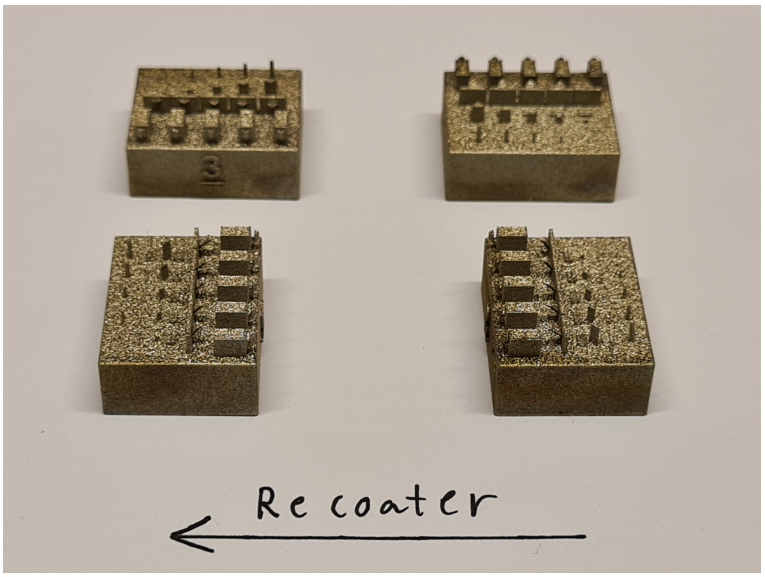

Figure A.36: Eight print of the artefact model where the recoating direction is shown and the orientation number from bottom left is 1, 2, 3 and 4 for each artefact.

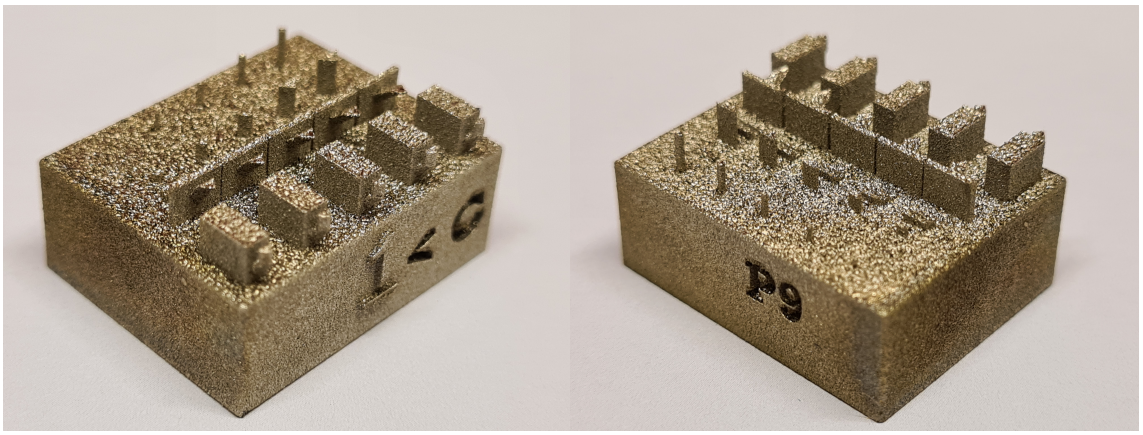

(a) Front-view of the artefact. **(b)** Back-view of the artefact.

Figure A.37: Front- and back -view of the artefact printed in orientation 1.

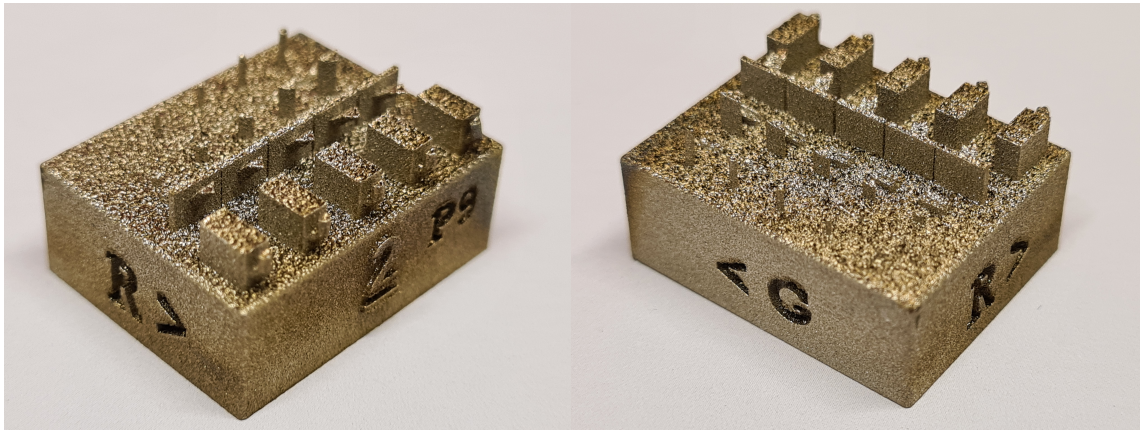

(a) Front-view of the artefact. **(b)** Back-view of the artefact.

Figure A.38: Front- and back -view of the artefact printed in orientation 2.

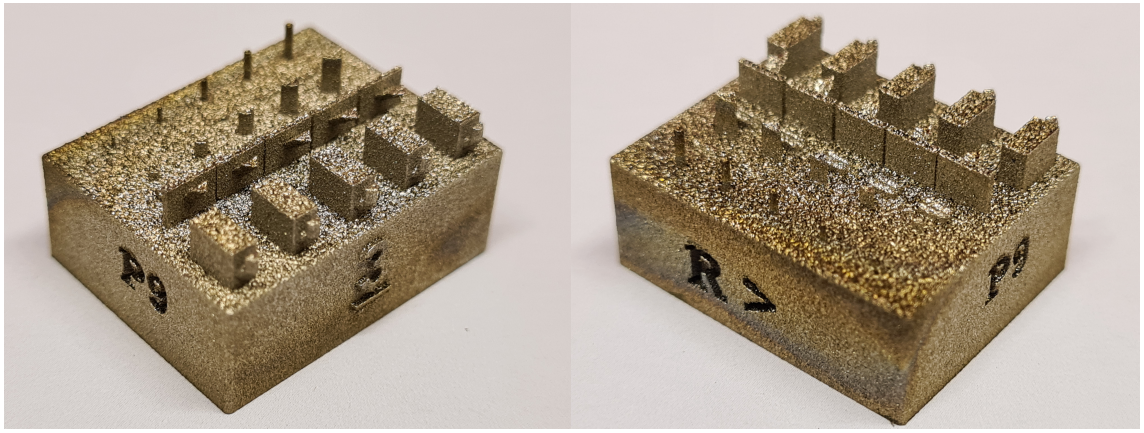

(a) Front-view of the artefact. **(b)** Back-view of the artefact.

Figure A.39: Front- and back -view of the artefact printed in orientation 3.

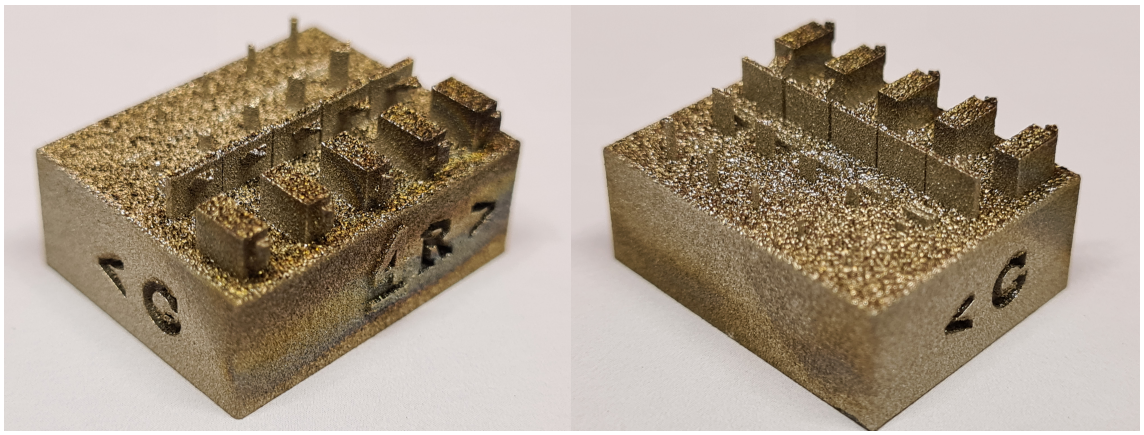

(a) Front-view of the artefact. **(b)** Back-view of the artefact.

Figure A.40: Front- and back -view of the artefact printed in orientation 4.

A.9 Ninth print repeatability of fourth print

It can be seen that the artefacts in this print resembles print 4 in terms of surface finish, however are cracks present. A closer view of each artefact can be found in Figure A.42, A.43, A.44 and A.45.

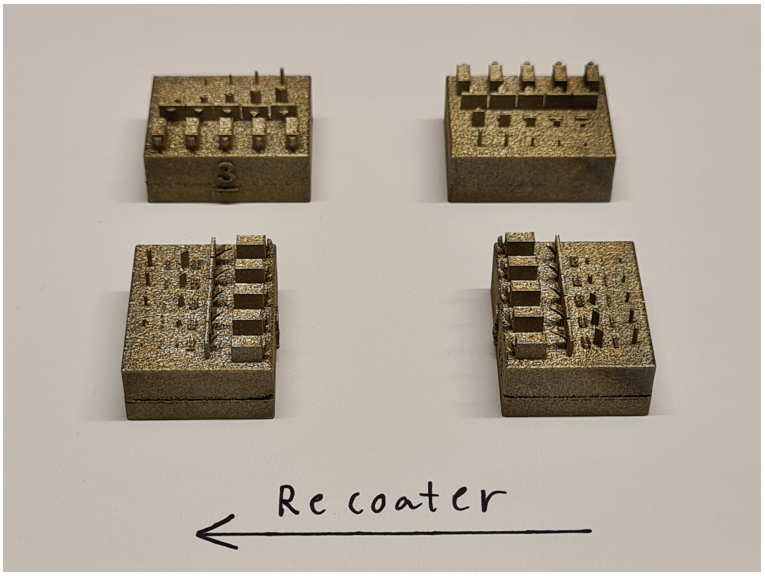

Figure A.41: Ninth print of the artefact model where the recoating direction is shown and the orientation number from bottom left is 1, 2, 3 and 4 for each artefact.

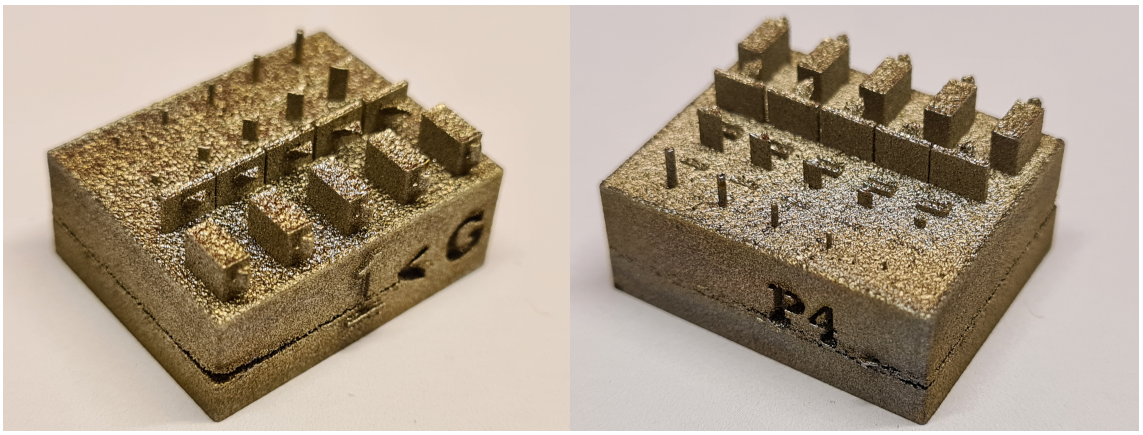

(a) Front-view of the artefact. **(b)** Back-view of the artefact.

Figure A.42: Front- and back -view of the artefact printed in orientation 1.

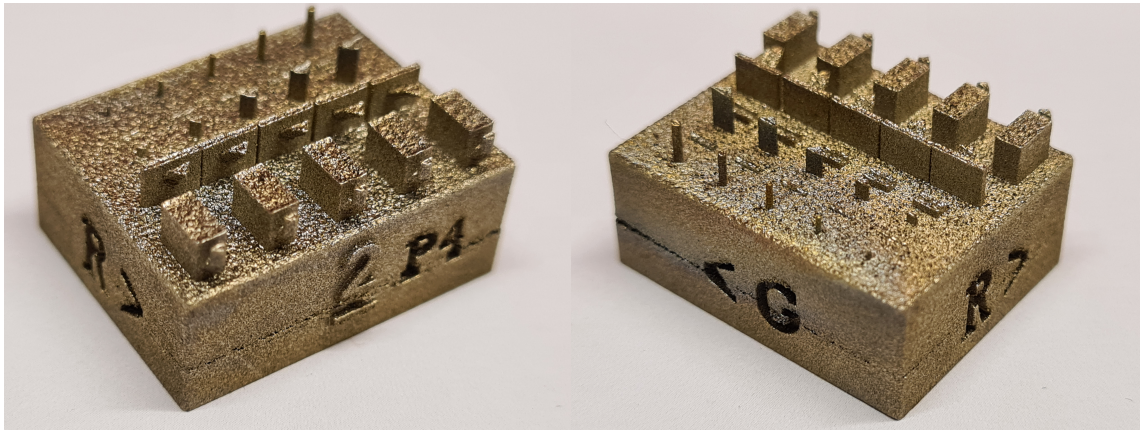

(a) Front-view of the artefact. **(b)** Back-view of the artefact.

Figure A.43: Front- and back -view of the artefact printed in orientation 2.

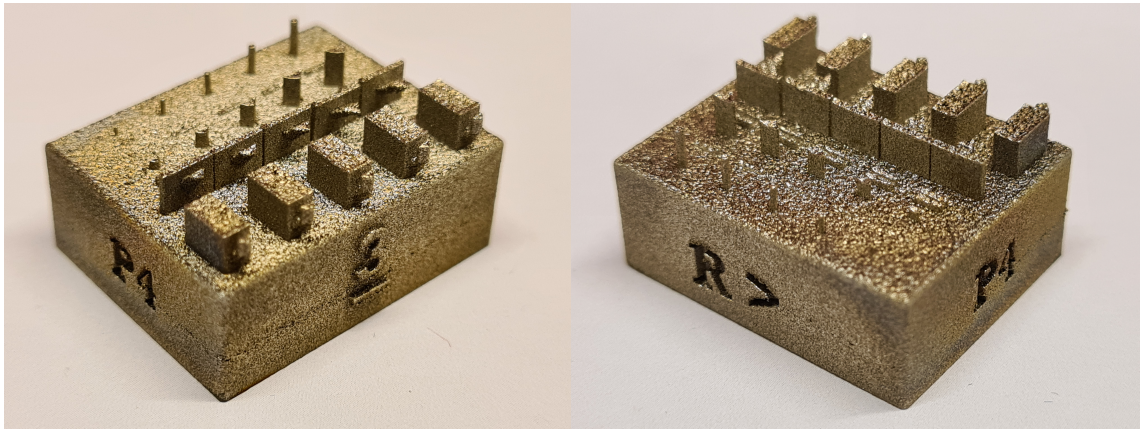

(a) Front-view of the artefact. **(b)** Back-view of the artefact.

Figure A.44: Front- and back -view of the artefact printed in orientation 3.

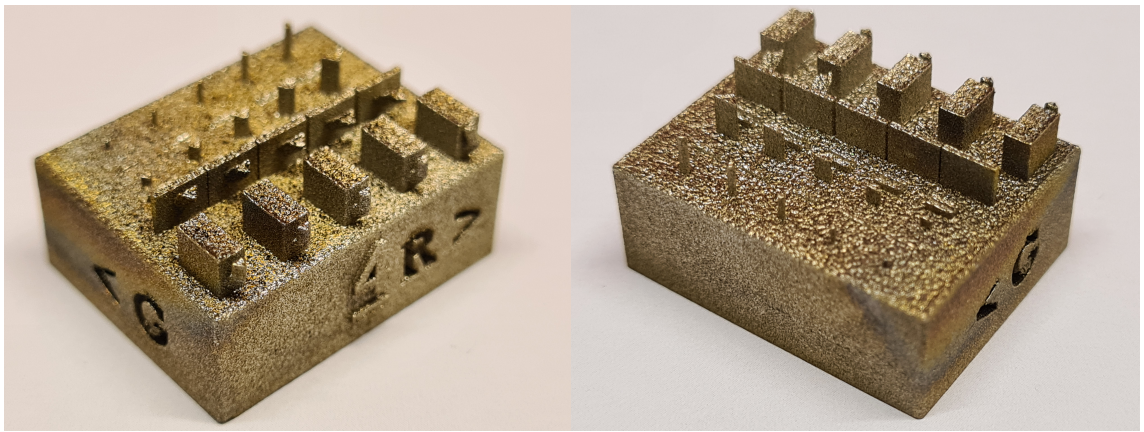

(a) Front-view of the artefact. **(b)** Back-view of the artefact.

Figure A.45: Front- and back -view of the artefact printed in orientation 4.

A.10 Tenth print binder jetting

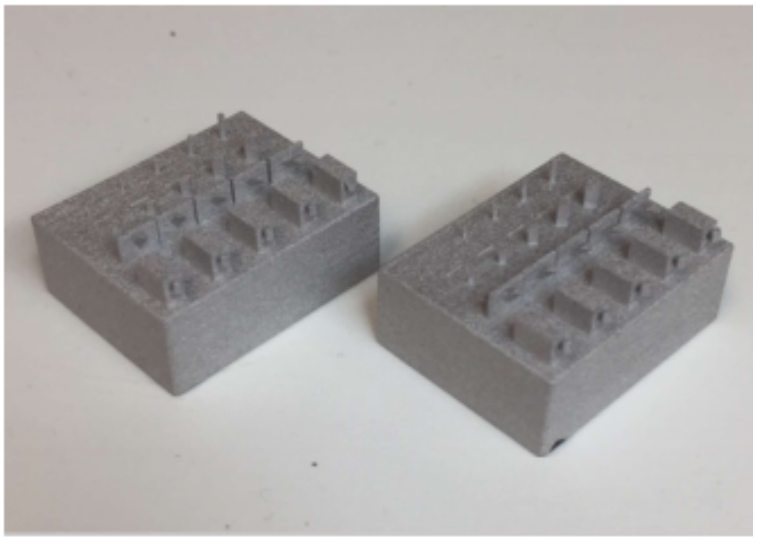

Figure A.46: Tenth print of the artefact where two artefacts were binder jetted.

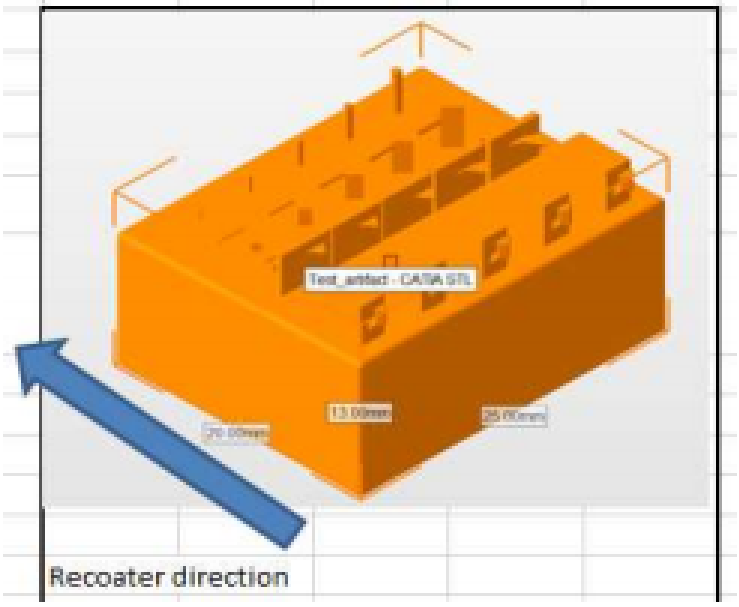

Figure A.47: Recoatin direction of the binder jetted artefacts.

Table A.1: Dimensions and weight of the binder jetted artefacts.

artefact	Measured dimensions			Weight [g]	Model dimensions		
[mm]	x	y	z		x	y	z
1	24.950	19.900	12.930	38.464	25.00	20.00	13.00
2	25.190	19.910	12,900	38.692	25.00	20.00	13.00

B

ESEM mesurements & Deviation tables

B.1 Pins

Pins which represent the fillets in the arrow are analyzed below for each print individually and finally a graph represents a pattern in the prints through which the process parameter is identified for each feature size.

- **Print 1**

  In the orientation 1, pin with radius 0.1 mm was not printed and pin with 0.2 mm radius is bent. In orientation 2, pin with 0.2 mm radius has 2 pins attached together while 0.25 mm and 0.3 mm are bent. In orientation 3, 0.25 mm print is bent. In orientation 4, 0.2 mm and 0.3 mm are bent. The possible cause could be of re-coater issues. The shapes of these pins were highly oval in nature. These issues in different pin sizes and shapes of the pins and the measurements can be seen from the Figure B.1.

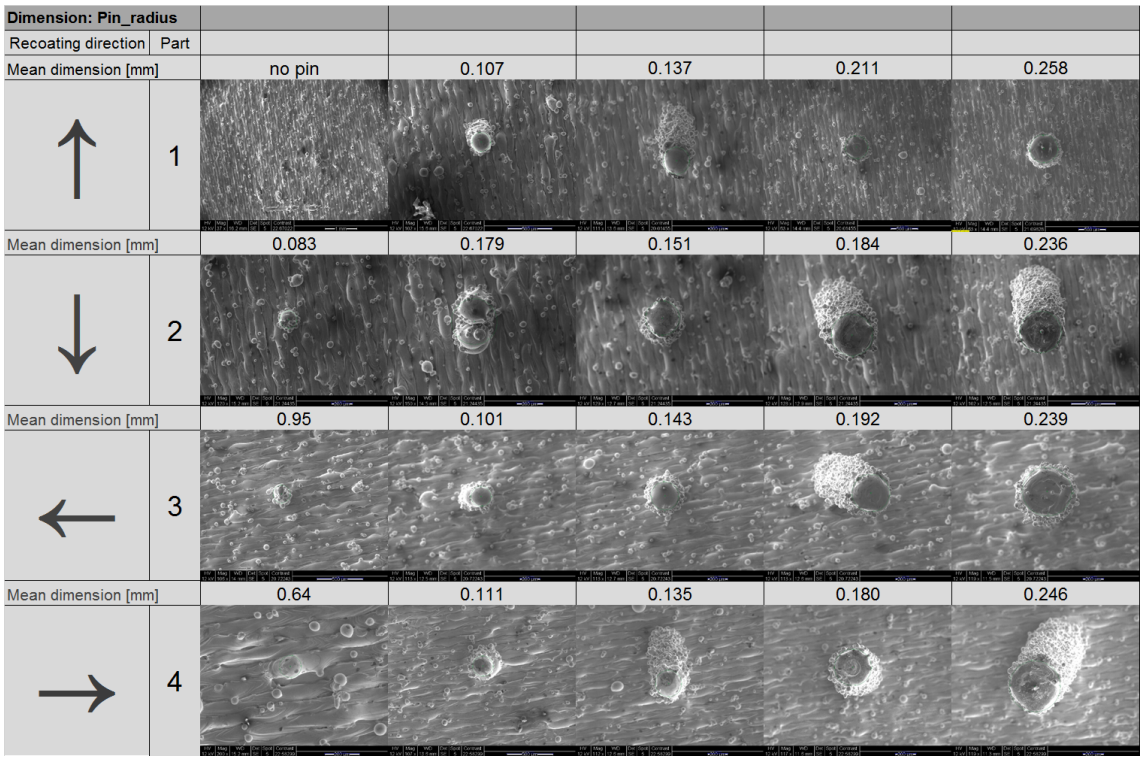

Figure B.1: ESEM images of pins of print 1.

Table B.1: Deviation of the pins for print 1.

Pin [r]	**0.1**		**0.15**		**0.2**		**0.25**		**0.3**	
Re-coat	[mm]	[%]	[mm]	[%]	[mm]	[%]	[mm]	[%]	[mm]	[%]
↑			-0.043	-28.66	-0.063	-31.5	-0.039	-15.6	-0.042	-14
↓	-0.02	-17	0.029	19.33	-0.049	-24.5	-0.066	-26.4	-0.064	-21.33
←	-0.01	-5	-0.049	-32.66	-0.057	-28.5	-0.058	-23.2	-0.061	-20.33
→	-0.036	-36	-0.039	-26	-0.065	-32.5	-0.07	-28	-0.054	-18

- **Print 2**

  In the orientation 1, pin with radius 0.15 mm is bent. In orientation 3, pin with 0.15 mm radius and 0.2 mm are bent. In orientation 3, 0.25 mm print is bent. In orientation 4, 0.2 mm and 0.3 mm are bent. The possible cause could be of re-coater issues. The shapes of these pins were circular in nature except for the pins with radius less than or equal to 0.15 mm in all the orientations. These issues in different pin sizes and shapes of the pins can be seen from the Figure B.2. The Table B.2 below shows the deviation of the pins with respect to the original CAD dimension.

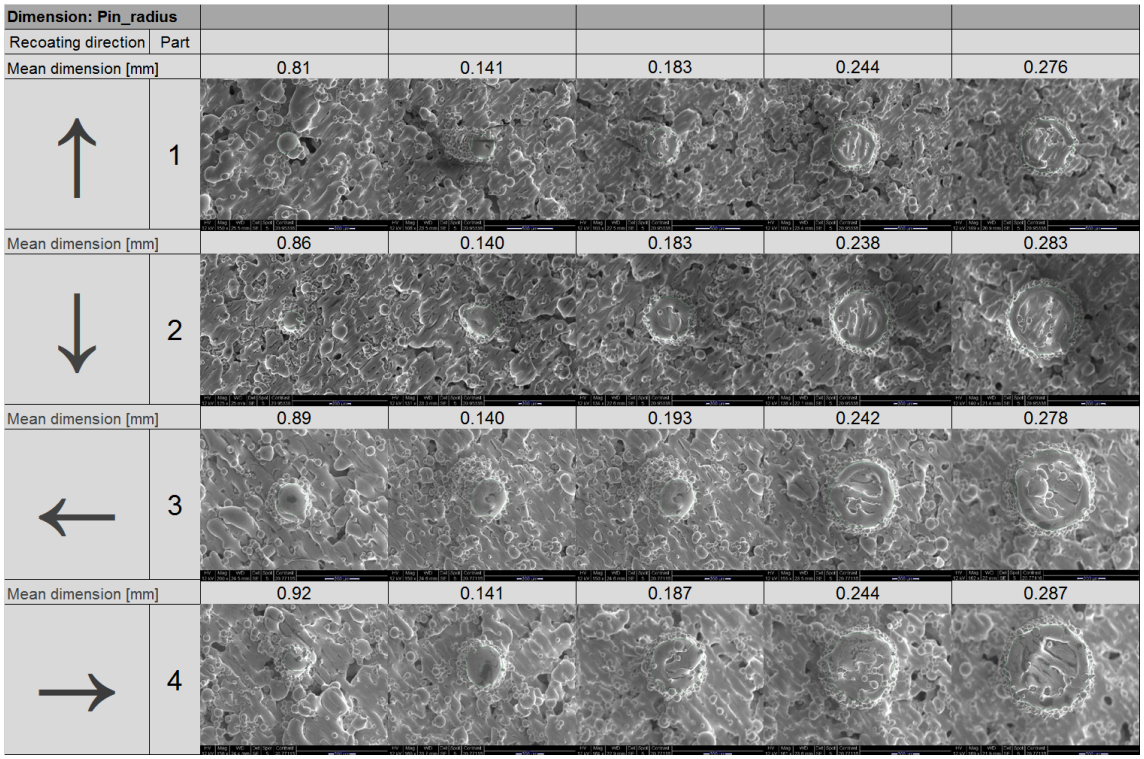

Figure B.2: ESEM images of pins of print 2.

Table B.2: Deviation of the pins for print 2.

Pin [r]	**0.1**		**0.15**		**0.2**		**0.25**		**0.3**	
Re-coat	[mm]	[%]	[mm]	[%]	[mm]	[%]	[mm]	[%]	[mm]	[%]
↑	-0.019	-19	-0.009	-6	-0.017	-8.5	-0.006	-2.4	-0.024	-8
↓	-0.014	-14	-0.01	-6.67	-0.017	-8.5	-0.012	-4.8	-0.017	-5.67
←	-0.011	-11	-0.01	-6.67	-0.007	-3.5	-0.008	-3.2	-0.022	-7.33
→	-0.008	-8	-0.009	-6	-0.013	-6.5	-0.006	-2.4	-0.013	-4.33

- **Print 3**

  In the orientation 1, pin with radius 0.1 mm was printed but had large size of half molten particle attached. In orientation 3 and orientation 4, pin with 0.1 mm radius and pin with 0.15 mm radius has high ovality shape. In orientation 3, 0.25 mm print is bent. In orientation 4, 0.2 mm and 0.3 mm are bent. These issues in different pin sizes and shapes of the pins can be seen from the Figure B.3. The Table B.3 below shows the deviation of the pins with respect to the original CAD dimension.

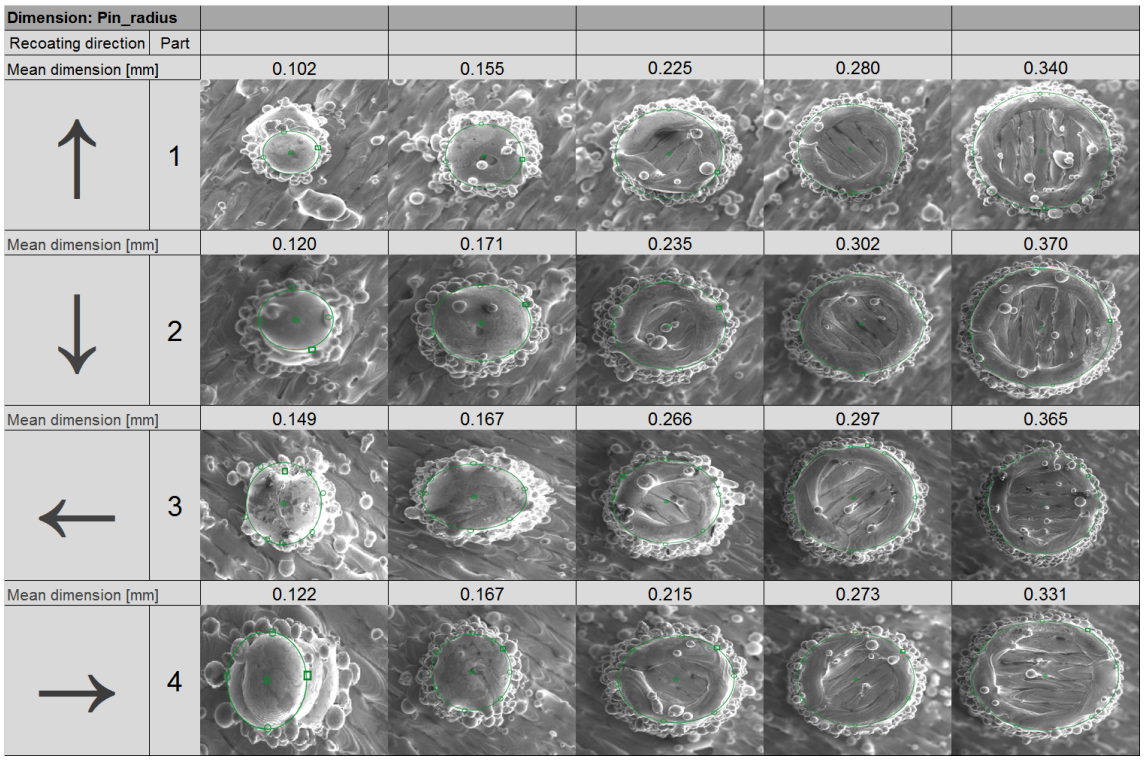

Figure B.3: ESEM images of pins of print 3.

Table B.3: Deviation of the pins for print 3.

Pin [r]	**0.1**		**0.15**		**0.2**		**0.25**		**0.3**	
Re-coat	[mm]	[%]	[mm]	[%]	[mm]	[%]	[mm]	[%]	[mm]	[%]
↑	0.002	0.005	0.005	3.33	0.025	12.5	0.03	12	0.04	13.33
↓	0.02	20	0.021	14	0.035	17.5	0.052	20.8	0.07	23.33
←	0.049	49	0.017	11.33	0.066	33	0.047	18.8	0.065	21.66
→	0.022	22	0.017	11.33	0.015	7.5	0.023	9.2	0.031	10.33

- **Print 4**

  In the orientation 3, pin with radius 0.1 mm has two pins attached. In orientation 4, the pin with radius 0.1 mm has too many half melted particles making the pin look bigger. The shapes of these pins were circular except few 0.1 mm radius pins. These issues in different pin sizes and shapes of the pins can be seen from the Figure B.4. The Table B.4 below shows the deviation of the pins with respect to the original CAD dimension.

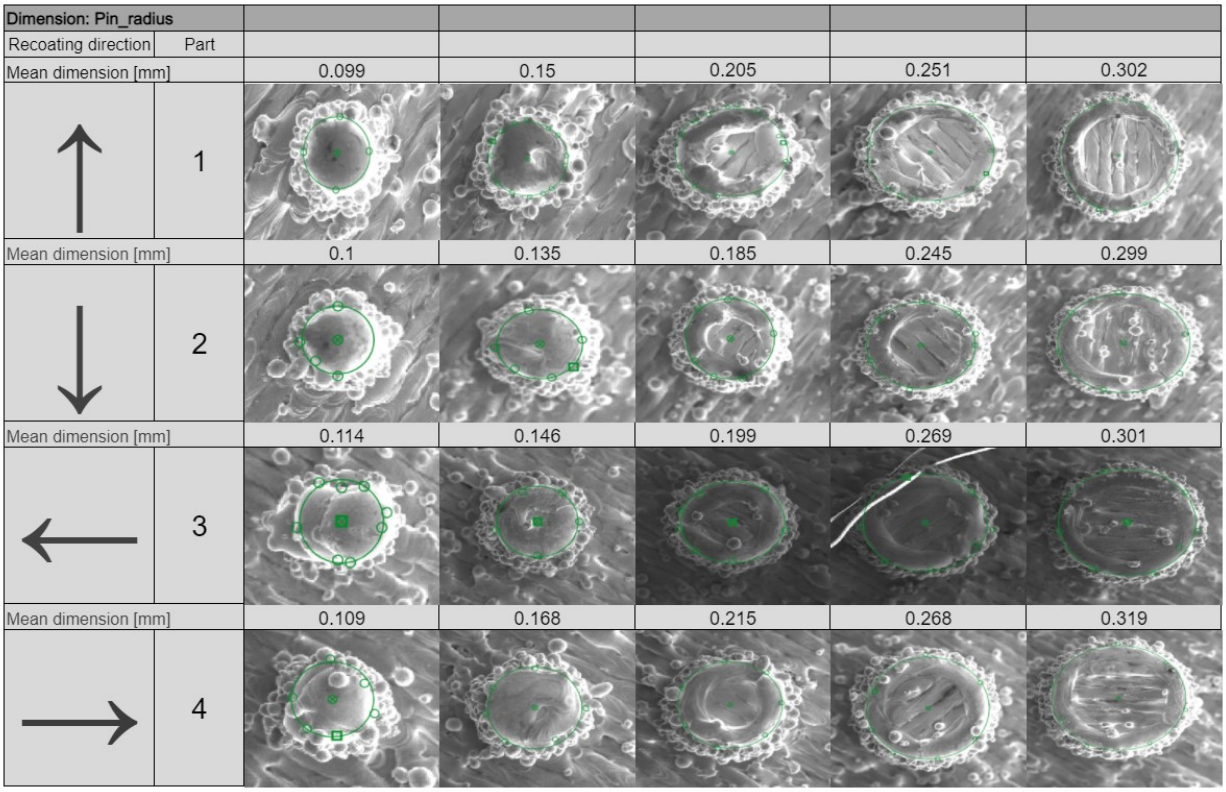

Figure B.4: ESEM images of pins of print 4.

Table B.4: Deviation of the pins for print 4.

Pin [r]	**0.1**		**0.15**		**0.2**		**0.25**		**0.3**	
Re-coat	[mm]	[%]	[mm]	[%]	[mm]	[%]	[mm]	[%]	[mm]	[%]
↑	-0.001	-1	0	0	0.005	2.5	0.001	0.4	0.002	0.66
↓	0	0	-0.015	-10	-0.015	-7.5	-0.005	-2	-0.001	-0.33
←	0.014	14	-0.004	-2.66	-0.001	-0.5	0.019	7.6	0.001	0.33
→	0.009	9	0.018	12	0.015	7.5	0.018	7.2	0.019	6.33

- **Print 5**

  In the orientation 3, pin with radius 0.1 mm has two pins attached. In orientation 2 and orientation 4, the pin with radius 0.1 mm has too many half melted particles making the pin look bigger and distorted. The shapes of all pins were circular. These issues in different pin sizes and shapes of the pins can be seen from the Figure B.5. The Table B.5 below shows the deviation of the pins with respect to the original CAD dimension.

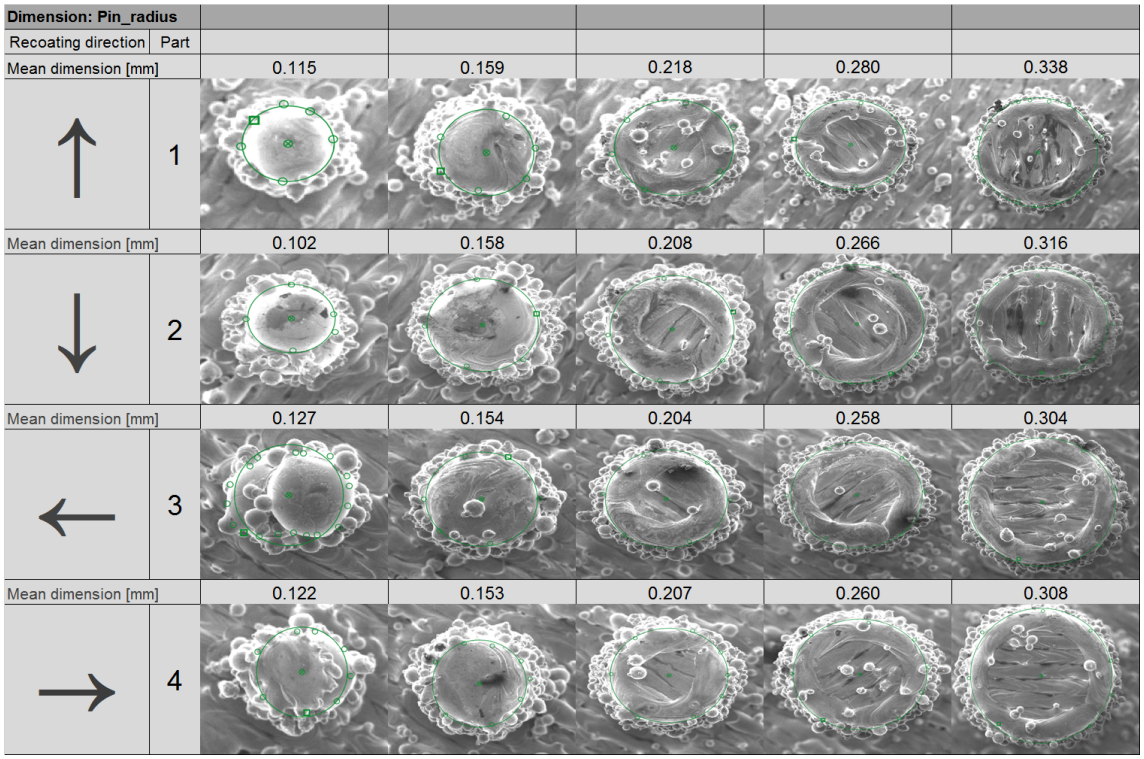

Figure B.5: ESEM images of pins of print 5.

Table B.5: Deviation of the pins for print 5.

Pin [r]	**0.1**		**0.15**		**0.2**		**0.25**		**0.3**	
Re-coat	[mm]	[%]	[mm]	[%]	[mm]	[%]	[mm]	[%]	[mm]	[%]
↑	0.02	15	0.009	6	0.018	9	0.03	12	0.038	12.66
↓	0.00	2	0.008	5.33	0.008	4	0.016	6.4	0.016	5.33
←	0.03	27	0.004	2.66	0.004	2	0.008	3.2	0.004	1.33
→	0.022	22	0.003	2	0.007	3.5	0.01	4	0.008	2.66

- **Print 6**

  In all the orientations, pins with radius 0.1 mm has large sized half melted particles making the pin shape look bigger. In orientation 3, pin with 0.1 mm radius has 2 pins attached together. In orienation 2, pin with 0.3 mm radius has a black shade on the top surface. Moreover small sized pores can be observed in the print. The shapes of these pins were approximately circular in nature. These issues in different pin sizes and shapes of the pins can be seen from the Figure B.6. The Table B.6 below shows the deviation of the pins with respect to the original CAD dimension.

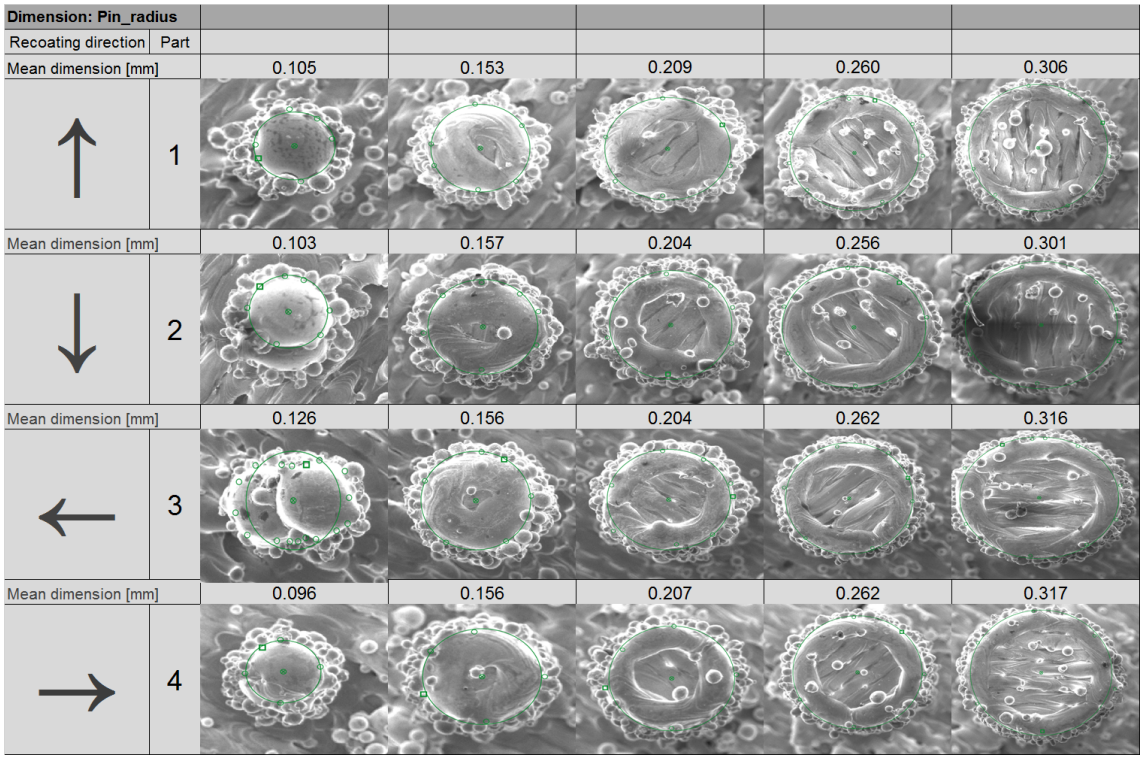

Figure B.6: ESEM images of pins of print 6.

Table B.6: Deviation of the pins for print 6.

Pin [r]	**0.1**		**0.15**		**0.2**		**0.25**		**0.3**	
Re-coat	[mm]	[%]	[mm]	[%]	[mm]	[%]	[mm]	[%]	[mm]	[%]
↑	0.00	5	0.003	2	0.009	4.5	0.01	4	0.006	2
↓	0.00	3	0.007	4.66	0.004	2	0.006	2.4	0.001	0.33
←	0.03	26	0.006	4	0.004	2	0.012	4.8	0.016	5.33
→	0.00	-4	0.006	4	0.007	3.5	0.012	4.8	0.017	5.66

- **Print 7**

  In the orientation 1, pin with radius 0.1 mm has half melted particles attached but the shapes are better than the previous prints. The shapes of these pins are circular. There are pores present in the print which is bigger than the previous print and presence of black shades can be seen in 0.25 mm radius pin in orientation 4. These issues in different pin sizes and shapes of the pins can be seen from the Figure B.7. The Table B.7 below shows the deviation of the pins with respect to the original CAD dimension.

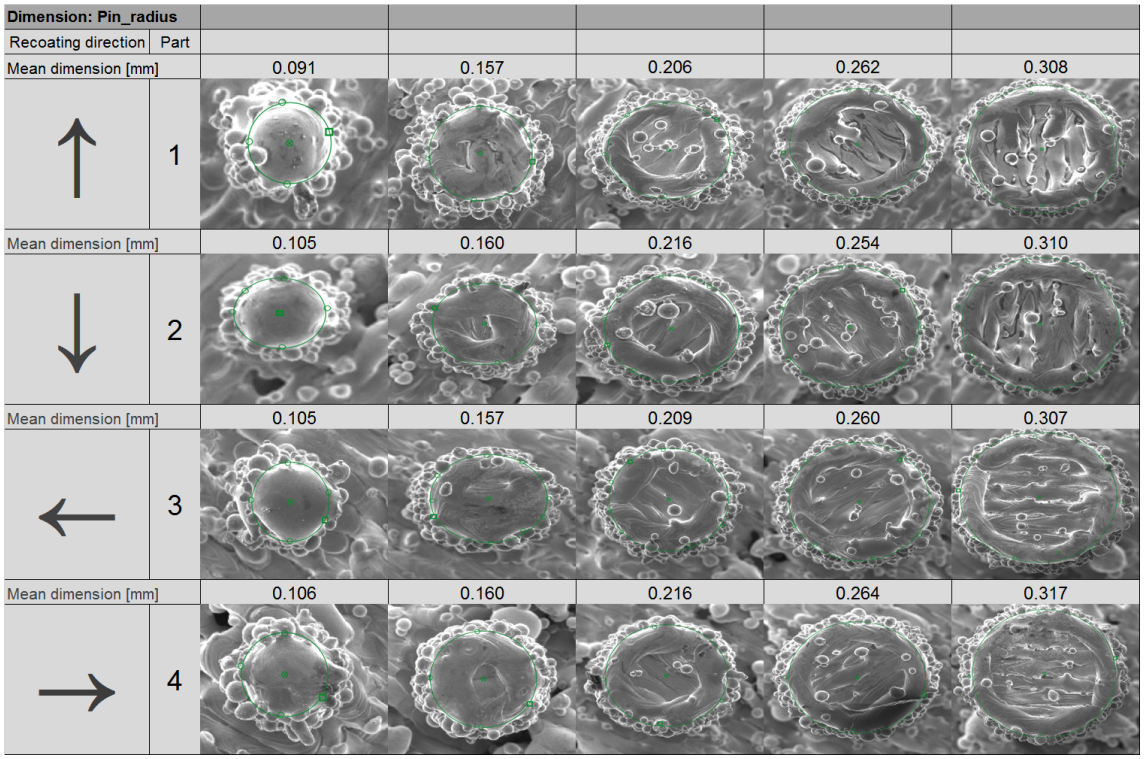

Figure B.7: ESEM images of pins of print 7.

Table B.7: Deviation of the pins for print 7.

Pin [r]	0.1		0.15		0.2		0.25		0.3	
Re-coat	[mm]	[%]	[mm]	[%]	[mm]	[%]	[mm]	[%]	[mm]	[%]
↑	-0.01	-9	0.007	4.66	0.006	3	0.012	4.8	0.008	2.66
↓	0.00	5	0.01	6.66	0.016	8	0.004	1.6	0.01	3.33
←	0.00	5	0.007	4.66	0.009	4.5	0.01	4	0.007	2.33
→	0.006	6	0.01	6.66	0.016	8	0.014	5.6	0.017	5.66

- **Print 8**

  In the orientation 1, pin with radius 0.3 mm is bent.In orientation 2, pin with 0.3 mm radius is bent. In orientation 2 and orientation 3, pins with 0.1 mm radius has big half melted particles attached. In orientation 3, 0.25 mm print is bent. In orientation 4, pin with radius 0.1 mm has two pins attached together. The shapes of these pins were highly oval in nature. These issues in different pin sizes and shapes of the pins can be seen from the Figure B.8. The Table B.8 below shows the deviation of the pins with respect to the original CAD dimension.

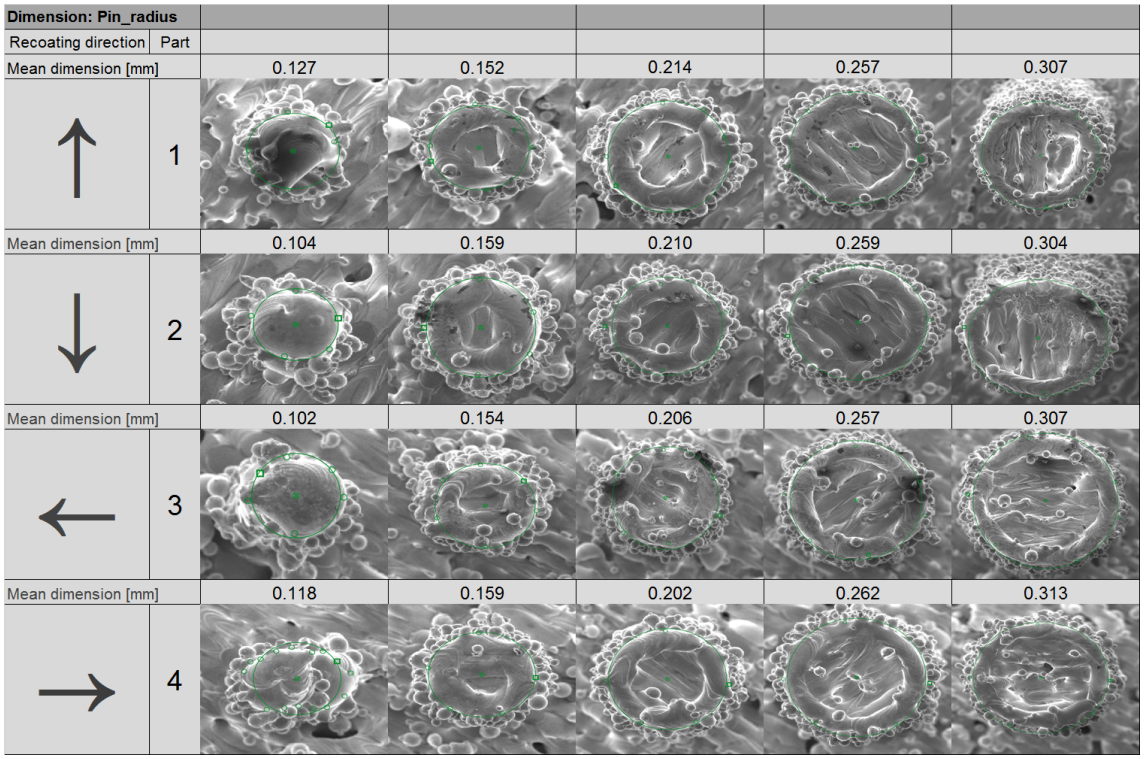

Figure B.8: ESEM images of pins of print 8.

Table B.8: Deviation of the pins for print 8.

Pin [r]	**0.1**		**0.15**		**0.2**		**0.25**		**0.3**	
Re-coat	[mm]	[%]	[mm]	[%]	[mm]	[%]	[mm]	[%]	[mm]	[%]
↑	0.03	27	0.002	1.33	0.014	7	0.007	2.8	0.007	2.33
↓	0.00	4	0.009	6	0.01	5	0.009	3.6	0.004	1.33
←	0.00	2	0.004	2.66	0.006	3	0.007	2.8	0.007	2.33
→	0.018	18	0.009	6	0.002	1	0.012	4.8	0.013	4.33

- **Print 9**

  In all the orientations, pins with 0.1 mm radius has big half melted particles attached. In orientation 4, pin with radius 0.1 mm has two pins attached together. The shapes of these pins were highly circular in nature. These issues in different pin sizes and shapes of the pins can be seen from the Figure B.9. The Table B.9 below shows the deviation of the pins with respect to the original CAD dimension.

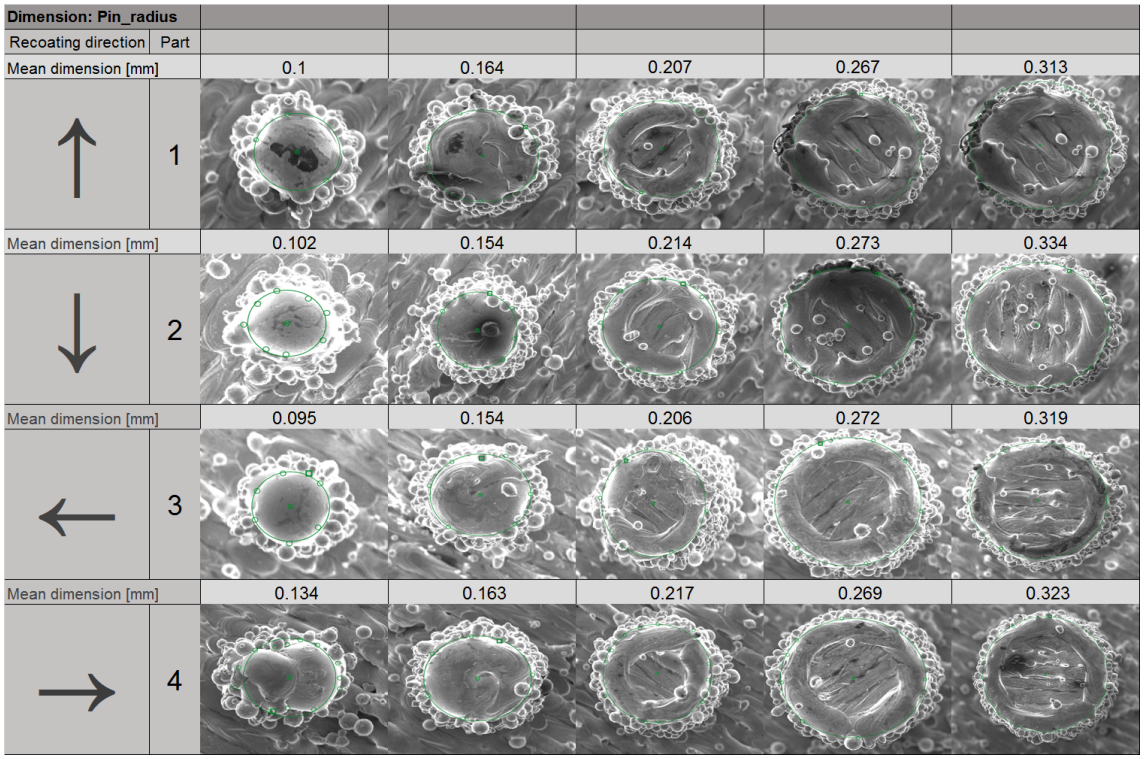

Figure B.9: ESEM images of the pins for print 9.

Table B.9: Deviation of the pins for print 9.

Pin [r]	0.1		0.15		0.2		0.25		0.3	
Re-coat	[mm]	[%]	[mm]	[%]	[mm]	[%]	[mm]	[%]	[mm]	[%]
↑	0.000	0.00	0.014	9.33	0.007	3.50	0.017	5.67	0.013	4.33
↓	0.002	2.00	0.004	2.67	0.014	7.00	0.023	7.67	0.034	11.33
←	-0.005	-5.00	0.004	2.67	0.006	3.00	0.022	7.33	0.019	6.33
→	0.034	34.00	0.013	8.67	0.017	8.50	0.019	6.33	0.023	7.67

- **Print 10**

  All the pins are highly bent. The resolution of pins are low but they are circular in shape. There are presence of pores in the print. These issues in different pin sizes and shapes of the pins can be seen from the Figure B.10. The Table B.10 below shows the deviation of the pins with respect to the original CAD dimension.

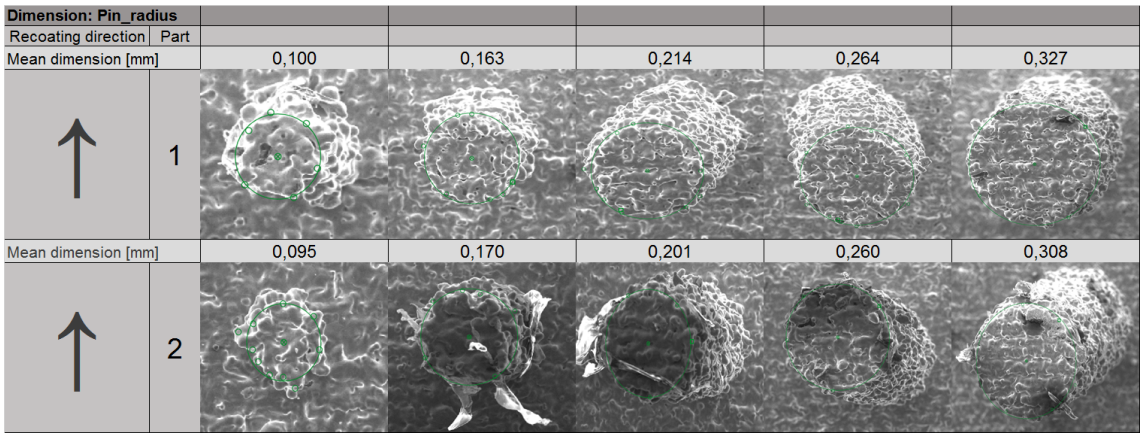

Figure B.10: ESEM images of the binder jetted pins of print 10.

Table B.10: Deviation of the pins for print 10.

Pin [r]		**0.1**		**0.15**		**0.2**		**0.25**		**0.3**	
Re-coat	Part	[mm]	[%]	[mm]	[%]	[mm]	[%]	[mm]	[%]	[mm]	[%]
↑	1	0.000	0.00	0.013	8.67	0.014	7.00	0.014	5.60	0.027	9.00
↑	2	-0.005	-5.00	0.020	13.33	0.001	0.50	0.010	4.00	0.008	2.67

B.2 Ribs

- **Print 1**

  In the orientation 1, rib with the diameter 0.2 mm is not printed properly. The edges along the length for all the ribs are not straight and contains half melted particles. These issues in different rib sizes can be seen from the Figure B.11. The Table B.11 below shows the deviation of the ribs with respect to the original CAD dimension.

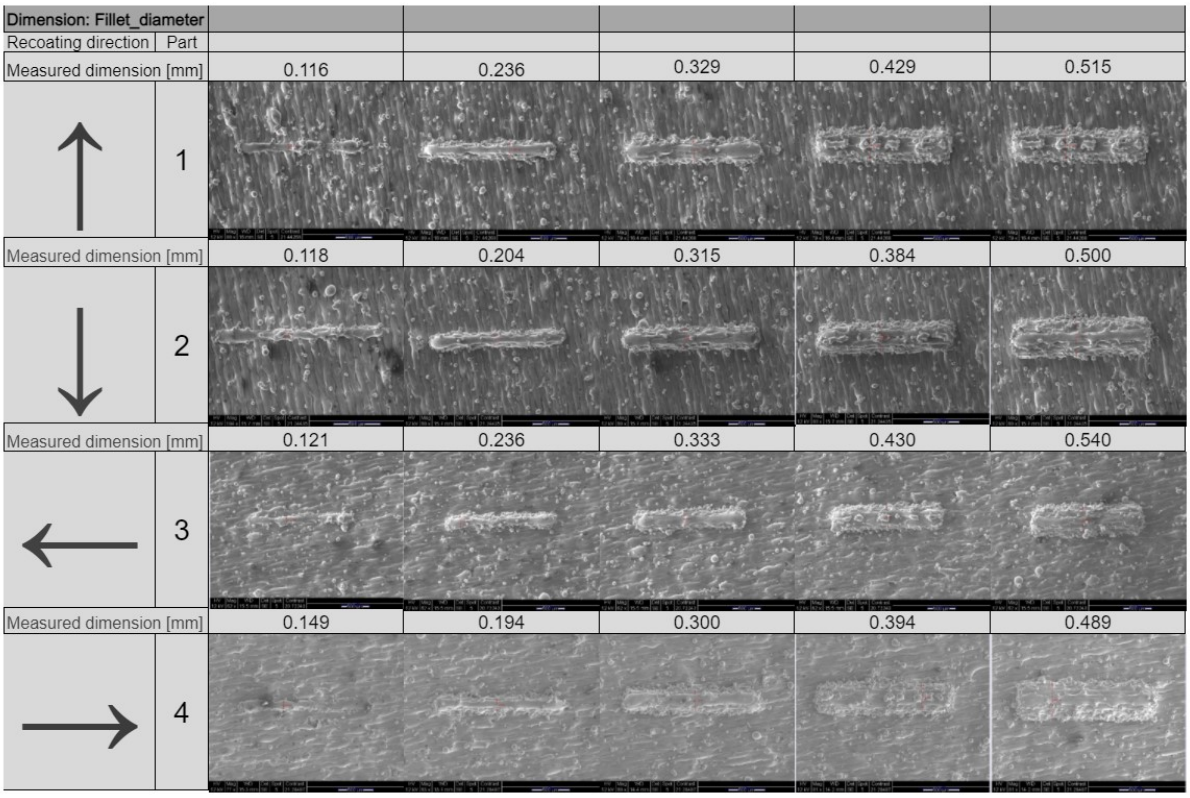

Figure B.11: ESEM images of ribs of print 1.

Table B.11: Deviation of the ribs for print 1.

Rib [ϕ]	0.2		0.3		0.4		0.5		0.6	
Re-coat	[mm]	[%]	[mm]	[%]	[mm]	[%]	[mm]	[%]	[mm]	[%]
↑	-0.084	-42	-0.064	-21.33	-0.071	-17.75	-0.071	-14.2	-0.085	-14.16
↓	-0.082	-41	-0.096	-32	-0.085	-21.25	-0.116	-23.2	-0.1	-16.66
←	-0.079	-39.5	-0.064	-21.33	-0.067	-16.75	-0.07	-14	-0.06	-10
→	-0.051	-25.5	-0.106	-35.33	-0.1	-25	-0.106	-21.2	-0.111	-18.5

- **Print 2**

  In all the orientations , rib with the diameter 0.2 mm is not printed properly. The edges along the length for all the ribs are not straight and contains half melted particles. The prints contain pores in it. A smooth curve cannot be seen in all the prints along the diameter. These issues in different rib sizes can be seen from the Figure B.12. The Table B.12 below shows the deviation of the ribs with respect to the original CAD dimension.

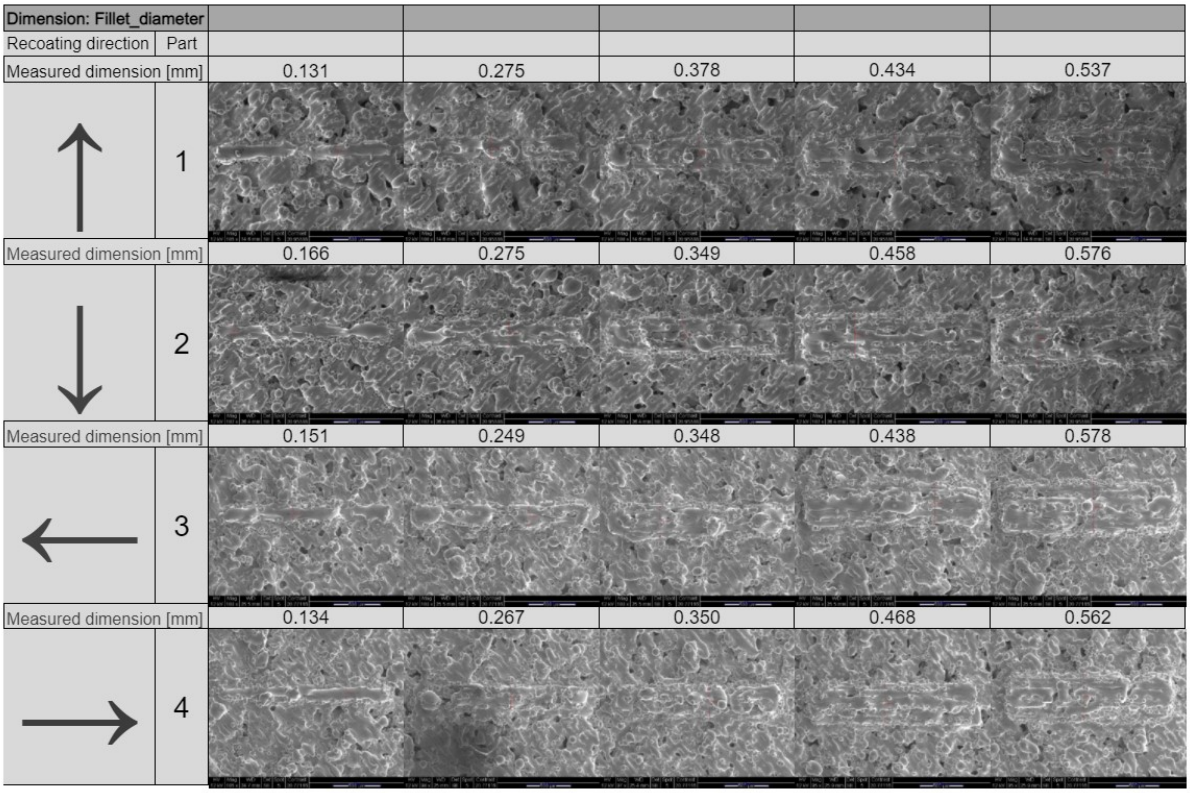

Figure B.12: ESEM images of ribs of print 2.

Table B.12: Deviation of the ribs for print 2.

Rib [ϕ]	**0.2**		**0.3**		**0.4**		**0.5**		**0.6**	
Re-coat	[mm]	[%]	[mm]	[%]	[mm]	[%]	[mm]	[%]	[mm]	[%]
↑	-0.069	-34.5	-0.025	-8.33	-0.022	-5.5	-0.066	-13.2	-0.063	-10.5
↓	-0.034	-17	-0.025	-8.33	-0.051	-12.75	-0.042	-8.4	-0.024	-4
←	-0.049	-24.5	-0.051	-17	-0.052	-13	-0.062	-12.4	-0.022	-3.66
→	-0.066	-33	-0.033	-11	-0.05	-12.5	-0.032	-6.4	-0.038	-6.33

- **Print 3**

  In all the orientations, ribs are printed. The edges along the length for the smaller diameter ribs are not straight and contains half melted particles. As the diameter increases the edges are seen straight with less deviation. A smooth curve can be seen in all the prints when compared to previous prints along the diameter. These issues in different rib sizes can be seen from the Figure B.13. The Table B.13 below shows the deviation of the ribs with respect to the original CAD dimension.

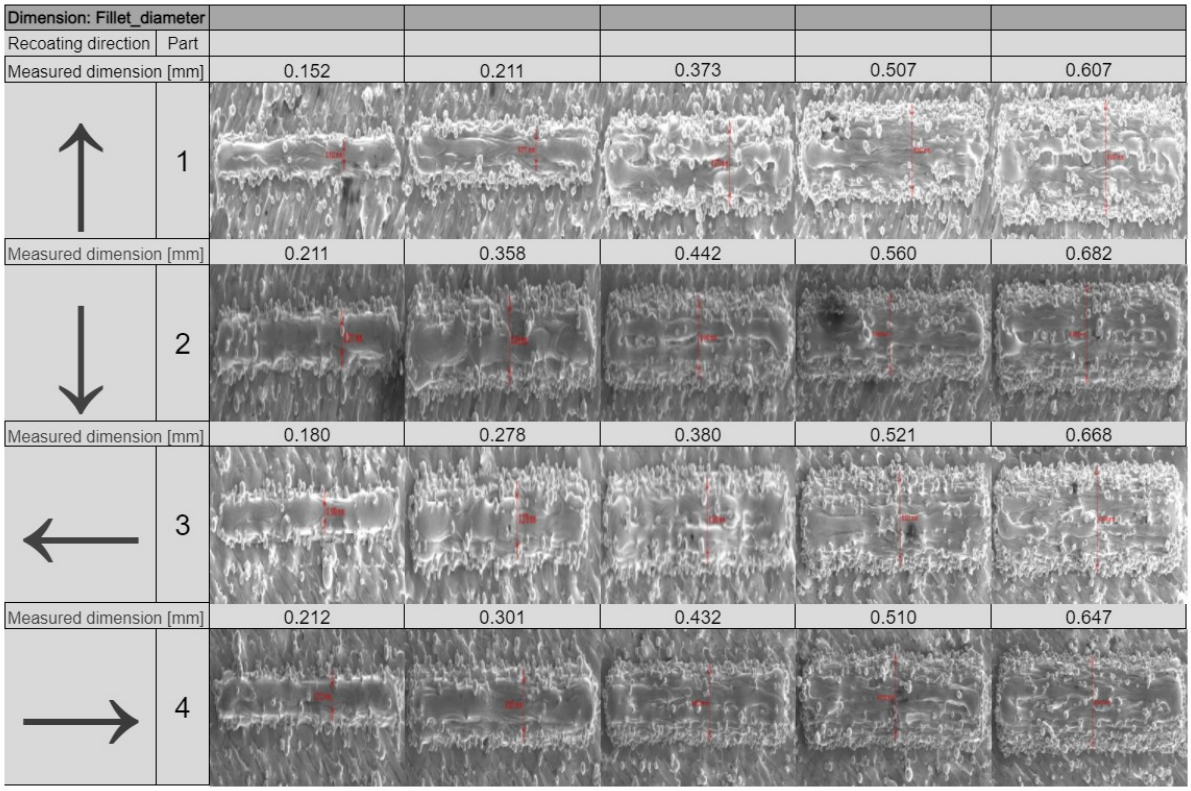

Figure B.13: ESEM images of ribs of print 3.

Table B.13: Deviation of the ribs for print 3.

Rib [ϕ]	**0.2**		**0.3**		**0.4**		**0.5**		**0.6**	
Re-coat	[mm]	[%]	[mm]	[%]	[mm]	[%]	[mm]	[%]	[mm]	[%]
↑	-0.048	-24	-0.089	-29.66	-0.027	-6.75	0.007	1.4	0.007	1.16
↓	0.011	5.5	0.058	19.33	0.042	10.5	0.06	12	0.082	13.66
←	-0.02	-10	-0.022	-7.33	-0.02	-5	0.021	4.2	0.068	11.33
→	0.012	6	0.001	0.33	0.032	8	0.01	2	0.047	7.83

- **Print 4**

  In all the orientations, ribs are printed. The edges along the length for the ribs are not perfect straight but it is better than previous prints and contains half melted particles. As the diameter increases the edges are seen straight with less deviation. A smooth curve can be seen in all the prints when compared to previous prints along the diameter. These issues in different rib sizes can be seen from the Figure B.14. The Table B.14 below shows the deviation of the ribs with respect to the original CAD dimension.

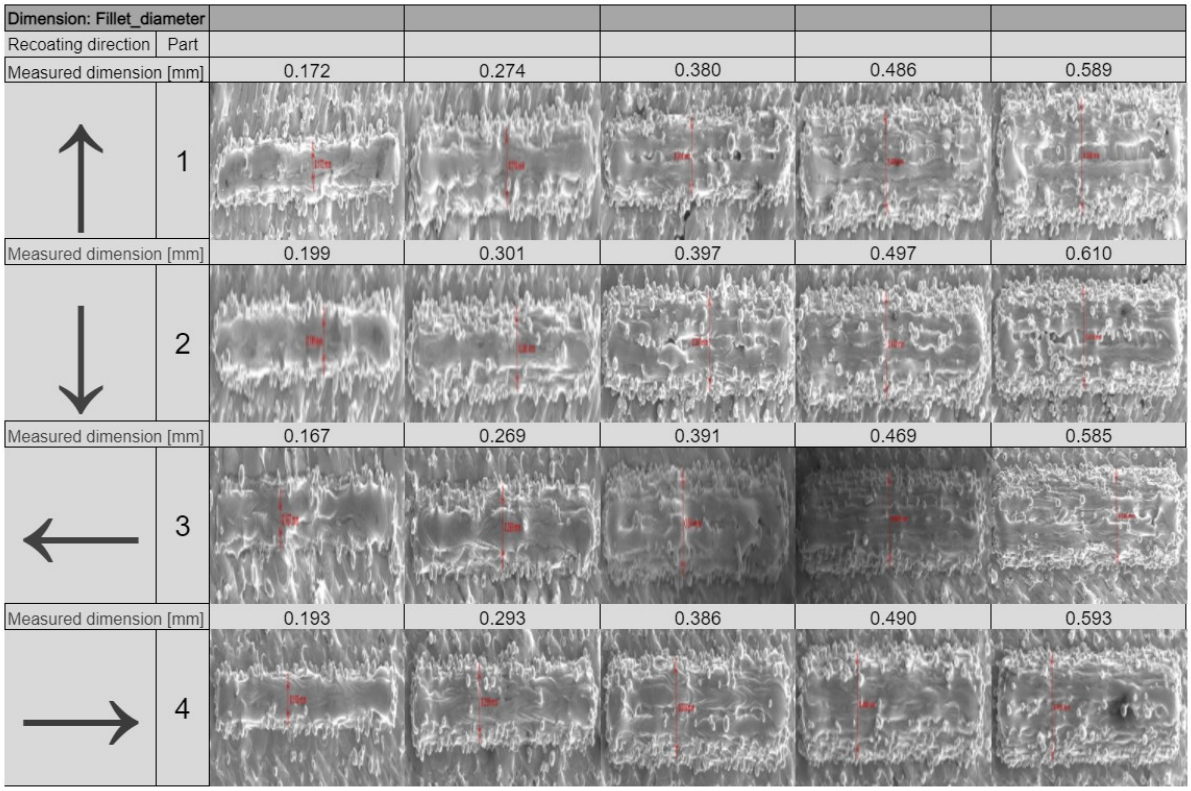

Figure B.14: ESEM images of ribs of print 4.

Table B.14: Deviation of the ribs for print 4.

Rib [ϕ]	0.2		0.3		0.4		0.5		0.6	
Re-coat	[mm]	[%]	[mm]	[%]	[mm]	[%]	[mm]	[%]	[mm]	[%]
↑	-0.028	-14	-0.026	-8.66	-0.02	-5	-0.014	-2.8	-0.011	-1.83
↓	-0.001	-0.5	0.001	0.33	-0.003	-0.75	-0.003	-0.6	0.01	1.66
←	-0.033	-16.5	-0.031	-10.33	-0.009	-2.25	-0.031	-6.2	-0.015	-2.5
→	-0.007	-3.5	-0.007	-2.33	-0.014	-3.5	-0.01	-2	-0.007	-1.16

- **Print 5**

  In all the orientations, ribs are printed. The edges along the length for the ribs are little straight and contains half melted particles. As the diameter increases the edges are seen straight with less deviation. A smooth curve can be seen in all the prints. There can be seen some smaller pores in the prints. These issues in different rib sizes can be seen from the Figure B.15. The Table B.15 below shows the deviation of the ribs with respect to the original CAD dimension.

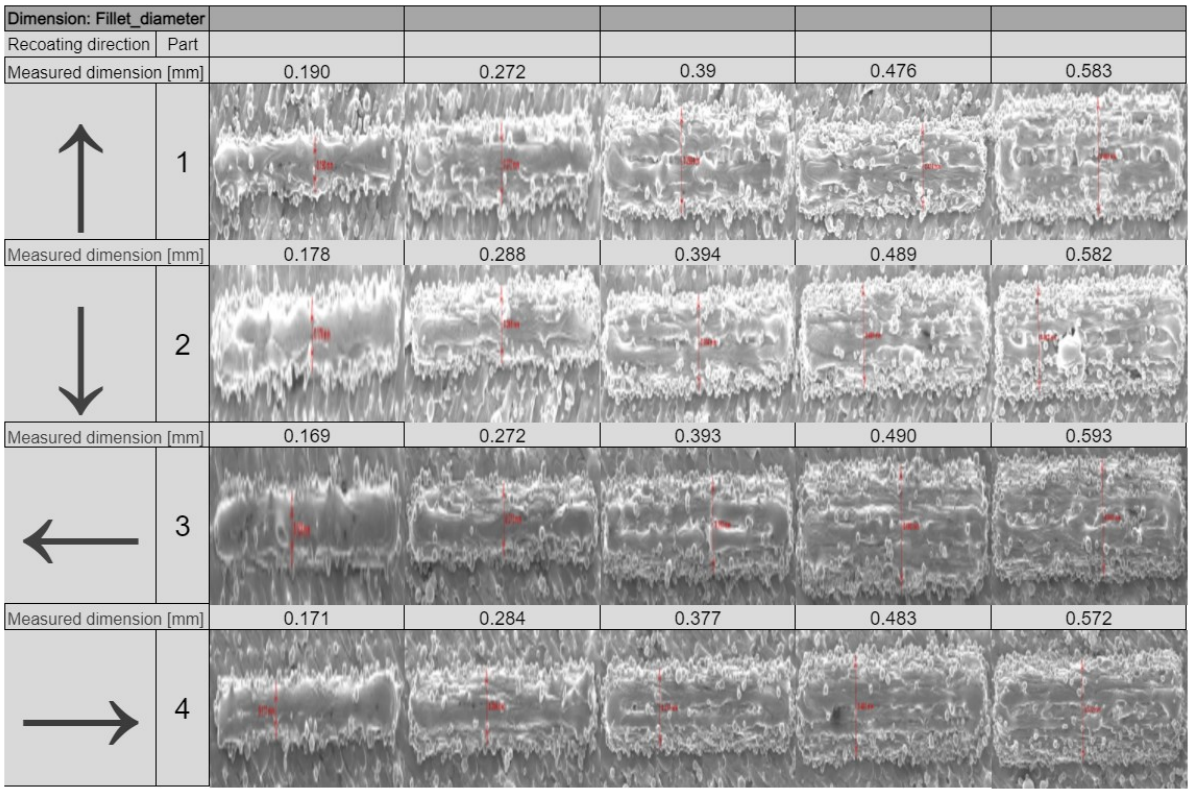

Figure B.15: ESEM images of ribs of print 5.

Table B.15: Deviation of the ribs for print 5.

Rib [ϕ]	0.2		0.3		0.4		0.5		0.6	
Re-coat	[mm]	[%]	[mm]	[%]	[mm]	[%]	[mm]	[%]	[mm]	[%]
↑	-0.01	-5	-0.028	-9.33	-0.01	-2.5	-0.024	-4.8	-0.017	-2.83
↓	-0.022	-11	-0.012	-4	-0.006	-1.5	-0.011	-2.2	-0.018	-3
←	-0.031	-15.5	-0.028	-9.33	-0.007	-1.75	-0.01	-2	-0.007	-1.16
→	-0.029	-14.5	-0.016	-5.33	-0.023	-5.75	-0.017	-3.4	-0.028	-4.66

- **Print 6**

  In all the orientations, ribs are printed. The edges along the length for the ribs are straight and better than previous prints and contains half melted particles. As the diameter increases the edges are seen straight with less deviation. A smooth curve can be seen in all the prints. There can be seen some smaller pores in the prints. These issues in different rib sizes can be seen from the Figure B.16. The Table B.16 below shows the deviation of the ribs with respect to the original CAD dimension.

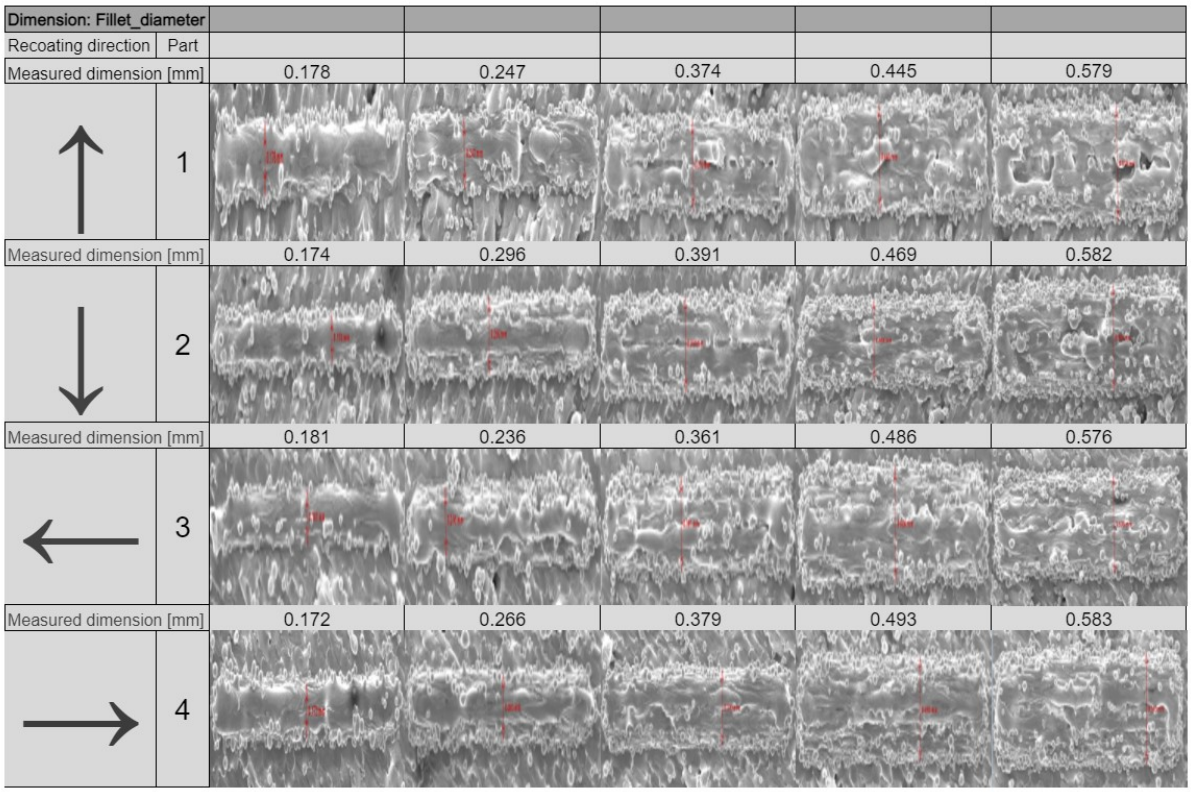

Figure B.16: ESEM images of ribs of print 6.

Table B.16: Deviation of the ribs for print 6.

Rib [ϕ]	0.2		0.3		0.4		0.5		0.6	
Re-coat	[mm]	[%]	[mm]	[%]	[mm]	[%]	[mm]	[%]	[mm]	[%]
↑	-0.095	-47.5	-0.147	-49	-0.191	-47.75	-0.24	-48	-0.294	-49
↓	-0.097	-48.5	-0.143	-47.66	-0.196	-49	-0.244	-48.8	-0.299	-49.83
←	-0.074	-37	-0.144	-48	-0.196	-49	-0.238	-47.6	-0.284	-47.33
→	-0.104	-52	-0.144	-48	-0.193	-48.25	-0.238	-47.6	-0.283	-47.16

- **Print 7**

  In all the orientations, ribs are printed. The edges along the length for the ribs are not straight and worse than all the prints. As the diameter increases the edges are seen straight with less deviation. The curve is not smooth in all the prints. There can be seen more smaller pores in the prints compared to all the prints. These issues in different rib sizes can be seen from the Figure B.17. The Table B.17 below shows the deviation of the ribs with respect to the original CAD dimension.

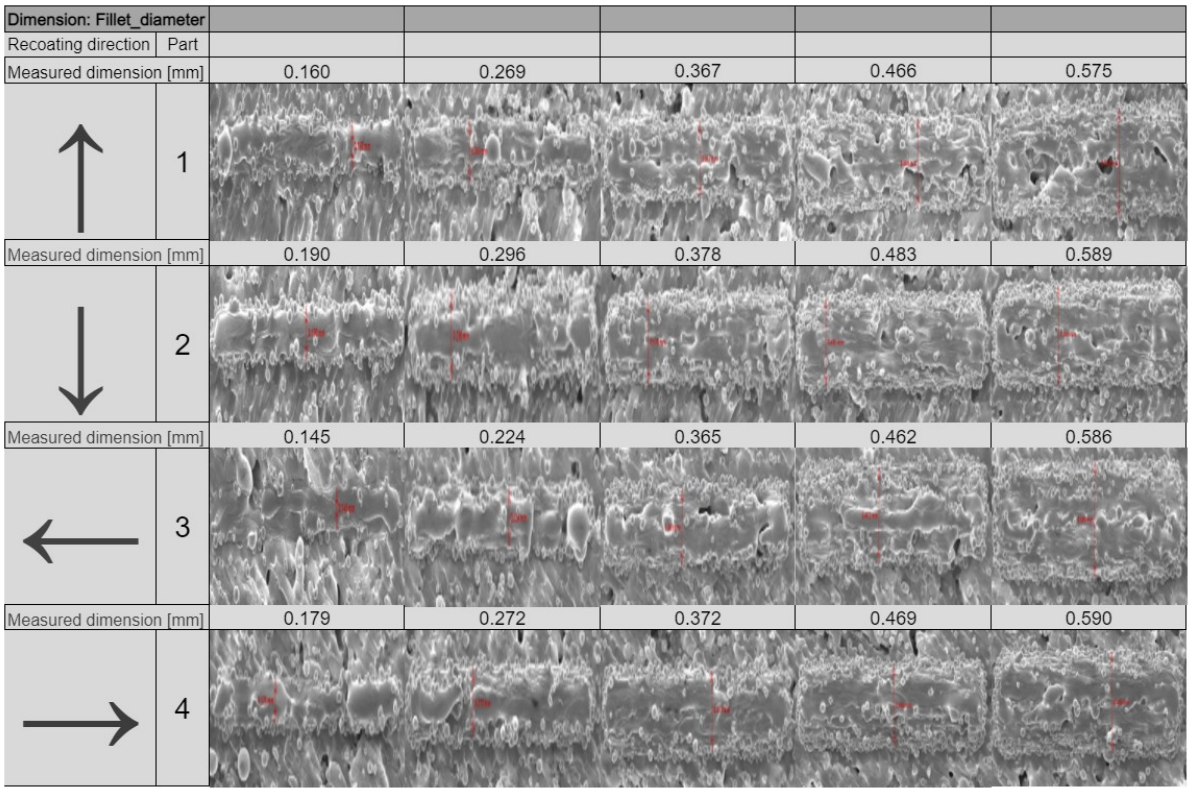

Figure B.17: ESEM images of ribs of print 7.

Table B.17: Deviation of the ribs for print 7.

Rib [ϕ]	0.2		0.3		0.4		0.5		0.6	
Re-coat	[mm]	[%]	[mm]	[%]	[mm]	[%]	[mm]	[%]	[mm]	[%]
↑	-0.04	-20	-0.031	-10.33	-0.033	-8.25	-0.034	-6.8	-0.025	-4.16
↓	-0.01	-5	-0.004	-1.33	-0.022	-5.5	-0.017	-3.4	-0.011	-1.83
←	-0.055	-27.5	-0.076	-25.33	-0.035	-8.75	-0.038	-7.6	-0.014	-2.33
→	-0.021	-10.5	-0.028	-9.33	-0.028	-7	-0.031	-6.2	-0.01	-1.66

- **Print 8**

  In the orientation 3, rib with diameter 0.2 mm was not printed. The edges along the length for the ribs are not good and worse than all the previous prints and contains half melted particles. Even the ribs that are bigger are not printed good. There can be seen smaller pores in the prints. These issues in different rib sizes can be seen from the Figure B.18. The Table B.18 below shows the deviation of the ribs with respect to the original CAD dimension.

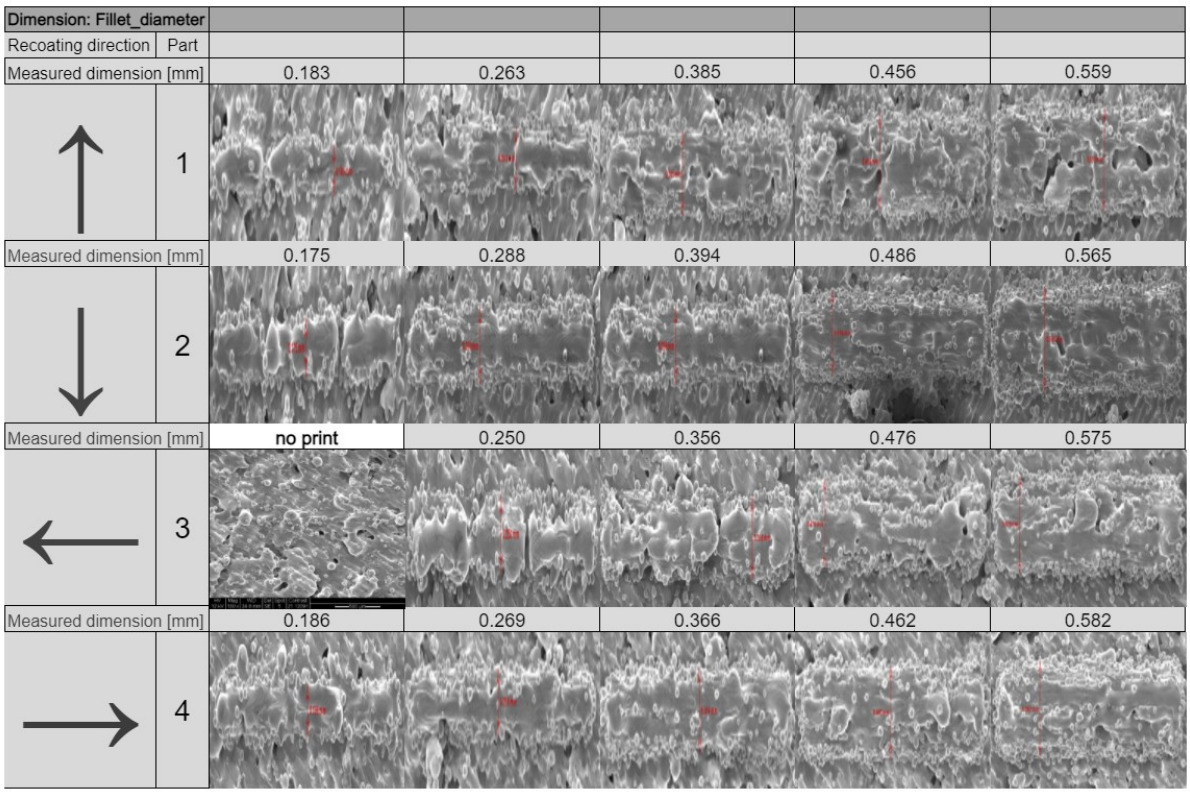

Figure B.18: ESEM images of ribs of print 8.

Table B.18: Deviation of the ribs for print 8.

Rib [ϕ]	0.2		0.3		0.4		0.5		0.6	
Re-coat	[mm]	[%]	[mm]	[%]	[mm]	[%]	[mm]	[%]	[mm]	[%]
↑	-0.017	-8.5	-0.037	-12.33	-0.015	-3.75	-0.044	-8.8	-0.041	-6.83
↓	-0.025	-12.5	-0.012	-4	-0.006	-1.5	-0.014	-2.8	-0.035	-5.83
←	-0.2	-100	-0.05	-16.66	-0.044	-11	-0.024	-4.8	-0.025	-4.16
→	-0.014	-7	-0.031	-10.33	-0.034	-8.5	-0.038	-7.6	-0.018	-3

- **Print 9**

  In all the orientations, ribs are printed. The edges along the length for the ribs are not perfect straight but it is better than previous prints and contains half melted particles. As the diameter increases the edges are seen straight with less deviation. A smooth curve can be seen in all the prints when compared to previous prints along the diameter. These issues in different rib sizes can be seen from the Figure B.19. The Table B.19 below shows the deviation of the ribs with respect to the original CAD dimension.

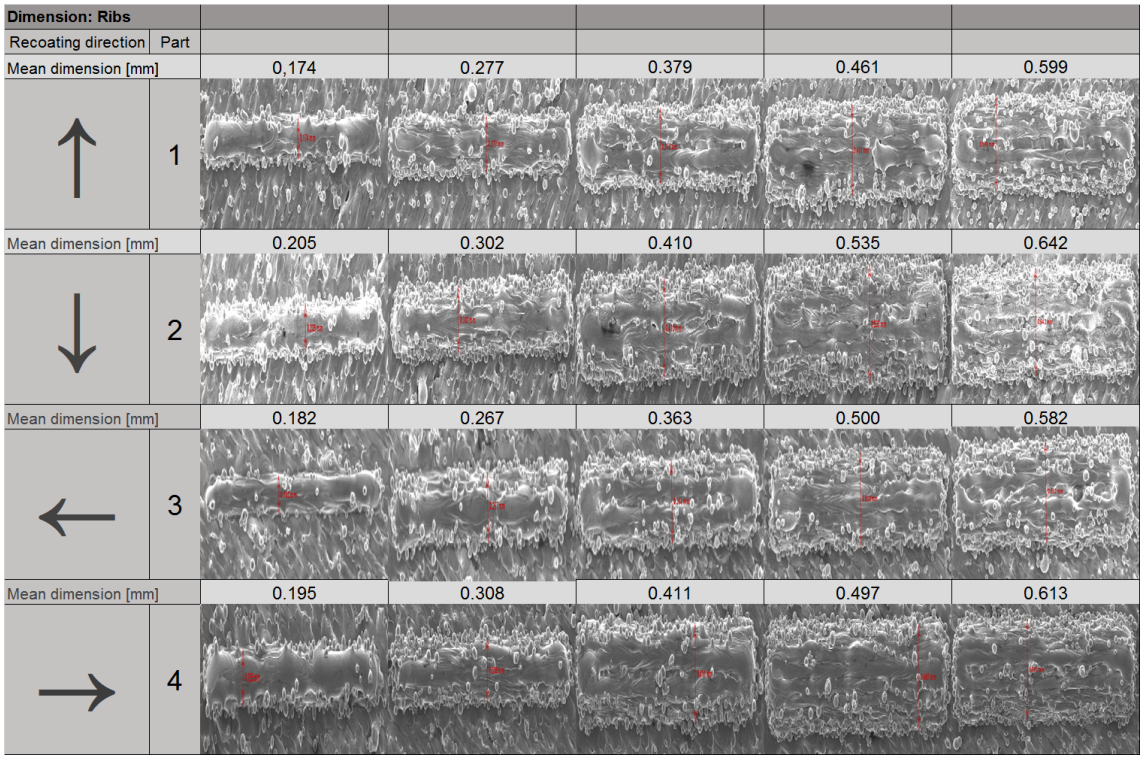

Figure B.19: ESEM images of the ribs for print 9.

Table B.19: Deviation of the ribs for print 9.

Rib [ϕ]	0.2		0.3		0.4		0.5		0.6	
Re-coat	[mm]	[%]	[mm]	[%]	[mm]	[%]	[mm]	[%]	[mm]	[%]
↑	-0.026	-13.00	-0.023	-7.67	-0.021	-5.25	-0.039	-6.50	-0.001	-0.17
↓	0.005	2.50	0.002	0.67	0.010	2.50	0.035	5.83	0.042	7.00
←	-0.018	-9.00	-0.033	-11.00	-0.037	-9.25	0	0.00	-0.018	-3.00
→	-0.005	-2.50	0.008	2.67	0.011	2.75	-0.003	-0.50	0.013	2.17

- **Print 10**

  All the ribs are printed. In all the prints step layers can be seen clearly. The edges are straight and better than LB-PBF prints. The presence of half molten particles are less. These issues in different rib sizes can be seen from the Figure B.20. The Table B.20 below shows the deviation of the ribs with respect to the original CAD dimension.

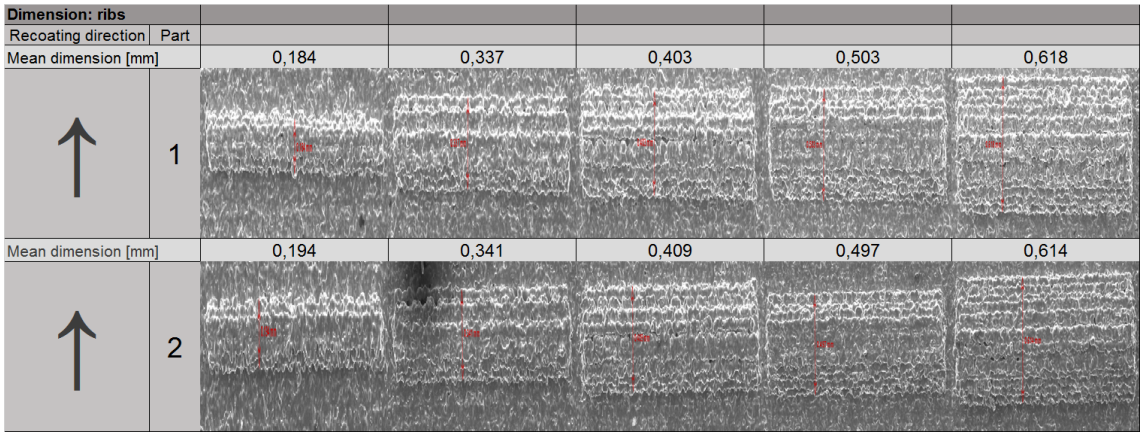

Figure B.20: ESEM images of the binder jetted ribs of print 10.

Table B.20: Deviation of the ribs for print 10.

Rib [ϕ]		**0.2**		**0.3**		**0.4**		**0.5**		**0.6**	
Re-coat	Part	[mm]	[%]	[mm]	[%]	[mm]	[%]	[mm]	[%]	[mm]	[%]
↑	1	-0.016	-8.00	0.037	12.33	0.003	0.75	0.003	0.60	0.018	3.00
↑	2	-0.006	-3.00	0.041	13.67	0.009	2.25	-0.003	-0.60	0.014	2.33

B.3 Arrowhead base

- **Print 1**

  All the arrowheads are printed but there can seen some issues in the arrowhead base of 0.849 mm where there are lots of bigger half melted particles attached in all the orientations. Smaller the arrowhead base higher is the natural fillets present at the corners causing the reduction in size. These issues in different arrowhead sizes can be seen from the Figure B.21. The Table B.21 below shows the deviation of the arrowheads with respect to the original CAD dimension.

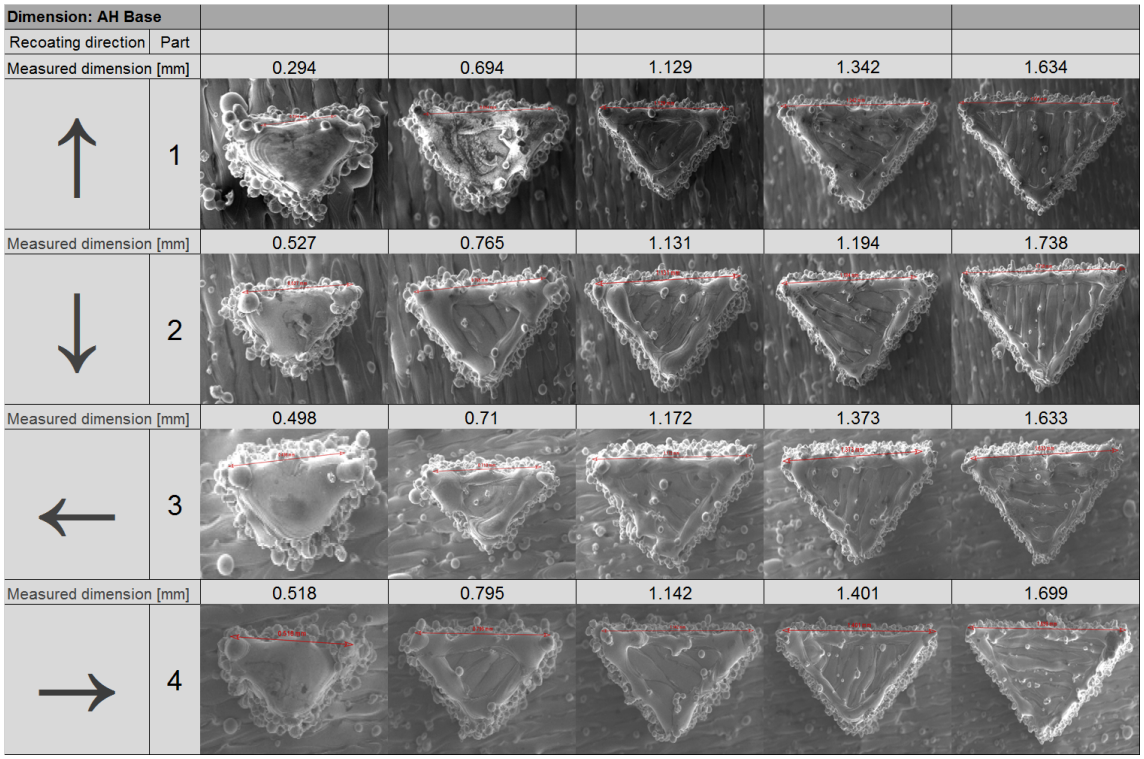

Figure B.21: ESEM images of arrowhead base of print 1.

Table B.21: Deviation of the arrowhead base for print 1.

Arrow base	0.849		1.131		1.414		1.697		1.98	
Re-coat	[mm]	[%]	[mm]	[%]	[mm]	[%]	[mm]	[%]	[mm]	[%]
↑	-0.555	-65.37	-0.437	-38.63	-0.285	-20.15	-0.355	-20.91	-0.346	-17.47
↓	-0.322	-37.92	-0.366	-32.36	-0.283	-20.01	-0.503	-29.64	-0.242	-12.22
←	-0.351	-41.34	-0.421	-37.22	-0.242	-17.11	-0.324	-19.09	-0.347	-17.52
→	-0.331	-38.98	-0.336	-29.70	-0.272	-19.23	-0.296	-17.44	-0.281	-14.19

- **Print 2**

  All the arrowheads are printed. There are half melted particles attached in all the arrowheads. There can be seen some pores on the print. The top surface is not smooth and has balling effect. These issues in different arrowhead sizes can be seen from the Figure B.22. The Table B.22 below shows the deviation of the arrowheads with respect to the original CAD dimension.

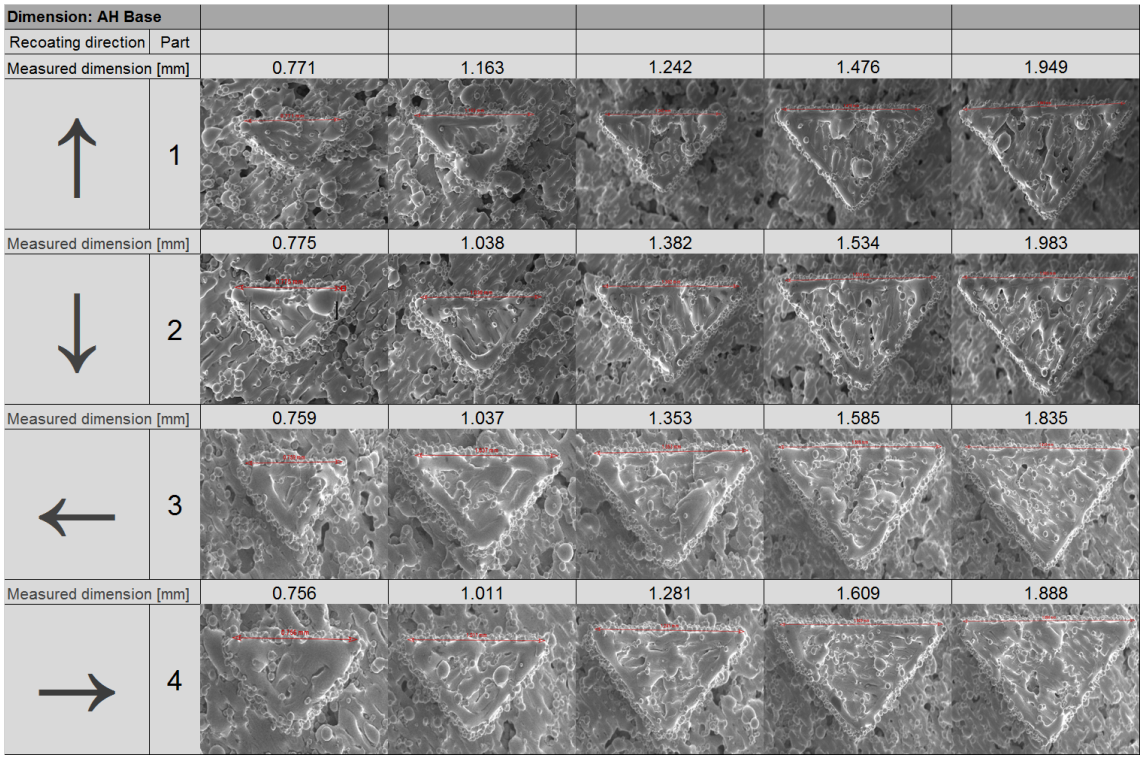

Figure B.22: ESEM images of arrowhead base of print 2.

Table B.22: Deviation of the arrowhead base for print 2.

Arrow base	0.849		1.131		1.414		1.697		1.98	
Re-coat	[mm]	[%]	[mm]	[%]	[mm]	[%]	[mm]	[%]	[mm]	[%]
↑	-0.078	-9.18	0.032	2.82	-0.172	-12.16	-0.221	-13.02	-0.031	-1.56
↓	-0.074	-8.71	-0.093	-8.22	-0.032	-2.26	-0.163	-9.60	0.003	0.15
←	-0.09	-10.60	-0.094	-8.31	-0.061	-4.31	-0.112	-6.59	-0.145	-7.32
→	-0.093	-10.95	-0.12	-10.61	-0.133	-9.40	-0.088	-5.18	-0.092	-4.64

- **Print 3**

  All the arrowheads are printed. There are half melted particles attached in all the arrowheads. The top surface is smooth compared to previous print. There can be seen some presence of natural fillets on the corners for the smaller arrowheads. These issues in different arrowhead sizes can be seen from the Figure B.23. The Table B.23 below shows the deviation of the arrowheads with respect to the original CAD dimension.

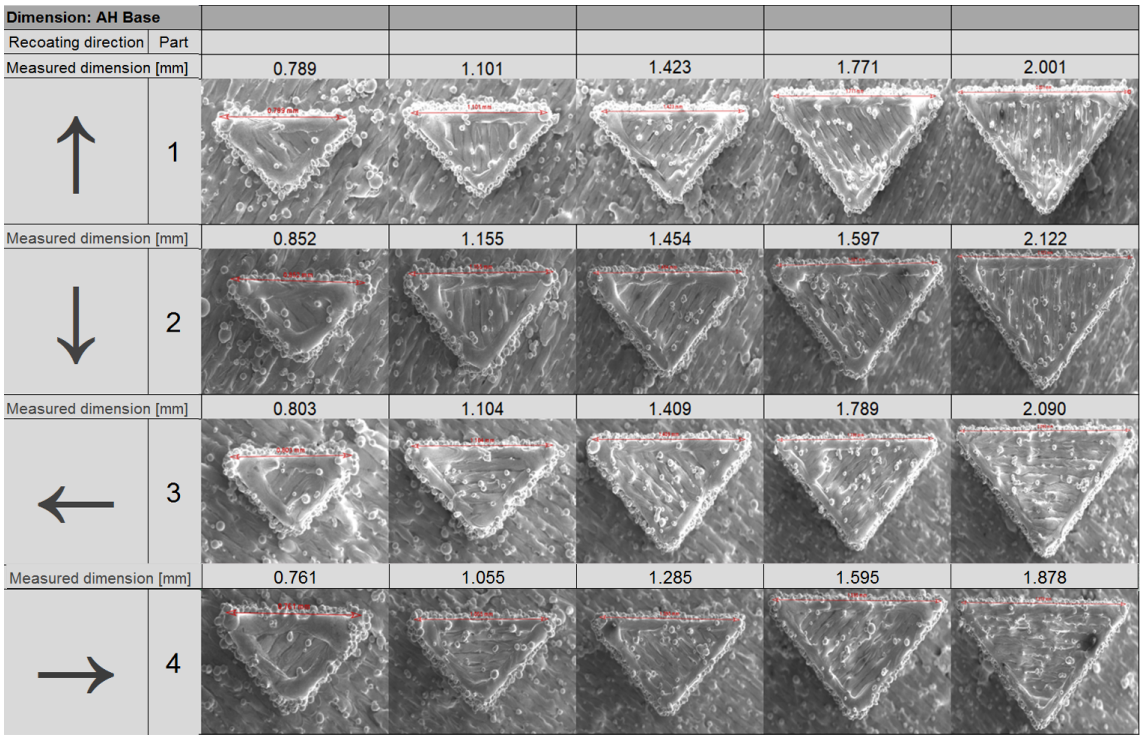

Figure B.23: ESEM images of arrowhead base of print 3.

Table B.23: Deviation of the arrowhead base for print 3.

Arrow base	0.849		1.131		1.414		1.697		1.98	
Re-coat	[mm]	[%]	[mm]	[%]	[mm]	[%]	[mm]	[%]	[mm]	[%]
↑	-0.06	-7.06	-0.03	-2.65	0.009	0.63	0.074	4.36	0.021	1.06
↓	0.003	0.35	0.024	2.12	0.04	2.82	-0.1	-5.89	0.142	7.17
←	-0.046	-5.41	-0.027	-2.38	-0.005	-0.35	0.092	5.42	0.11	5.55
→	-0.088	-10.36	-0.076	-6.71	-0.129	-9.12	-0.102	-6.01	-0.102	-5.15

- **Print 4**

  All the arrowheads are printed. There are half melted particles attached in all the arrowheads. The top surface is smooth. There can be seen some presence of smaller radius natural fillets on the corners for all the arrowheads. The arrowheads are almost similar to the CAD model with respect to shape and measurements. These issues in different arrowhead sizes can be seen from the Figure B.24. The Table B.24 below shows the deviation of the arrowheads with respect to the original CAD dimension.

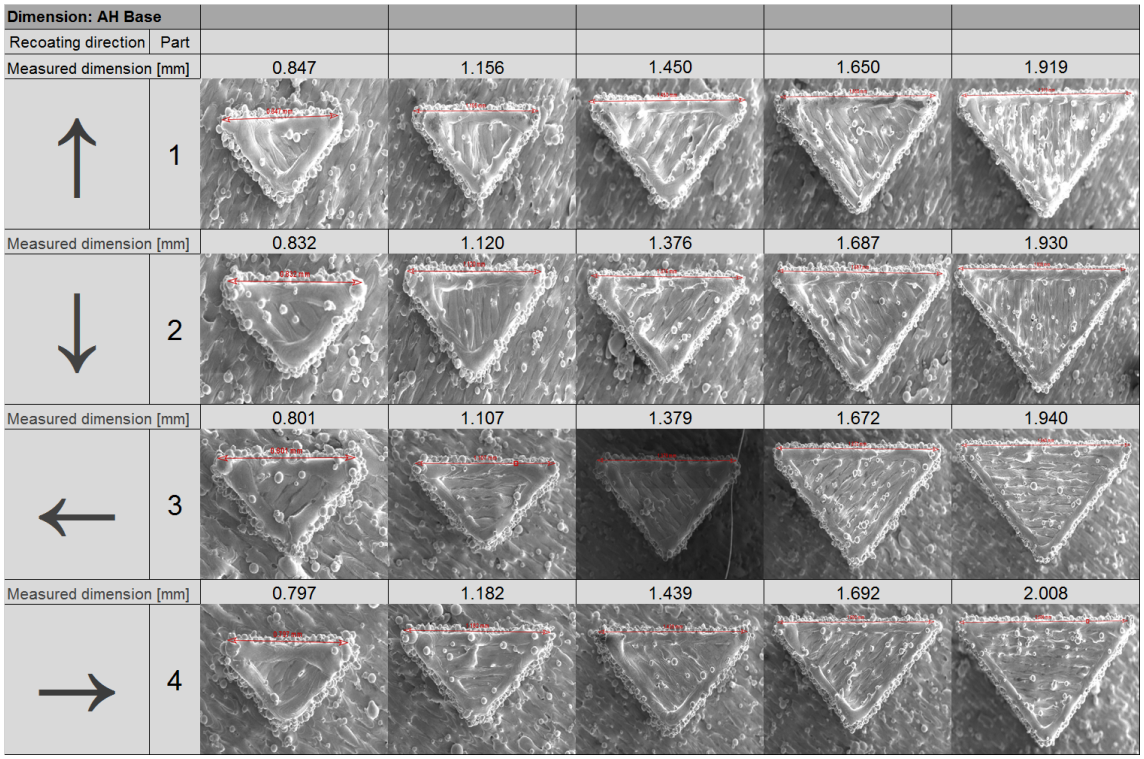

Figure B.24: ESEM images of arrowhead base of print 4.

Table B.24: Deviation of the arrowhead base for print 4.

Arrow base	0.849		1.131		1.414		1.697		1.98	
Re-coat	[mm]	[%]	[mm]	[%]	[mm]	[%]	[mm]	[%]	[mm]	[%]
↑	-0.002	-0.23	0.025	2.21	0.036	2.54	-0.047	-2.76	-0.061	-3.08
↓	-0.017	-2.00	-0.011	-0.97	-0.038	-2.68	-0.01	-0.58	-0.05	-2.52
←	-0.048	-5.65	-0.024	-2.12	-0.035	-2.47	-0.025	-1.47	-0.04	-2.02
→	-0.052	-6.12	0.051	4.50	0.025	1.76	-0.005	-0.29	0.028	1.41

- **Print 5**

  All the arrowheads are printed. There are half melted particles attached in all the arrowheads. The top surface is smooth. There can be seen some presence of smaller radius natural fillets on the corners for all the arrowheads. The arrowheads are almost similar to the CAD model with respect to shape and measurements. These issues in different arrowhead sizes can be seen from the Figure B.25. The Table B.25 below shows the deviation of the arrowheads with respect to the original CAD dimension.

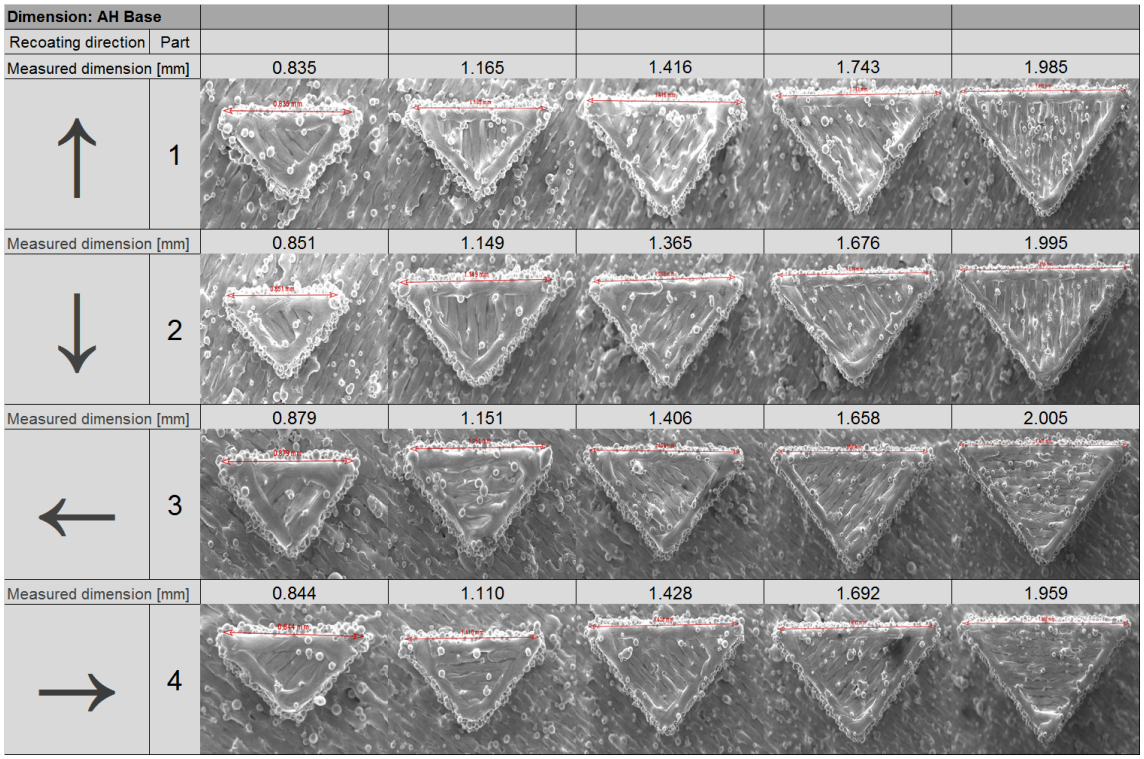

Figure B.25: ESEM images of arrowhead base of print 5.

Table B.25: Deviation of the arrowhead base for print 5.

Arrow base	0.849		1.131		1.414		1.697		1.98	
Re-coat	[mm]	[%]	[mm]	[%]	[mm]	[%]	[mm]	[%]	[mm]	[%]
↑	-0.014	-1.64	0.034	3.00	0.002	0.14	0.046	2.71	0.005	0.25
↓	0.002	0.23	0.018	1.59	-0.049	-3.46	-0.021	-1.23	0.015	0.75
←	0.03	3.53	0.02	1.76	-0.008	-0.56	-0.039	-2.29	0.025	1.26
→	-0.005	-0.58	-0.021	-1.85	0.014	0.99	-0.005	-0.29	-0.021	-1.06

- **Print 6**

  All the arrowheads are printed. There are half melted particles attached in all the arrowheads. The top surface is smooth. There can be seen some presence of smaller radius natural fillets on the corners for all the arrowheads. The arrowheads are almost similar to the CAD model with respect to shape and measurements. There are lots of pores present in the print. These issues in different arrowhead sizes can be seen from the Figure B.26. The Table B.26 below shows the deviation of the arrowheads with respect to the original CAD dimension.

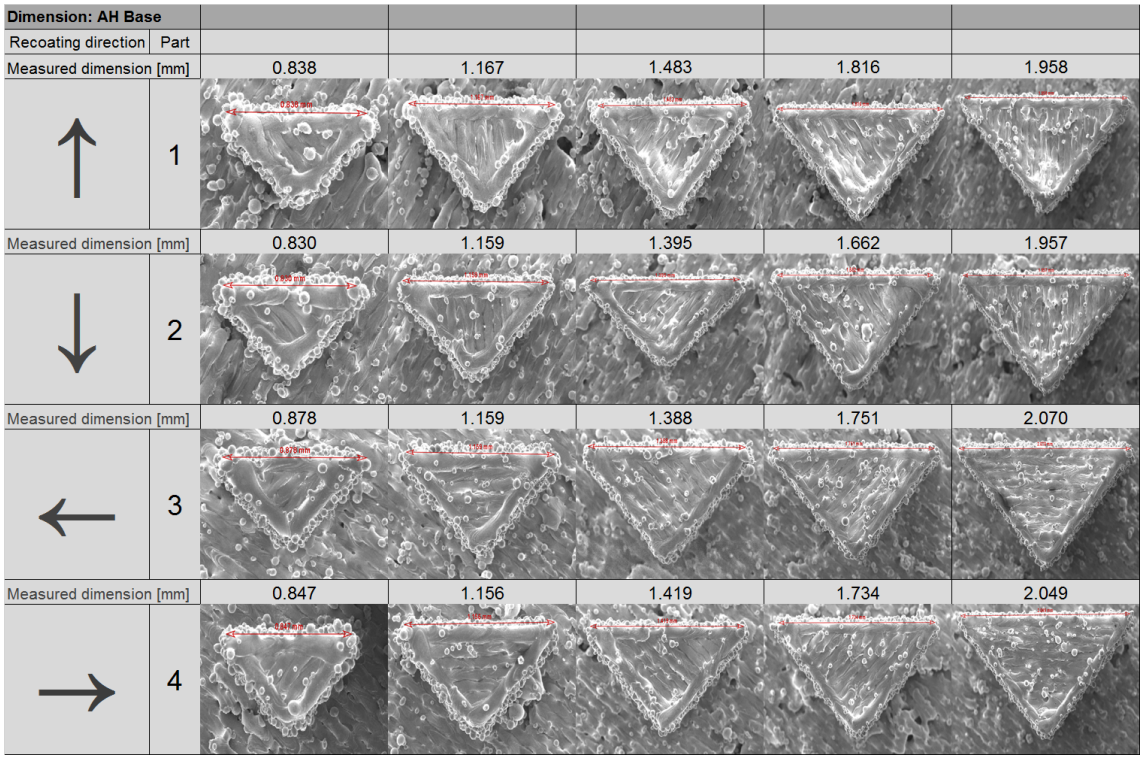

Figure B.26: ESEM images of arrowhead base of print 6.

Table B.26: Deviation of the arrowhead base for print 6.

Arrow base	0.849		1.131		1.414		1.697		1.98	
Re-coat	[mm]	[%]	[mm]	[%]	[mm]	[%]	[mm]	[%]	[mm]	[%]
↑	-0.011	-1.29	0.036	3.18	0.069	4.87	0.119	7.01	-0.022	-1.11
↓	-0.019	-2.23	0.028	2.47	-0.019	-1.34	-0.035	-2.06	-0.023	-1.16
←	0.029	3.41	0.028	2.47	-0.026	-1.83	0.054	3.18	0.09	4.54
→	-0.002	-0.23	0.025	2.21	0.005	0.35	0.037	2.18	0.069	3.48

- **Print 7**

  All the arrowheads are printed. There are half melted particles attached in all the arrowheads. The top surface is showing balling effect. There can be seen some presence of smaller radius natural fillets on the corners for all the arrowheads. The arrowheads are almost similar to the CAD model with respect to shape and measurements. There are lots of pores present in the print. These issues in different arrowhead sizes can be seen from the Figure B.27. The Table B.27 below shows the deviation of the arrowheads with respect to the original CAD dimension.

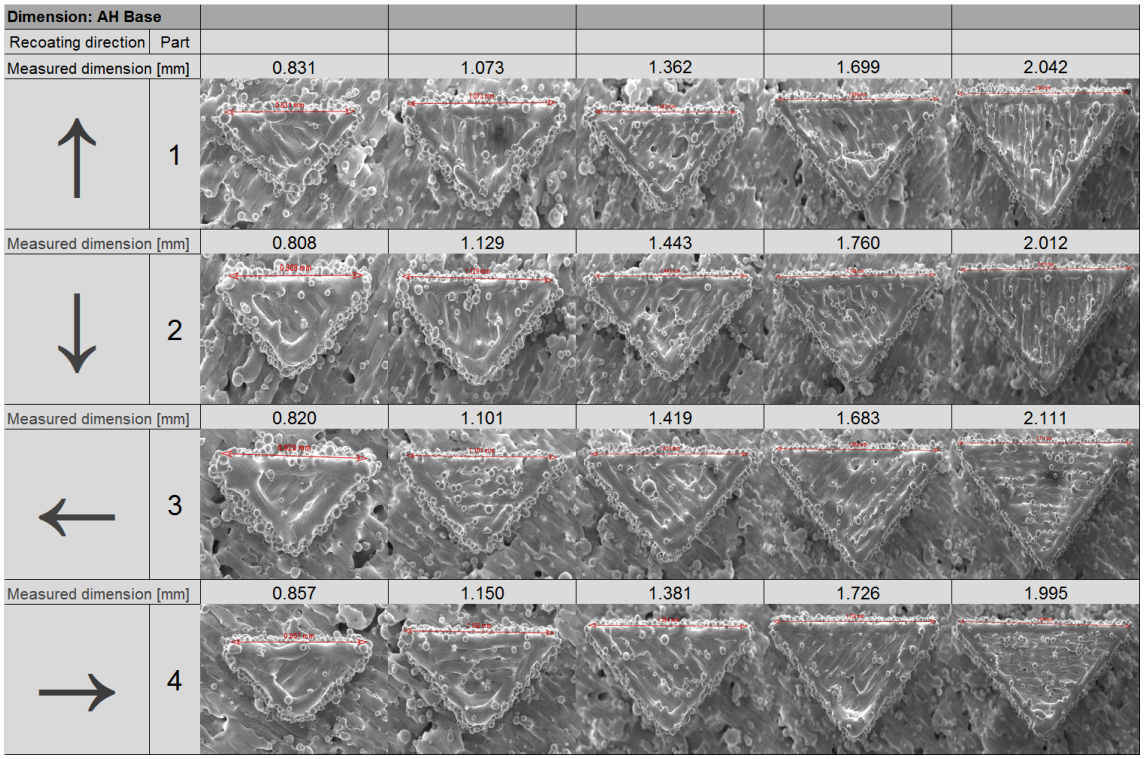

Figure B.27: ESEM images of arrowhead base of print 7.

Table B.27: Deviation of the arrowhead base for print 7.

Arrow base	0.849		1.131		1.414		1.697		1.98	
Re-coat	[mm]	[%]	[mm]	[%]	[mm]	[%]	[mm]	[%]	[mm]	[%]
↑	-0.018	-2.12	-0.058	-5.12	-0.052	-3.67	0.002	0.11	0.062	3.13
↓	-0.041	-4.82	-0.002	-0.17	0.029	2.05	0.063	3.71	0.032	1.61
←	-0.029	-3.41	-0.03	-2.65	0.005	0.35	-0.014	-0.82	0.131	6.61
→	0.008	0.94	0.019	1.67	-0.033	-2.33	0.029	1.70	0.015	0.75

- **Print 8**

  All the arrowheads are printed. There are bigger sized half melted particles attached in all the arrowheads. The top surface is not good and is showing high balling effect. There can be seen some presence of smaller radius natural fillets on the corners for all the arrowheads. The arrowheads are almost similar to the CAD model with respect to shape and measurements. There are lots of pores present in the print. These issues in different arrowhead sizes can be seen from the Figure B.28. The Table B.28 below shows the deviation of the arrowheads with respect to the original CAD dimension.

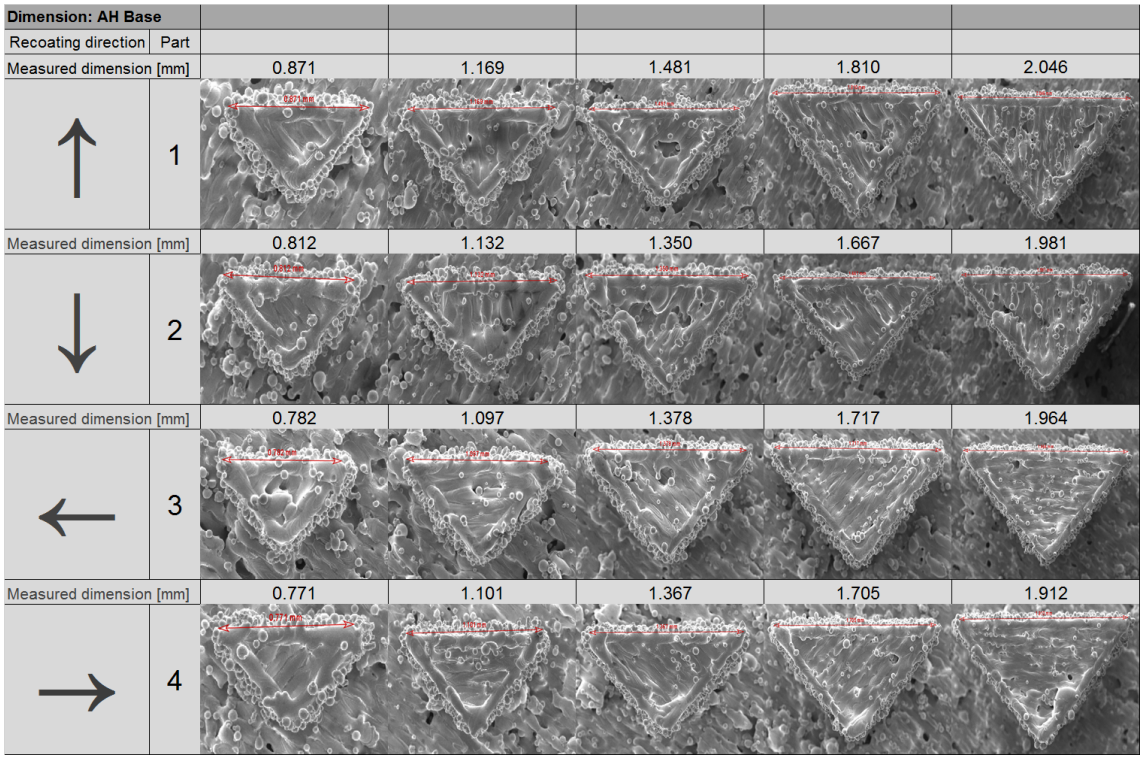

Figure B.28: ESEM images of arrowhead base of print 8.

Table B.28: Deviation of the arrowhead base for print 8.

Arrow base	0.849		1.131		1.414		1.697		1.98	
Re-coat	[mm]	[%]	[mm]	[%]	[mm]	[%]	[mm]	[%]	[mm]	[%]
↑	0.022	2.59	0.038	3.35	0.067	4.73	0.113	6.65	0.066	3.33
↓	-0.037	-4.35	0.001	0.08	-0.064	-4.52	-0.03	-1.76	0.001	0.05
←	-0.067	-7.89	-0.034	-3.00	-0.036	-2.54	0.02	1.17	-0.016	-0.80
→	-0.078	-9.18	-0.03	-2.65	-0.047	-3.32	0.008	0.47	-0.068	-3.43

- **Print 9**

  All the arrowheads are printed. There are half melted particles attached in all the arrowheads. The top surface is smooth. There can be seen some presence of smaller radius natural fillets on the corners for all the arrowheads. The arrowheads are almost similar to the CAD model with respect to shape and measurements. These issues in different arrowhead sizes can be seen from the Figure B.29. The Table B.29 below shows the deviation of the arrowheads with respect to the original CAD dimension.

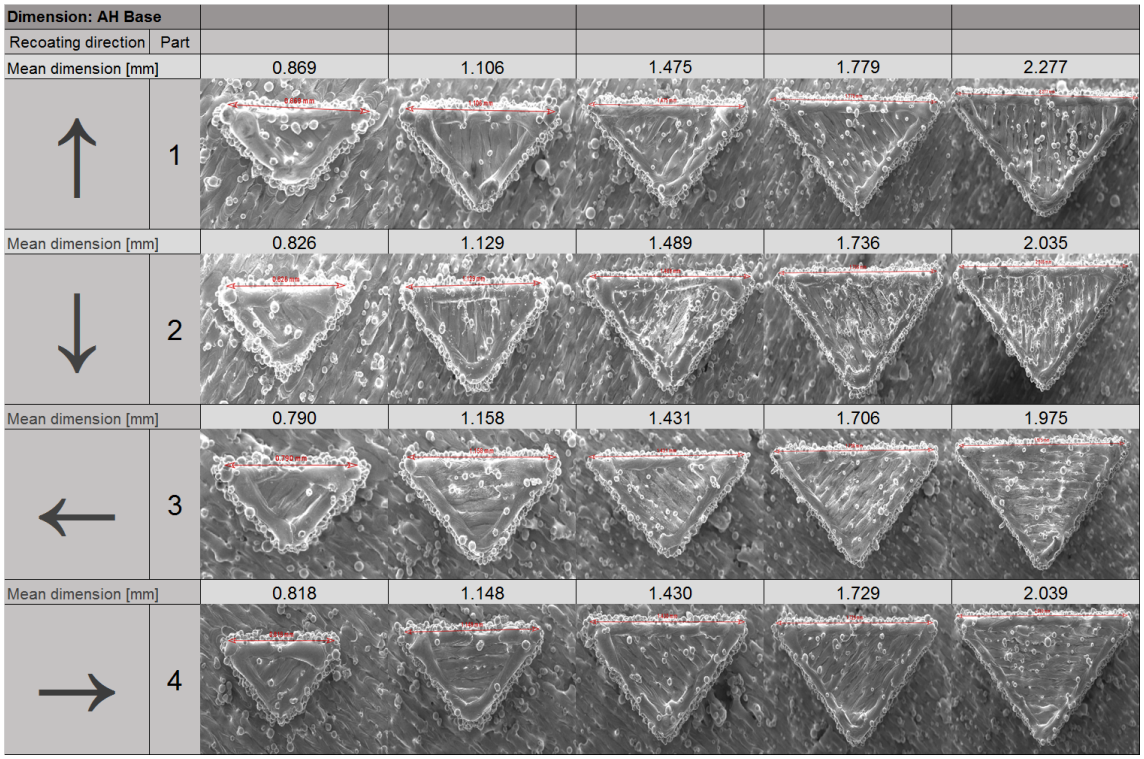

Figure B.29: ESEM images of the arrowhead base for print 9.

Table B.29: Deviation of the arrowhead base for print 9.

Arrow base	0.849		1.131		1.414		1.697		1.98	
Re-coat	[mm]	[%]	[mm]	[%]	[mm]	[%]	[mm]	[%]	[mm]	[%]
↑	0.020	2.36	-0.025	-2.21	0.061	4.31	0.082	4.14	0.297	15.00
↓	-0.023	-2.71	-0.002	-0.18	0.075	5.30	0.039	1.97	0.055	2.78
←	-0.059	-6.95	0.027	2.39	0.017	1.20	0.009	0.45	-0.005	-0.25
→	-0.031	-3.65	0.017	1.50	0.016	1.13	0.032	1.62	0.059	2.98

- **Print 10**

  All the arrowheads are printed. The arrowhead with lower base values have some distortions in the geometry but the corners are better compared to the LB-PBF prints. These issues in different arrowhead sizes can be seen from the Figure B.30. The Table B.30 below shows the deviation of the arrowheads with respect to the original CAD dimension.

L

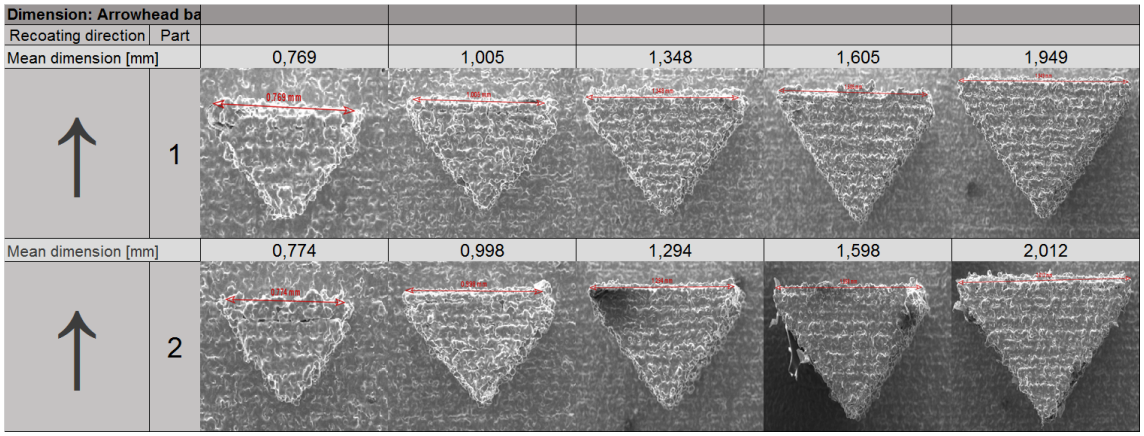

Figure B.30: ESEM images of the binder jetted arrowhead of print 10.

Table B.30: Deviation of the binder jetted arrowhead base for print 10.

Arrow base		0.849		1.131		1.414		1.697		1.98	
Re-coat	Part	[mm]	[%]	[mm]	[%]	[mm]	[%]	[mm]	[%]	[mm]	[%]
↑	1	-0.080	-9.42	-0.126	-11.14	-0.066	-4.67	-0.092	-5.42	-0.031	-1.57
↑	2	-0.075	-8.83	-0.133	-11.76	-0.120	-8.49	-0.099	-5.83	0.032	1.62

B.4 Grooves

- **Print 1**

  All the grooves were printed good. There are half melted particles attached to the grooves. These issues in different grooves can be seen from the Figure B.31. The Table B.31 below shows the deviation of the grooves with respect to the original CAD dimension.

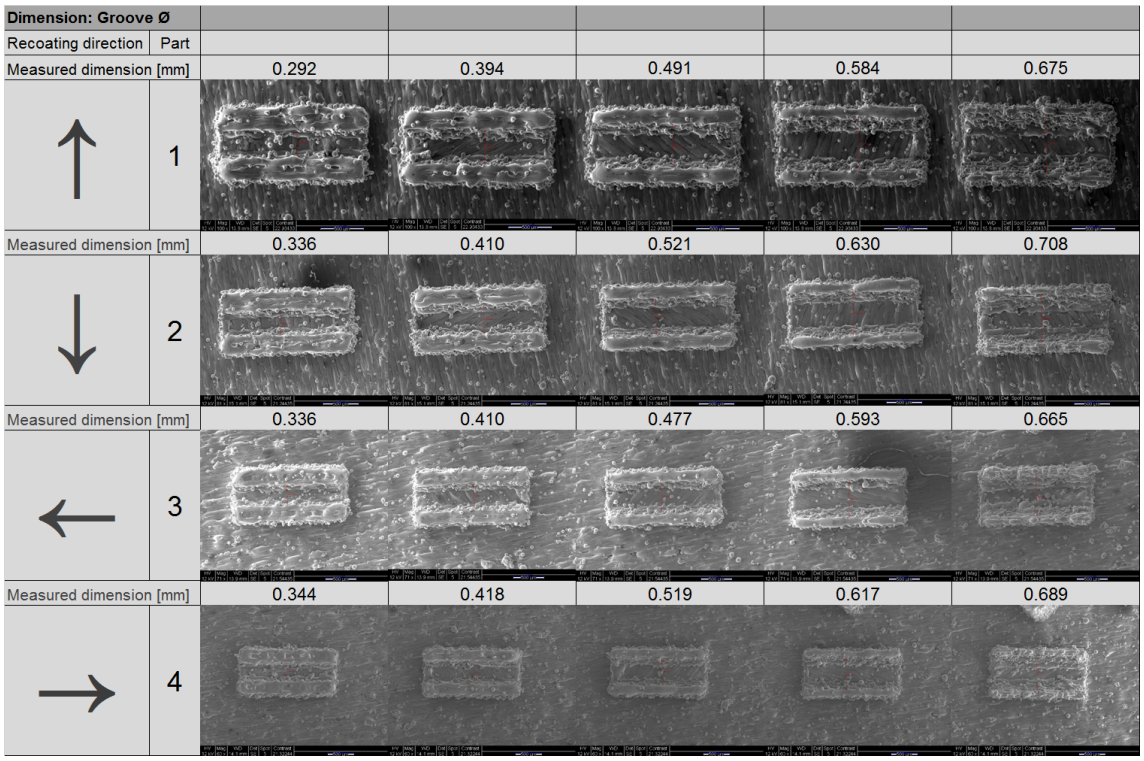

Figure B.31: ESEM images of the grooves for print 1.

Table B.31: Deviation of the grooves for print 1.

Groove [ϕ]	**0.3**		**0.4**		**0.5**		**0.6**		**0.7**	
Re-coat	[mm]	[%]	[mm]	[%]	[mm]	[%]	[mm]	[%]	[mm]	[%]
↑	-0.008	-2.66	-0.006	-1.5	-0.009	-1.8	-0.016	-2.66	-0.025	-3.57
↓	0.036	12	0.01	2.5	0.021	4.2	0.03	5	0.008	1.14
←	0.036	12	0.01	2.5	-0.023	-4.6	-0.007	-1.16	-0.035	-5
→	0.044	14.66	0.018	4.5	0.019	3.8	0.017	2.83	-0.011	-1.57

- **Print 2**

  All the grooves were printed good. There are half melted particles attached to the grooves. There are too many pores in the print. The prints surface are not smooth. These issues in different grooves can be seen from the Figure B.32. The Table B.32 below shows the deviation of the grooves with respect to the original CAD dimension.

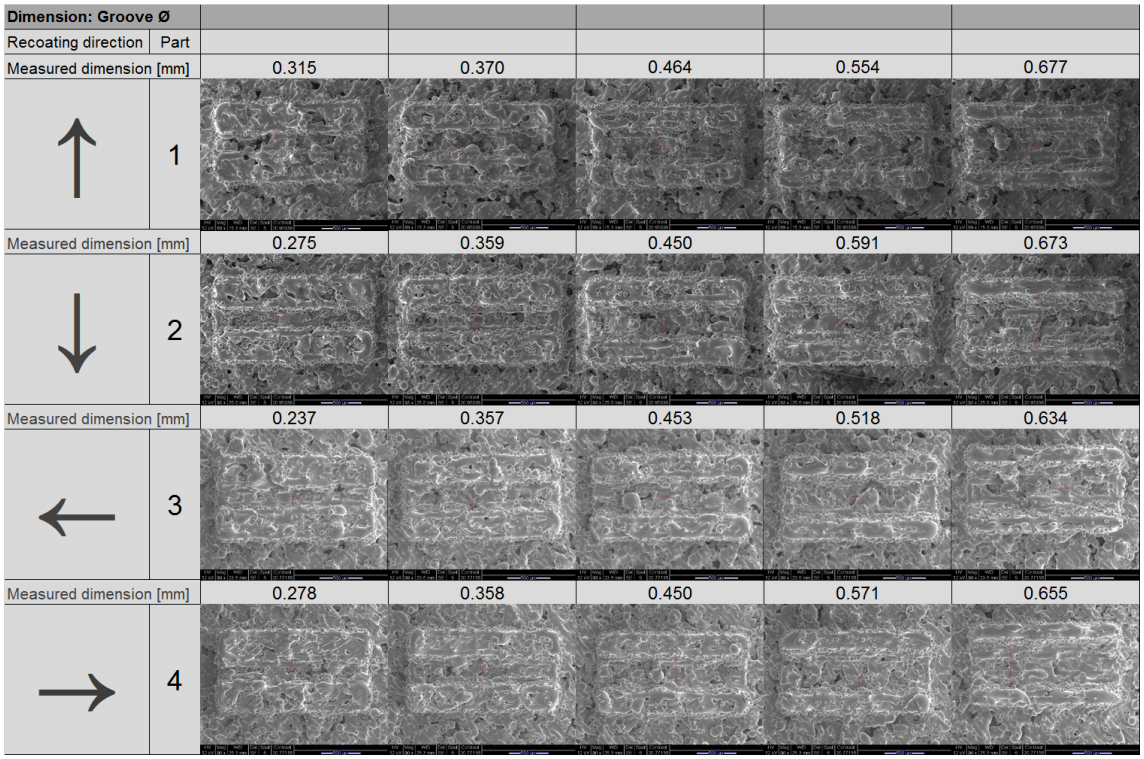

Figure B.32: ESEM images of the grooves for print 2.

Table B.32: Deviation of the grooves for print 2.

Groove [ϕ]	0.3		0.4		0.5		0.6		0.7	
Re-coat	[mm]	[%]	[mm]	[%]	[mm]	[%]	[mm]	[%]	[mm]	[%]
↑	0.015	5	-0.03	-7.5	-0.036	-7.2	-0.046	-7.66	-0.023	-3.28
↓	-0.025	-8.33	-0.041	-10.25	-0.05	-10	-0.009	-1.5	-0.027	-3.85
←	-0.063	-21	-0.043	-10.75	-0.047	-9.4	-0.082	-13.66	-0.066	-9.42
→	-0.022	-7.33	-0.042	-10.5	-0.05	-10	-0.029	-4.83	-0.045	-6.42

- **Print 3**

  All the grooves were printed good. There are half melted particles attached to the grooves. The prints surface are better than the previous prints. These issues in different grooves can be seen from the Figure B.33. The Table B.33 below shows the deviation of the grooves with respect to the original CAD dimension.

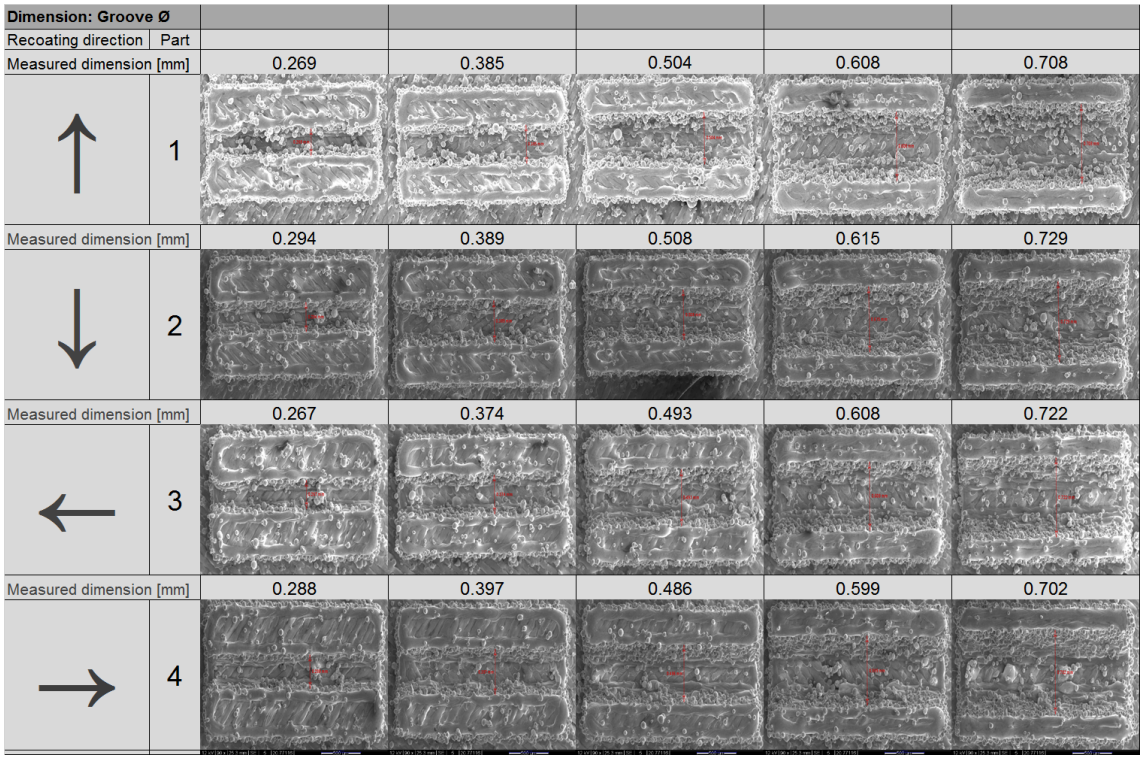

Figure B.33: ESEM images of the grooves for print 3.

Table B.33: Deviation of the grooves for print 3.

Groove [ϕ]	**0.3**		**0.4**		**0.5**		**0.6**		**0.7**	
Re-coat	[mm]	[%]	[mm]	[%]	[mm]	[%]	[mm]	[%]	[mm]	[%]
↑	-0.031	-10.33	-0.015	-3.75	0.004	0.8	0.008	1.33	0.008	1.14
↓	-0.006	-2	-0.011	-2.75	0.008	1.6	0.015	2.5	0.029	4.14
←	-0.033	-11	-0.026	-6.5	-0.007	-1.4	0.008	1.33	0.022	3.14
→	-0.012	-4	-0.003	-0.75	-0.014	-2.8	-0.001	-0.16	0.002	0.28

- **Print 4**

  All the grooves were printed good. There are half melted particles attached to the grooves. The prints surface are good. Traces of very small pores can be seen in the print. These issues in different grooves can be seen from the Figure B.34. The Table B.34 below shows the deviation of the grooves with respect to the original CAD dimension.

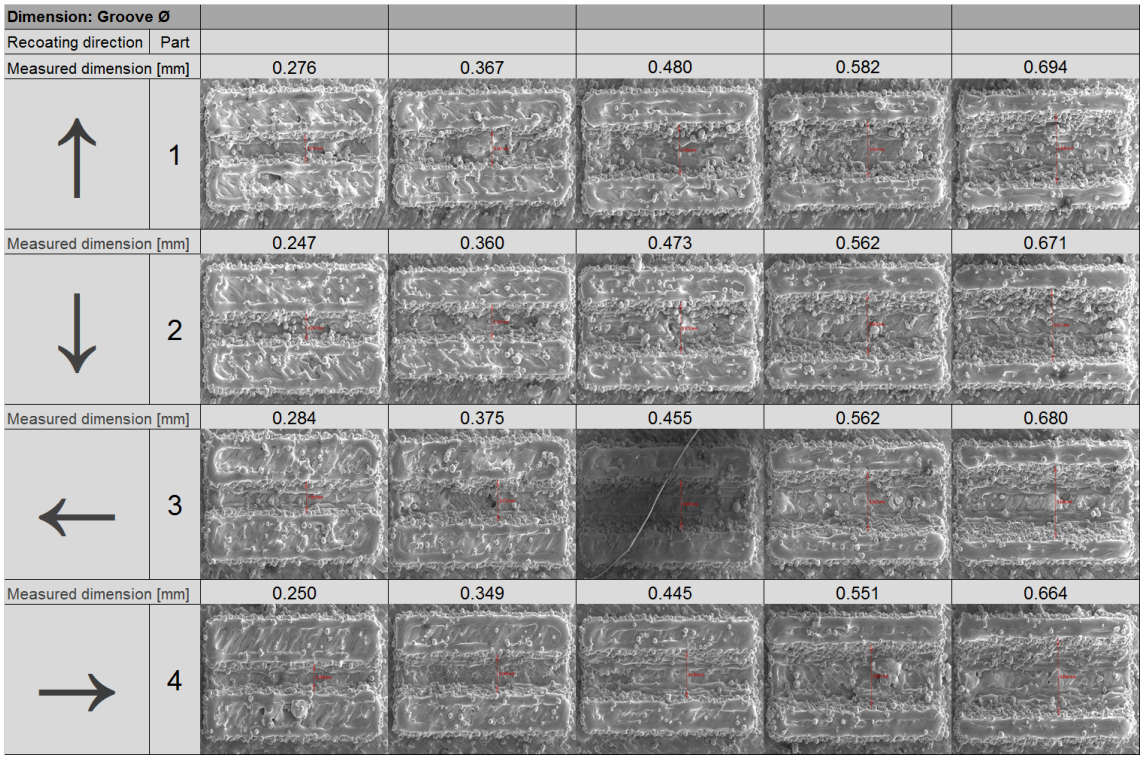

Figure B.34: ESEM images of the grooves for print 4.

Table B.34: Deviation of the grooves for print 4.

Groove [ϕ]	**0.3**		**0.4**		**0.5**		**0.6**		**0.7**	
Re-coat	[mm]	[%]	[mm]	[%]	[mm]	[%]	[mm]	[%]	[mm]	[%]
↑	-0.024	-8	-0.033	-8.25	-0.02	-4	-0.018	-3	-0.006	-0.85
↓	-0.053	-17.66	-0.04	-10	-0.027	-5.4	-0.038	-6.33	-0.029	-4.14
←	-0.016	-5.33	-0.025	-6.25	-0.045	-9	-0.038	-6.33	-0.02	-2.85
→	-0.05	-16.66	-0.051	-12.75	-0.055	-11	-0.049	-8.16	-0.036	-5.14

- **Print 5**

  All the grooves were printed good. There are half melted particles attached to the grooves. The prints surface are good. Traces of very small pores can be seen in the print. These issues in different grooves can be seen from the Figure B.35. The Table B.35 below shows the deviation of the grooves with respect to the original CAD dimension.

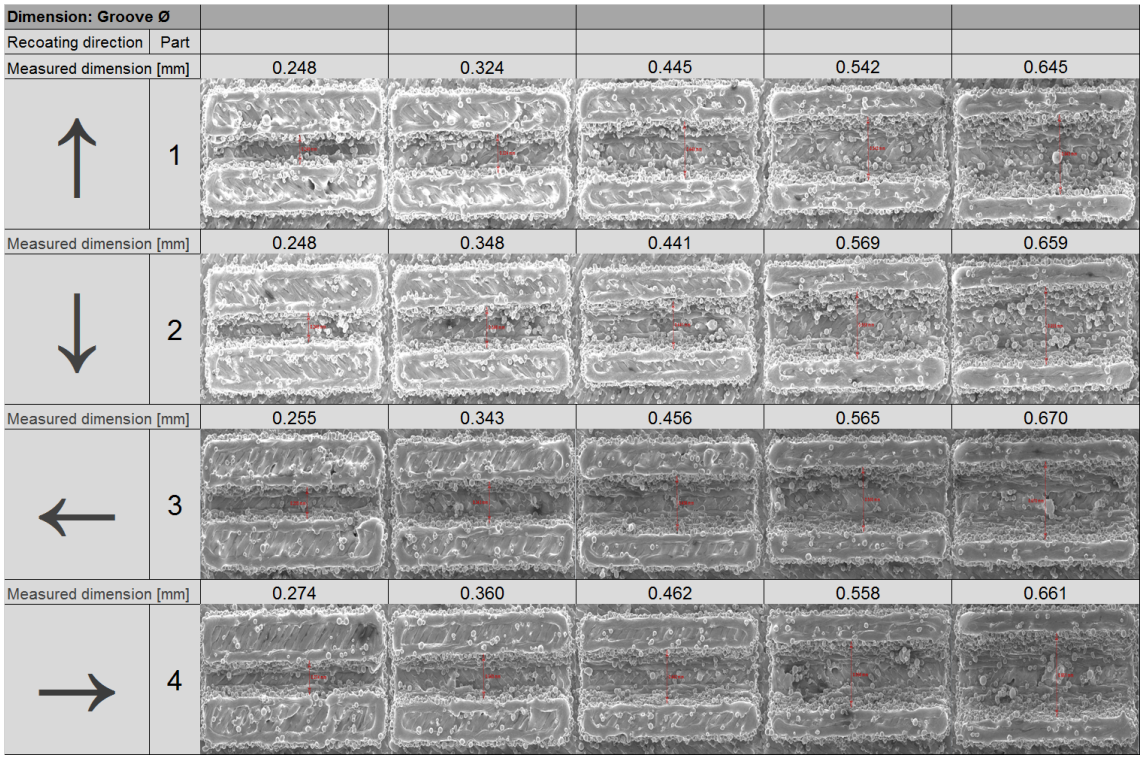

Figure B.35: ESEM images of the grooves for print 5.

Table B.35: Deviation of the grooves for print 5.

Groove [ϕ]	**0.3**		**0.4**		**0.5**		**0.6**		**0.7**	
Re-coat	[mm]	[%]	[mm]	[%]	[mm]	[%]	[mm]	[%]	[mm]	[%]
↑	-0.052	-17.33	-0.076	-19	-0.055	-11	-0.058	-9.66	-0.055	-7.85
↓	-0.052	-17.33	-0.052	-13	-0.059	-11.8	-0.031	-5.16	-0.041	-5.85
←	-0.045	-15	-0.057	-14.25	-0.044	-8.8	-0.035	-5.83	-0.03	-4.28
→	-0.026	-8.66	-0.04	-10	-0.038	-7.6	-0.042	-7	-0.039	-5.57

- **Print 6**

  All the grooves were printed good. There are half melted particles attached to the grooves. The prints surface are not good. Traces of larger sized pores can be seen in the print. These issues in different grooves can be seen from the Figure B.36. The Table B.36 below shows the deviation of the grooves with respect to the original CAD dimension.

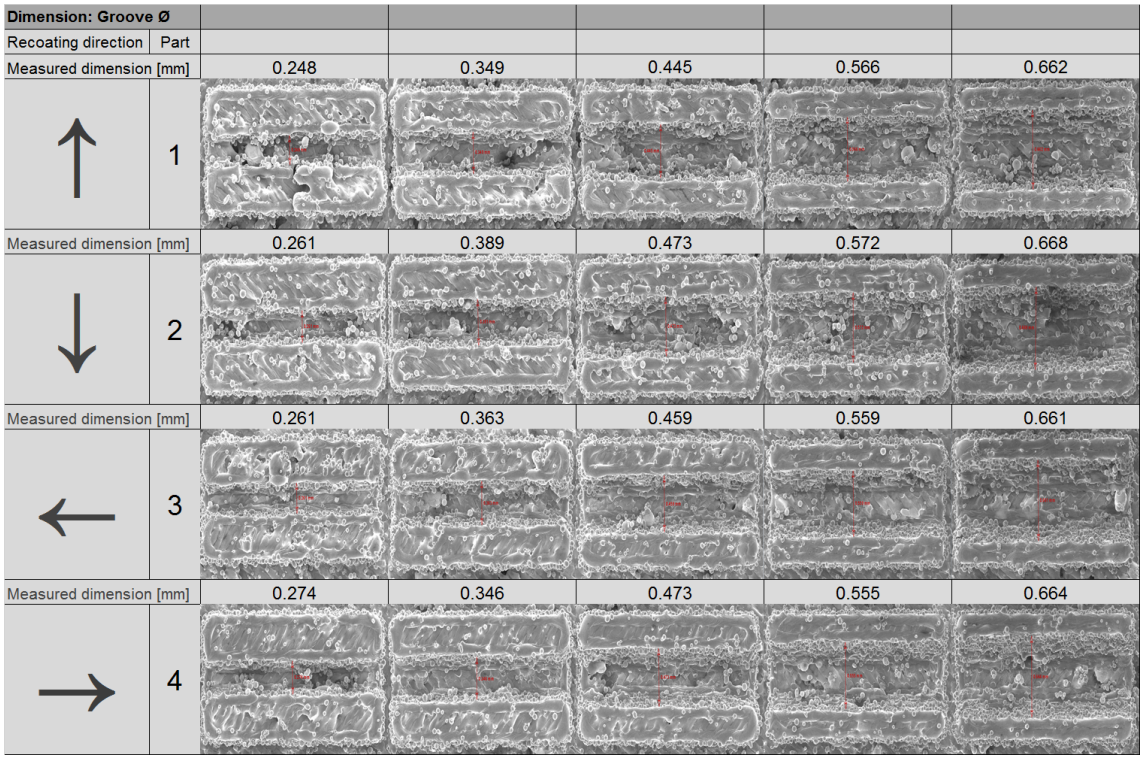

Figure B.36: ESEM images of the grooves for print 6.

Table B.36: Deviation of the grooves for print 6.

Groove [ϕ]	0.3		0.4		0.5		0.6		0.7	
Re-coat	[mm]	[%]	[mm]	[%]	[mm]	[%]	[mm]	[%]	[mm]	[%]
↑	-0.052	-17.33	-0.051	-12.75	-0.055	-11	-0.034	-5.66	-0.038	-5.42
↓	-0.039	-13	-0.011	-2.75	-0.027	-5.4	-0.028	-4.66	-0.032	-4.57
←	-0.039	-13	-0.037	-9.25	-0.041	-8.2	-0.041	-6.83	-0.039	-5.57
→	-0.026	-8.66	-0.054	-13.5	-0.027	-5.4	-0.045	-7.5	-0.036	-5.14

- **Print 7**

  All the grooves were printed good. There are larges sized half melted particles attached to the grooves. The prints surface are not good and worse than all the prints. Traces of larger sized pores can be seen in the print compared to previous prints. These issues in different grooves can be seen from the Figure B.37. The Table B.37 below shows the deviation of the grooves with respect to the original CAD dimension.

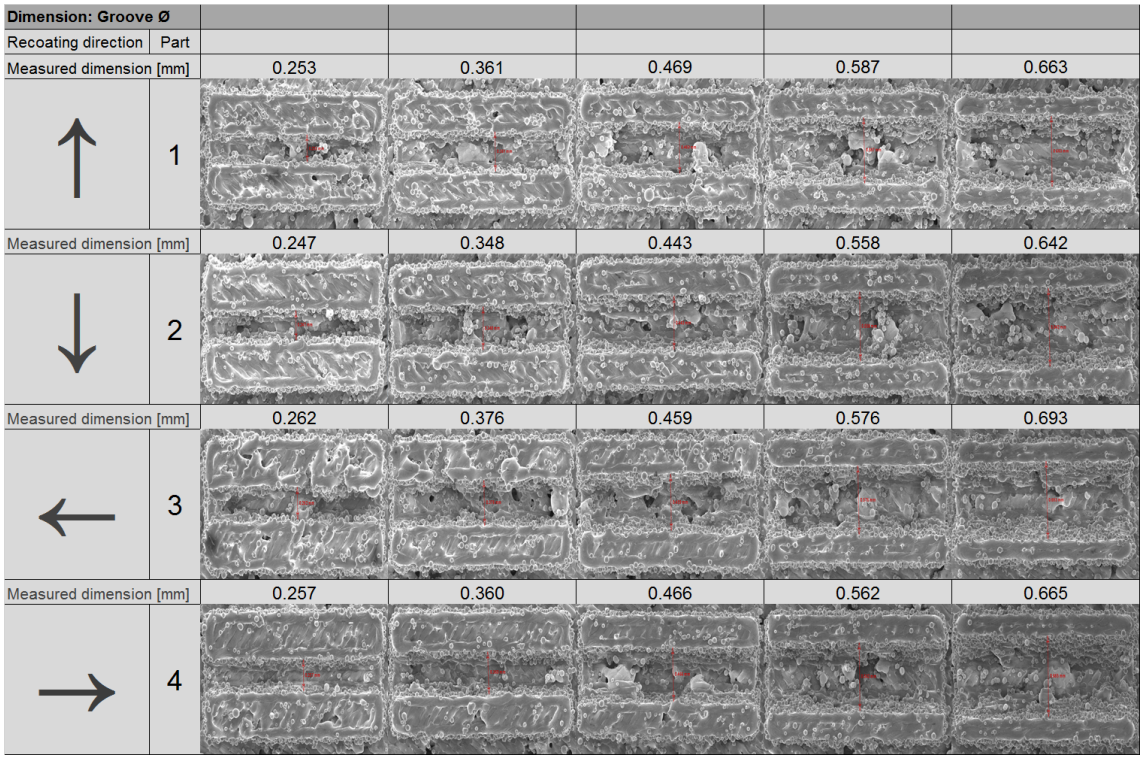

Figure B.37: ESEM images of the grooves for print 7.

Table B.37: Deviation of the grooves for print 7.

Groove [ϕ]	**0.3**		**0.4**		**0.5**		**0.6**		**0.7**	
Re-coat	[mm]	[%]	[mm]	[%]	[mm]	[%]	[mm]	[%]	[mm]	[%]
↑	-0.047	-15.66	-0.039	-9.75	-0.031	-6.2	-0.013	-2.16	-0.037	-5.28
↓	-0.053	-17.66	-0.052	-13	-0.057	-11.4	-0.042	-7	-0.058	-8.28
←	-0.038	-12.66	-0.024	-6	-0.041	-8.2	-0.024	-4	-0.007	-1
→	-0.043	-14.33	-0.04	-10	-0.034	-6.8	-0.038	-6.33	-0.035	-5

- **Print 8**

  All the grooves were printed good. There are larges sized half melted particles attached to the grooves. The prints surface are not good and worse than all the prints. Traces of larger sized pores can be seen in the print compared to previous prints. These issues in different grooves can be seen from the Figure B.38. The Table B.38 below shows the deviation of the grooves with respect to the original CAD dimension.

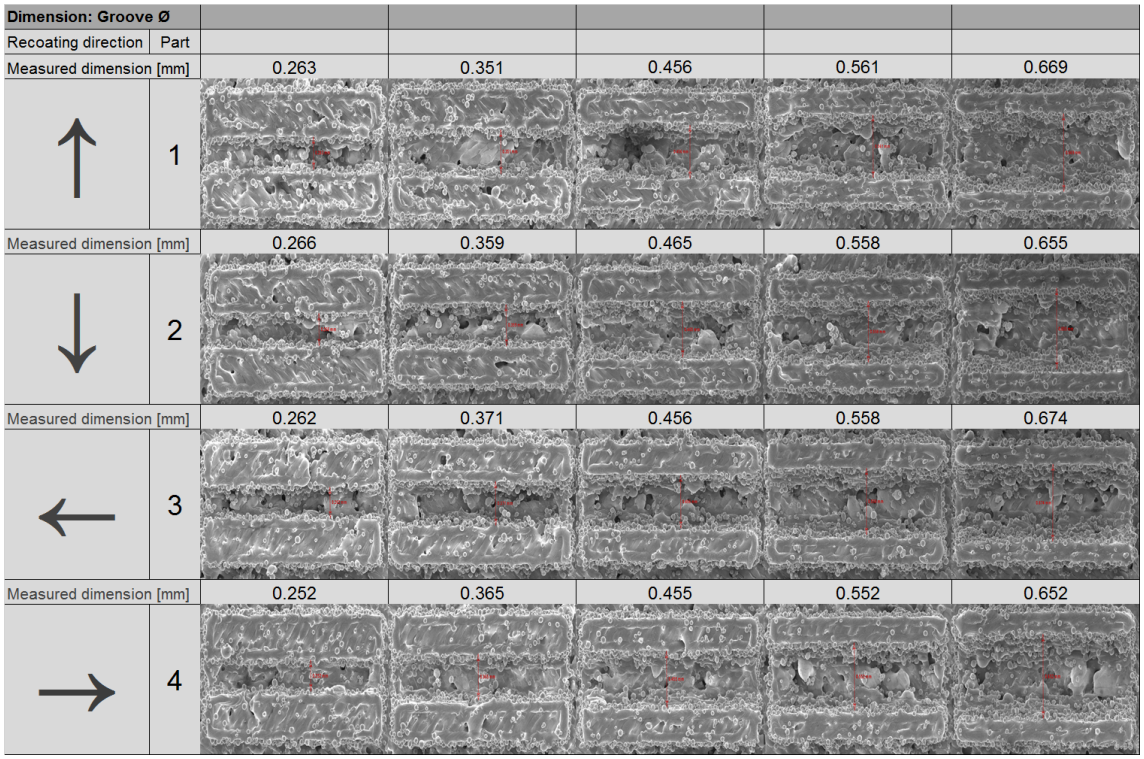

Figure B.38: ESEM images of the grooves for print 8.

Table B.38: Deviation of the grooves for print 8.

Groove [ϕ]	0.3		0.4		0.5		0.6		0.7	
Re-coat	[mm]	[%]	[mm]	[%]	[mm]	[%]	[mm]	[%]	[mm]	[%]
↑	-0.037	-12.33	-0.049	-12.25	-0.044	-8.8	-0.039	-6.5	-0.031	-4.42
↓	-0.034	-11.33	-0.041	-10.25	-0.035	-7	-0.042	-7	-0.045	-6.42
←	-0.038	-12.66	-0.029	-7.25	-0.044	-8.8	-0.042	-7	-0.026	-3.71
→	-0.048	-16	-0.035	-8.75	-0.045	-9	-0.048	-8	-0.048	-6.85

- **Print 9**

  All the grooves were printed good. There are half melted particles attached to the grooves. The prints surface are good. Traces of very small pores can be seen in the print. These issues in different grooves can be seen from the Figure B.39. The Table B.39 below shows the deviation of the grooves with respect to the original CAD dimension.

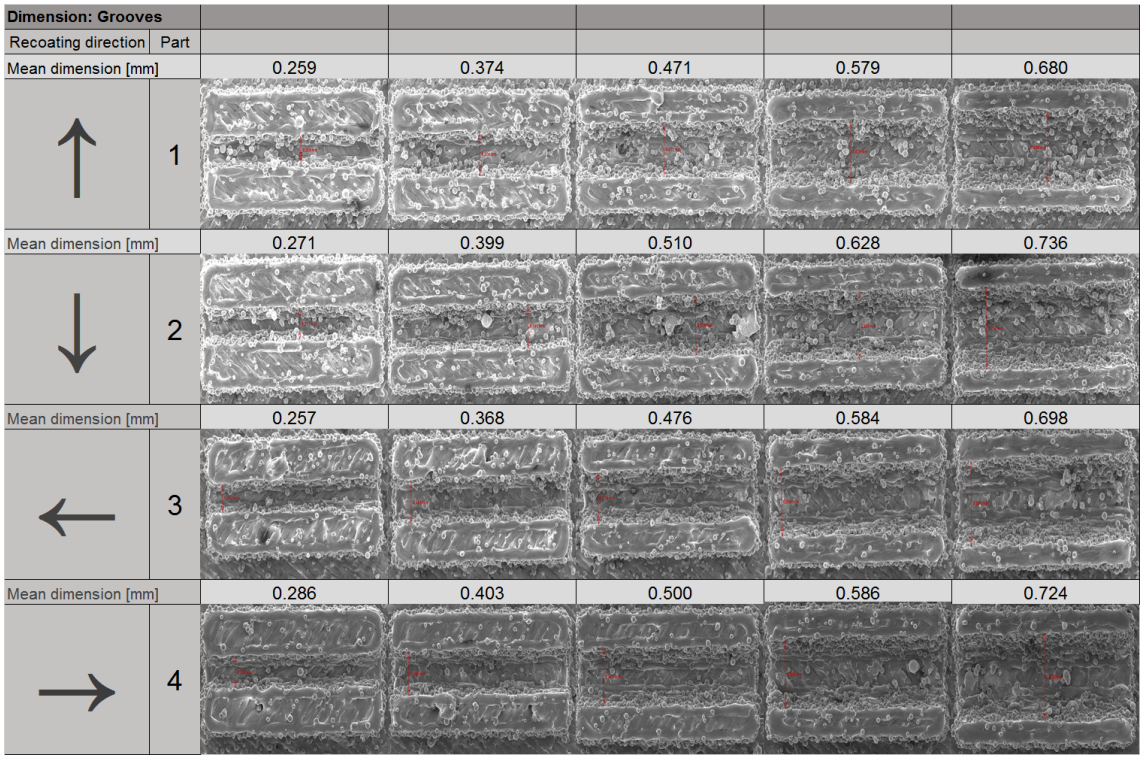

Figure B.39: ESEM images of the grooves for print 9.

Table B.39: Deviation of the grooves for print 9.

Groove [ϕ]	0.3		0.4		0.5		0.6		0.7	
Re-coat	[mm]	[%]	[mm]	[%]	[mm]	[%]	[mm]	[%]	[mm]	[%]
↑	-0.041	-13.67	-0.026	-6.50	-0.029	-5.80	-0.021	-3.00	-0.020	-2.86
↓	-0.029	-9.67	-0.001	-0.25	0.010	2.00	0.028	4.00	0.036	5.14
←	-0.043	-14.33	-0.032	-8.00	-0.024	-4.80	-0.016	-2.29	-0.002	-0.29
→	-0.014	-4.67	0.003	0.75	0.000	0.00	-0.014	-2.00	0.024	3.43

- **Print 10**

  All the grooves are printed. Although the edges are straight, they are hard to identify during measurements. These issues in different grooves can be seen from the Figure B.40. The Table B.40 below shows the deviation of the grooves with respect to the original CAD dimension.

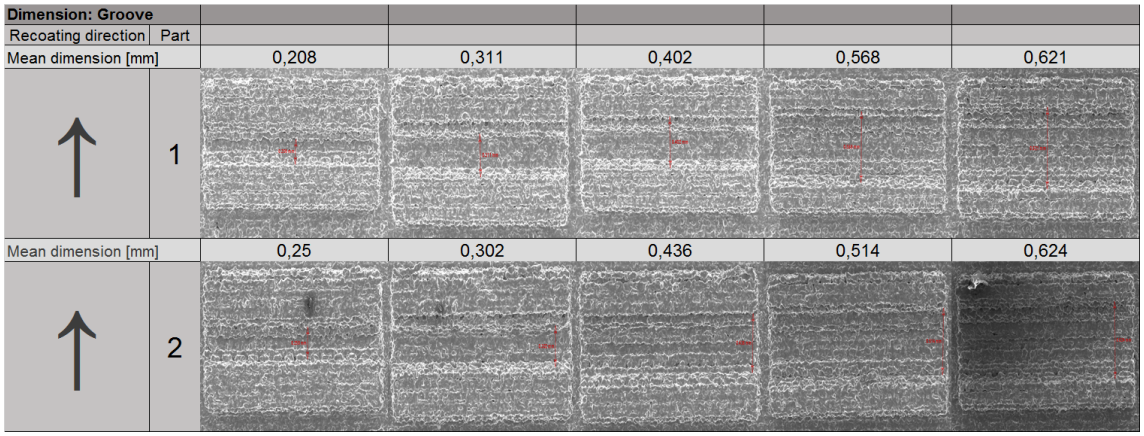

Figure B.40: ESEM images of the binder jetted grooves of print 10.

Table B.40: Deviation of the grooves for print 10.

Groove[ϕ]	**0.3**		**0.4**		**0.5**		**0.6**		**0.7**	
Re-coat	[mm]	[%]	[mm]	[%]	[mm]	[%]	[mm]	[%]	[mm]	[%]
↑	-0.092	-30.67	-0.089	-22.25	-0.098	-19.60	-0.032	-5.33	-0.079	-11.29
↑	-0.050	-16.67	-0.098	-24.50	-0.064	-12.80	-0.086	-14.33	-0.076	-10.86

B.5 Arrowfoot

- **Print 1**
  All the arrows were printed but there are some defects in them. In orientation 4, the first arrow and the third arrow are bent possibly due to re-coater issues. In other arrows some of the arrows had circularity issues in the fillets. The arrows were attached with half molten particles. These issues in different arrowfoot can be seen from the Figure B.41. The Table B.41 below shows the deviation of the arrowfoot with respect to the original CAD dimension.

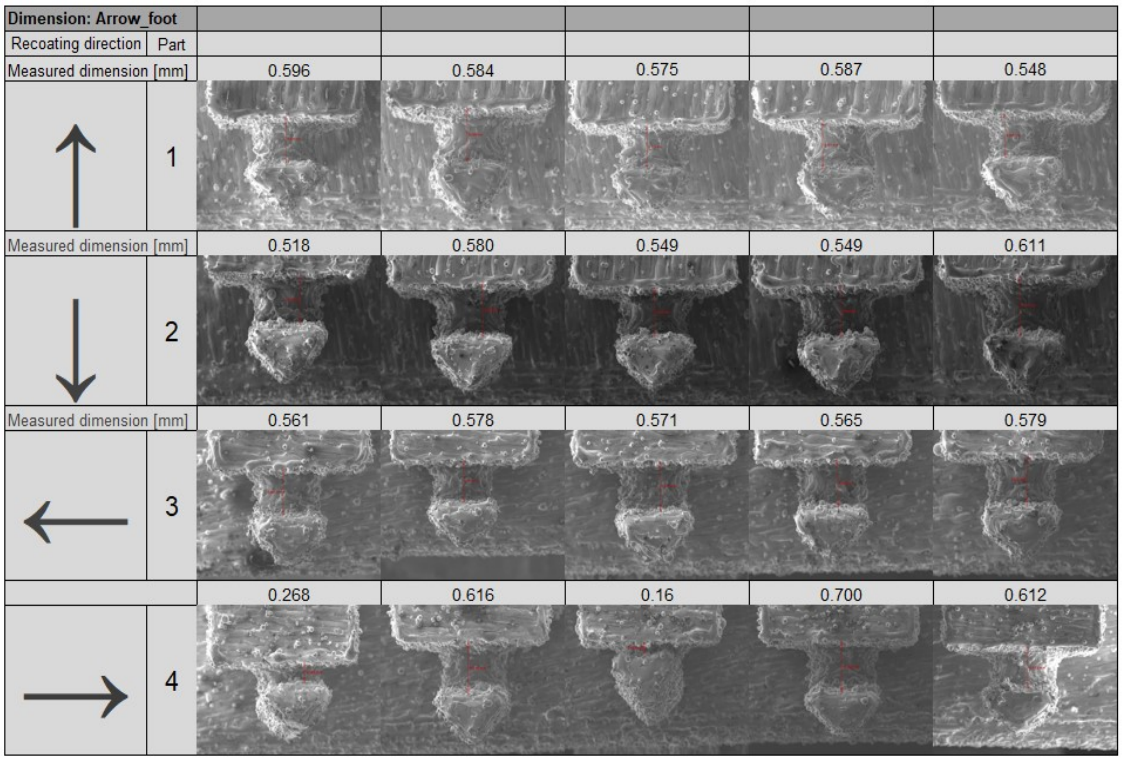

Figure B.41: ESEM images of arrowfoot of print 1.

Table B.41: Deviation of arrowfoot of print 1.

Arrowfoot	**0.5**		**0.5**		**0.5**		**0.5**		**0.5**	
Re-coat	[mm]	[%]	[mm]	[%]	[mm]	[%]	[mm]	[%]	[mm]	[%]
↑	0.096	19.2	0.084	16.8	0.075	15	0.087	17.4	0.048	9.6
↓	0.018	3.6	0.08	16	0.049	9.8	0.049	9.8	0.111	22.2
←	0.061	12.2	0.078	15.6	0.071	14.2	0.065	13	0.079	15.8
→	-0.232	-46.4	0.116	23.2	-0.34	-68	0.2	40	0.112	22.4

- **Print 2**
  All the arrows were printed but there are some defects in them. In orientation 2, the fifth arrow has some external particles attached. In other arrows some of the arrows had circularity issues in the fillets. There are pores present in the print. The arrows were attached with half molten particles. The top surface is not smooth. These issues in different arrowfoot can be seen from the Figure B.42. The Table B.42 below shows the deviation of the arrowfoot with respect to the original CAD dimension.

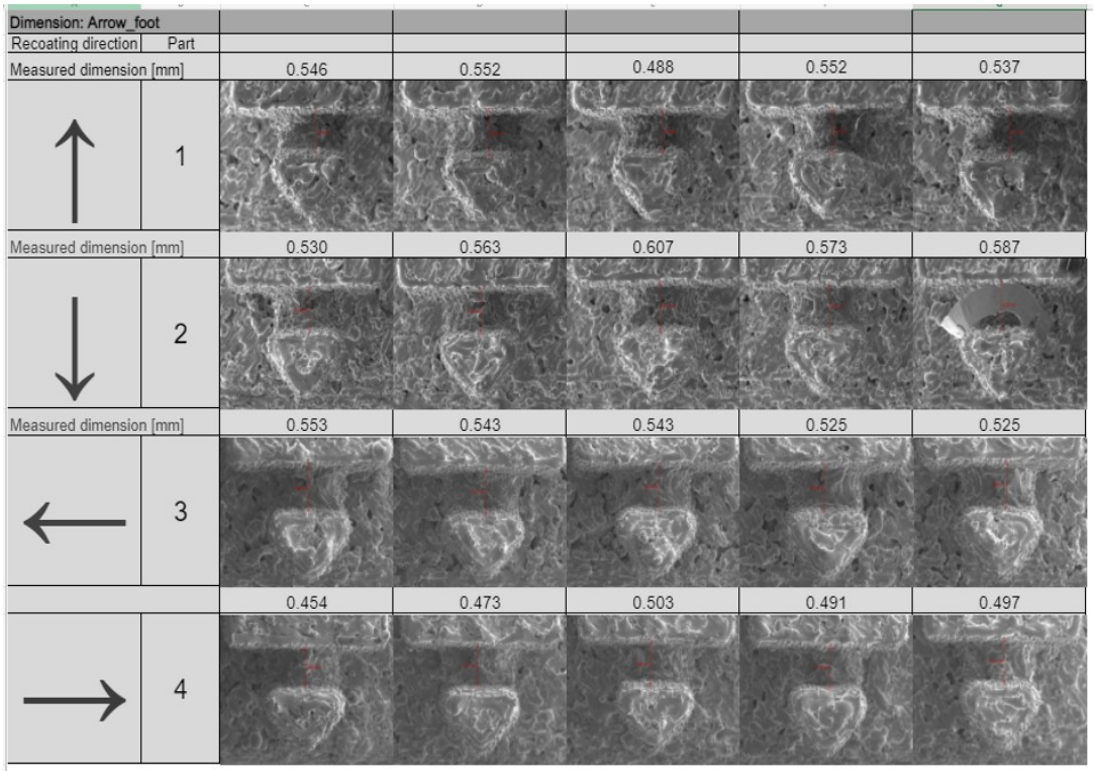

Figure B.42: ESEM images of arrowfoot of print 2.

Table B.42: Deviation of arrowfoot of print 2.

Arrowfoot	0.5		0.5		0.5		0.5		0.5	
Re-coat	[mm]	[%]	[mm]	[%]	[mm]	[%]	[mm]	[%]	[mm]	[%]
↑	0.046	9.2	0.052	10.4	-0.012	-2.4	0.052	10.4	0.037	7.4
↓	0.03	6	0.063	12.6	0.107	21.4	0.073	14.6	0.087	17.4
←	0.053	10.6	0.043	8.6	0.043	8.6	0.025	5	0.025	5
→	-0.046	-9.2	-0.027	-5.4	0.003	0.6	-0.009	-1.8	-0.003	-0.6

- **Print 3**
  All the arrows were printed but there are some defects in them. In other arrows some of the arrows has circularity issues in the nose section of the arrows. The arrows were attached with half molten particles. The top surface is not smooth. These issues in different arrowfoot can be seen from the Figure B.43. The Table B.43 below shows the deviation of the arrowfoot with respect to the original CAD dimension.

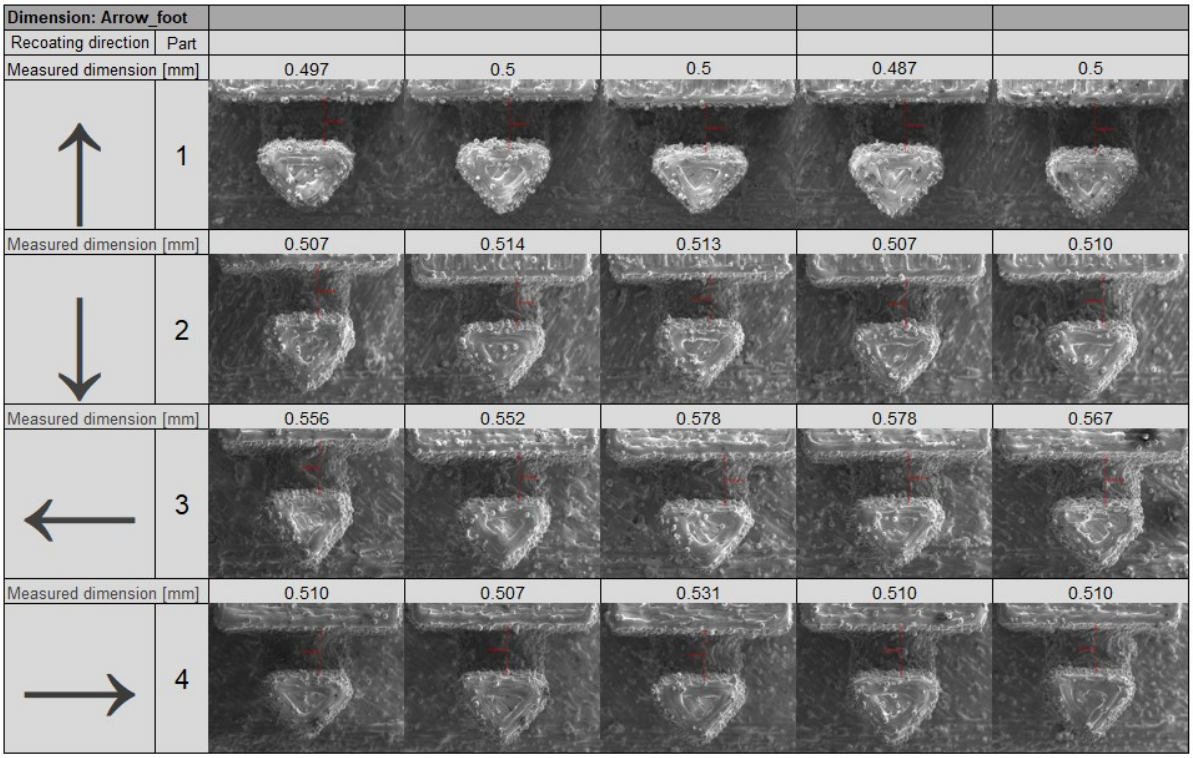

Figure B.43: ESEM images of arrowfoot of print 3.

Table B.43: Deviation of arrowfoot of print 3.

Arrowfoot	0.5		0.5		0.5		0.5		0.5	
Re-coat	[mm]	[%]	[mm]	[%]	[mm]	[%]	[mm]	[%]	[mm]	[%]
↑	-0.003	-0.6	0	0	0	0	-0.013	-2.6	0	0
↓	0.007	1.4	0.014	2.8	0.013	2.6	0.007	1.4	0.01	2
←	0.056	11.2	0.052	10.4	0.078	15.6	0.078	15.6	0.067	13.4
→	0.01	2	0.007	1.4	0.031	6.2	0.01	2	0.01	2

- **Print 4**
  All the arrows were printed but there are some defects in them. In orientation 2, the fourth arrow had some crack on the surface. In orientation 4, the the fifth arrow is bent. Arrow shapes are better than previous prints. The arrows were attached with half molten particles. The top surface is smooth. These issues in different arrowfoot can be seen from the Figure B.44. The Table B.44 below shows the deviation of the arrowfoot with respect to the original CAD dimension.

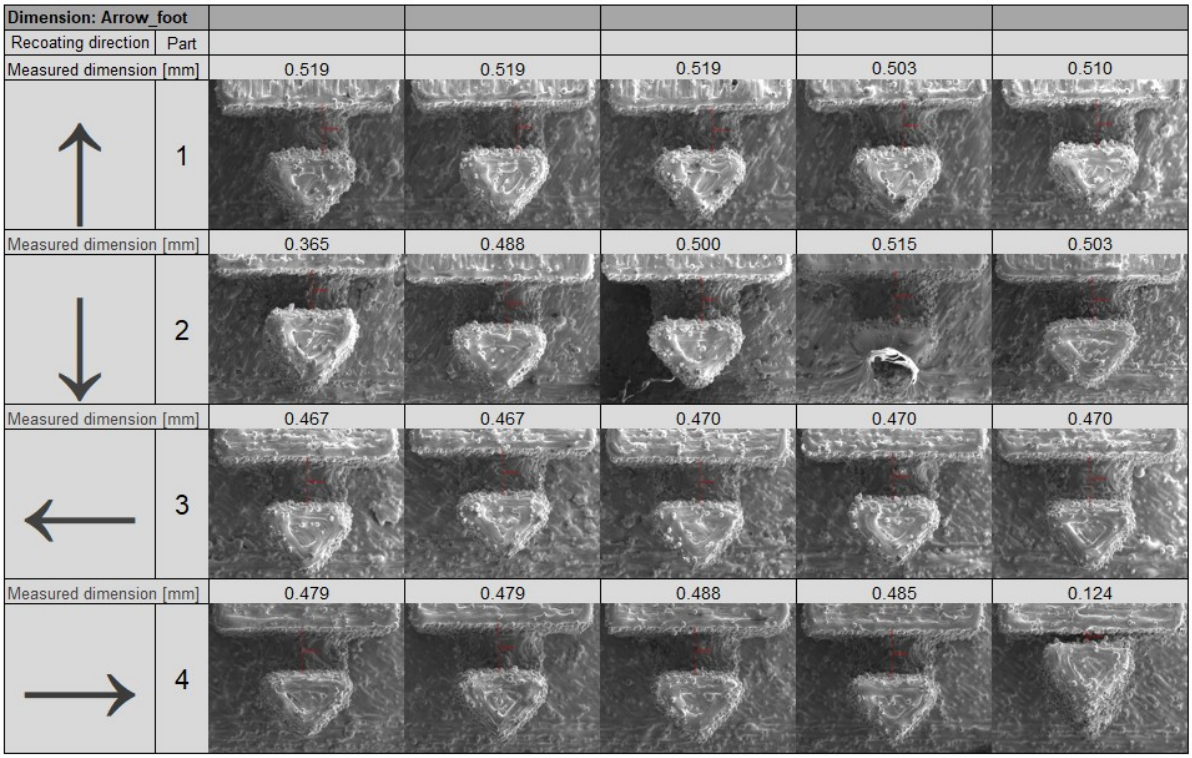

Figure B.44: ESEM images of arrowfoot of print 4.

Table B.44: Deviation of arrowfoot of print 4.

Arrowfoot	0.5		0.5		0.5		0.5		0.5	
Re-coat	[mm]	[%]	[mm]	[%]	[mm]	[%]	[mm]	[%]	[mm]	[%]
↑	0.019	3.8	0.019	3.8	0.019	3.8	0.003	0.6	0.01	2
↓	-0.135	-27	-0.012	-2.4	0	0	0.015	3	0.003	0.6
←	-0.033	-6.6	-0.033	-6.6	-0.03	-6	-0.03	-6	-0.03	-6
→	-0.021	-4.2	-0.021	-4.2	-0.012	-2.4	-0.015	-3	-0.376	-75.2

- **Print 5**
  All the arrows were printed. The arrows were attached with half molten particles. The top surface is smooth. The shapes of the arrows are consistent and better than all the previous prints. These issues in different arrowfoot can be seen from the Figure B.45. The Table B.45 below shows the deviation of the arrowfoot with respect to the original CAD dimension.

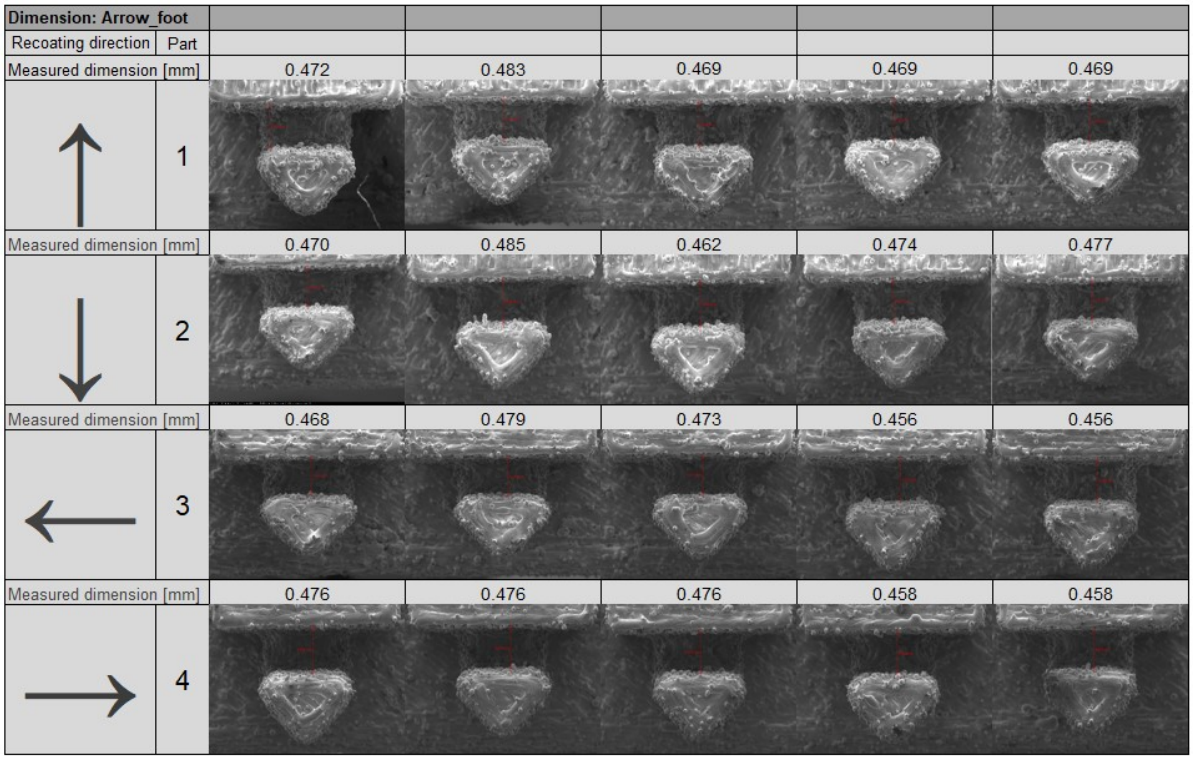

Figure B.45: ESEM images of arrowfoot of print 5.

Table B.45: Deviation of arrowfoot of print 5.

Arrowfoot	0.5		0.5		0.5		0.5		0.5	
Re-coat	[mm]	[%]	[mm]	[%]	[mm]	[%]	[mm]	[%]	[mm]	[%]
↑	-0.028	-5.6	-0.017	-3.4	-0.031	-6.2	-0.031	-6.2	-0.031	-6.2
↓	-0.030	-6	-0.015	-3	-0.038	-7.6	-0.026	-5.2	-0.023	-4.6
←	-0.032	-6.4	-0.021	-4.2	-0.027	-5.4	-0.044	-8.8	-0.044	-8.8
→	-0.024	-4.8	-0.024	-4.8	-0.024	-4.8	-0.042	-8.4	-0.042	-8.4

- **Print 6**
  All the arrows were printed but there are some defects in them. There are pores present on the part. The arrows were attached with half molten particles. The top surface is smooth and the shape of the arrows are consistent. These issues in different arrowfoot can be seen from the Figure B.46. The Table B.46 below shows the deviation of the arrowfoot with respect to the original CAD dimension.

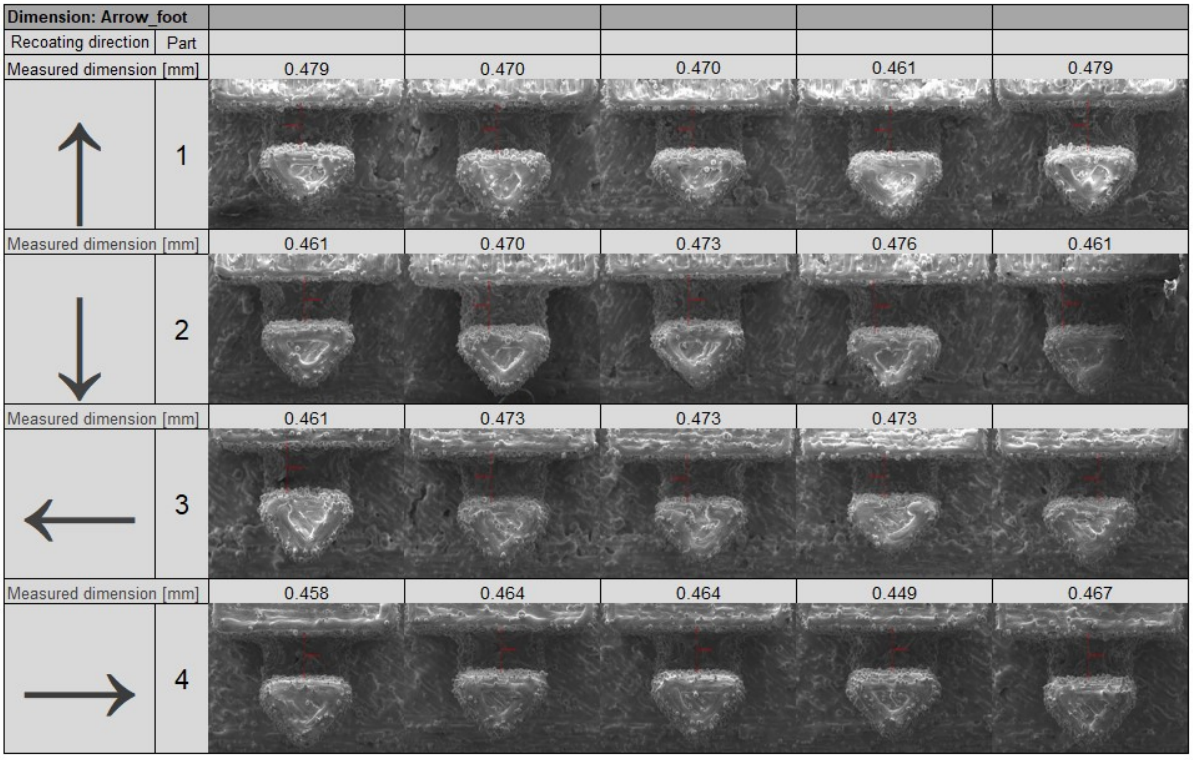

Figure B.46: ESEM images of arrowfoot of print 6.

Table B.46: Deviation of arrowfoot of print 6.

Arrowfoot	0.5		0.5		0.5		0.5		0.5	
Re-coat	[mm]	[%]	[mm]	[%]	[mm]	[%]	[mm]	[%]	[mm]	[%]
↑	-0.021	-4.2	-0.03	-6	-0.03	-6	-0.039	-7.8	-0.021	-4.2
↓	-0.039	-7.8	-0.03	-6	-0.027	-5.4	-0.024	-4.8	-0.039	-7.8
←	-0.039	-7.8	-0.027	-5.4	-0.027	-5.4	-0.027	-5.4	-0.027	-5.4
→	-0.042	-8.4	-0.036	-7.2	-0.036	-7.2	-0.051	-10.2	-0.033	-6.6

- **Print 7**
  All the arrows were printed but there are some defects in them. There are pores present on the part. The arrows were attached with half molten particles. The top surface is not smooth but the shape of the arrows are consistent. These issues in different arrowfoot can be seen from the Figure B.47. The Table B.47 below shows the deviation of the arrowfoot with respect to the original CAD dimension.

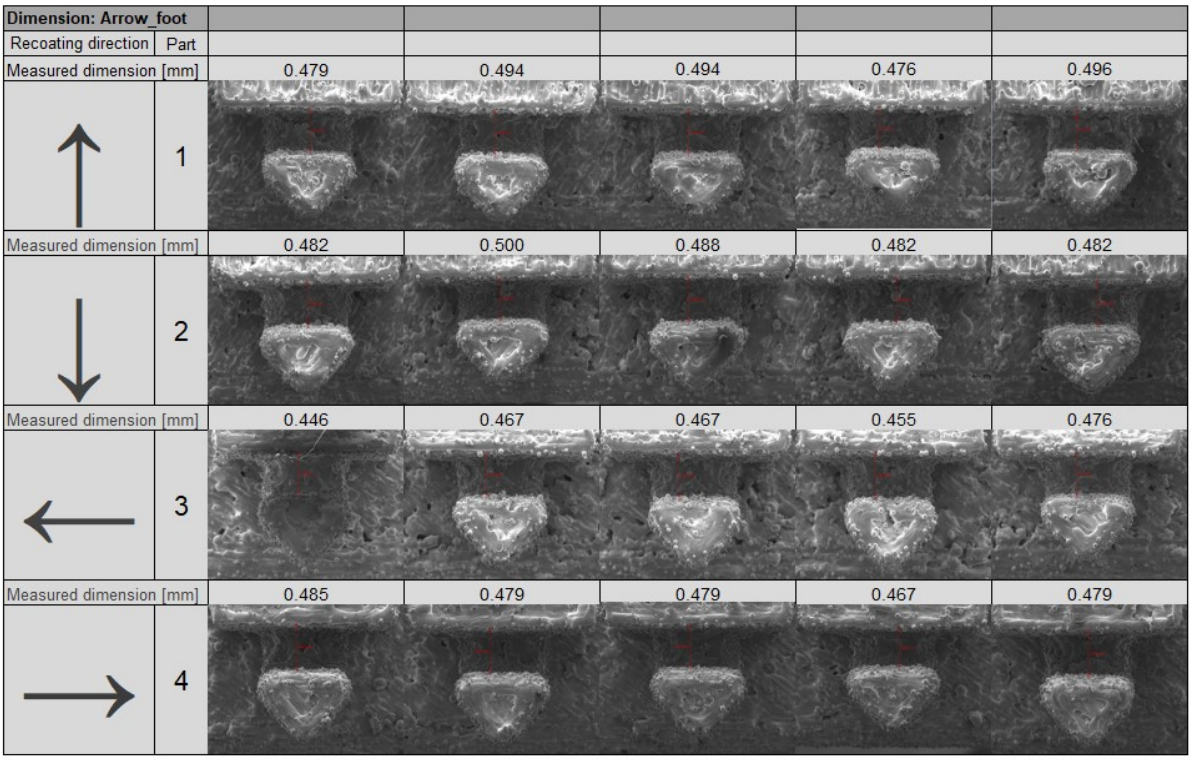

Figure B.47: ESEM images of arrowfoot of print 7.

Table B.47: Deviation of arrowfoot of print 7.

Arrowfoot	0.5		0.5		0.5		0.5		0.5	
Re-coat	[mm]	[%]	[mm]	[%]	[mm]	[%]	[mm]	[%]	[mm]	[%]
↑	-0.021	-4.2	-0.006	-1.2	-0.006	-1.2	-0.024	-4.8	-0.004	-0.8
↓	-0.018	-3.6	0	0	-0.012	-2.4	-0.018	-3.6	-0.018	-3.6
←	-0.054	-10.8	-0.033	-6.6	-0.033	-6.6	-0.045	-9	-0.024	-4.8
→	-0.015	-3	-0.021	-4.2	-0.021	-4.2	-0.033	-6.6	-0.021	-4.2

- **Print 8**
  All the arrows were printed but there are some defects in them. There are pores present on the part. In orientation 2, the fifth arrow is bent. The arrows are attached with half molten particles. The top surface is not smooth but the shape of the arrows are consistent. These issues in different arrowfoot can be seen from the Figure B.48. The Table B.48 below shows the deviation of the arrowfoot with respect to the original CAD dimension.

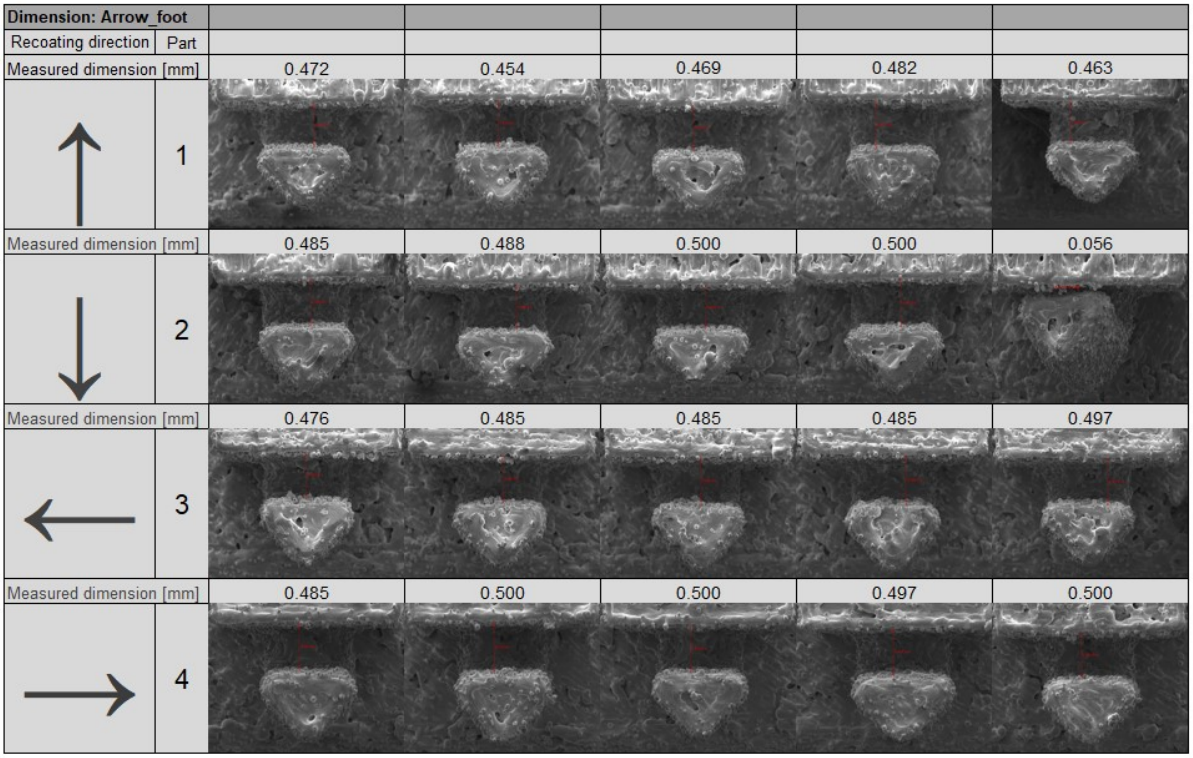

Figure B.48: ESEM images of arrowfoot of print 8.

Table B.48: Deviation of arrowfoot of print 8.

Arrowfoot	0.5		0.5		0.5		0.5		0.5	
Re-coat	[mm]	[%]	[mm]	[%]	[mm]	[%]	[mm]	[%]	[mm]	[%]
↑	-0.028	-5.6	-0.046	-9.2	-0.031	-6.2	-0.018	-3.6	-0.037	-7.4
↓	-0.015	-3	-0.012	-2.4	0	0	0	0	-0.444	-88.8
←	-0.024	-4.8	-0.015	-3	-0.015	-3	-0.015	-3	-0.003	-0.6
→	-0.015	-3	0	0	0	0	-0.003	-0.6	0	0

- **Print 9**
  All the arrows were printed but there are some defects in them. In orientation 1 and orientation 4, the fifth arrow are bent. Arrow shapes are good. The arrows were attached with half molten particles. The top surface is smooth. These issues in different arrowfoot can be seen from the Figure B.49. The Table B.49 below shows the deviation of the arrowfoot with respect to the original CAD dimension.

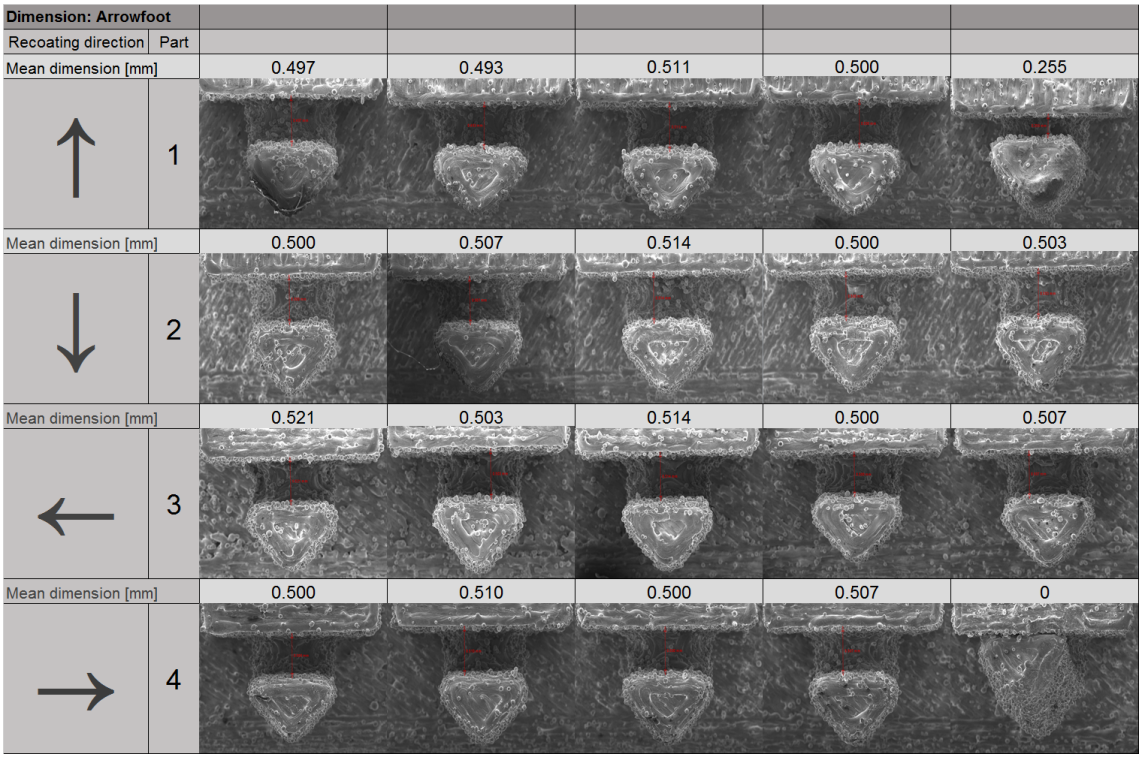

Figure B.49: ESEM images of the arrowfoot of print 9.

Table B.49: Deviation of arrowfoot of print 9.

Arrowfoot	0.5		0.5		0.5		0.5		0.5	
Re-coat	[mm]	[%]	[mm]	[%]	[mm]	[%]	[mm]	[%]	[mm]	[%]
↑	-0.003	-0.60	-0.007	-1.40	0.011	2.20	0	0.00	-0.245	-49.00
↓	0.000	0.00	0.007	1.40	0.014	2.80	0	0.00	0.003	0.60
←	0.021	4.20	0.003	0.60	0.014	2.80	0	0.00	0.007	1.40
→	0.000	0.00	0.010	2.00	0.000	0.00	0.007	1.40	-0.500	-100.00

- **Print 10**
  All the arrows are printed but there are some defects present. In part 1 and part 2, the fifth arrow is bent which is seen in both the technologies. Moreover the dimensions are the least compared to other prints. These issues in different arrowfoot can be seen from the Figure B.50. The Table B.50 below shows the deviation of the arrowfoot with respect to the original CAD dimension.

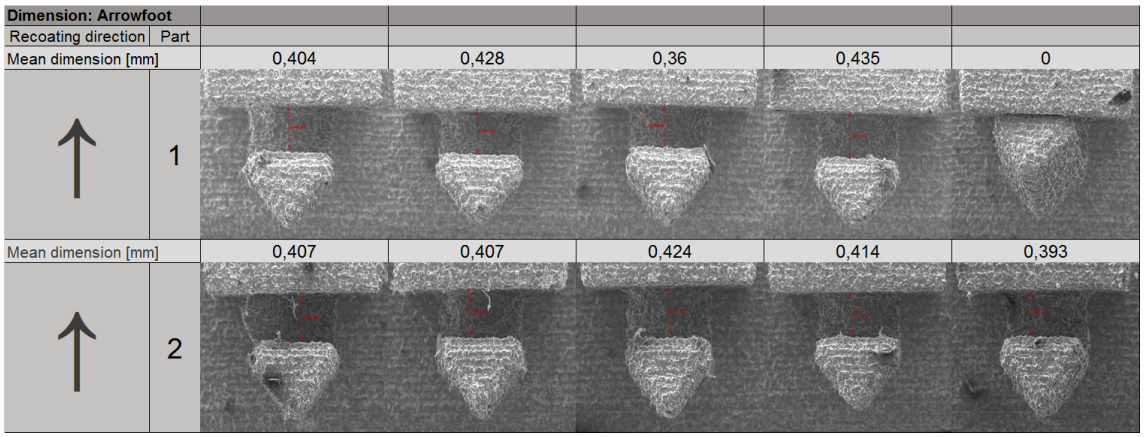

Figure B.50: ESEM images of the binder jetted arrowfoot of print 10.

Table B.50: Deviation of the arrowfoot for print 10.

Arrowfoot	**0.5**		**0.5**		**0.5**		**0.5**		**0.5**	
Re-coat	[mm]	[%]	[mm]	[%]	[mm]	[%]	[mm]	[%]	[mm]	[%]
↑	-0.096	-19.2	-0.072	-14.4	-0.14	-28	-0.065	-13	-0.5	-100
↑	-0.093	-18.6	-0.093	-18.6	-0.076	-15.2	-0.086	-17.2	-0.107	-21.4

B.6 Arrow shape area

This method is not very accurate in measurement of area of the arrow. As it can be seen in the Figure B.51, the arrow shapes look different and not easy to extract with the half molten particles attached to the sides of the arrow. This either increases the area or decreases when eliminating the noise in the image. The original CAD area of the arrow from the top view is 0.429 mm^2. The arrow shape which is red is indicating the bent which increases the arrow area. Therefore this method was not used for the further prints.

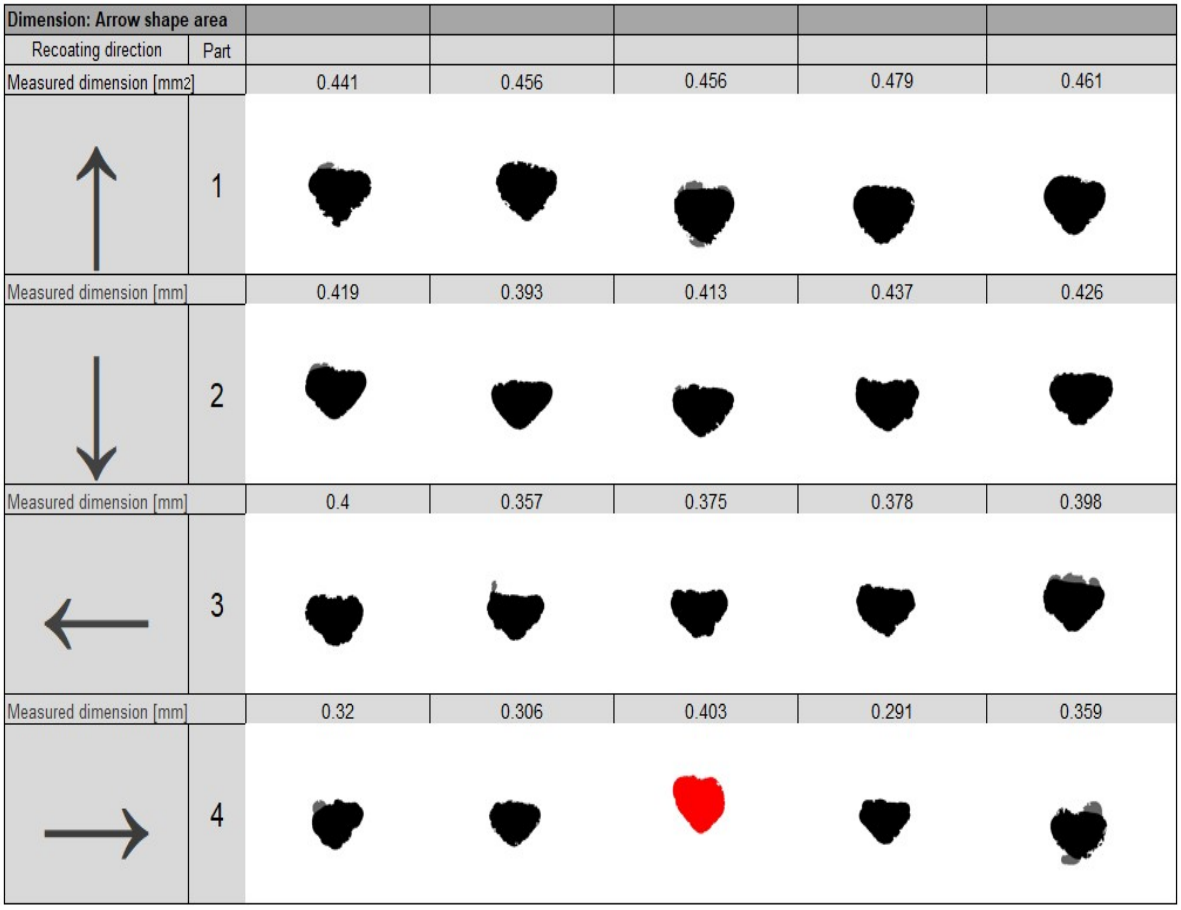

Figure B.51: Images of arrow shape area of print 1.

Table B.51: Deviation for the arrow area expressed in distance and percentage.

Arrowarea	**0.429**		**0.429**		**0.429**		**0.429**		**0.429**	
Re-coat	[mm]	[%]	[mm]	[%]	[mm]	[%]	[mm]	[%]	[mm]	[%]
↑	0.012	2.797	0.027	6.294	0.027	6.294	0.05	11.66	0.032	7.459
↓	-0.01	-2.33	-0.04	-8.39	-0.02	-3.73	0.008	1.865	-0	-0.7
←	-0.03	-6.76	-0.07	-16.8	-0.05	-12.6	-0.05	-11.9	-0.03	-7.23
→	-0.11	-25.4	-0.12	-28.7	-0.03	-6.06	-0.14	-32.2	-0.07	-16.3

C

SOM mesurements & Deviation tables

C.1 Print 1 comparison between ESEM & SOM measurements

C.1.1 Pins

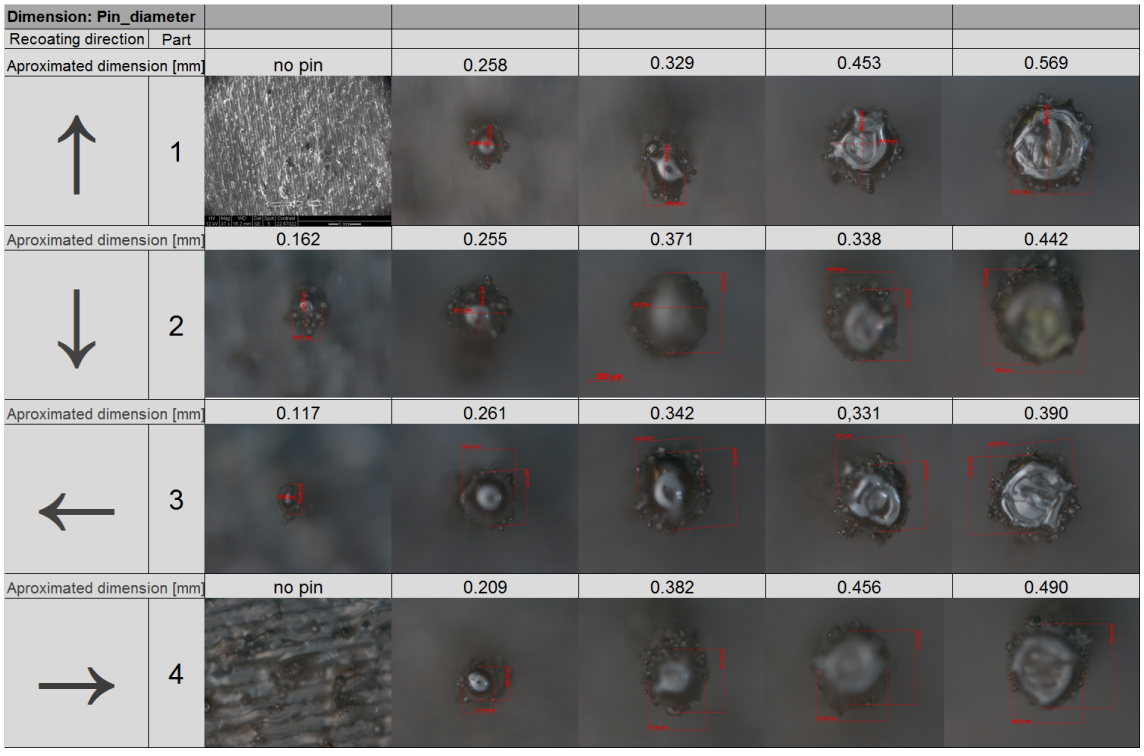

Figure C.1: SOM images of pins for print 1.

C.1.2 Arrowhead base

Dimension: AH base						
Recoating direction	Part					
Measured dimension [mm]		0.445	0.698	0.888	0.847	0.879
↑	1	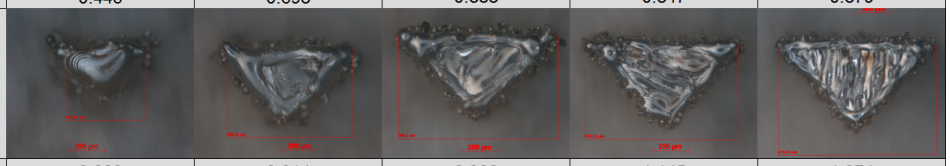				
Measured dimension [mm]		0.609	0.914	0.960	1.145	1.074
↓	2					
Measured dimension [mm]		0.556	0.853	0.964	1.152	1.150
←	3					
Measured dimension [mm]		0.597	0.789	1.170	1.061	1.223
→	4					

Figure C.2: SOM images of arrowhead base for print 1.

C.1.3 Grooves

Dimension: Groove Ø						
Recoating direction	Part					
Measured dimension [mm]		0.386	0.518	0.563	0.647	0.670
↑	1	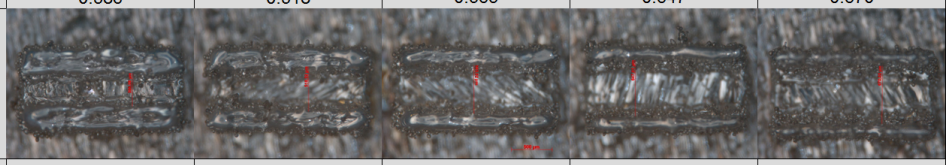				
Measured dimension [mm]		0.359	0.470	missing messurment	0.634	0.703
↓	2	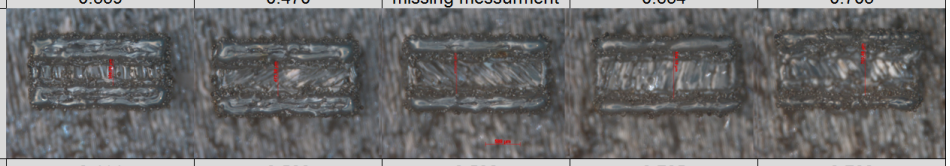				
Measured dimension [mm]		0.414	0.500	0.592	0.705	0.762
←	3					
Measured dimension [mm]		0.553	0.545	0.636	0.723	0.752
→	4	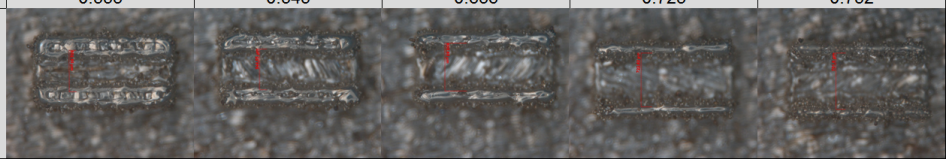				

Figure C.3: SOM images of grooves for print 1.

C.2 Gaps

- **Print 1**
  All the gaps are visible without any attachments to the nearest part. The SOM images and measurements of each gap can be seen in the Figure C.4. The Table C.1 below shows the deviation of the grooves with respect to the original CAD dimension. If the gaps are smaller than the original dimension, then it is a result of irregular shape of the part and half molten particles attached. If the gaps are bigger than the original dimension, then it can be due to shrinkage and irregular shape of the part.

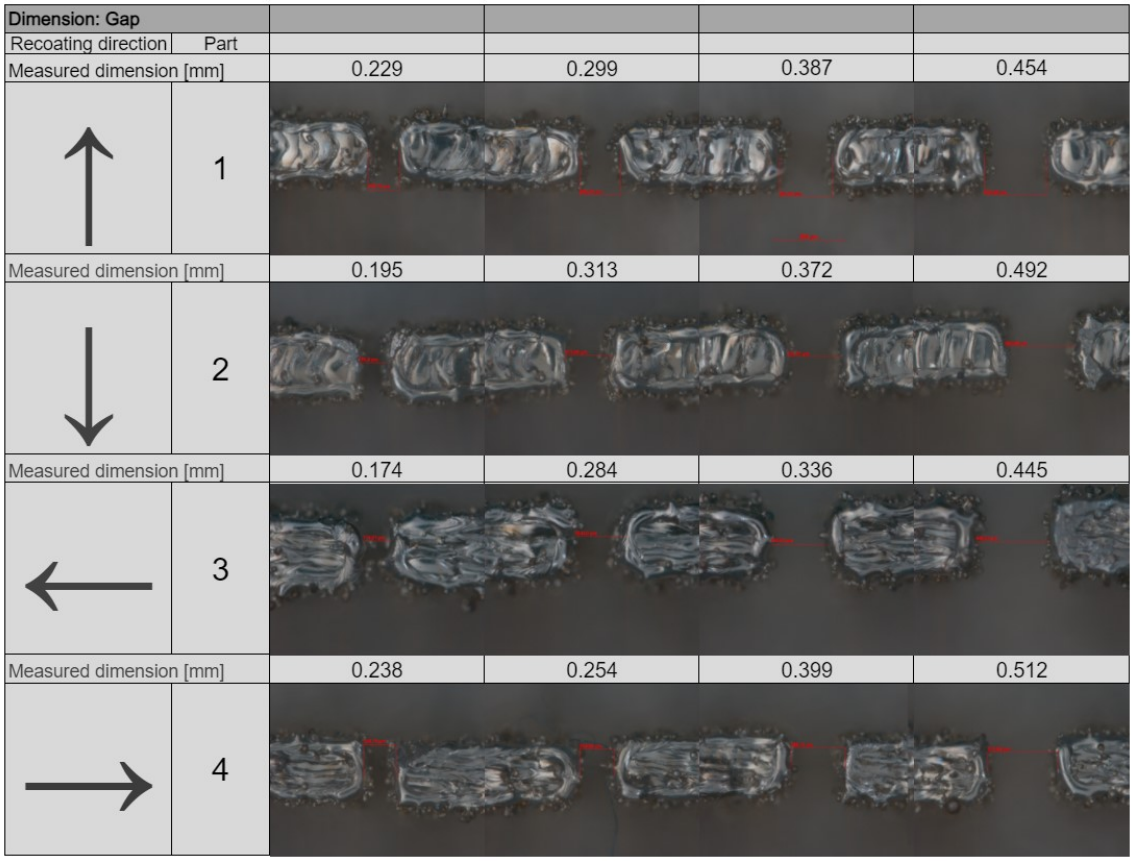

Figure C.4: SOM images of the gaps for print 1.

Table C.1: Deviation of the gaps for print 1.

Gap	0.1		0.2		0.3		0.4	
Re-coat	[mm]	[%]	[mm]	[%]	[mm]	[%]	[mm]	[%]
↑	0.129	129	0.099	49.5	0.087	29	0.054	13.5
↓	0.095	95	0.113	56.5	0.072	24	0.092	23
←	0.074	74	0.084	42	0.036	12	0.045	11.25
→	0.138	138	0.054	27	0.099	33	0.112	28

- **Print 2**
  The gaps are visible without any attachments to the nearest part except for the first gaps in all orientations. The SOM images and measurements of each gap can be seen in the Figure C.5. The Table C.2 below shows the deviation of the grooves with respect to the original CAD dimension. If the gaps are smaller than the original dimension, then it is a result of irregular shape of the part and half molten particles attached. If the gaps are bigger than the original dimension, then it can be due to shrinkage and irregular shape of the part.

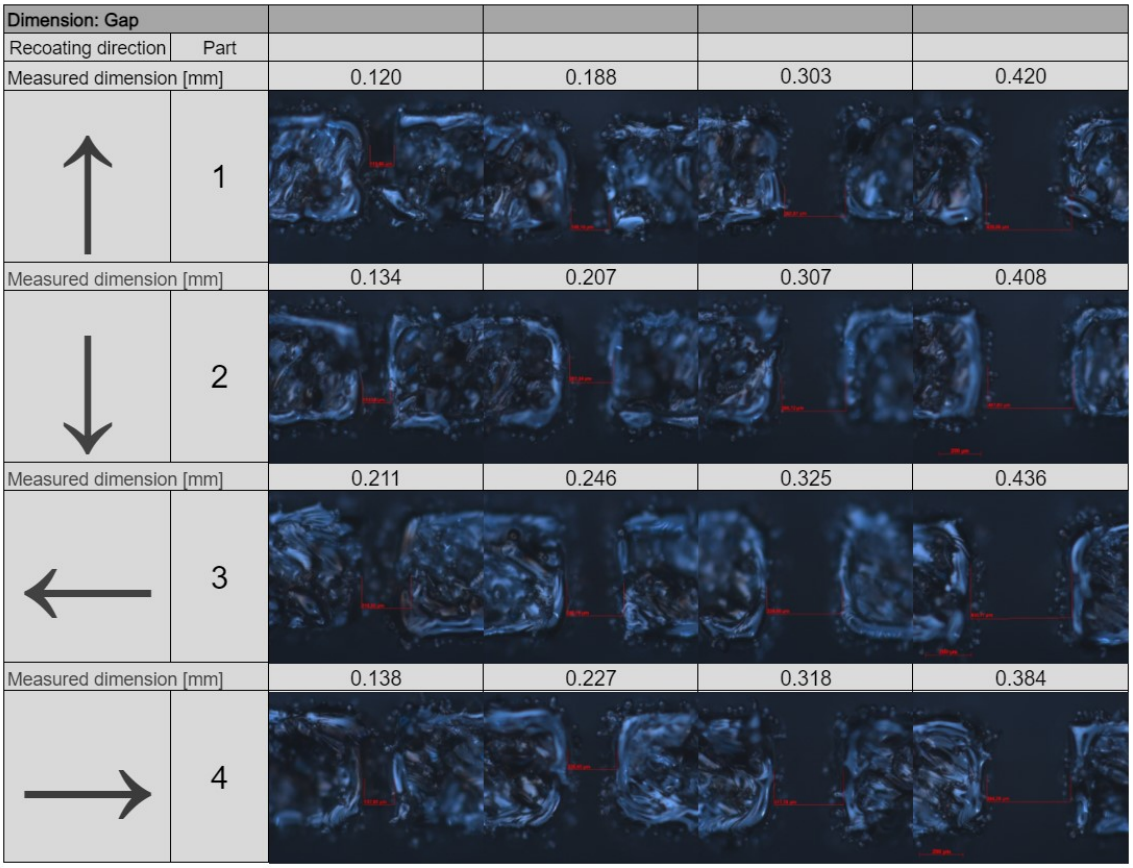

Figure C.5: SOM images of the gaps for print 2.

Table C.2: Deviation of the gaps for print 2.

Gap	0.1		0.2		0.3		0.4	
Re-coat	[mm]	[%]	[mm]	[%]	[mm]	[%]	[mm]	[%]
↑	0.02	20	-0.012	-6	0.003	1	0.02	5
↓	0.034	34	0.007	3.5	0.007	2.33	0.008	2
←	0.111	111	0.046	23	0.025	8.33	0.036	9
→	0.038	38	0.027	13.5	0.018	6	-0.016	-4

- **Print 3**
  The gaps are visible without any attachments to the nearest part except for the first gaps in all orientations. The SOM images and measurements of each gap can be seen in the Figure C.6. The Table C.3 below shows the deviation of the grooves with respect to the original CAD dimension. If the gaps are smaller than the original dimension, then it is a result of irregular shape of the part and half molten particles attached. If the gaps are bigger than the original dimension, then it can be due to shrinkage and irregular shape of the part.

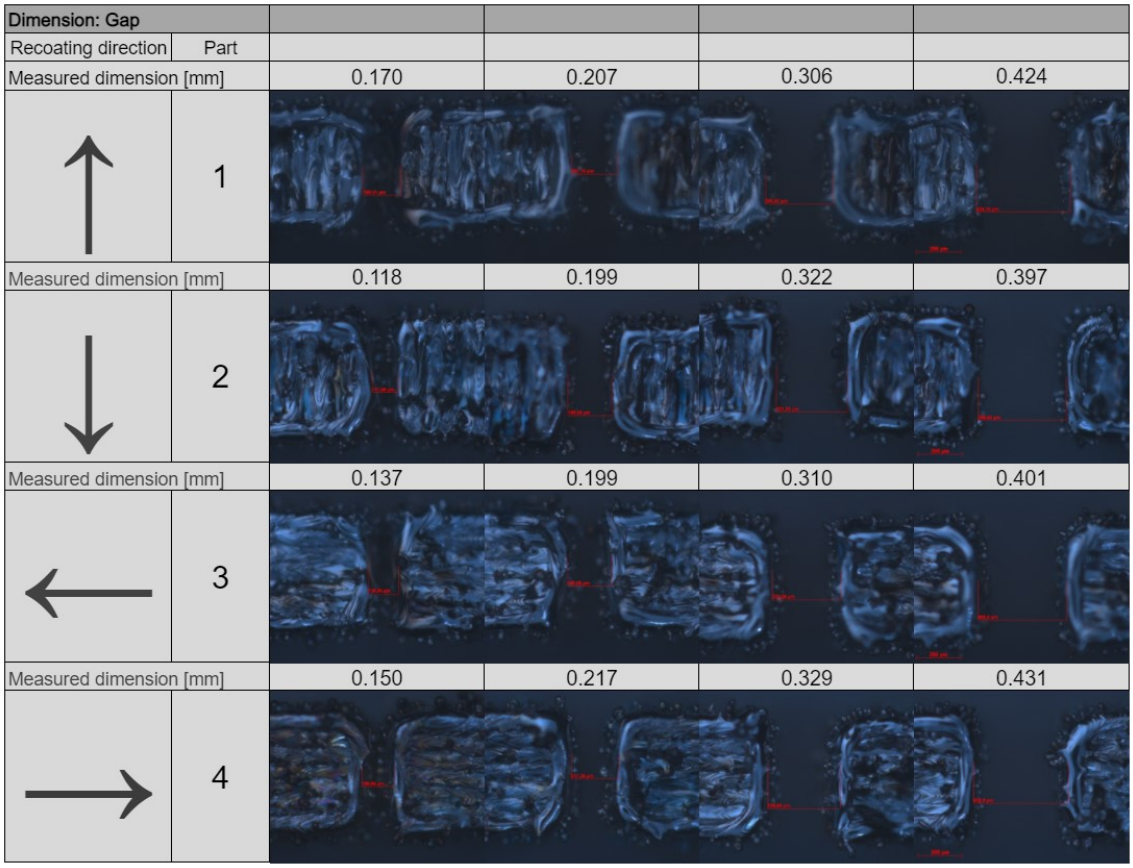

Figure C.6: SOM images of the gaps for print 3.

Table C.3: Deviation of the gaps for print 3.

Gap	0.1		0.2		0.3		0.4	
Re-coat	[mm]	[%]	[mm]	[%]	[mm]	[%]	[mm]	[%]
↑	0.07	70	0.007	3.5	0.006	2	0.024	6
↓	0.018	18	-0.001	-0.5	0.022	7.33	-0.003	-0.75
←	0.037	37	-0.001	-0.5	0.01	3.33	0.001	0.25
→	0.05	50	0.017	8.5	0.029	9.66	0.031	7.75

- **Print 4**
  The gaps are visible without any attachments to the nearest part except for the first gaps in all orientations. The SOM images and measurements of each gap can be seen in the Figure C.7. The Table C.4 below shows the deviation of the grooves with respect to the original CAD dimension. If the gaps are smaller than the original dimension, then it is a result of irregular shape of the part and half molten particles attached. If the gaps are bigger than the original dimension, then it can be due to shrinkage and irregular shape of the part.

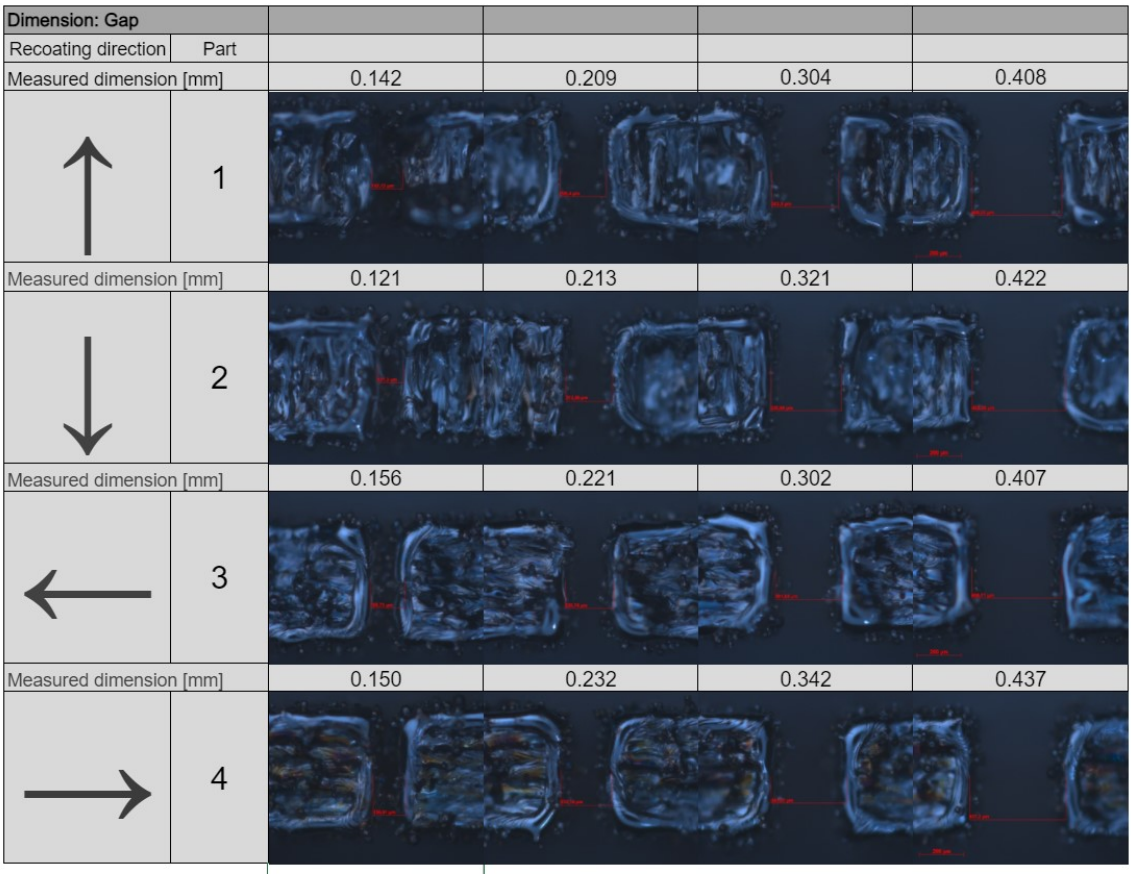

Figure C.7: SOM images of the gaps for print 4.

Table C.4: Deviation of the gaps for print 4.

Gap	0.1		0.2		0.3		0.4	
Re-coat	[mm]	[%]	[mm]	[%]	[mm]	[%]	[mm]	[%]
↑	0.042	42	0.009	4.5	0.004	1.33	0.008	2
↓	0.021	21	0.013	6.5	0.021	7	0.022	5.5
←	0.056	56	0.021	10.5	0.002	0.66	0.007	1.75
→	0.05	50	0.032	16	0.042	14	0.037	9.25

- **Print 5** The gaps are visible without any attachments to the nearest part except for the first gaps in all orientations. The SOM images and measurements of each gap can be seen in the Figure C.8. The Table C.5 below shows the deviation of the grooves with respect to the original CAD dimension. If the gaps are smaller than the original dimension, then it is a result of irregular shape of the part and half molten particles attached. If the gaps are bigger than the original dimension, then it can be due to shrinkage and irregular shape of the part.

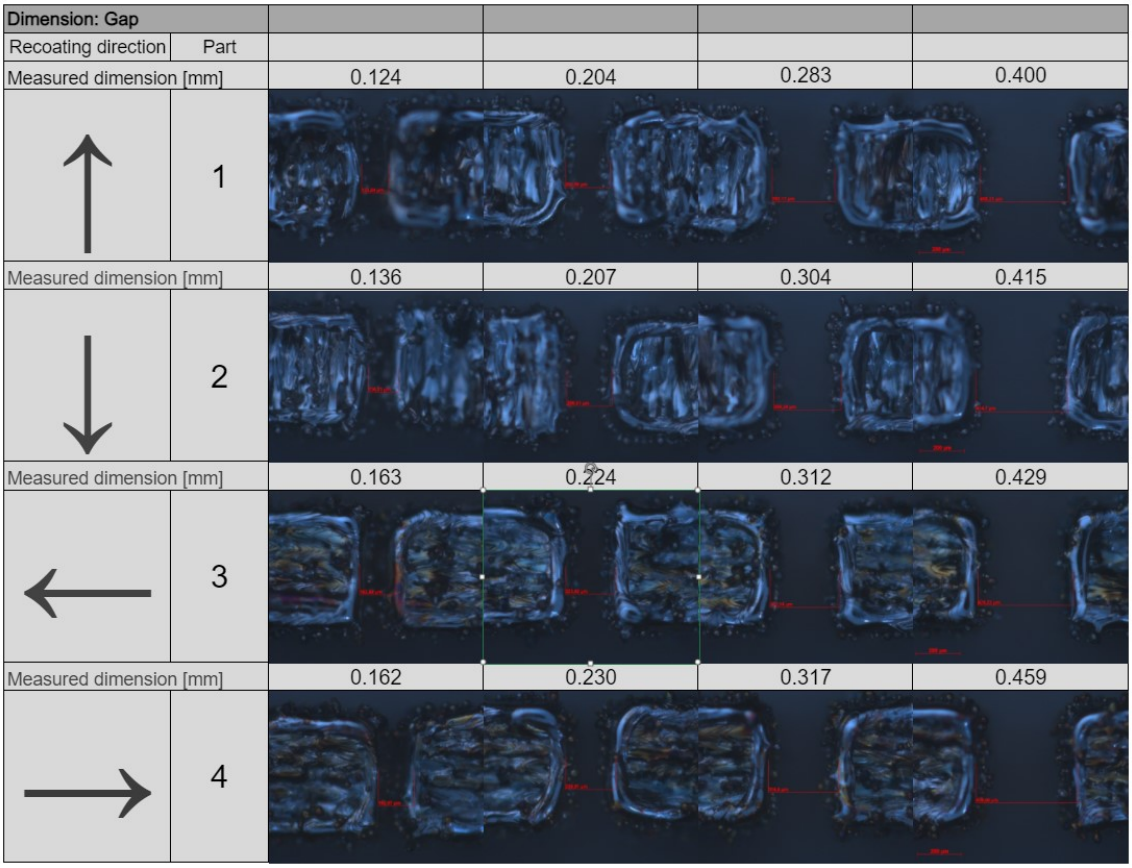

Figure C.8: SOM images of the gaps for print 5.

Table C.5: Deviation of the gaps for print 5.

Gap	0.1		0.2		0.3		0.4	
Re-coat	[mm]	[%]	[mm]	[%]	[mm]	[%]	[mm]	[%]
↑	0.024	24	0.004	2	-0.017	-5.67	0	0
↓	0.036	36	0.007	3.5	0.004	1.33	0.015	3.75
←	0.063	63	0.024	12	0.012	4.00	0.029	7.25
→	0.062	62	0.03	15	0.017	5.67	0.059	14.75

- **Print 6**
  The gaps are visible without any attachments to the nearest part except for the first gaps in all orientations. The SOM images and measurements of each gap can be seen in the Figure C.9. The Table C.6 below shows the deviation of the grooves with respect to the original CAD dimension. If the gaps are smaller than the original dimension, then it is a result of irregular shape of the part and half molten particles attached. If the gaps are bigger than the original dimension, then it can be due to shrinkage and irregular shape of the part.

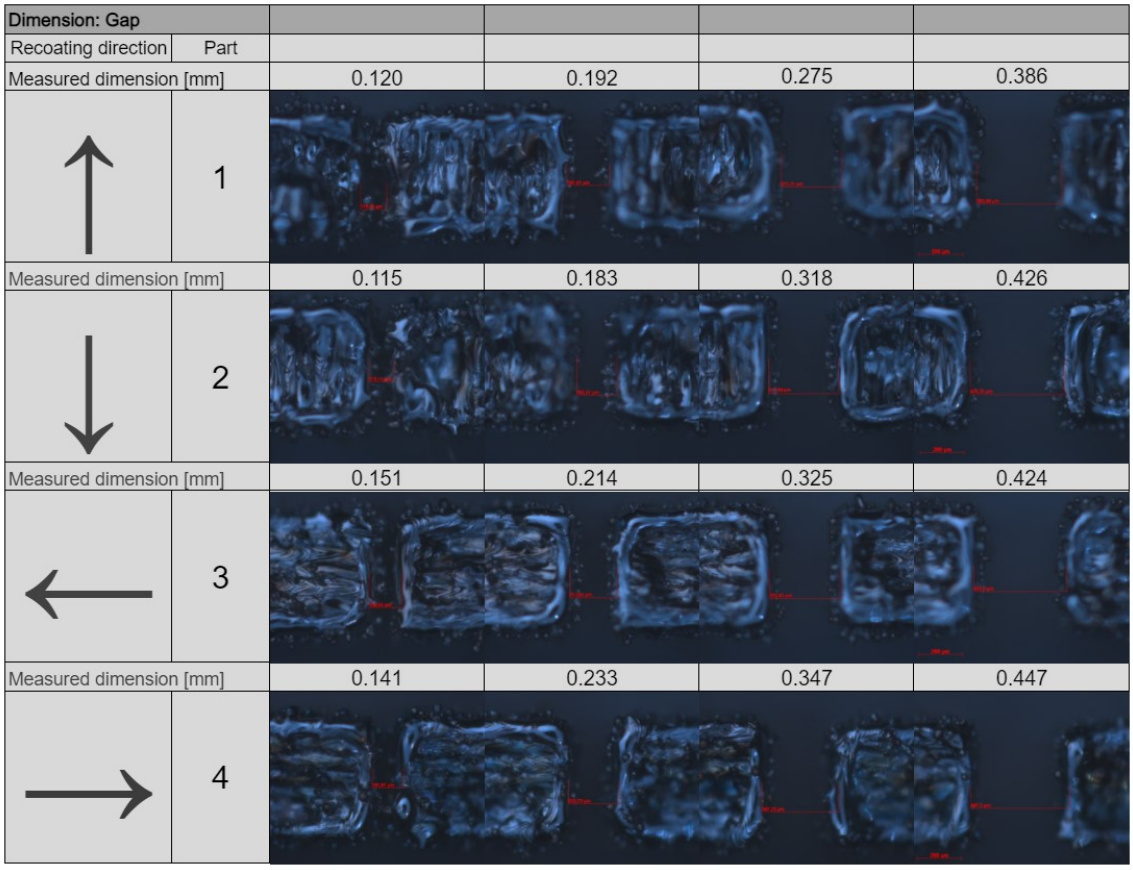

Figure C.9: SOM images of the gaps for print 6.

Table C.6: Deviation of the gaps for print 6.

Gap	0.1		0.2		0.3		0.4	
Re-coat	[mm]	[%]	[mm]	[%]	[mm]	[%]	[mm]	[%]
↑	0.02	20	-0.008	-4	-0.025	-8.33	-0.014	-3.5
↓	0.015	15	-0.017	-8.5	0.018	6.00	0.026	6.5
←	0.051	51	0.014	7	0.025	8.33	0.024	6
→	0.041	41	0.033	16.5	0.047	15.67	0.047	11.75

- **Print 7**
  The gaps are visible without any attachments to the nearest part except for the first gaps in all orientations. The SOM images and measurements of each gap can be seen in the Figure C.10. The Table C.7 below shows the deviation of the grooves with respect to the original CAD dimension. If the gaps are smaller than the original dimension, then it is a result of irregular shape of the part and half molten particles attached. If the gaps are bigger than the original dimension, then it can be due to shrinkage and irregular shape of the part.

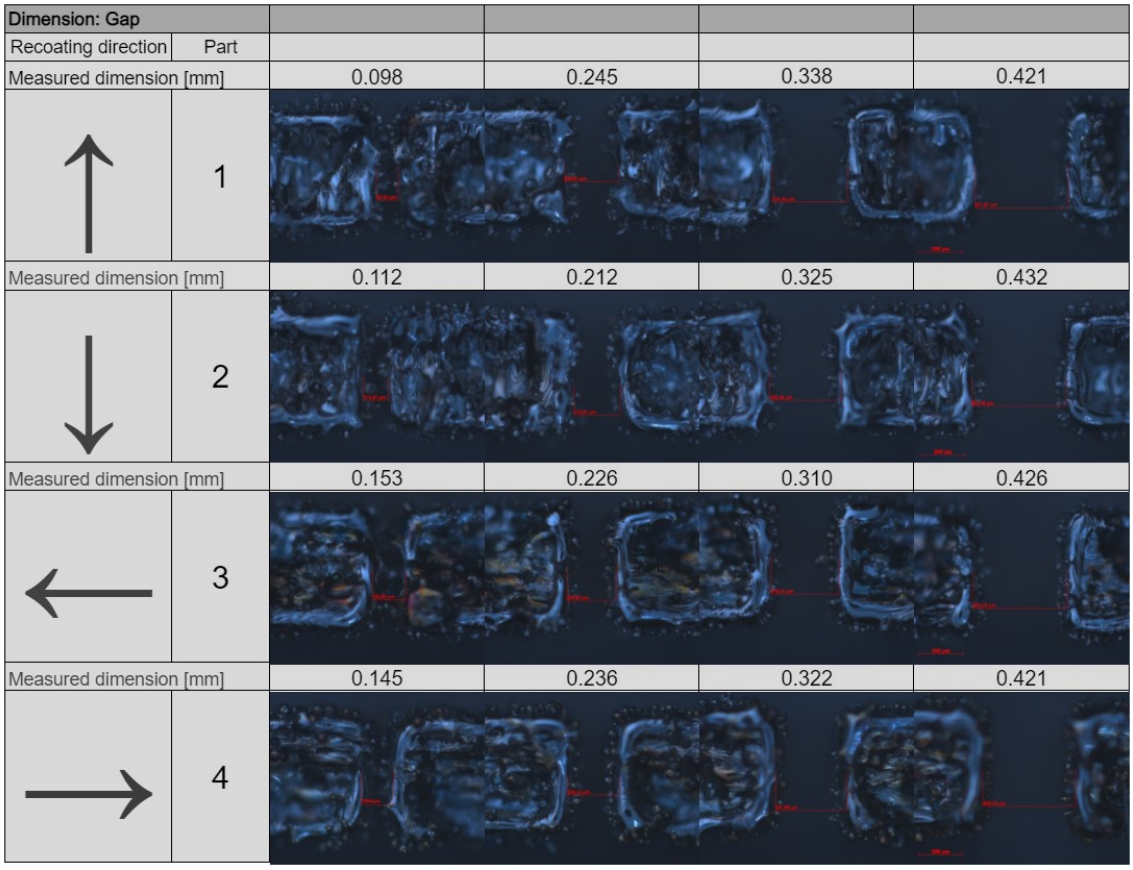

Figure C.10: SOM images of the gaps for print 7.

Table C.7: Deviation of the gaps for print 7.

Gap	0.1		0.2		0.3		0.4	
Re-coat	[mm]	[%]	[mm]	[%]	[mm]	[%]	[mm]	[%]
↑	-0.002	-2	0.045	22.5	0.038	12.67	0.021	5.25
↓	0.012	12	0.012	6	0.025	8.33	0.032	8
←	0.053	53	0.026	13	0.01	3.33	0.026	6.5
→	0.045	45	0.036	18	0.022	7.33	0.021	5.25

- **Print 8**

  The gaps are visible without any attachments to the nearest part except for the first gaps in all orientations. The SOM images and measurements of each gap can be seen in the Figure C.11. The Table C.8 below shows the deviation of the grooves with respect to the original CAD dimension. If the gaps are smaller than the original dimension, then it is a result of irregular shape of the part and half molten particles attached. If the gaps are bigger than the original dimension, then it can be due to shrinkage and irregular shape of the part.

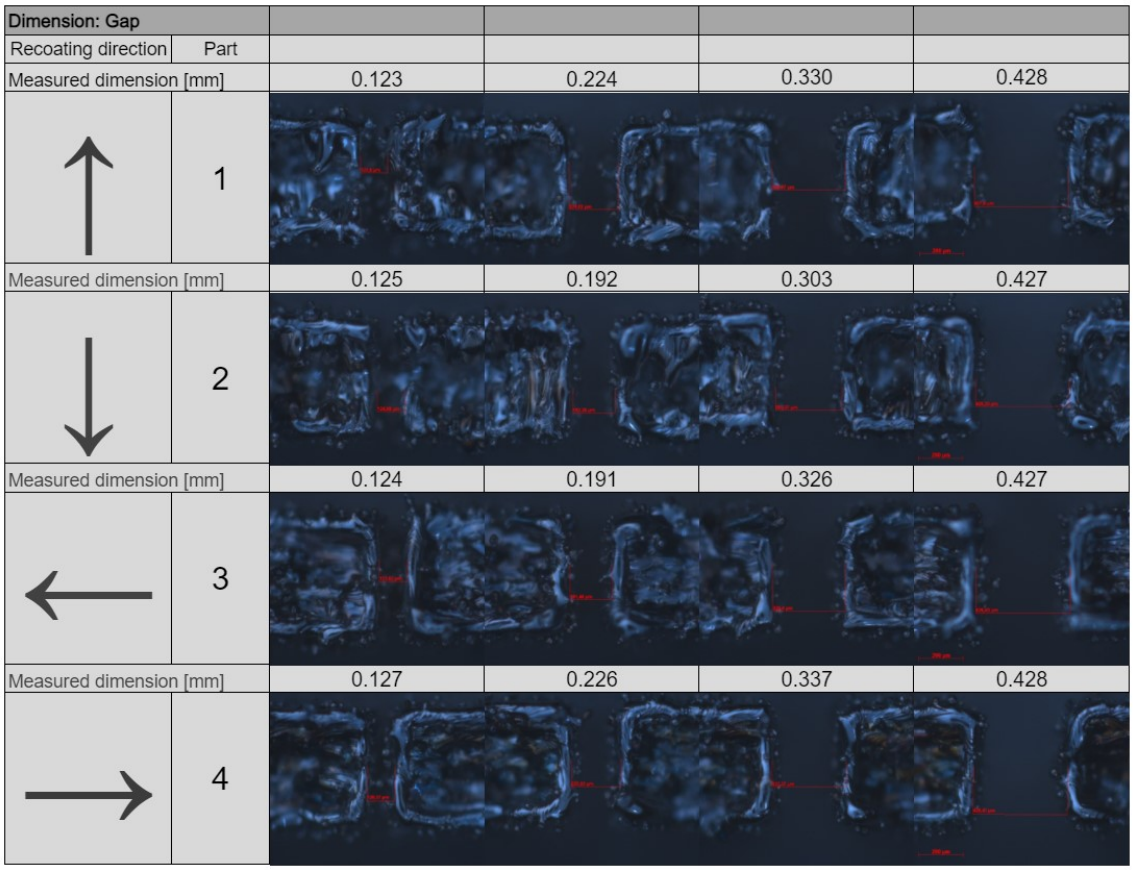

Figure C.11: SOM images of the gaps for print 8.

Table C.8: Deviation of the gaps for print 8.

Gap	0.1		0.2		0.3		0.4	
Re-coat	[mm]	[%]	[mm]	[%]	[mm]	[%]	[mm]	[%]
↑	0.023	23	0.024	12	0.03	10	0.028	7
↓	0.025	25	-0.008	-4	0.003	1	0.027	6.75
←	0.024	24	-0.009	-4.5	0.026	8.67	0.027	6.75
→	0.027	27	0.026	13	0.037	12.33	0.028	7

C.3 Angles

- **Print 2**
  SOM images were taken for angle in position 1 and 5 for each artefact in order to predict the range of deviation, due to the limited accessibility to take images of the angles located in the middle of the artefact. The measurements of the angles 1 and 5 for print 2 together with the calculated deviation can be seen in Figure C.12 and the tables below.

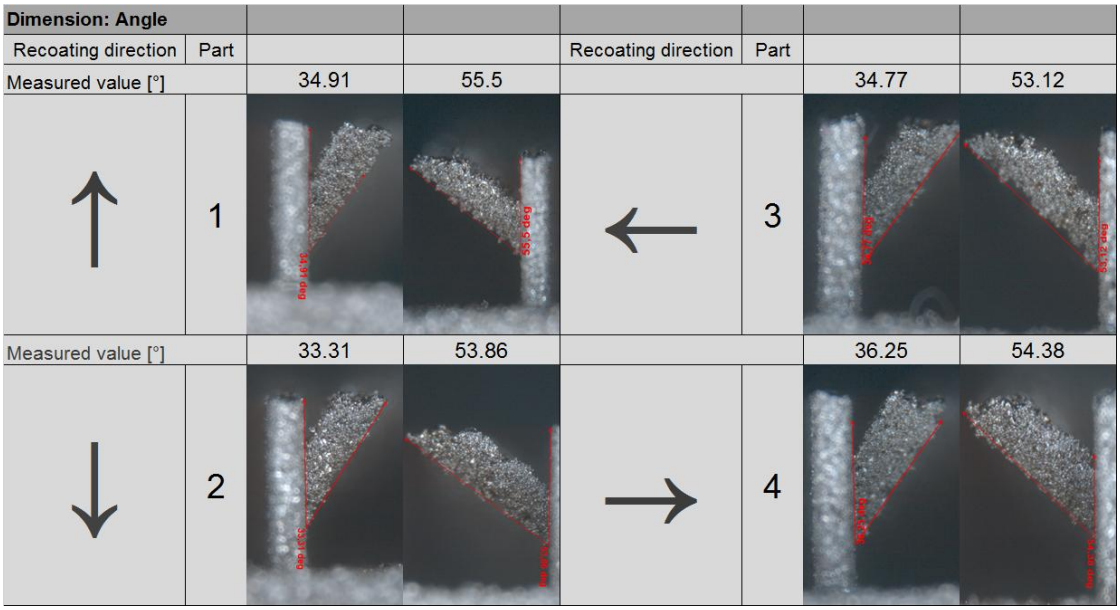

Figure C.12: SOM images of angle 1 and 5 for print 2.

Table C.9: Deviation of angles for print 2

Deviation: Angle		35°		55°	
Recoating direction	Part	[°]	[%]	[mm]	[%]
↑	1	-0.09	-0.2571	0.5	0.90909
↓	2	-1.69	-4.8286	-1.14	-2.0727
←	3	-0.23	-0.6571	-1.88	-3.4182
→	4	1.25	3.57143	-0.62	-1.1273

- **Print 3**
  SOM images were taken for angle in position 1 and 5 for each artefact in order to predict the range of deviation, due to the limited accessibility to take images of the angles located in the middle of the artefact. The measurements of the angles 1 and 5 for print 3 together with the calculated deviation can be seen in Figure C.13 and the tables below.

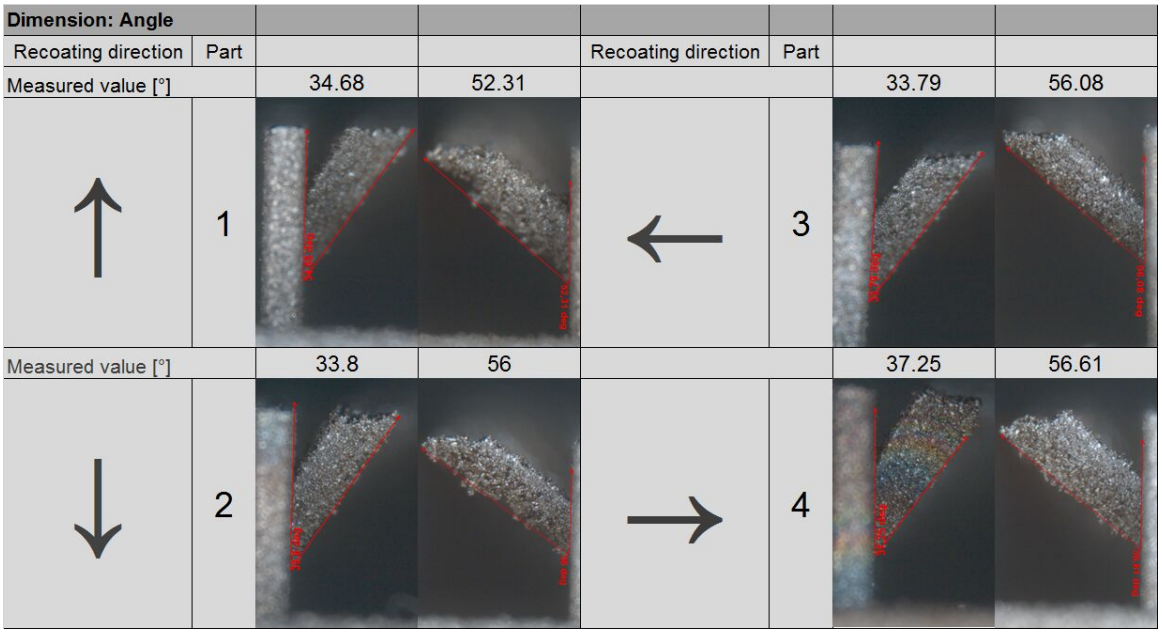

Figure C.13: SOM images of angle 1 and 5 for print 3.

Table C.10: Deviation of angles for print 3

Deviation: Angle		35°		55°	
Recoating direction	Part	[°]	[%]	[mm]	[%]
↑	1	-0.32	-0.9143	-2.69	-4.8909
↓	2	-1.2	-3.4286	1	1.81818
←	3	-1.21	-3.4571	1.08	1.96364
→	4	2.25	6.42857	1.61	2.92727

- **Print 4**
  SOM images were taken for angle in position 1 and 5 for each artefact in order to predict the range of deviation, due to the limited accessibility to take images of the angles located in the middle of the artefact. The measurements of the angles 1 and 5 for print 4 together with the calculated deviation can be seen in Figure C.14 and the tables below.

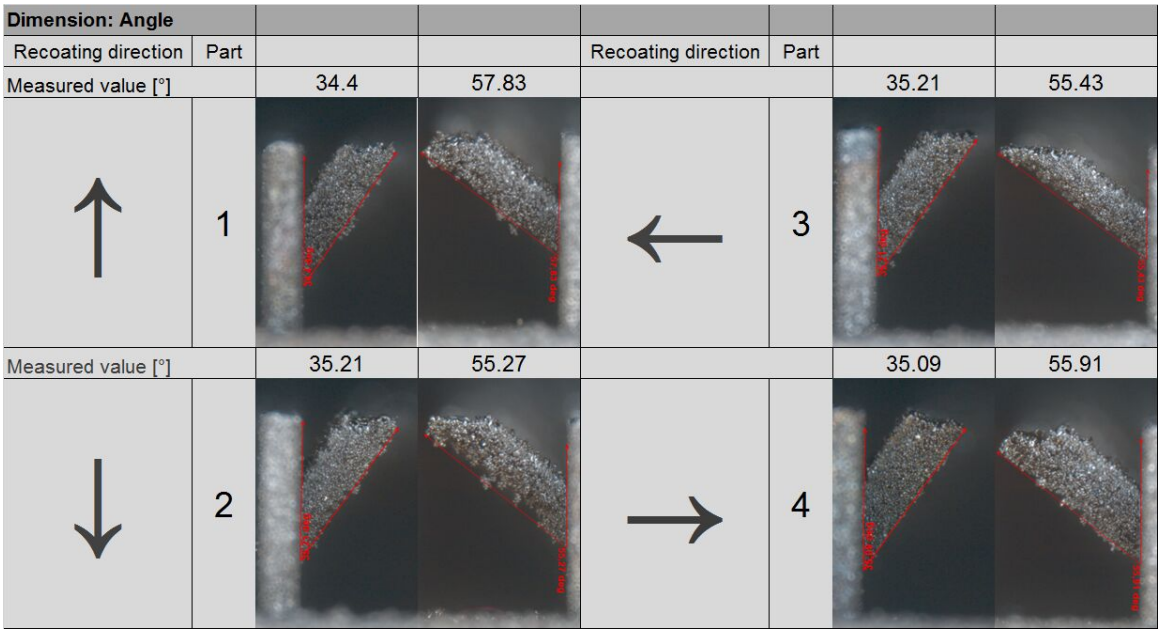

Figure C.14: SOM images of angle 1 and 5 for print 4.

Table C.11: Deviation of angles for print 4

Deviation: Angle		35°		55°	
Recoating direction	Part	[°]	[%]	[mm]	[%]
↑	1	-0.6	-1.7143	2.83	5.14545
↓	2	0.21	0.6	0.27	0.49091
←	3	0.21	0.6	0.43	0.78182
→	4	0.09	0.25714	0.91	1.65455

- **Print 5**
  SOM images were taken for angle in position 1 and 5 for each artefact in order to predict the range of deviation, due to the limited accessibility to take images of the angles located in the middle of the artefact. The measurements of the angles 1 and 5 for print 5 together with the calculated deviation can be seen in Figure C.15 and the tables below.

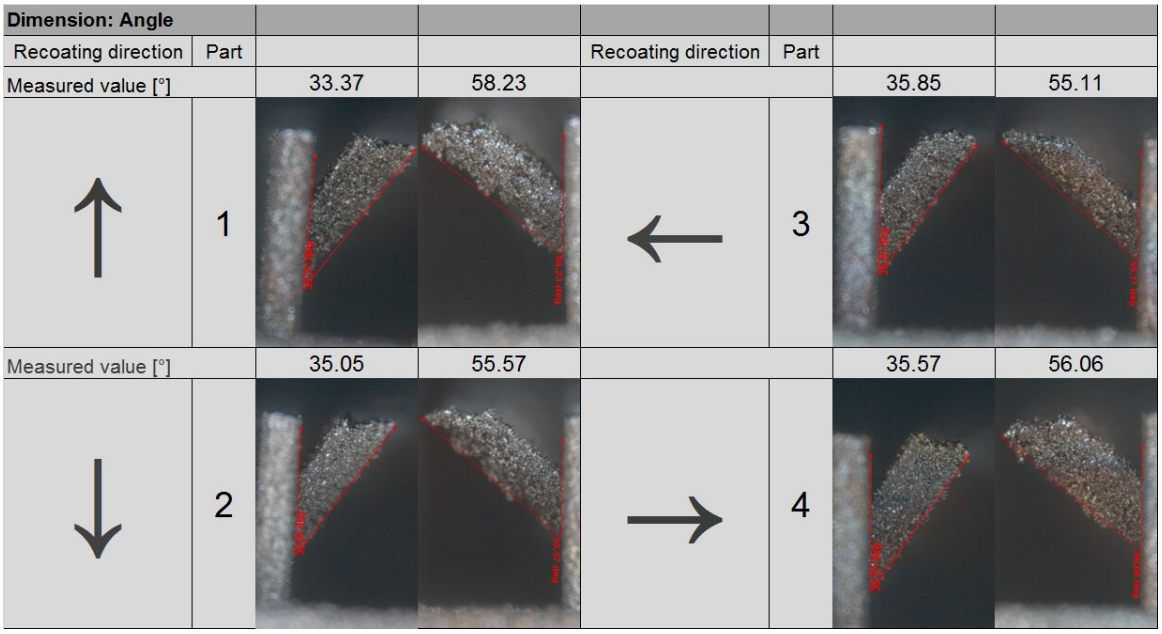

Figure C.15: SOM images of angle 1 and 5 for print 5.

Table C.12: Deviation of angles for print 5

Deviation: Angle		35°		55°	
Recoating direction	Part	[°]	[%]	[mm]	[%]
↑	1	-1.63	-4.6571	3.23	5.87273
↓	2	0.05	0.14286	0.57	1.03636
←	3	0.85	2.42857	0.11	0.2
→	4	0.57	1.62857	1.06	1.92727

- **Print 6**
  SOM images were taken for angle in position 1 and 5 for each artefact in order to predict the range of deviation, due to the limited accessibility to take images of the angles located in the middle of the artefact. The measurements of the angles 1 and 5 for print 6 together with the calculated deviation can be seen in Figure C.16 and the tables below.

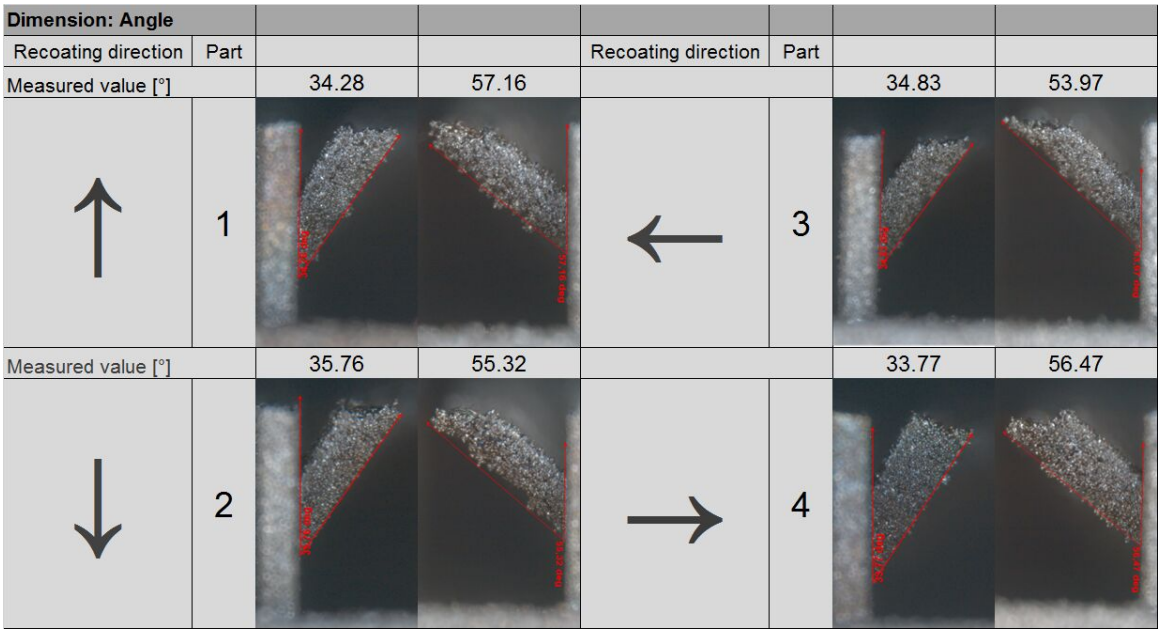

Figure C.16: SOM images of angle 1 and 5 for print 6.

Table C.13: Deviation of angles for print 6

Deviation: Angle		35°		55°	
Recoating direction	Part	[°]	[%]	[mm]	[%]
↑	1	-0.72	-2.0571	2.16	3.92727
↓	2	0.76	2.17143	0.32	0.58182
←	3	-0.17	-0.4857	-1.03	-1.8727
→	4	-1.23	-3.5143	1.47	2.67273

- **Print 7**
  SOM images were taken for angle in position 1 and 5 for each artefact in order to predict the range of deviation, due to the limited accessibility to take images of the angles located in the middle of the artefact. The measurements of the angles 1 and 5 for print 7 together with the calculated deviation can be seen in Figure C.17 and the tables below.

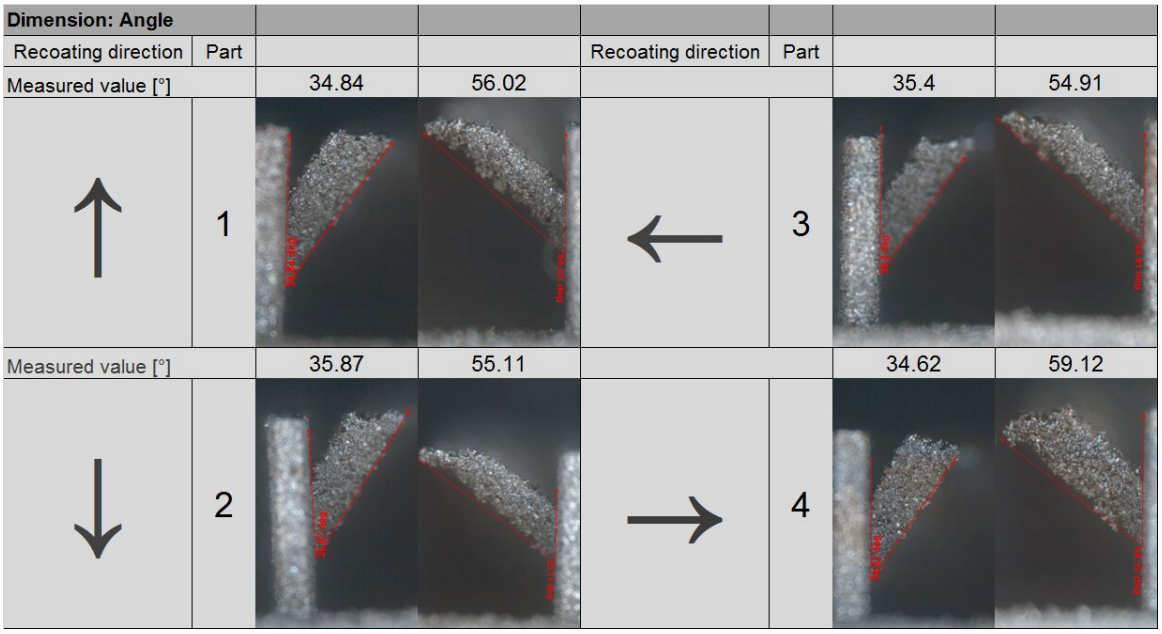

Figure C.17: SOM images of angle 1 and 5 for print 7.

Table C.14: Deviation of angles for print 7

Deviation: Angle		35°		55°	
Recoating direction	Part	[°]	[%]	[mm]	[%]
↑	1	-0.16	-0.4571	1.02	1.85455
↓	2	0.87	2.48571	0.11	0.2
←	3	0.4	1.14286	-0.09	-0.1636
→	4	-0.38	-1.0857	4.12	7.49091

- **Print 8**
  SOM images were taken for angle in position 1 and 5 for each artefact in order to predict the range of deviation, due to the limited accessibility to take images of the angles located in the middle of the artefact. The measurements of the angles 1 and 5 for print 8 together with the calculated deviation can be seen in Figure C.18 and the tables below.

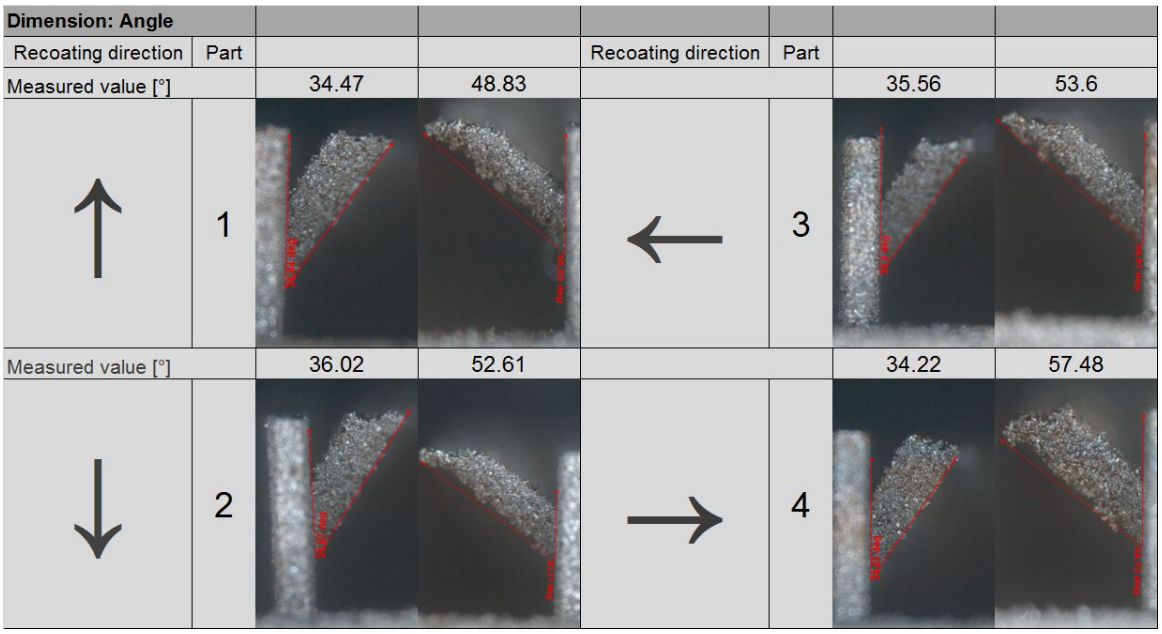

Figure C.18: SOM images of angle 1 and 5 for print 8.

Table C.15: Deviation of angles for print 8

Deviation: Angle		**35°**		**55°**	
Recoating direction	Part	[°]	[%]	[mm]	[%]
↑	1	-0.53	-1.5143	-6.17	-11.218
↓	2	1.02	2.91429	-2.39	-4.3455
←	3	0.56	1.6	-1.4	-2.5455
→	4	-0.78	-2.2286	2.48	4.50909

C.4 Arrow angle & height

- **Print 2**
  SOM images were taken of the arrow height and angle for print 2 in order to investigate the deviation in reputability which can be seen in Figure C.19 and the tables below.

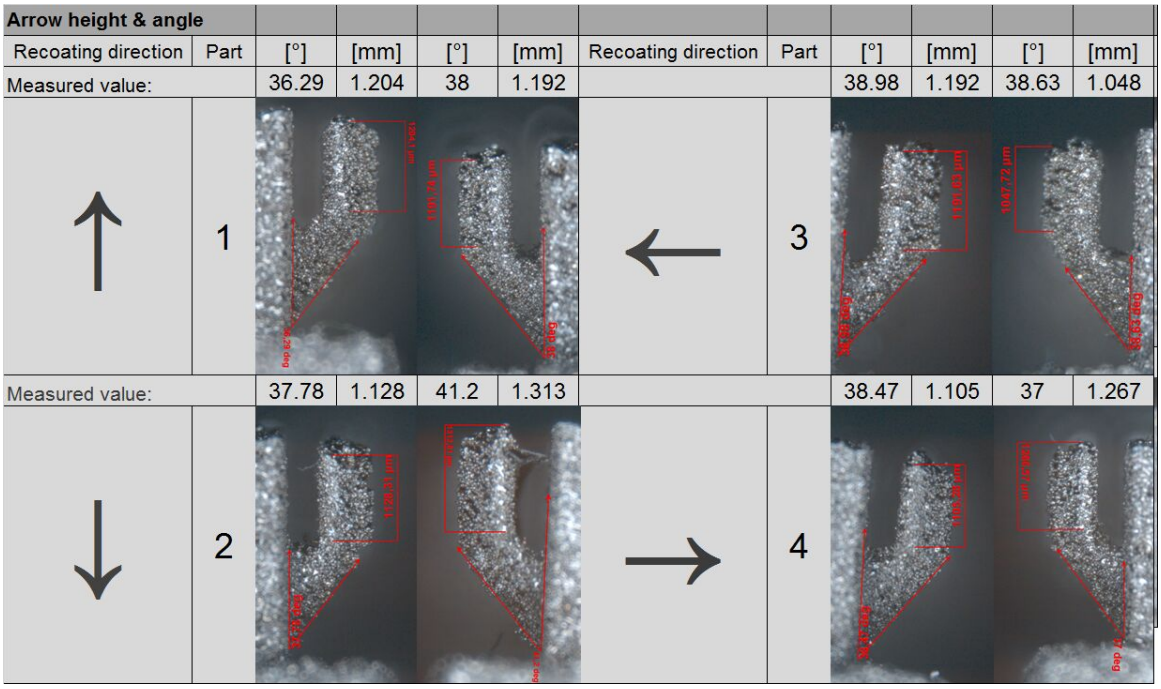

Figure C.19: SOM images of arrow 1 and 5 for print 2.

Table C.16: Deviation of arrowfoot angle for print 2.

Arrowfoot angle	40°		40°	
Re-coat	[°]	[%]	[°]	[%]
↑	-3.71	-9.28	-2.00	-5.00
↓	-2.22	-5.55	1.20	3.00
←	-1.02	-2.55	-1.37	-3.42
→	-1.53	-3.83	-3.00	-7.50

Table C.17: Deviation of arrowhead height for print 2.

Arrowhead height	1.15		1.15	
Re-coat	[mm]	[%]	[mm]	[%]
↑	0.05	4.70	0.04	3.65
↓	-0.02	-1.91	0.16	14.17
←	0.04	3.65	-0.10	-8.87
→	-0.04	-3.91	0.12	10.17

- **Print 3**
  SOM images were taken of the arrow height and angle for print 3 in order to investigate the deviation in reputability which can be seen in Figure C.20 and the tables below.

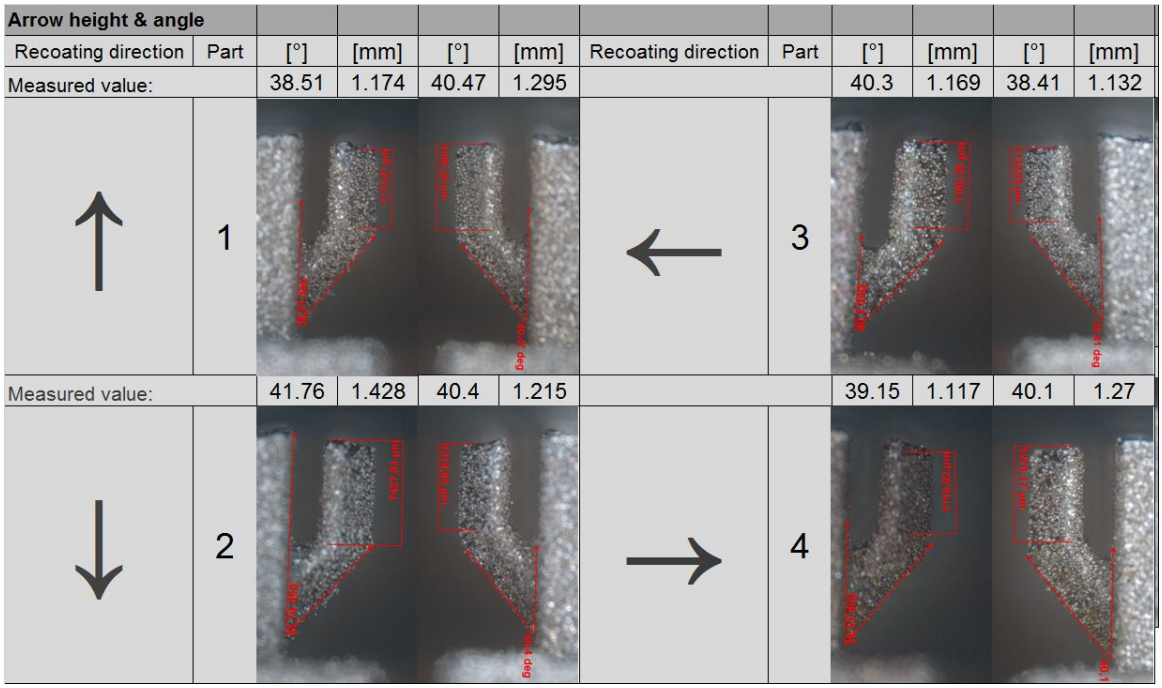

Figure C.20: SOM images of arrow 1 and 5 for print 3.

Table C.18: Deviation of arrowfoot angle for print 3.

Arrowfoot angle	40°		40°	
Re-coat	[°]	[%]	[°]	[%]
↑	-1.49	-3.73	0.47	1.18
↓	1.76	4.40	0.40	1.00
←	0.30	0.75	-1.59	-3.98
→	-0.85	-2.13	0.10	0.25

Table C.19: Deviation of arrowhead height for print 3.

Arrowhead height	1.15		1.15	
Re-coat	[mm]	[%]	[mm]	[%]
↑	0.02	2.09	0.15	12.61
↓	0.28	24.17	0.07	5.65
←	0.02	1.65	-0.02	-1.57
→	-0.03	-2.87	0.12	10.43

- **Print 4**
  SOM images were taken of the arrow height and angle for print 4 in order to investigate the deviation in reputability which can be seen in Figure C.21 and the tables below.

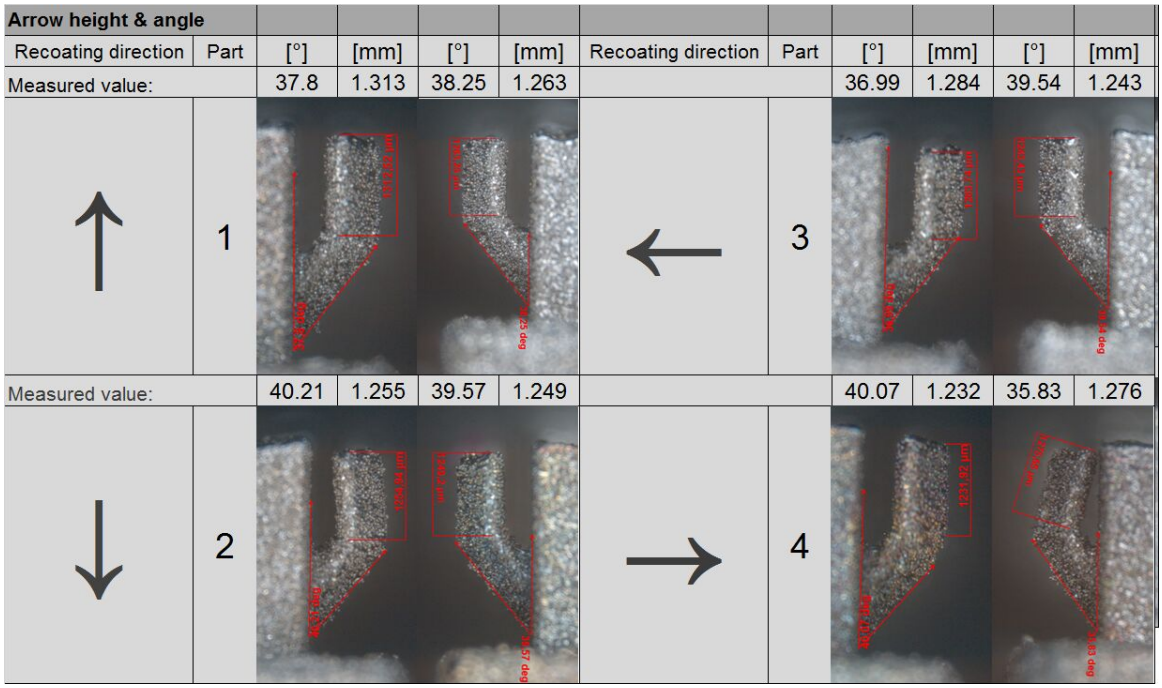

Figure C.21: SOM images of arrow 1 and 5 for print 4.

Table C.20: Deviation of arrowfoot angle for print 4.

Arrowfoot angle	40°		40°	
Re-coat	[°]	[%]	[°]	[%]
↑	-2.20	-5.50	-1.75	-4.38
↓	0.21	0.53	-0.43	-1.08
←	-3.01	-7.53	-0.46	-1.15
→	0.07	0.18	-4.17	-10.43

Table C.21: Deviation of arrowhead height for print 4.

Arrowhead height	40°		40°	
Re-coat	[°]	[%]	[°]	[%]
↑	-2.20	-5.50	-1.75	-4.38
↓	0.21	0.53	-0.43	-1.08
←	-3.01	-7.53	-0.46	-1.15
→	0.07	0.18	-4.17	-10.43

- **Print 5**
  SOM images were taken of the arrow height and angle for print 5 in order to investigate the deviation in reputability which can be seen in Figure C.22 and the tables below.

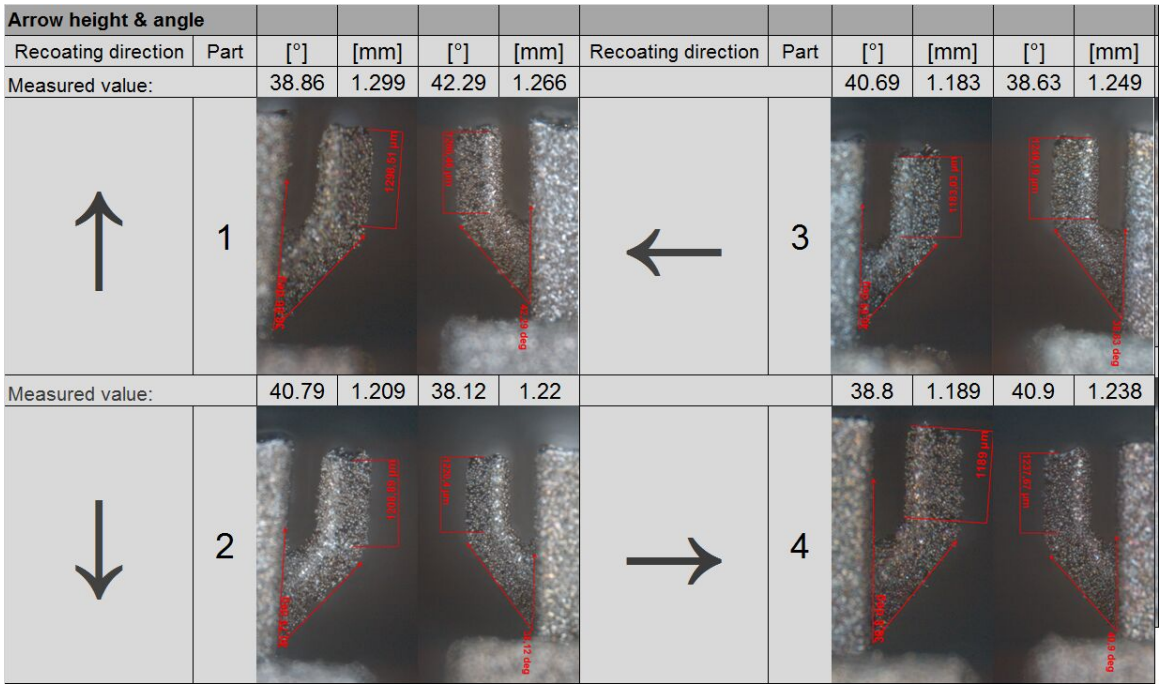

Figure C.22: SOM images of arrow 1 and 5 for print 5.

Table C.22: Deviation of arrowfoot angle for print 5.

Arrowfoot angle	40°		40°	
Re-coat	[°]	[%]	[°]	[%]
↑	-1.14	-2.85	2.29	5.73
↓	0.79	1.98	-1.88	-4.70
←	0.69	1.72	-1.37	-3.42
→	-1.20	-3.00	0.90	2.25

Table C.23: Deviation of arrowhead height for print 5.

Arrowhead height	1.15		1.15	
Re-coat	[mm]	[%]	[mm]	[%]
↑	0.15	12.96	0.12	10.09
↓	0.06	5.13	0.07	6.09
←	0.03	2.87	0.10	8.61
→	0.04	3.39	0.09	7.65

- **Print 6**
  SOM images were taken of the arrow height and angle for print 6 in order to investigate the deviation in reputability which can be seen in Figure C.23 and the tables below.

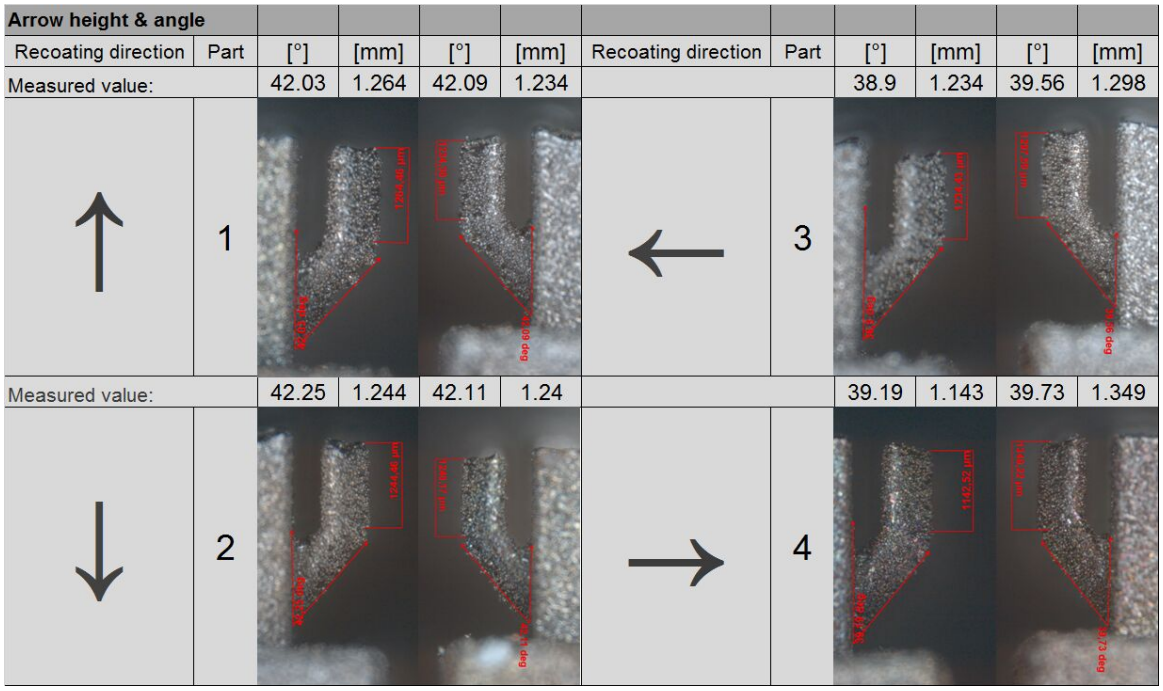

Figure C.23: SOM images of arrow 1 and 5 for print 6.

Table C.24: Deviation of arrowfoot angle for print 6.

Arrowfoot angle	40°		40°	
Re-coat	[°]	[%]	[°]	[%]
↑	2.03	5.08	2.09	5.23
↓	2.25	5.63	2.11	5.28
←	-1.10	-2.75	-0.44	-1.10
→	-0.81	-2.03	-0.27	-0.68

Table C.25: Deviation of arrowhead height for print 6.

Arrowhead height	1.15		1.15	
Re-coat	[mm]	[%]	[mm]	[%]
↑	0.11	9.91	0.08	7.30
↓	0.09	8.17	0.09	7.83
←	0.08	7.30	0.15	12.87
→	-0.01	-0.61	0.20	17.30

- **Print 7**
  SOM images were taken of the arrow height and angle for print 7 in order to investigate the deviation in reputability which can be seen in Figure C.24 and the tables below.

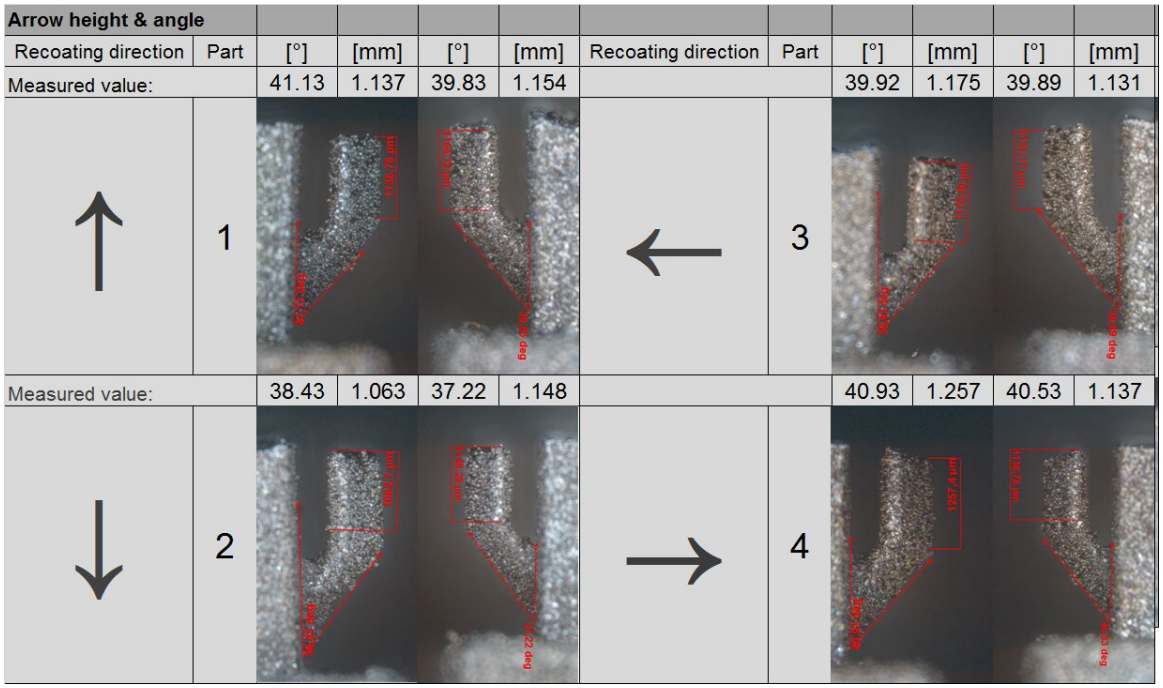

Figure C.24: SOM images of arrow 1 and 5 for print 7.

Table C.26: Deviation of arrowfoot angle for print 7.

Arrowfoot angle	40°		40°	
Re-coat	[°]	[%]	[°]	[%]
↑	1.13	2.83	-0.17	-0.43
↓	-1.57	-3.93	-2.78	-6.95
←	-0.08	-0.20	-0.11	-0.27
→	0.93	2.33	0.53	1.33

Table C.27: Deviation of arrowhead height for print 7.

Arrowhead height	1.15		1.15	
Re-coat	[mm]	[%]	[mm]	[%]
↑	-0.01	-1.13	0.00	0.35
↓	-0.09	-7.57	0.00	-0.17
←	0.03	2.17	-0.02	-1.65
→	0.11	9.30	-0.01	-1.13

- **Print 8**
  SOM images were taken of the arrow height and angle for print 8 in order to investigate the deviation in reputability which can be seen in Figure C.25 and the tables below.

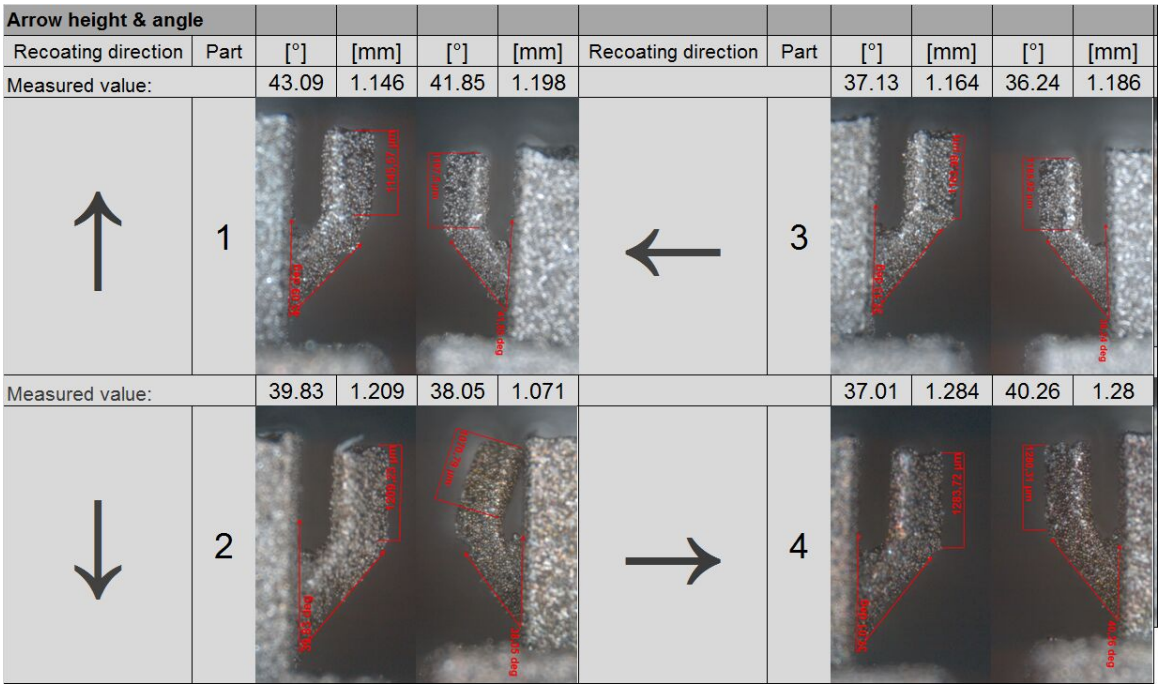

Figure C.25: SOM images of arrow 1 and 5 for print 8.

Table C.28: Deviation of arrowfoot angle for print 8.

Arrowfoot angle	40°		40°	
Re-coat	[°]	[%]	[°]	[%]
↑	3.09	7.73	1.85	4.63
↓	-0.17	-0.43	-1.95	-4.88
←	-2.87	-7.17	-3.76	-9.40
→	-2.99	-7.48	0.26	0.65

Table C.29: Deviation of arrowhead height for print 8.

Arrowhead height	1.15		1.15	
Re-coat	[mm]	[%]	[mm]	[%]
↑	0.00	-0.35	0.05	4.17
↓	0.06	5.13	-0.08	-6.87
←	0.01	1.22	0.04	3.13
→	0.13	11.65	0.13	11.30

DEPARTMENT OF INDUSTRIAL AND MATERIAL SCIENCE (IMS)
CHALMERS UNIVERSITY OF TECHNOLOGY
Gothenburg, Sweden
www.chalmers.se



CHALMERS
UNIVERSITY OF TECHNOLOGY